

## **2.12.4 Engineering Test Results**

The engineering test unit (ETU) was built in half-scale, and incorporated only those features considered necessary for the evaluation of the planned tests. The primary purpose of the tests was to evaluate the puncture resistance of the package. The engineering test described herein addressed the following package design issues:

- *Resistance to Puncture.* While puncture on the body (including oblique orientation) was not expected to present any difficulty, puncture drop tests on or near the containment O-ring seal were of concern. The design of the lid end impact limiter includes an extra thickness shell to prevent perforation, thus completely protecting the seal area from puncture bar attack. Two different (half-scale) thicknesses were present on the ETU: 1/8-inch and 5/32-inch thick. The impact limiters were constructed using two thicknesses to allow for possible optimization of the design. The lesser thickness was tested first. If it had allowed perforation, the greater thickness would have been tested. However, the thinner shell prevented puncture, thus the thicker shell was not tested.
- *Containment Shell Stability.* Although non-linear FEA analyses show that the containment shell will not buckle during any of the NCT or HAC events, the ETU was fabricated using prototypic shell geometry.
- *Effect of thick shell on impact limiter behavior.* On a package of this size and weight, impact limiter shells of the proposed thickness will have a significant effect on impact force. Therefore, the test plan includes a 30-ft free drop to evaluate the impact limiter shell thickness effect.

Since the engineering tests were designed to evaluate specific performance parameters of the MFFP design, the regulatory test sequence stipulated by 10 CFR §71.73(c) was not adhered to. The certification testing, which is summarized in Appendix 2.12.3, *Certification Test Results*, was performed in accordance with the 10 CFR §71.73(c) regulatory test sequence as primary evidence of the MFFP robust design.

### **2.12.4.1 Engineering Test Unit Configuration**

The ETU was a half-scale model of the MFFP and partially prototypic. The design features reproduced in the test unit were primarily those related to the structural behavior of either the seal area or of the impact limiters. The specific features of the test unit and their purpose were as follows:

1. The closure lid and shell flange regions were prototypic with regard to structural strength. The closure lid contained a single O-ring seal instead of three since leakage rate testing was performed by the pressure drop method rather than helium mass spectrometry. A pipe fitting was included in the package shell sidewall for pressurizing and monitoring the cavity (see Figure 2.12.4-1).
2. Only 12 closure bolts were used instead of the full quantity of 24 since the worst case load for the bolts (the inside-out impact of the contents in an end drop) was not being evaluated. The effect of fewer bolts on the seal area puncture deformation was not considered to be significant.
3. The package shell had a half-scale prototypic thickness of 9/32 inches (full-scale 9/16-inch thickness).

4. The impact limiters were retained by prototypic means, including six necked-down bolts, the shell bolt lugs, and the impact limiter internal attachments.
5. The impact limiter shells, shape, attachment means, and foam density of the impact limiters were essentially prototypic. For testing convenience, the thicker shells were used at the bottom end, and the thinner shells used at the lid end.
6. The limiter used at the bottom end of the package featured the thicker shells, which were made from Type 304 stainless steel in order to exactly model their resistance to perforation/tearing. All the flat shell sections and half the curved shells (cylindrical and tapered sections) were 11-gauge (0.120-inches) material. The other half of the curved shell was 5/32-inches thick. The limiter used at the lid (top) end of the package featured the thinner shell made from carbon steel, since no resistance to perforation was expected. All of the thin shell material of the top end limiter was 16-gauge (0.060-inches) material.
7. The foam in the thicker-shell limiter was nominally  $10 \text{ lb}_m/\text{ft}^3$  and the thinner-shell limiter foam was nominally  $11.5 \text{ lb}_m/\text{ft}^3$ . These densities were analytically calculated to give essentially the same force deflection curve. Impact limiter crush performance in the free drop was expected to be similar.
8. The steel material used for the package shell and lid was ASTM A572 Grade 50. For modest strain levels this material will have a similar stress strain curve as the actual XM-19 steel based on a simple comparison of yield and tangent modulus. The minimum yield strengths are approximately the same (55 ksi for XM-19 and 50 ksi for A572). The ultimate strength and elongation for XM-19 and A572 are 100 ksi - 40%, and 65 ksi - 21%, respectively. The tangent moduli (calculated using engineering values) are therefore 112.5 ksi and 71.4 ksi, respectively. The test material has conservatively lower strain hardening, compared to the XM-19 material. The material report on the A572 shell material listed an yield strength of 52 ksi, which demonstrates the conservatism of using this material.
9. The strongback was not replicated in the ETU. The weight of the strongback and fuel assemblies was included as non-structural steel rods.

Although the engineering tests were not completely prototypic, the results are relevant in supporting the conclusions regarding the MFFP that: 1) the impact limiter shells, with exception of the recessed end plate, are puncture resistant, 2) the effect of puncture through the recessed end plate onto the closure lid is of little consequence, 3) the containment body shell is stable during a 30-foot side drop, and 4) the containment body shell is capable of sustaining direct puncture impact.

#### **2.12.4.1.1 Interim Impact Limiter**

During the testing of the thick shell sections, puncture impacts took place at the bottom end of the package and secondary impacts occurred at the lid end. To prevent damage to the thin shell limiter and the lid end from secondary impacts, an interim impact limiter was installed (refer to Figure 2.12.4-2).

#### **2.12.4.1.2 Dummy Payload**

A dummy payload was used to simulate the weight of the strongback and three fuel assemblies. The equivalent full-scale weight of the dummy payload is 6,616 pounds and essentially evenly distributed. In half-scale, the dummy payload weighed 827 pounds. A bundle of approximately

(181) 1/2-inch diameter round bars  $\times 82 \pm 1/2$  inches long were used. This dummy payload arrangement had an approximate diameter of 7½ inches. The bars were strapped together at each end. In this configuration, the dummy payload had little structural strength in bending. The axial clearance to the package cavity was approximately 3/4 inches. The radial clearance was approximately 3½ inches. Wooden blocks were strapped to the bundle at several locations along its length to maintain a gap between the bundle and the shell wall, which kept the payload from affording any puncture resistance (backing).

**2.12.4.1.3 Test Facility**

The tests were conducted using a drop pad consisting of 12-inches of reinforced concrete over 18-inches of packed gravel, topped by a 2-inch thick, 9  $\times$  10 ft steel plate. The plate was connected to the concrete using high-strength grout. The combined weight of the steel and concrete was approximately 20,000 pounds. The weight of the half-scale model was 1,641 pounds (see Table 2.12.4-1), which is less than one-tenth of the weight of the drop pad.

**Table 2.12.4-1 – Summary of Engineering Test Unit Component Weights**

<b>Component</b>	<b>Actual Half-Scale Weight, pounds</b>	<b>Full-Scale Weight = 8 <math>\times</math> [Half-Scale Weight], pounds</b>
Bundle of Rebar (mock payload)	827	6,616
Containment Body	467	3,736
Stainless Impact Limiter	200	1,600
Carbon Steel Impact Limiter	147	1,176
<b>Total Weight</b>	<b>1,641</b>	<b>13,128</b>

The half-scale puncture bar was 3-inches in diameter and made from mild steel, having a maximum 1/8-inch radius. The bar was socket welded and gusseted to a 1½-inch thick baseplate, which was welded to the drop pad. The free length of bar was 16-inches, which was adequate to reach full depth before the outer surface of the impact limiter came in contact with the gussets.

**2.12.4.2 Pre-Test Activities**

Prior to free drop or puncture testing, the following activities were performed.

1. The quality assurance data package was reviewed to ensure that the ETU was adequate for the test requirements.
2. All ETU components were weighed. Separate weights were recorded for the package shell assembly, the package lid, each impact limiter, the interim impact limiter, and the dummy payload.

**2.12.4.2.1 Leakage Rate Test Calibration**

Damage to the seal area due to puncture drop testing was evaluated by means of a pressure drop test. It was assumed, for the purposes of this test program, that the seal would either perform adequately or it would exhibit a gross leak, and therefore sophisticated leakage rate test procedures were not required. The seal area was evaluated by pressurizing the package

internally, and monitoring the pressure over a brief time period. The arrangement of the leakage rate test components is shown in Figure 2.12.4-1.

1. *Pressure Integrity of Package.* Before testing, the pressure holding behavior of the package was confirmed. First, the closure lid was assembled by installing the O-ring seal and tightening the closure bolts according to the drawing. The package cavity was pressurized to 5 psig using regulated air to the package cavity through a shut-off valve. The pressure was monitored within the cavity, and when the pressure stabilized at 5 psig, the shut-off valve was closed. The pressure within the package was monitored for 45 minutes without variation of the internal pressure. Thus, the pressure integrity of the package was verified.
2. *Pressure Drop vs. Time.* Using a pipe plug with a 1/32-inch drilled hole, the package was re-pressurized and the pressure was monitored. The behavior of such a leak was characterized by noting the pressure drop vs. time. This information was used to establish an appropriate dwell time and pressure drop magnitude for use in later post-puncture leak testing.

### **2.12.4.3 Summary of Engineering Test Results**

#### **2.12.4.3.1 Test 1**

Test 1 was an oblique puncture drop onto the conical portion of the 1/8-inch thick stainless steel impact limiter. The actual drop angle of the package axis with respect to horizontal was 69 degrees and the drop height was slightly greater than 40 inches, measured from the top of the puncture bar to the point of impact. The impact resulted in an indentation of 7/8 inches to 1 1/8 inches, depending on measurement method. There was no sign of cracking or tearing of the impact limiter shell. The planned drop orientation is shown in Figure 2.12.4-3. A photo record of the drop results is shown in Figure 2.12.4-4.

#### **2.12.4.3.2 Test 2**

Test 2 was an oblique puncture drop onto the cylindrical portion of the 1/8-inch thick stainless steel impact limiter. The actual drop angle of the package axis with respect to horizontal was 24 degrees and the drop height was slightly greater than 40 inches, measured from the top of the puncture bar to the point of impact. The impact resulted in an indentation of 3/4 inches. There was no sign of cracking or tearing of the impact limiter shell. The drop orientation is shown in Figure 2.12.4-5. A photo record of the drop results is shown in Figure 2.12.4-6.

#### **2.12.4.3.3 Test 3**

Test 3 was an oblique puncture drop onto the recessed end plate (1/8-inch thick) of the stainless steel impact limiter. The actual drop angle of the package axis with respect to horizontal was 64 degrees and the drop height was slightly greater than 40 inches, measured from the top of the puncture bar to the point of impact. The impact resulted in an indentation of 1 1/8 inches. There was a very small crescent tear over approximately 160 degrees of the puncture circle. The drop orientation is shown in Figure 2.12.4-7. A photo record of the drop results is shown in Figure 2.12.4-8.

#### **2.12.4.3.4 Test 4**

Test 4 was a side puncture drop onto containment body shell as near to the O-ring seal area as possible without contacting the impact limiter. The actual drop angle of the package axis with

respect to horizontal was 0 degrees and the drop height was slightly greater than 40 inches, measured from the top of the puncture bar to the point of impact. The impact resulted in a 3/8-inch indentation. There was no sign of cracking or tearing of the body shell. Following the test, a leakage rate check was performed. The actual internal pressure was 5.5 psi and held without change for 5 minutes. The drop orientation is shown in Figure 2.12.4-9. A photo record of the drop results is shown in Figure 2.12.4-10.

#### **2.12.4.3.5 Test 5**

Test 5 was an end puncture drop onto the thin shell (1/16-inch thick), carbon steel impact limiter. The actual drop angle of the package axis with respect to horizontal was 90 degrees and the drop height was slightly greater than 40 inches, measured from the top of the puncture bar to the point of impact. The impact resulted in a puncture of the shell of 2 3/4 inches. The package remained vertical for several seconds and slowly turned off the bar. The bar did not bend and there was very little 'tearout' damage. Following the test, a leakage rate check was performed. The actual internal pressure was 5.0 psi and held without change for 5 minutes. The drop orientation is shown in Figure 2.12.4-11. A photo record of the drop results is shown in Figure 2.12.4-12. Appearance of the photo notwithstanding, the puncture bar was still welded to the drop pad.

#### **2.12.4.3.6 Test 6**

Test 6 was a 30-foot side drop. The actual drop angle of the package axis with respect to horizontal was 0 degrees and the drop height was slightly greater than 30 feet. The impact caused no noticeable permanent deformation of the shell. The drop orientation is shown in Figure 2.12.4-13. A photo record of the drop results is shown in Figure 2.12.4-14. The small hollow tubes were aluminum crush gages used to measure crush distance.

#### **2.12.4.3.7 Test 7**

Test 7 was a side puncture drop onto the center of the containment body shell. The actual drop angle of the package axis with respect to horizontal was 0 degrees and the drop height was slightly greater than 40 inches, measured from the top of the puncture bar to the point of impact. The impact resulted in an indentation of 1 1/8 inches maximum depth. The deformation gradually decreased to zero by approximately 18 inches from the impact point. At a distance of 3 inches from the point of impact, the deformation was approximately 1/2 inches, and at 6 inches distant, the deformation was approximately 5/32 inches. There was no sign of cracking or tearing of the containment body shell. The full scale dent depth would be twice the 1 1/8 inches, or 2 1/4 inches. The drop orientation is shown in Figure 2.12.4-15. A photo record of the drop results is shown in Figure 2.12.4-16.

#### **2.12.4.3.8 Test 8**

Test 8 was an oblique puncture drop onto the conical portion of the 1/8-inch thick stainless steel impact limiter. This test was very similar to Test 1, except that the impact point was closer to the cylindrical-to-conical shell joint. The actual drop angle of the package axis with respect to horizontal was 77 degrees and the drop height was slightly greater than 40 inches, measured from the top of the puncture bar to the point of impact. The impact resulted in an indentation of approximately 2 inches. There was no sign of cracking or tearing of the impact limiter shell. Following the test a leakage rate check was performed. The actual internal pressure was 4.95 psi and held without change for 4 minutes. The planned drop orientation is shown in Figure 2.12.4-17. A photo record of the drop results is shown Figure 2.12.4-18.

### 2.12.4.3.9 Conclusions

Following the engineering tests, the test article was returned to the shop for final inspection of the O-ring seal area. No appreciable change of the seal region dimensions was noted. Based on the success of the 1/8-inch thick impact limiter shells in resisting perforation, the final design of the lid end impact limiter was determined to have 1/4-inch thick stainless steel shells (full-scale), and consequently, puncture bar impact on the seal region, and exposure of the seal region to HAC fire temperatures, is precluded. The engineering test also demonstrated the ability of the closure lid to resist puncture loads and remain sealed, although due to the perforation resistance of the impact limiter shells, this feature is not expected to be necessary. Because the recessed end plate did tear slightly, the plate thickness was increased from a full-scale thickness of 1/4 inches to 5/16 inches. Since no puncture resistance at the bottom end of the package is necessary (since there are no penetrations or elastomer seals located there), to minimize weight, the shell of the bottom end impact limiter was determined to have a full-scale thickness of 1/8-inch stainless steel.

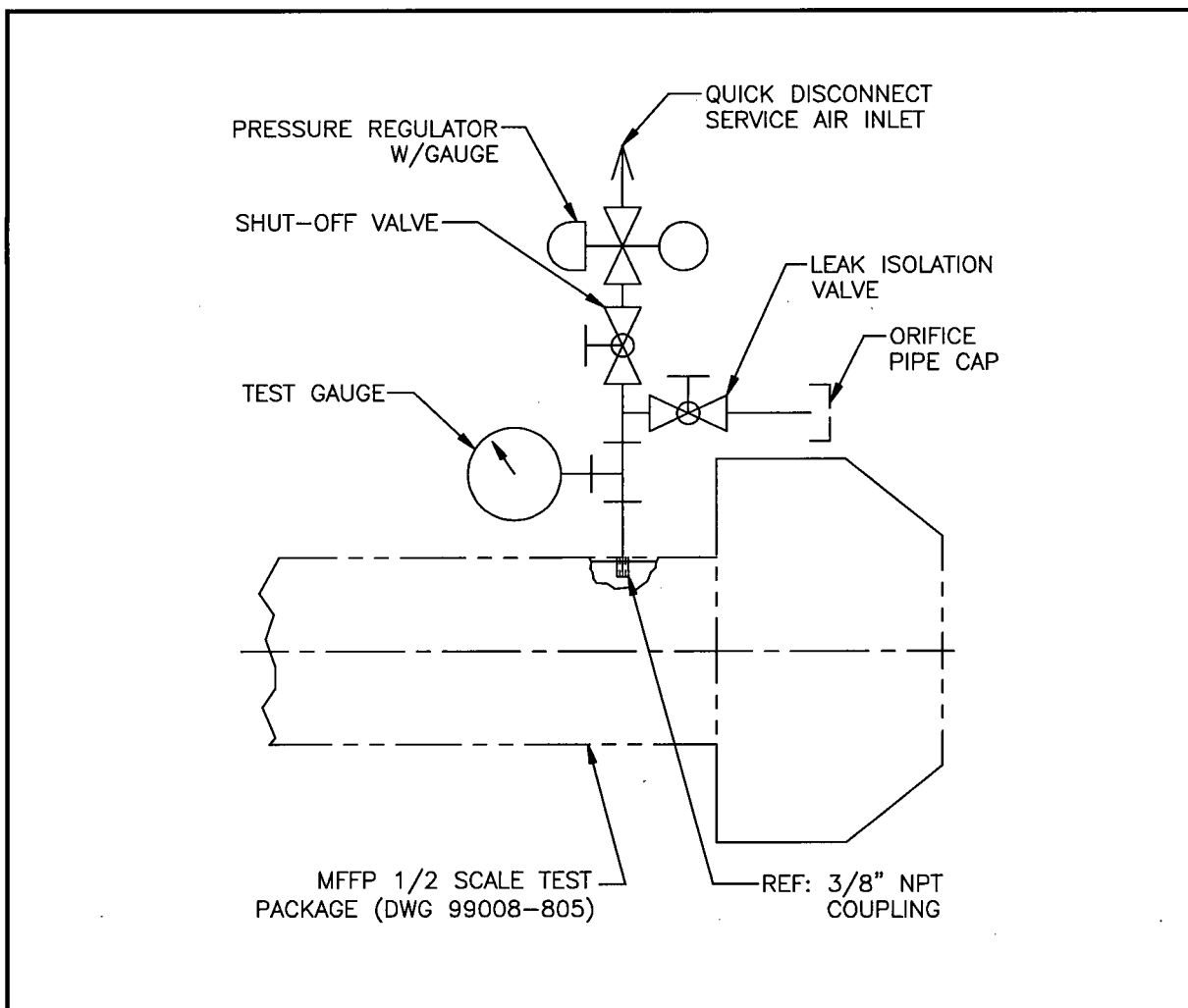


**Figure 2.12.4-1 – ETU Leakage Rate Test Plumbing Schematic**



**Figure 2.12.4-2 – ETU Initial Configuration (with Interim Impact Limiter)**

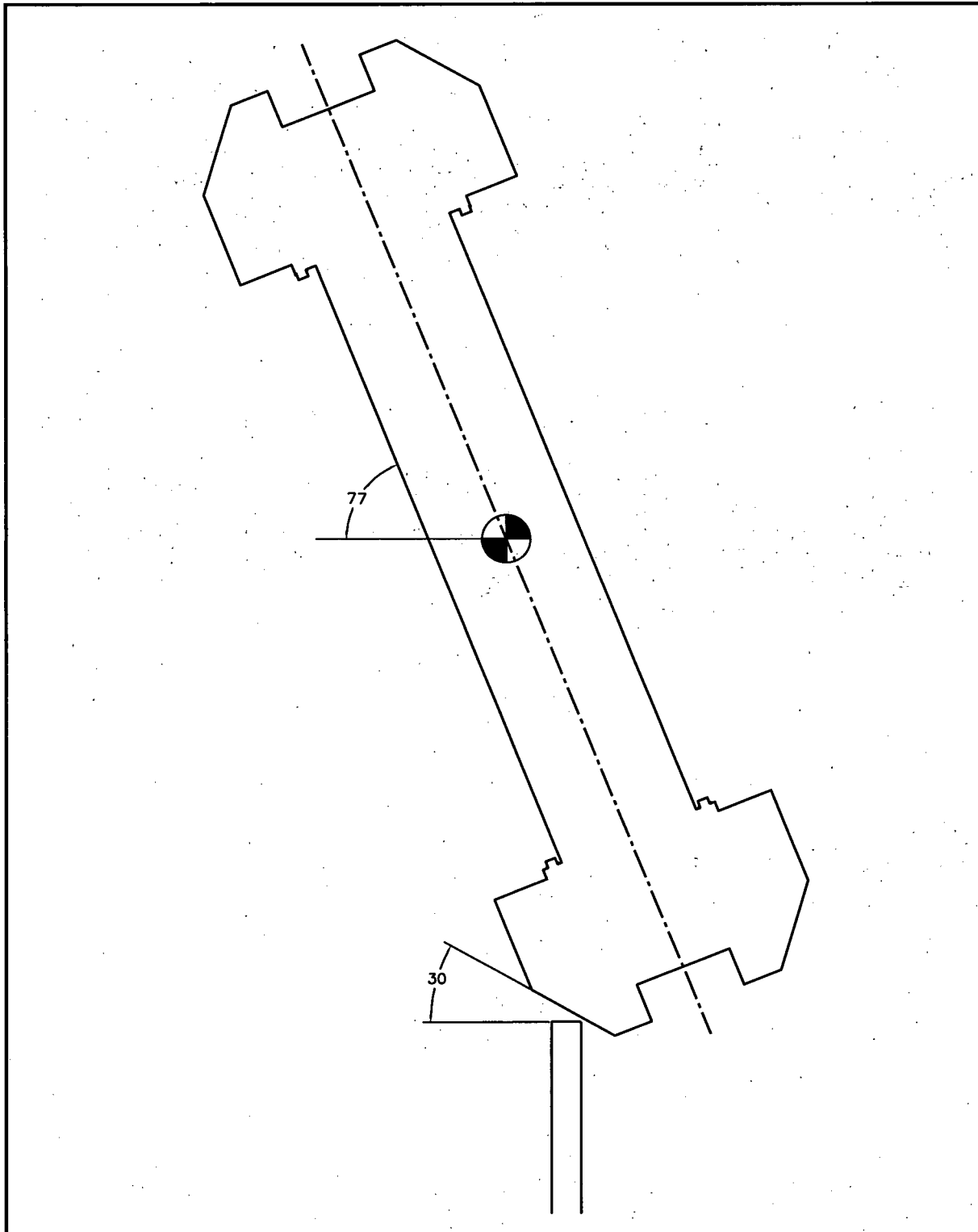


**Figure 2.12.4-3 – ETU Test 1 Drop Orientation**

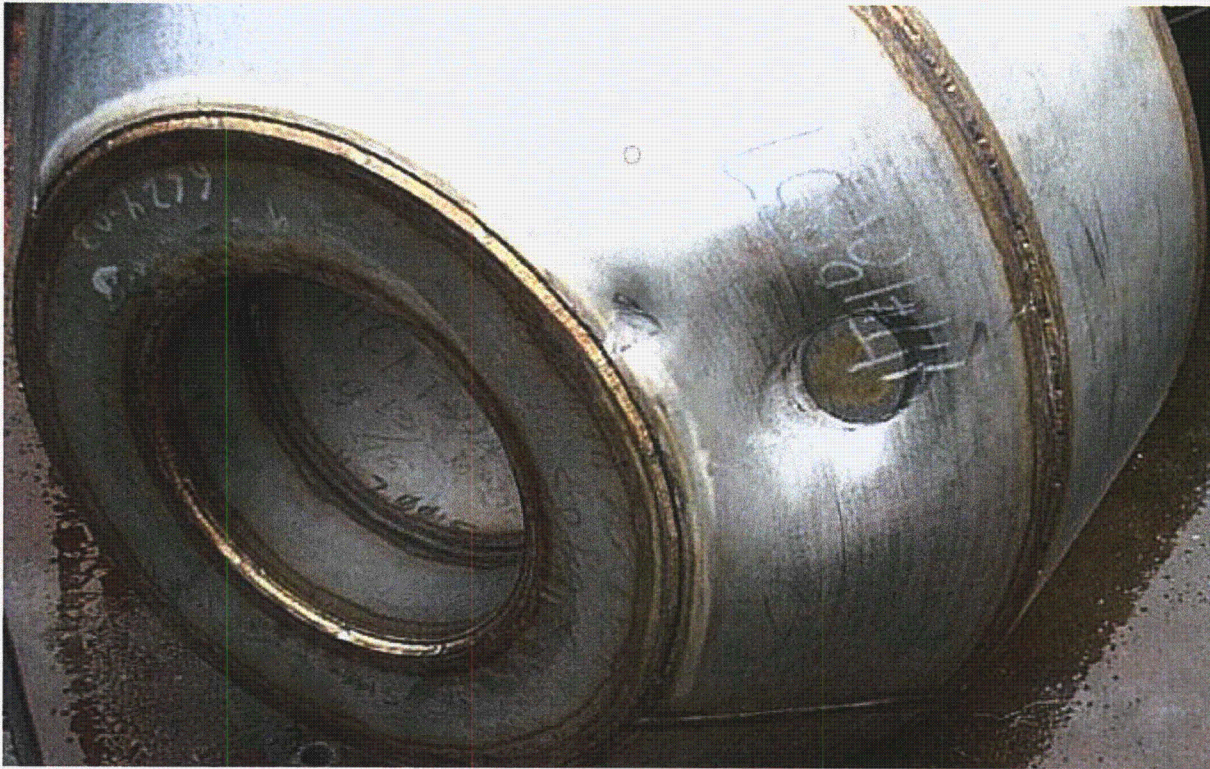


Figure 2.12.4-4 – ETU Test 1: View of Puncture Damage; ~1" Deep

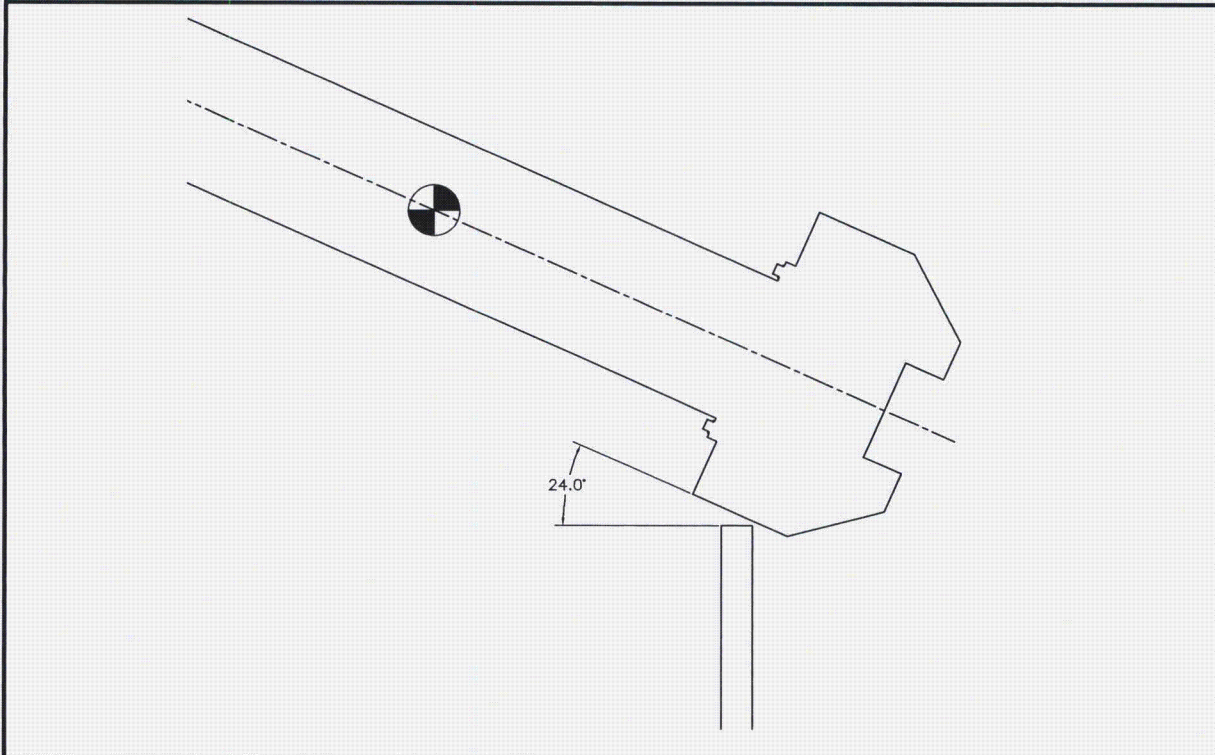


Figure 2.12.4-5 – ETU Test 2 Drop Orientation



Figure 2.12.4-6 – ETU Test 2: View of Puncture Damage; ~3/4" Deep

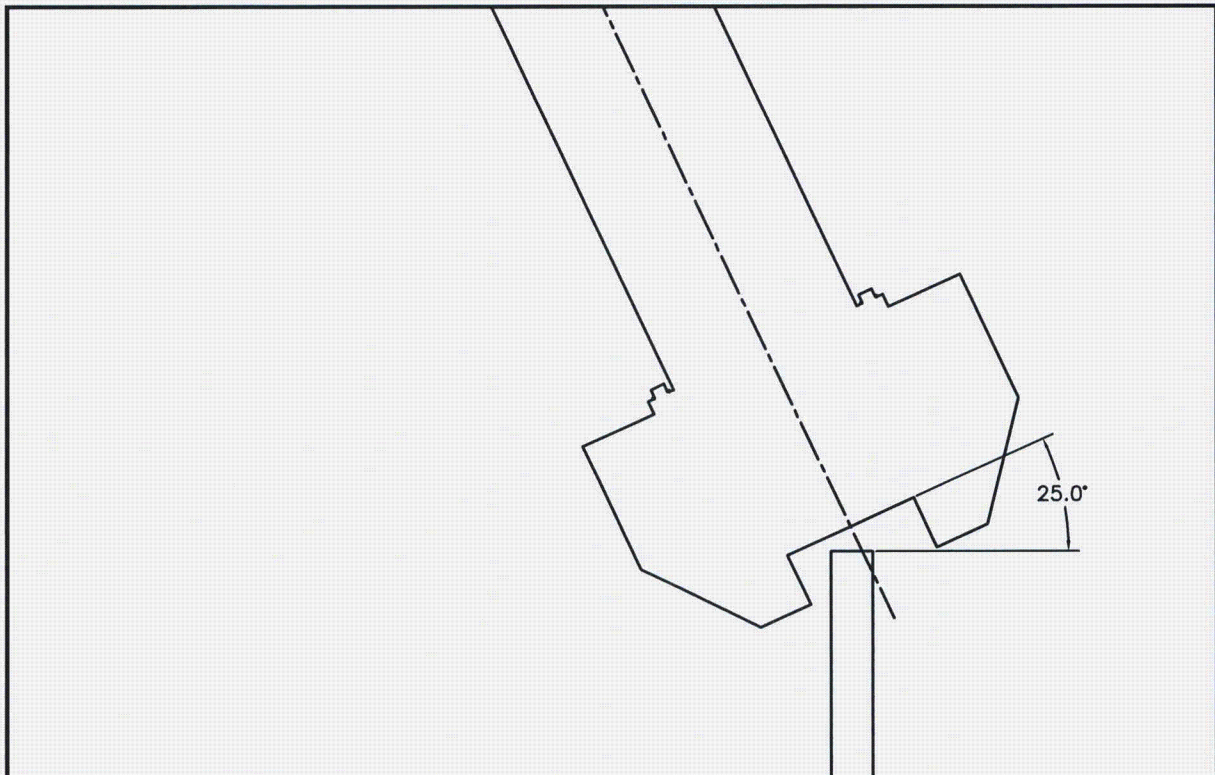


Figure 2.12.4-7 – ETU Test 3 Drop Orientation



Figure 2.12.4-8 – ETU Test 3: View of Puncture Damage;  $\sim 1\frac{1}{8}$ " Deep

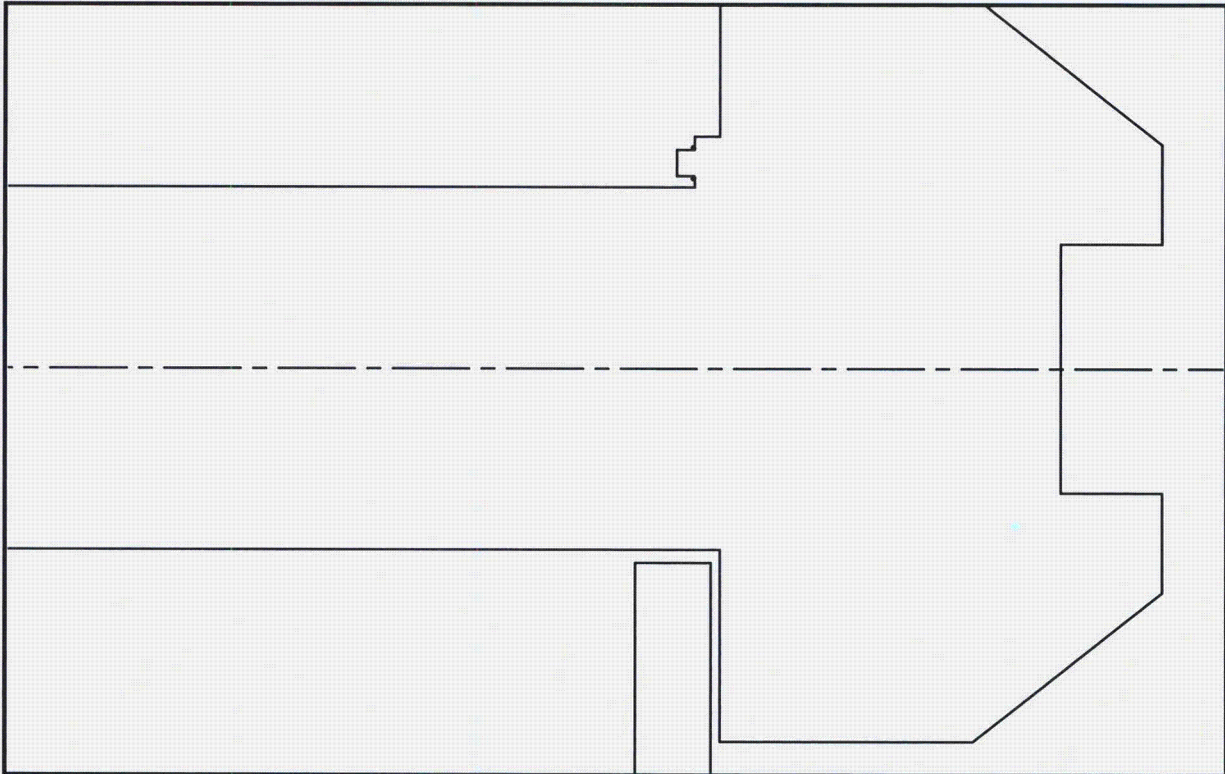


Figure 2.12.4-9 – ETU Test 4 Drop Orientation



Figure 2.12.4-10 – ETU Test 4: View of Puncture Damage; ~3/8" Deep

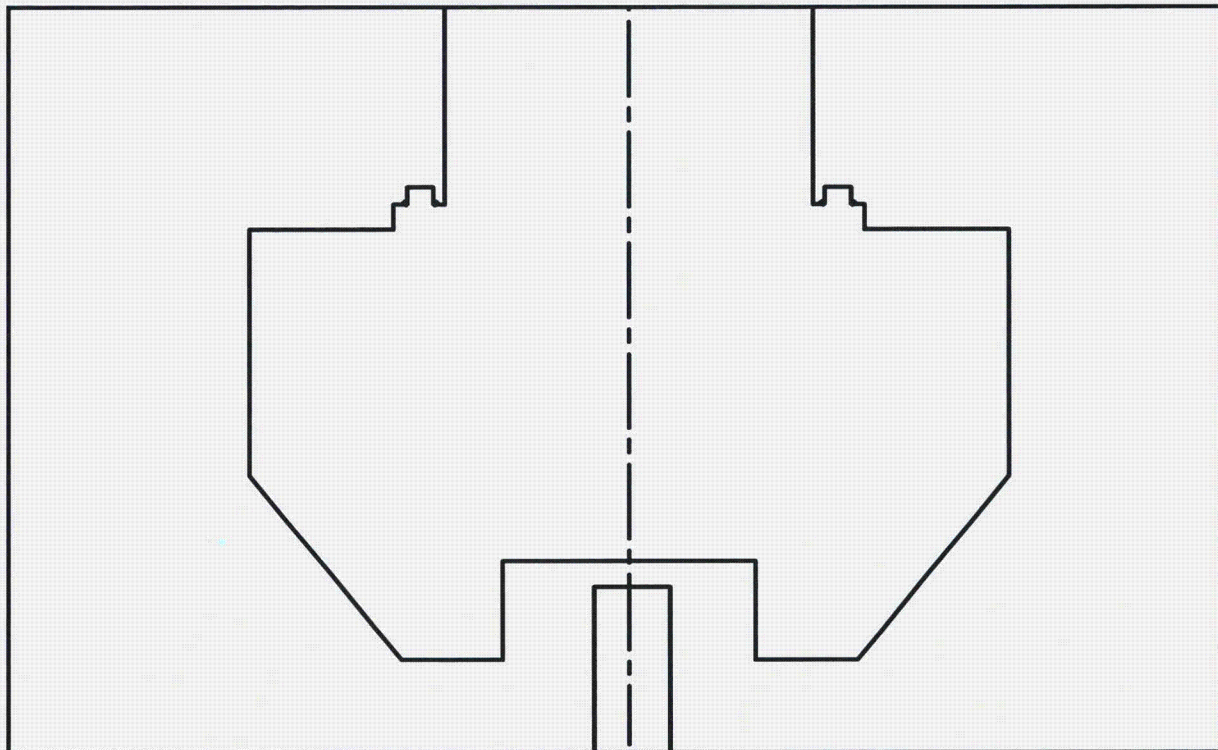


Figure 2.12.4-11 – ETU Test 5 Drop Orientation



**Figure 2.12.4-12 – ETU Test 5: View of Puncture Damage; ~2<sup>3</sup>/<sub>4</sub>" Deep**



**Figure 2.12.4-13 – ETU Test 6 Drop Orientation**



Figure 2.12.4-14 – ETU Test 6: View of Free Drop Damage

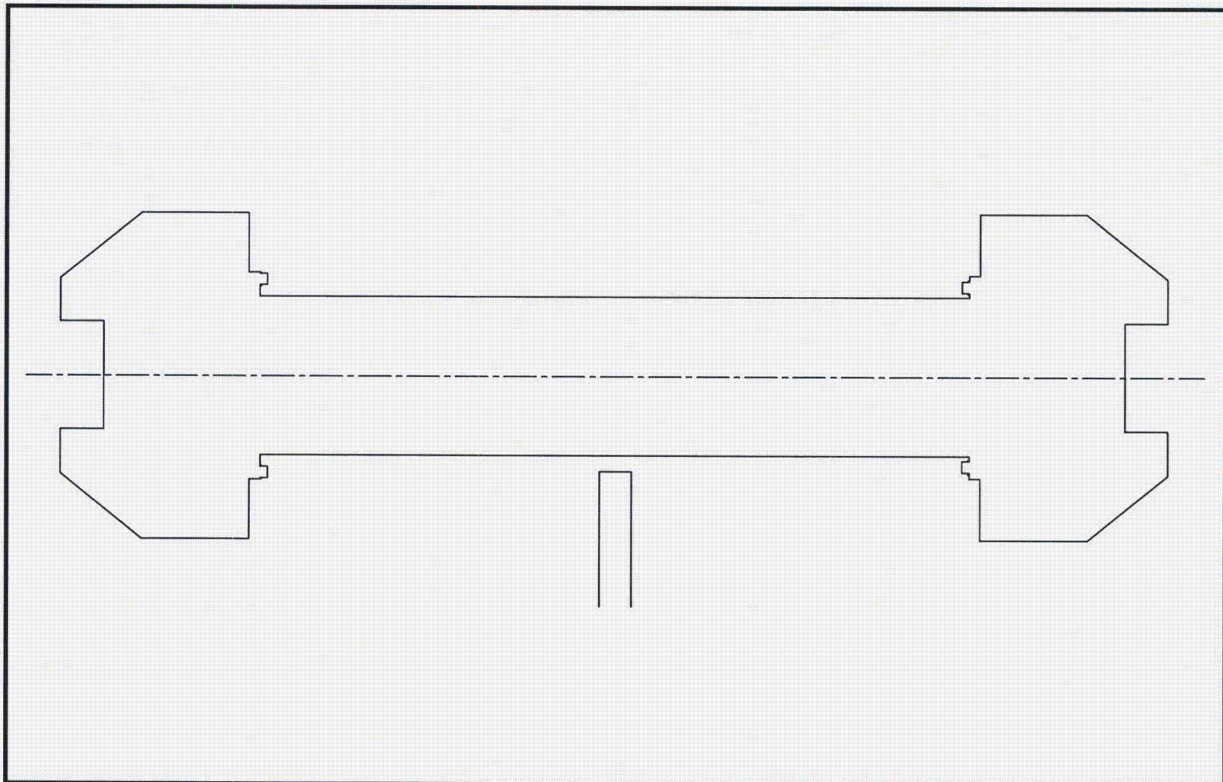
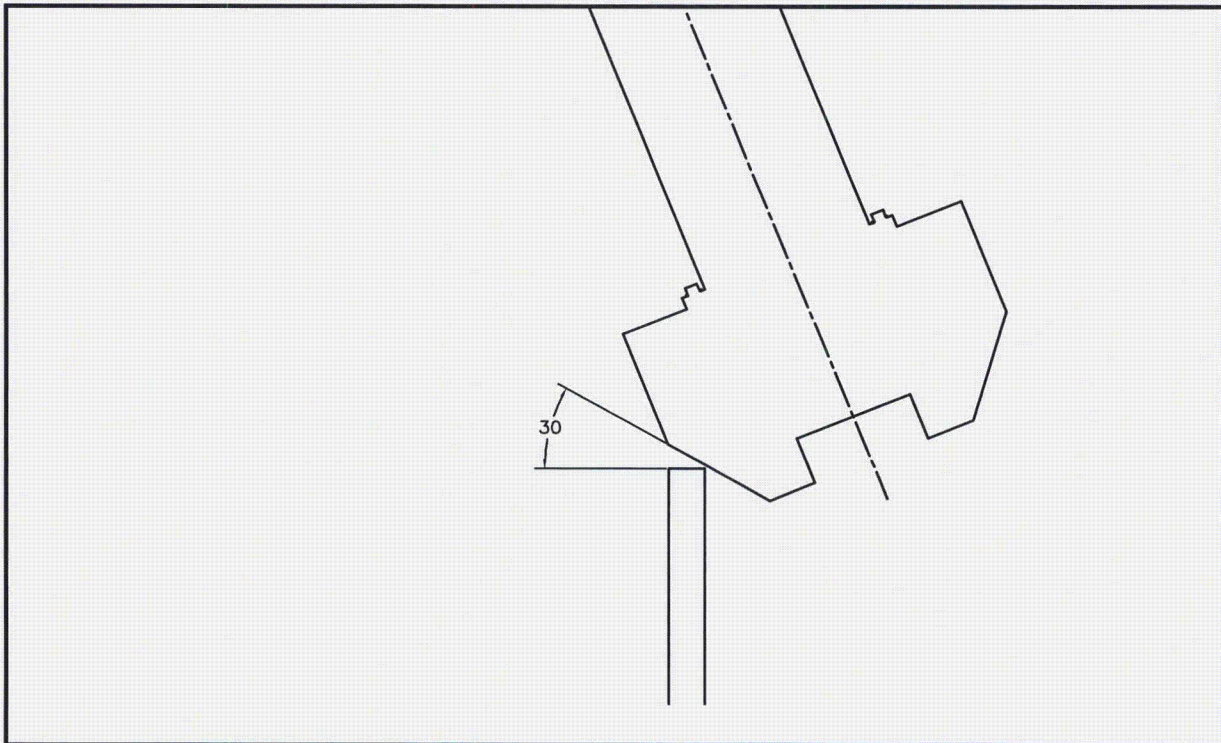


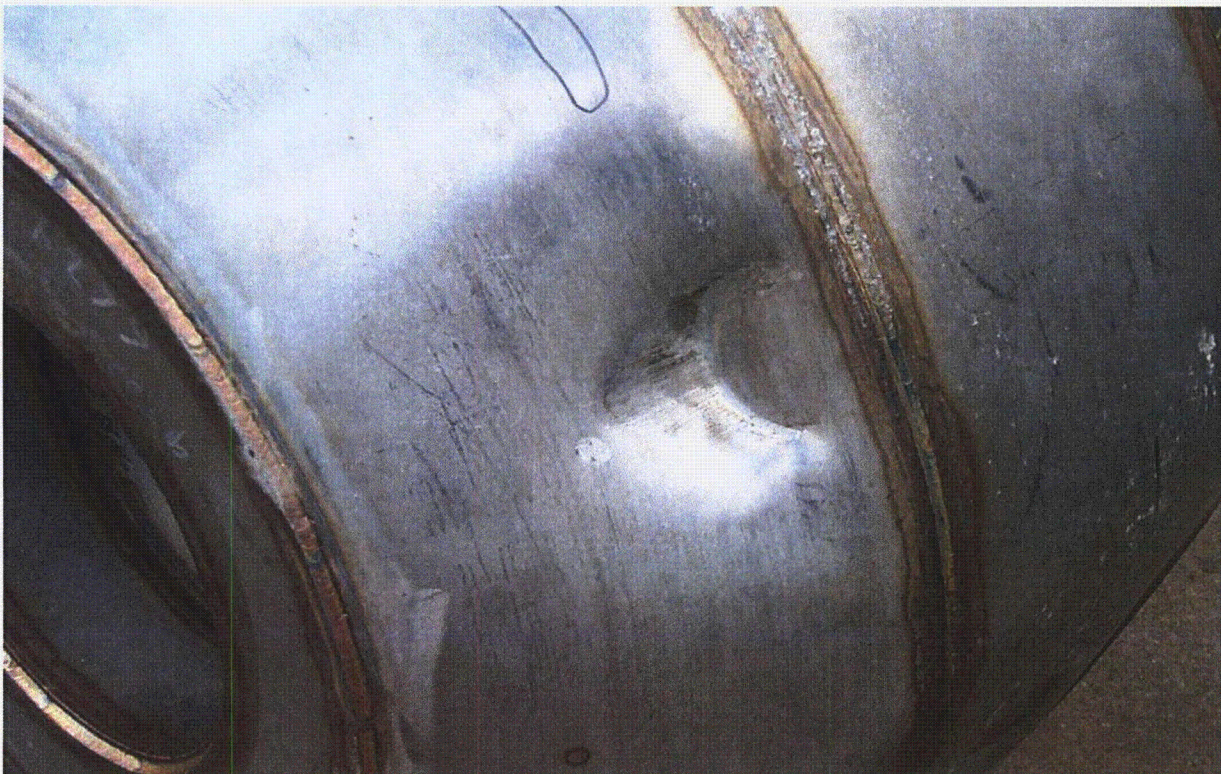
Figure 2.12.4-15 – ETU Test 7 Drop Orientation



Figure 2.12.4-16 – ETU Test 7: View of Puncture Damage; ~1 $\frac{1}{8}$ " Deep



**Figure 2.12.4-17 – ETU Test 8 Drop Orientation**



**Figure 2.12.4-18 – ETU Test 8: View of Puncture Damage; ~2" Deep**



This page left intentionally blank.

## 2.12.5 Fuel Control Structure Evaluation

As discussed in Appendix 2.12.3, *Certification Test Results*, the 80 degrees-from-horizontal, 30-foot free drop resulted in lateral deformation of the fuel rods. The focus of this evaluation is the vertical or near-vertical free drop orientations. Geometric control of the fuel is required during the vertical or near-vertical orientations for criticality considerations, as discussed in Chapter 6.0, *Criticality Evaluation*. Horizontal orientations are considered in the evaluation of the strongback longitudinal structure. Although the fuel control structures (FCSs) are not specifically required to control the fuel for horizontal orientation impacts, the strongback longitudinal weldment provides separation of the fuel. This appendix demonstrates the FCS design satisfies all stability and stress requirements.

The FCS provides a fixed geometric boundary surrounding the fuel assembly (FA), preventing excessive pitch expansion and controlling lateral deformations of the fuel rods. Two primary design features of the FCS are important to the criticality evaluation.

1. The FCS provides a support structure for the neutron poison plates surrounding the exterior of the FA.
2. The FCS, with clamp arms, controls and limits the distortion of the fuel to a cross-section of 8.70 inches square, restricting an increase in the fuel rod pitch.

Since the FCSs were not included in the certification tests, the structural integrity for the hypothetical accident condition (HAC) free drops defined in 10 CFR §71.73(c)(1)<sup>1</sup> is demonstrated analytically in this appendix.

### 2.12.5.1 Summary of Results

The results of the evaluations contained in the following sections of this appendix demonstrate that:

- The fuel rod forces used to evaluate the FCS and strongback core are highly conservative and based on simple determination methods. Section 2.12.5.7, *Vertically Loaded Fuel Load Determination*, and Section 2.12.5.8, *Horizontally Loaded Fuel Load Determination*, present the fuel rod load derivations.
- The FCS structure provides significant geometric control of the MK-BW/MOX1 fuel assemblies as well as serving as a substrate to support additional neutron poison, thereby providing significant criticality margin. Section 2.12.5.6, *Stability Criteria*, through Section 2.12.5.13, *Lock Plate and Hinge Mounting Brackets*, provide the structural evaluation of the FCS.
- The structural integrity of the strongback is demonstrated in Section 2.12.5.14, *Strongback Global Stability*, through Section 2.12.5.20, *Strongback Stress Calculations - Horizontal Loads*, for the increased weight and effects of the FCS. These calculations included comprehensive checks of the stress and stability conditions.

---

<sup>1</sup> Title 10, Code of Federal Regulations, Part 71 (10 CFR 71), *Packaging and Transportation of Radioactive Materials*, Final Rule, 01-26-04.

### 2.12.5.2 Conditions Analyzed

The FCS is evaluated using four bounding loading conditions. Three of these conditions are comprised of maximum near vertical load plus a lateral loading applied by the FA rods. The fourth loading condition is comprised of maximum lateral loading only.

The loading cases are as follows:

1. LC1: 120g's vertical plus lateral loads applied by the FA rods on inside *pin block* box panel. Lateral loads are parallel to the local 'Y' axis (refer to Figure 2.12.5-5 for geometry).
2. LC2: 120g's vertical plus lateral loads applied by the FA rods on inside *hinge block* box panel. Lateral loads are parallel to the local 'X' axis (refer to Figure 2.12.5-5 for geometry).
3. LC3: 120g's vertical plus lateral loads applied by the FA rods on both hinge and pin block box panels.

The vertical g-loading in LC 1-3 is perpendicular to the lateral FA rod loading and is based on the 80 degrees from horizontal, 30-foot drops (Certification Test Series 2, Test 1 and Data Test 11) performed in the certification testing (Appendix 2.12.3, *Certification Test Results*). The lateral loads applied to the FCS by the FA rods are determined within this appendix.

The FCS is attached to the strongback and applies loads locally to the primary structure of the strongback. The worst-case reaction FCS load to the strongback results from a horizontal drop. Fuel buckling is not a concern during this horizontal drop. A fourth load case is performed to determine the worst-case FCS reaction forces on the strongback.

4. LC4: 180g's horizontal including inertia loads applied by the FA rods on inside hinge block box panel.

The hinge block of the FCS is mounted in close proximity to the strongback triangular core, while the pin block is mounted near the unsupported edge of the strongback angle plate, see Figure 2.12.5-5. Therefore, applying the acceleration and fuel support load perpendicular to the inside surface of the hinge block box panel causes loads to concentrate at the hinge, thus maximizing local loadings to the strongback.

### 2.12.5.3 FCS Geometry

The function of the FCSs is to control the geometry of the fuel assemblies to prevent excessive lateral displacement when subjected to a 120g vertical acceleration loading, including the lateral fuel loading.

The MFFP strongback is constructed as shown in Appendix 1.4.2, *Packaging General Arrangement Drawings*, Drawing 99008-30. The primary structural components are:

- The strongback core, which provides the longitudinal structure of the strongback.
- The top and bottom plates of the strongback, which interface with the ends of the FA and the containment body.
- The clamp arm assemblies, which provide the interface of the fuel to the strongback and restrain the fuel at the grid straps during all conditions of transport.
- The FCSs, which restrict the lateral movement of the fuel rods.

The MK-BW/MOX-1 FA physical characteristics important to this evaluation are geometry and weight. Table 2.12.5-1 and Figure 2.12.5-1 re-state the FA geometry and weight information from Section 1.2.3, *Contents of Packaging*.

The neutron poison plates and angle supports attached to the fuel segment angle are conservatively assumed to not provide any structural reinforcement, and therefore are not included in the FEA model. However, their mass is included with the angle component to account for their effect on the hinges and stiffeners associated with the drop acceleration load.

#### **2.12.5.4 FCS Material Properties**

The material properties used for the analyses herein are fully presented in Section 2.2, *Materials*, and are summarized in Table 2.12.5-2.

The FCS consists of four primary structural components; the box angle, channel stiffeners, hinge block, and pin block, see Figure 2.12.5-5. The material for the channel stiffeners, hinge block, and pin block is XM-19 stainless steel. These components are welded together (or machined as one) and subsequently bolted to the box angle. The pins used to connect the FCS to the strongback are ASTM A564 Grade 630 H1100 (17-4PH). The box angle is Type 304 stainless steel and the fasteners are ASTM F835 flat countersunk head cap screws. The chemical and mechanical requirements of F835<sup>2</sup> are similar to A574 (for regular socket head cap screws). The ASTM minimum tensile loads for both F835 and A574 are based on the same ultimate strength of 180 ksi. The primary difference between the two specifications is the product form; i.e. flat countersunk head cap screws versus regular socket head cap screws. Therefore, the material properties in Table 2.12.5-2 for A574 are considered to be applicable for determining the allowable stresses of F835 fasteners in the subsequent evaluations. The tangent modulus for XM-19 and Type 304 is determined below for use in the non-linear ANSYS<sup>®</sup> model.

The tangent modulus is defined as the slope of the true stress-strain curve between the material yield point and the ultimate breaking strength, given as:

$$E_{\text{TAN}} = \frac{(S_u - S_y)}{(\epsilon_u - 0.002)}$$

where  $S_u$  is the ultimate true stress,  $S_y$  is the yield true stress, and  $\epsilon_u$  is the ultimate true strain, and the elongation or strain at the yield point is defined as 0.2%, or 0.002. Since the data is in the form of engineering stress-strain data, it must first be converted to true stress-strain data before use in the equation above for the tangent modulus. This conversion can be performed using the following relations<sup>3</sup>:

$$\sigma_{\text{true}} = \sigma_{\text{eng}}(1 + e_{\text{eng}})$$

$$\epsilon_{\text{true}} = \ln(1 + e_{\text{eng}})$$

<sup>2</sup> ASTM International, *Fasteners; Rolling Element Bearings*, Section 1, Volume 01.08, 2003

<sup>3</sup> W. Johnson, P. B. Mellor, *Engineering Plasticity*, Halstead Press/Wiley and Sons, New York, 1983.

where  $\sigma_{eng}$  is the engineering stress value, and  $e_{eng}$  is the elongation (as a decimal value, percent divided by 100).

The data for XM-19 at 200 °F from Table 2.12.5-2 is first converted from engineering to true stress-strain and then used to calculate the tangent modulus. First, the true ultimate tensile strength is:

$$S_u = \sigma_{eng}(1 + e_{eng}) = 99,400 \times (1 + 0.35) = 134,190 \text{ psi}$$

where  $\sigma_{eng}$  is 99,400 psi and  $e_{eng}$  is 35.0% elongation<sup>4</sup>. Similarly, the true yield strength is

$$S_y = \sigma_{eng}(1 + e_{eng}) = 47,100 \times (1 + 0.002) = 47,194 \text{ psi}$$

where  $\sigma_{eng}$  is the stress at 0.2% strain of 47,100 psi. The true ultimate strain is:

$$\epsilon_u = \ln(1 + e_{eng}) = \ln(1 + 0.35) = 0.30$$

The tangent modulus for XM-19 at 200 °F is therefore:

$$E_{TAN} = \frac{(S_u - S_y)}{(\epsilon_u - 0.002)} = \frac{(134,190 - 47,194)}{(0.30 - 0.002)} = 291,933 \text{ psi}$$

The data for Type 304 at 200 °F from Table 2.12.5-2 is first converted from engineering to true stress-strain and then used to calculate the tangent modulus. First, the true ultimate tensile strength is:

$$S_u = \sigma_{eng}(1 + e_{eng}) = 71,000 \times (1 + 0.40) = 99,400 \text{ psi}$$

where  $\sigma_{eng}$  is 71,000 psi and  $e_{eng}$  is 40.0% elongation<sup>4</sup>. Similarly, the true yield strength is:

$$S_y = \sigma_{eng}(1 + e_{eng}) = 25,000 \times (1 + 0.002) = 25,050 \text{ psi}$$

where  $\sigma_{eng}$  is the stress at 0.2% strain of 25,000 psi. The true ultimate strain is:

$$\epsilon_u = \ln(1 + e_{eng}) = \ln(1 + 0.40) = 0.34$$

The tangent modulus for Type 304 at 200 °F is therefore:

$$E_{TAN} = \frac{(S_u - S_y)}{(\epsilon_u - 0.002)} = \frac{(99,400 - 25,050)}{(0.34 - 0.002)} = 219,970 \text{ psi}$$

### 2.12.5.5 FCS Stress Criteria

The stress criteria used for the analyses herein are fully presented in Section 2.1.2, *Design Criteria*, and are summarized in Table 2.12.5-3. The FCS is a criticality control structure component that is only required for HAC. Therefore, a combination of plastic and elastic analysis techniques from ASME Appendix F<sup>5</sup> is utilized. The only sections that will use acceptance criteria from elastic

<sup>4</sup> American Society of Mechanical Engineers (ASME) Boiler and Pressure Vessel Code, Section II, *Materials*, Part A, *Properties*, 2001 Edition with 2002 and 2003 Addenda.

<sup>5</sup> American Society of Mechanical Engineers (ASME) Boiler and Pressure Vessel Code, Section III, *Rules for Construction of Nuclear Power Plant Components*, 2001 Edition with 2002 and 2003 addenda.

analysis are those related to the pinned connections in accordance with Appendix F, Section F-1336. All other evaluations utilize the plastic analysis acceptance criteria.

### 2.12.5.6 FCS Stability Criteria

The function of the strongback is to maintain the position of the neutron poison plates between the regions of "active" fuel. The structure is acceptable, provided global stability is maintained. HAC free drop loads and HAC criteria are used in this stability demonstration.

### 2.12.5.7 FCS Vertically Loaded Fuel Load Determination

This calculation evaluates the loads applied to the FCS during a near-vertical free drop in which the fuel rods buckle. The loads on the FCS are normal to the longitudinal axis and FCS panels, and are caused by restraining the lateral displacement of the fuel rods. The geometry and related data needed for this determination is given in Table 2.12.5-1. Since the fuel is in a  $17 \times 17$  array with a 0.496-inch pitch and a single rod diameter of 0.374 inches, the bounds of the array are  $16(0.496) + 0.374 = 8.31$  inches. The clearance between the FCS and the fuel rods is therefore  $0.5(8.70 - 8.31) = 0.2$  inches. Some deflection of the FCS is expected to occur under loading from the fuel rods. Therefore, for purposes of calculation, the total clearance is increased by 0.05 inches to a total of 0.25 inches, to account for the full possible range of movement of the rods. This value bounds the worst-case calculated FCS deflections as shown in Figure 2.12.5-15. The buckling magnitude and buckling forces are the greatest in the space between clamp arms (hereafter called 'bay') which is nearest to the ground. The one long bay (length equal to 24.13 inches) is not governing, since the force applied by the fuel rods is proportional to the angle of deformation, and the angle is smaller in the longer bay than in the shorter ones. Thus, for analysis purposes, the free length of the rods is equal to the shorter distance between clamp arms of 20.5 inches.

The following assumptions govern this evaluation:

- The action of each fuel rod under the applied loading is Euler buckling caused by self weight under the impact loading. The resulting lateral deflection of the rods brings them into contact with the FCS, the strongback core, and with each other.
- Conservatively, all rods buckle in the same direction within a bay, and in opposite directions in adjacent bays. For example, if the rods deflect towards the FCS in the lowest bay, they deflect towards the strongback core in the next bay above it.
- Conservatively, those rods which are in contact stack up in perfect columns behind each other such that rod forces accumulate without loss. This assumption is conservative, since, as seen in Figure 2.12.5-2, the planes of deformation of the rods are not all perfectly parallel, and the rods, which are smooth, actually tend to slip past each other with only partial transfer of the lateral buckling load.
- The grid structures serve as points of inflection for the deflected rods. As shown in Figure 2.12.5-2 and in Figure 2.12.3-20, the spacing distances in the grid remain essentially unchanged. Also, it is noted that there is essentially no bending (and therefore zero moment) in the grids. Thus, the grids supply lateral support for the rods, but no moment support. Also, no axial friction support is assumed.

Since each rod deforms in a sine shape with inflection points at the grids, the deflection distance of any rod to the left and to the right is equal. In other words, the leftward deflection in the upper bay shown in Figure 2.12.5-3 is equal to the rightward deflection of the same rod in the lower bay. Given this fact, the magnitude of rod deflection is controlled by the first point of contact above or below the grid, whichever occurs first. For example (referring to Figure 2.12.5-3), row 1 deflects the least because it contacts the FCS after deflection through a distance equal to the gap of 0.25 inches between the rods and the FCS. Similarly, row 17 deflects the same amount, since it contacts the strongback core after deflecting through 0.25 inches in the adjacent bay. Note that the rods could deflect in the opposite direction, in which case the roles of the FCS and strongback core would be reversed in the above statements. Regardless of direction, the fuel has the strongback on one side and the FCS on the other. Other rows deflect through greater distances, owing to the clearance gaps between the rod rows. For example, the deflection of rows 2 and 16 is greater than for rows 1 and 17; the deflection of rows 3 and 15 is greater still; rows 4 and 14 greater still, and so on. The center row, row 9, deflects the most, and is the only row to contact other rods both above and below the grid.

Figure 2.12.5-4 depicts the free body diagram of a rod in a typical row (number 1 to 8) on the left of the figure, and a free body diagram of a rod in the central row (no. 9), on the right. Since rows 10 – 17 load the strongback core, they are not considered in this analysis.

For the general case, as discussed above, the segment is deflected equally at the top and bottom by the amount  $x_i$ . The force  $F_i$  represents the contact force of rod  $i$  with the rod to its left, or in the case where  $i = 1$ , with the FCS. The force  $F_{Gi}$  represents the force supplied by the grid in maintaining the row spacing. The force  $P$  is the buckling force along the rod axis, and the moment  $M_i$  is the bending moment in the rod. A free body diagram for a smaller segment is shown in the lower left of the figure. By symmetry, only half of the total contact force  $F_i$  is applied to the free body detail figure. Summing moments about the lower end, clockwise positive,

$$P(2x_i) - F_{Gi} \frac{L}{2} - 2M_i = 0$$

from which:

$$F_{Gi} = \frac{4(Px_i - M_i)}{L}$$

Summing forces in the horizontal direction, positive to the right, readily shows that  $F_i = 2F_{Gi}$ , so that the contact force is:

$$F_i = \frac{8(Px_i - M_i)}{L}$$

For the case of a rod in row 9, again summing moments about the lower end, clockwise positive,

$$P(2x_9) - \frac{1}{2}F_9L - 2M_9 = 0$$

By symmetry, the grid force is zero. The rod force is:

$$F_9 = \frac{4(Px_9 - M_9)}{L}$$

Before computing the rod forces, the parameters  $P$ ,  $x_i$ , and  $M_i$  must be evaluated. In the following, any needed fuel assembly or cladding parameters are taken from Table 2.12.5-1.

The buckling force P, axial to the rod, is simply:

$$P = W_e g$$

where  $W_e$  is the effective weight of the rod, and  $g$  is the impact, which is bounded by 120 g. The weight of the rod which is above the bay where maximum buckling occurs is fully effective. The weight of the rod in the bay of interest is only 1/3 effective<sup>6</sup>. Since the rod is 152.4 inches long, and the length of the bay is  $L = 20.5$  inches, the total effective weight of the rod is:

$$W_e = \left[ \frac{(152.4 - 20.5)}{152.4} + \frac{20.5}{152.4} \left( \frac{1}{3} \right) \right] \times 5.33 = 4.85 \text{ lb}_f$$

where the weight of the entire rod is 5.33 lb<sub>f</sub>. For purposes of analysis, the weight  $W_e$  will be applied in a lumped manner above the bay of interest. Note that  $W_e$  equals 91% of the total rod weight. The load P is therefore equal to  $4.85 \times 120 = 582$  lb<sub>f</sub> per rod.

The lateral deflections of the rods are:

$$x_i = C + (i - 1)G_r$$

where the clearance between the surface row (i.e., row 1) and the FCS is  $C = 0.25$  inches, and the gap between rows,  $G_r = 0.496 - 0.374 = 0.122$  inches, where 0.496 inches is the row pitch, and 0.374 inches is the rod diameter. Parameter  $i$  is the row number. For example, for the third row ( $i = 3$ ):

$$x_3 = 0.250 + (3 - 1)0.122 = 0.494 \text{ inches}$$

The moment in the rod,  $M_i$ , can be evaluated from the common expression:

$$M = EI \frac{d^2 y}{dx^2}$$

where, for consistency with the nomenclature of most references,  $y$  is the lateral deflection of the rod, and  $x$  is the axial position along the rod, equal to zero at a point of inflection (in this case, at a grid). Since the equation of the elastic curve of an Euler column<sup>7</sup> is:

$$y = A \sin \pi \frac{x}{L}$$

where  $A$  is the maximum lateral deflection, and  $L$  is the length of one half-wave, then the second derivative of the deflection,  $y$ , is:

$$\frac{d^2 y}{dx^2} = \left( \frac{\pi}{L} \right)^2 A \sin \pi \frac{x}{L}$$

and the maximum value, when  $x = L/2$ , is:

$$\frac{d^2 y}{dx^2}_{\text{MAX}} = \left( \frac{\pi}{L} \right)^2 A$$

<sup>6</sup> This is by analogy to the case of a longitudinally vibrating rod with a mass at the free end. The solution to the vibration problem may be carried out assuming that 1/3 of the distributed mass of the rod is lumped in with the end mass. See Harris, Cyril M., *Shock and Vibration Handbook*, Third Edition, McGraw-Hill, 1988, Table 7.2.

<sup>7</sup> Beer, Ferdinand P., and Johnson, E. Russell Jr., *Mechanics of Materials*, McGraw-Hill, 1981.

The moment in the rod is then:

$$M_{MAX} = EI \frac{d^2y}{dx^2}_{MAX} = EI \left( \frac{\pi}{L} \right)^2 A$$

However, this elastic moment is limited by the plastic hinge moment, which can be found from the product of the shape factor and the yield moment. The shape factor<sup>8</sup>, SF, is:

$$SF = 1.698 \frac{R^4 - R_i^3 R}{R^4 - R_i^4} = 1.351$$

where the rod outer diameter,  $R = 0.374/2 = 0.187$  inches, and the inner diameter,  $R_i = R - t = 0.1645$  inches, where the wall thickness  $t = 0.0225$  inches. The moment of inertia of the rod is:

$$I = \frac{\pi}{4} (R^4 - R_i^4) = 3.853(10^{-4}) \text{ in}^4$$

The yield strength of the rod cladding material at a bounding temperature of 200 °F is  $S_y = 31,222$  psi. The bending moment for first yield of the cladding material is therefore:

$$M_y = \frac{S_y I}{R} = 64.3 \text{ in-lb}$$

Consequently the plastic hinge moment is:

$$M_p = (SF)M_y = 86.9 \text{ in-lb}$$

Since the elastic modulus,  $E$ , of the cladding material is  $12.8(10^6)$  psi at 200 °F, the rod moment is equal to:

$$M_i = EI \left( \frac{\pi}{L} \right)^2 A = 115.8x_i \text{ in-lb}, \leq 86.9 \text{ in-lb}$$

where  $x_i$ , substituted for  $A$ , is the maximum deflection of any rod from its neutral position, and  $L$  equals 20.5 inches.

The total force applied to the FCS can now be determined. The force of an individual rod is equal to  $F_i$  above. The total force of that row is equal to  $F_i$  multiplied times the number of active rods in the row (see Figure 2.12.5-1). Some rows have up to five inactive spaces (empty guide tubes) which, due to their stiffer cross section and low weight loading (tributary weight of one nozzle of less than one pound each), do not need to be included in the loading calculation. Finally, the total force is the sum of the force contributions of each row. The calculations are detailed in Table 2.12.5-4. Thus, the maximum force applied to the FCS from the buckled fuel rods is 17,452 pounds.

### **2.12.5.8 FCS Horizontal Fuel Load Determination**

This section considers the loads applied to the FCS during a horizontal HAC free drop (including the secondary impact of a slapdown orientation). The loads on the FCS are normal to the fuel rod axis and FCS panels, and are the result of the fuel rod lateral displacements. The geometry

<sup>8</sup>Young, Warren C., *Roark's Formulas for Stress and Strain*, Sixth Edition, McGraw-Hill, 1989, Table 1, Case 15.

relevant to the determination of the fuel load on the FCS is free span between clamp arms. With exception to the bottom most set of clamp arms, the center-to-center distance is 20.50 inches. The bottom set has a center-to-center distance of 24.13 inches. The clamp pads are 2.25 inches wide.

Each fuel rod weighs 5.3 pounds and is 152.4 inches long. The unit weight of fuel rod is therefore  $5.3/152.4 = 0.035$  lb<sub>f</sub>/inch. The horizontal drop load is determined assuming the fuel rods load both the clamp arms and FCS channel. The fuel rod load tributary to the FCS channel is simply determined by multiplying the unit weight of the fuel rod by the tributary length of fuel rod. For the bottom set of FCSs, the tributary length is  $(24.13-2.25)/2 = 10.94$  inches, assuming the FCS channel share the load equally with the clamp arms. There are 264 fuel rods per fuel assembly. Therefore, the maximum load which may be applied to the FCS channel supports at 1g of acceleration is:  $0.035(10.94)(264) = 101.1$  pounds. For the 180 g horizontal acceleration, the horizontal load on the FCS attributed to a single fuel assembly is 18,198 pounds; however 19,000 pounds will conservatively be used.

### 2.12.5.9 Evaluation Assumptions and Methodology

ANSYS® Version 8.0 and Version 8.1 were utilized to perform finite element analysis on the FCS for the load cases stated in Section 2.12.5.2, *Conditions Analyzed*. The model includes the full geometry of each item, excluding clearance chamfers, and pin and bolt holes. Stresses for the pin hole sections are calculated manually in Section 2.12.5.19, *Evaluation of Strongback Response to FCS Loads*, using reaction forces extracted from the FEA runs. The FEA model uses coupled coincident nodes in the bolt locations. The component forces are collected at these locations and used to determine the bolt stresses in Section 2.12.5.12, *Fastener Analysis*.

The MOX strongback utilizes seven fuel control structures per fuel assembly. Therefore, there are a total of twenty one per strongback. Each FCS spans the length between two adjacent strongback clamp arms. The typical FCS span is 20.50 inches. The span between the bottom strongback endplate and adjacent clamp arm is 24.13 inches. The clamp pads are 2.25 inches wide. The bottom three FCSs are identical to the typical span versions, except the angle and neutron poison is slightly longer. The finite element analysis (FEA) model is adjusted to have a mass equivalent to that of the longer FCS, bounding stresses with respect to the vertical acceleration.

The fuel load determined in Section 2.12.5.7, *FCS Vertically Loaded Fuel Load Determination*, and Section 2.12.5.8, *FCS Horizontally Loaded Fuel Load Determination*, are applied as a pressure to the angle in the region backed by the stiffener. The maximum NCT hot temperature for the strongback structure, as determined in Section 3.4, *Thermal Evaluation for Normal Conditions of Transport*, is 178 °F. The structural evaluation of the FCS conservatively uses 200 °F. The stress acceptance criteria are determined using mechanical properties summarized in Table 2.12.5-2.

The model consists of SOLID45 3-D structural 4-node solid elements with CONTAC49 3-D point-to-surface contact elements between the primary bolted surfaces. Friction between the bolted surfaces is conservatively ignored. The material properties correspond to 200 °F and the tangent moduli for XM-19 and Type 304 used in the FEA model are calculated in Section 2.12.5.4 as 291,933 psi and 219,970 psi, respectively. Corresponding runs were made for load cases 1 through 3 with the tangent moduli set at 5% of the Modulus of Elasticity (i.e., 1,380,000 psi).

Table 2.12.5-5 provides summary results for comparison between the lower and higher tangent moduli. Results for the lower tangent moduli are taken from Table 2.12.5-7. The maximum

plastic strain is low (less than 3%) and the difference in plastic strain between the lower and higher tangent moduli is negligible. Stresses for both lower and higher tangent moduli runs are approximately the same, with only more redistribution of stress in the lower tangent modulus runs. The lower tangent modulus runs had slightly more net displacement or deflection as expected. Therefore, the lower tangent moduli calculated in Section 2.12.5.4 are considered conservative as the stresses are minimally affected and displacements are larger. Using the lower tangent moduli provides a more conservative evaluation of the FCS stability.

The FEA model has an approximately 0.31 inch longer channel on the hinge block side than the actual design. The hinge block side channel is a symmetry copy of the pin block side channel for model generation. The minor additional length is considered negligible in regard to the reaction loads and bounding with respect to weight and stresses. The bending stresses in the channel will be conservative because the load is applied over a slightly longer unsupported span. The pin block side of the channel is approximately 0.16 inches shorter than shown on the General Arrangement Drawing 99008-34. This difference is less than 2%, which is not significant considering the margins of safety shown in Table 2.12.5-6 and Table 2.12.5-7. The bending stress increases linearly with a set load and an increase in length. Therefore, the channel stress would increase by less than 2%, which is not a significant impact considering the lowest margin of safety for this part is 0.59.

The fuel lateral load is 17,452 pounds, however 18,000 pounds is conservatively used in load cases 1-3. The load is applied as a pressure to the angle in the region backed by the channel. This method is based on test results collected during certification testing. A prototypic fuel assembly was shown to undergo first mode Euler buckling, where it displaced perpendicular to its axis at the center of the span between clamp arms, see Figure 2.12.3-22 of Appendix 2.12.3, *Certification Test Results*.

#### 2.12.5.10 FCS Finite Element Analysis (FEA)

Each component of the FCS is evaluated in the FEA model for general primary membrane stress intensity ( $P_m$ ) and maximum primary membrane stress intensity ( $P_{max}$ ).  $P_m$  is determined by looking at the stress intensity plots and plotting paths thru sections with high stress. The stress intensity is linearized across the path using the ANSYS® “prsect” and/or “plsect” command.  $P_{max}$  is conservatively taken as the maximum stress intensity from the component plots, which include peak stresses from geometrical discontinuities and local applications of boundary constraints. The plastic analysis acceptance criteria are per Table 2.12.5-3.

Table 2.12.5-6 and Table 2.12.5-7 demonstrate the FCS meets all the plastic analysis acceptance criteria. Margins of safety (MS) greater than or equal to zero are acceptable. Stress and displacement plots of the FEA are provided in Figure 2.12.5-11 through Figure 2.12.5-25, and Figure 2.12.5-36 through Figure 2.12.5-44.

During horizontal drop orientations in which the acceleration vector is primarily normal to the longitudinal axis of the fuel, fuel rod pitch is not of concern, and therefore the FCS geometry is not required to control the reactivity of the fuel. Because the FCS geometry is not required during horizontal drops, the FCS is not evaluated for LC4 (the horizontal load case). However, the connection points on the strongback longitudinal weldment are evaluated for LC4 to show that the side drop loads do not cause failure of non-FCS strongback components.

**FEA Reaction and Bolt Loads**

Contained in Table 2.12.5-8 through Table 2.12.5-11 are the reaction loads from the four analyzed conditions, as reported by the FEA model. Similarly, Table 2.12.5-12 through Table 2.12.5-14 contains the bolt loads from the three analyzed conditions. The reaction loads are used for the pinned connection elastic analysis and the bolt loads are used for the fastener analysis. Node reaction and bolt locations are shown in Figure 2.12.5-10.

**2.12.5.11 Pinned Connection Elastic Analysis**

The pinned sections of the FCS pin and hinge blocks are evaluated elastically according to the criteria in Table 2.12.5-3. The reaction loads from the FEA runs are used as the loads that act over the corresponding pinned section. The lug of the pin block and the bounding center lug of the hinge block are the pinned sections evaluated. The bounding reaction loads both come from Load Case 2 where the pressure load is applied to the hinge block side of the angle. The total reaction force perpendicular to the axis of the fuel assembly is the Square Root of the Sum of the Squares (SRSS) of the x and y direction reactions. The axial, z direction, reactions do not affect the pinned sections. Their related stresses are included in  $P_m$  and  $P_{max}$  in Section 2.12.5.10, *FCS Finite Element Analysis (FEA)*, for the plastic analysis.

The pin and hinge blocks are fabricated from Type XM-19 stainless steel. The stress allowable, based on the stress criteria in Table 2.12.5-3 and the material properties of Type XM-19 at 200 °F are summarized below.

<b>Allowable Stresses</b>	
Shear, $S_\tau$ (psi)	$S_\tau = 0.42S_u = 0.42(99,400) = 41,748$
Bearing, $S_{bearing}$ (psi)	$S_{bearing} = 2.1S_u = 2.1(99,400) = 208,740$
<b>Pin Block Shear (See Figure 2.12.5-8)</b>	
Net shear tear-out area, $A_s$ (in <sup>2</sup> )	$A_s = (\text{min. edge length})(\text{lug length})$ $= (0.22)(1.5) = 0.33$
Bounding reaction load, $P$ (lbf)	$P = 8,898$ (LC2, Table 2.12.5-9)
Shear Stress, $\tau$ (psi)	$\tau = P/2A_s = 8,898/(2(0.33)) = 13,482$
Margin of Safety	$MS = \frac{S_\tau}{\tau} - 1.0 = \frac{41,748}{13,482} - 1.0 = +2.10$
<b>Pin Block Bearing (See Figure 2.12.5-8)</b>	
Projected bearing area, $A_b$ (in <sup>2</sup> )	$A_b = (\text{pin dia})(\text{lug length}) = (0.375)(1.5) = 0.56$
Bounding reaction load, $P$ (lbf)	$P = 8,898$ (LC2, Table 2.12.5-9)
Bearing Stress, $\sigma_b$ (psi)	$\sigma_b = P/A_b = 8,898/0.56 = 15,889$
Margin of Safety	$MS = \frac{S_{bearing}}{\sigma_b} - 1.0 = \frac{208,740}{15,889} - 1.0 = +12.14$

<b>Hinge Block Center Lug Shear Stress</b>	
Net shear tear-out area, $A_s$ (in <sup>2</sup> )	$A_s = (\text{min. edge length})(\text{lug length})$ $= (0.24)(1.5) = 0.36$
Bounding reaction load, $P$ (lb <sub>f</sub> )	$P = 7,590$ (LC2, Table 2.12.5-9)
Shear Stress, $\tau$ (psi)	$\tau = P/2A_s = 7,590/(2(0.36)) = 10,542$
Margin of Safety	$MS = \frac{S_\tau}{\tau} - 1.0 = \frac{41,748}{10,542} - 1.0 = +2.96$
<b>Hinge Block Center Lug Bearing Stress</b>	
Projected bearing area, $A_b$ (in <sup>2</sup> )	$A_b = (\text{pin dia})(\text{lug length}) = (0.375)(1.5) = 0.56$
Bounding reaction load, $P$ (lb <sub>f</sub> )	$P = 7,590$ (LC2, Table 2.12.5-9)
Bearing Stress, $\sigma_b$ (psi)	$\sigma_b = P/A_b = 7,590/0.56 = 13,554$
Margin of Safety	$MS = \frac{S_{\text{bearing}}}{\sigma_b} - 1.0 = \frac{208,740}{13,554} - 1.0 = +14.40$
<b>Hinge Block Outer Lug Shear Stress (See Figure 2.12.5-8)</b>	
Net shear tear-out area, $A_s$ (in <sup>2</sup> )	$A_s = (\text{min. edge length})(\text{lug length})$ $= (0.24)(1.0) = 0.24$
Bounding reaction load, $P$ (lb <sub>f</sub> )	$P = 4,377$ (LC1, Table 2.12.5-8)
Shear Stress, $\tau$ (psi)	$\tau = P/2A_s = 4,377/[2(0.24)] = 9,119$
Margin of Safety	$MS = \frac{S_\tau}{\tau} - 1.0 = \frac{41,748}{9,119} - 1.0 = +3.58$
<b>Hinge Block Outer Lug Bearing Stress</b>	
Projected bearing area, $A_b$ (in <sup>2</sup> )	$A_b = (\text{pin dia})(\text{lug length}) = (0.375)(1.0) = 0.38$
Bounding reaction load, $P$ (lb <sub>f</sub> )	$P = 4,377$ (LC1, Table 2.12.5-8)
Bearing Stress, $\sigma_b$ (psi)	$\sigma_b = P/A_b = 4,377/0.38 = 11,518$
Margin of Safety	$MS = \frac{S_{\text{bearing}}}{\sigma_b} - 1.0 = \frac{208,740}{11,518} - 1.0 = +17.12$

**Quick-Release Pin Shear Load:**

The quick-release pins used in conjunction with the FCS and strongback are Avibank (or equivalent) 3/8-inch diameter quick-release pins. The body and spindle are fabricated from corrosion resistant 17-4PH or PH15-7MO material. The calculated double shear strength per the manufacturer for this quick-release pin is 20,600 pounds.

Bounding reaction load (lb<sub>f</sub>):  $P = 5,078$  (LC2, Table 2.12.5-9) (single shear)

Allowable Load (lb <sub>f</sub> ):	$P_{\text{allow-DS}} = 20,600$	(double shear)
	$P_{\text{allow-SS}} = 20,600/2 = 10,300$	(single shear)
Margin of Safety:	$MS = \frac{P_{\text{allow-SS}}}{P} - 1.0 = \frac{10,300}{5,078} - 1.0 = +1.03$	

**Quick Release Pin Bearing Stress:**

Projected bearing area (in <sup>2</sup> ):	$A_b = (\text{pin dia})(\text{lug length}) = (0.375)(1.5) = 0.56 \text{ in}^2$
Bounding reaction load (lb <sub>f</sub> ):	$P = 8,898$ (LC2, Table 2.12.5-9)
Bearing Stress (psi):	$\sigma_b = P/A_b = 8,898/0.56 = 15,889$
Allowable Stress (psi):	$S_{\text{bearing}} = 2.1S_u = 2.1(140,000) = 294,000$
Margin of Safety:	$MS = \frac{S_{\text{bearing}}}{\sigma_b} - 1.0 = \frac{294,000}{15,889} - 1.0 = +17.50$

**2.12.5.12 Fastener Analysis**

The welded hinge block/pin block/stiffener assembly is secured to the box angle with socket head screws, see Figure 2.12.5-9. The maximum tensile and shear loads are extracted from the FEA runs and used to check the screw stresses in accordance with Table 2.12.5-3.

The fasteners material is A574. The stress allowable, based on the stress criteria in Table 2.12.5-3 and the material properties of A574 at 200°F are summarized below.

<b>Allowable Stresses</b>	
Tensile, $F_{tb}$ (psi)	$0.7S_u = 0.7(180,000) = 126,000$
Shear, $F_{vb}$ (psi)	$0.42S_u = 0.42(180,000) = 75,600$
Bearing, $S_{\text{bearing}}$ (psi)	$2.1S_u = 2.1(99,400) = 208,740$
<b>Screw Tensile Stress</b>	
Net tensile area, $A_t$ (in <sup>2</sup> )	$A_t = 0.0364$ (1/4-28 UNF Table 8-2 <sup>9</sup> )
Bounding tensile load, $P$ (lb <sub>f</sub> )	$P = 240$ (LC1, Table 2.12.5-12)
Tensile Stress, $f_t$ (psi)	$f_t = P/A_t = 240/0.0364 = 6,593$
Margin of Safety	$MS = \frac{F_{tb}}{f_t} - 1.0 = \frac{126,000}{6,593} - 1.0 = +18.11$

<sup>9</sup> Shigley, J. E., Mischke, C. R., *Mechanical Engineering Design*, Fifth Edition, McGraw-Hill, 1989, New York, NY.

<b>Screw Shear Stress</b>	
Net shear area, $A_s$ (in <sup>2</sup> )	$A_s = 0.0326$ (1/4-28 UNF Table 8-2 <sup>8</sup> )
Bounding reaction load, $P$ (lb <sub>f</sub> )	$P = 2,204$ (LC1, Table 2.12.5-12)
Shear Stress, $f_v$ (psi)	$f_v = P / A_s = 2,204 / 0.0326 = 67,607$
Margin of Safety	$MS = \frac{F_{vb}}{f_v} - 1.0 = \frac{75,600}{67,607} - 1.0 = +0.12$
<b>Bolt Tensile and Shear Stress Combination</b>	
Bolt Tension + Shear Stress	$f_t^2/F_{tb}^2 + f_v^2/F_{vb}^2 \leq 1$
	$(6,593)^2/(126,000)^2 + (67,607)^2/(75,600)^2 = 0.80 < 1$
<b>Allowable Stress</b>	
The strongback longitudinal plate material is Type 304 stainless steel. The allowable stress, based on the stress criteria in Table 2.12.5-3 and the material properties of Type 304 at 200 °F, are summarized below.	
Ultimate Stress, $S_u$ (psi)	71,000
Shear, $S_\tau$ (psi)	$0.42S_u = 0.42(71,000) = 29,820$
<b>Minimum Edge Distance Check</b>	
The minimum edge distance calculated is for the maximum square root, sum of the squares (SRSS) load from the screws near the edge of the angle.	
Projected screw angle area, $A_p$ (in <sup>2</sup> )	$A_p = (\text{screw head mean diameter})(\text{angle thickness})$ $= \frac{1}{2}(0.480 + 0.25)(0.125) = 0.37(0.125) = 0.046$
Bounding reaction load, $P$ (lb <sub>f</sub> )	$P = 1,380$ (LC1, Table 2.12.5-12)
Projected Area Stress, $f_p$ (psi)	$f_p = P/A_p = 1,380/0.046 = 30,000$
Min. Angle Bolt Edge Distance	$L/d \geq [0.5 + 1.2(f_p/S_u)]$ $0.50/0.37 \geq [0.50 + 1.2(35,935/71,000)] \Rightarrow 1.35 \geq 1.01$
	$f_p/S_u \leq 2.1 \Rightarrow 30,000/71,000 \leq 2.1 \Rightarrow 0.42 < 2.1$
<b>Tensile Pull-Out Shear Stress</b>	
The angle is evaluated for tensile pull-out of the countersunk SHCS. The shear area of the angle is assumed to be the cylindrical area under the maximum countersunk head diameter (see Figure 2.12.5-9).	
Net axial shear area, $A_s$ (in <sup>2</sup> )	$A_s = \pi(t)(\text{head diameter}) = \pi(0.125)(0.480) = 0.188$
Bounding reaction load, $P$ (lb <sub>f</sub> )	$P = 240$ (LC1, Table 2.12.5-12)
Shear Stress, $\tau$ (psi)	$\tau = P/A_s = 240/0.188 = 1,277$
Margin of Safety	$MS = \frac{S_\tau}{\tau} - 1.0 = \frac{29,820}{1,277} - 1.0 = +22.35$

**2.12.5.13 Lock Plate and Hinge Mounting Brackets**

The lock plate and two hinge mounting brackets are reciprocal XM-19 components to the pin and hinge blocks that are bolted directly to the strongback angle plates. The lock plate is bolted near the outer edge of the strongback angle plate and is the component that the FCS pin block is pinned to. There are two identical hinge mounting brackets, for one FCS, that bolt to the strongback angle plate near the triangular core. The FCS hinge block is pinned to the hinge mounting brackets. See Figure 2.12.5-5 for the global orientation and coordinate system. Figure 2.12.5-27 and Figure 2.12.5-28 illustrate the details and coordinate systems for the lock plate and hinge mounting bracket evaluations. The coordinate systems in Figure 2.12.5-27 and Figure 2.12.5-28, correspond to that in Figure 2.12.5-5 and the FEA analysis.

**2.12.5.13.1 Pinned Connection Elastic Analysis**

The pinned sections of the lock plate and hinge mounting bracket are evaluated similarly to the pin and hinge blocks in Section 2.12.5.11, *Pinned Connection Elastic Analysis*. The stress criteria used are for elastic analysis from Table 2.12.5-3. The reaction loads from the FEA runs are used as the loads that act over the corresponding pinned section. The bounding reaction loads both come from Load Case 2 where the pressure load is applied to the hinge block side of the angle.

The pin and hinge blocks are fabricated from Type XM-19 stainless steel. The stress allowable, based on the stress criteria in Table 2.12.5-3 and the material properties of Type XM-19 at 200 °F are summarized below.

<b>Allowable Stress</b>	
Shear, $S_\tau$ (psi)	$0.42S_u = 0.42(99,400) = 41,748$
Bearing, $S_{bearing}$ (psi)	$2.1S_u = 2.1(99,400) = 208,740$
<b>Lock Plate Shear Tear-Out</b>	
Net shear tear-out area, $A_s$ (in <sup>2</sup> )	$A_s = (\text{min edge length})(\text{lug no})(\text{lug width} - \text{chamfer})$ $= (0.24)2(0.59 - 0.13) = 0.22$
Bounding reaction load, $P$ (lb <sub>f</sub> )	$P = 8,898$ (LC1, Table 2.12.5-8)
Shear Stress, $\tau$ (psi)	$\tau = \frac{P}{2A_s} = \frac{8,898}{2(0.22)} = 20,223$
Margin of Safety	$MS = \frac{S_\tau}{\tau} - 1.0 = \frac{41,748}{20,223} - 1.0 = +1.06$
<b>Lock Plate Axial Shear</b>	
The axial shear is evaluated for the lock plate, because it is not included in the FEA and the lug width and shear area are smaller than any of the other pinned components. The bounding axial load is from LC 1.	
Net axial shear area, $A$ (in <sup>2</sup> )	$A = (\text{lug width})(\text{plate thickness}) = (0.59)(0.67) = 0.40$
Bounding reaction load, $P$ (lb <sub>f</sub> )	$P = 1,126$ (LC2, Table 2.12.5-9)
Shear Stress, $\tau$ (psi)	$\tau = \frac{P}{A} = \frac{1,126}{0.40} = 2,815$

Margin of Safety	$MS = \frac{S_{\tau}}{\tau} - 1.0 = \frac{41,748}{2,815} - 1.0 = +13.83$
<b>Lock Plate Bearing</b>	
Projected bearing area, $A_b$ (in <sup>2</sup> )	$A_b = (\text{pin dia})(\text{lug no})(\text{lug width}) = (0.375)(2)(0.59) = 0.44$
Bounding reaction load, P (lb <sub>f</sub> )	$P = 8,898$ (LC2, Table 2.12.5-9)
Bearing Stress, $\sigma_b$ (psi)	$\sigma_b = \frac{P}{A_b} = \frac{8,898}{0.44} = 20,223$
Margin of Safety	$MS = \frac{S_{\text{bearing}}}{\sigma_b} - 1.0 = \frac{208,062}{20,223} - 1.0 = +9.32$
<b>Hinge Mounting Bracket Axial Shear</b>	
The axial shear is evaluated for the hinge mounting bracket, because it is not included in the FEA analysis. The bounding axial load is from Load Case 1.	
Net shear area, A (in <sup>2</sup> )	$A = (\text{lug width})(\text{plate thickness}) = (2.44)(0.69) = 1.68$
Bounding reaction load, P (lb <sub>f</sub> )	$P = 1,974$ (LC1, Table 2.12.5-8)
Shear Stress, $\tau$ (psi)	$\tau = \frac{P}{A} = \frac{1,974}{1.68} = 1,175$
Margin of Safety	$MS = \frac{S_{\tau}}{\tau} - 1.0 = \frac{41,748}{1,175} - 1.0 = +34.53$
<b>Hinge Mounting Bracket Shear</b>	
Net shear tear-out area, $A_s$ (in <sup>2</sup> )	$A_s = (\text{min edge length})(\text{width})$ $= (0.24)(2.44 - 2(0.13)) = 0.52$
Bounding reaction load, P (lb <sub>f</sub> )	$P = 7,325$ (LC2, Table 2.12.5-9)
Shear Stress, $\tau$ (psi)	$\tau = \frac{P}{2A_s} = \frac{7,325}{2(0.52)} = 7,043$
Margin of Safety	$MS = \frac{S_{\tau}}{\tau} - 1.0 = \frac{41,748}{7,043} - 1.0 = +4.93$
<b>Hinge Mounting Bracket Bearing</b>	
Projected bearing area, $A_b$ (in <sup>2</sup> )	$A_b = (\text{pin dia})(\text{lug width}) = (0.375)(2.44) = 0.92$
Bounding reaction load, P (lb <sub>f</sub> )	$P = 7,325$ (LC2, Table 2.12.5-9)
Bearing Stress, $\sigma_b$ (psi)	$\sigma_b = \frac{P}{A_b} = \frac{7,325}{0.92} = 7,962$
Margin of Safety	$MS = \frac{S_{\text{bearing}}}{\sigma_b} - 1.0 = \frac{208,062}{7,962} - 1.0 = +25.22$

**2.12.5.13.2 Fastener Analysis**

**Lock Plate Fasteners**

The lock plate is used with the pin block and lock pin to hold the FCS in a closed position. The lock plate is fastened to the strongback angle plate with three, 3/8 – 16 UNC countersunk socket head cap screws (SHCS),  $A_t = .078 \text{ in}^2$ , in a triangular pattern as shown in Figure 2.12.5-27. The fastener loads and stresses are determined as follows.

The FEA analysis of the FCS calculates reaction loads at the lock pin. These reaction loads are applied to the lock plate to determine the loads on the lock plate fasteners. The three loads are  $F_x$  (out of the plane of the lock plate, creating tensile fastener loads from prying), and  $F_y$  and  $F_z$  (in plane, creating shear loads). The shear loads arise from direct shear loading as well as from a torsional moment created by the axial acceleration.

The parameters affecting the load calculations, as depicted on Figure 2.12.5-26 and Figure 2.12.5-27, are (inches):

$$y_{\text{bar}} = \frac{2 \times A_t \times L_3}{3 \times A_t} = \frac{2 \times 0.078 \times 0.62}{3 \times 0.078} = 0.41 \quad \text{fastener group centroid to the single fastener}$$

$$r = \sqrt{\left(\frac{w_1}{2}\right)^2 + (L_3 - y_{\text{bar}})^2}$$

= 0.78 fastener group centroid to one of the fasteners in the two-fastener row

$L_1 = 0.46$  lock pin center to pivot edge

$L_2 = 0.73$  pivot edge to single fastener

$L_3 = 0.62$  single fastener row to two-fastener row

$w_1 = 1.5$  width between fasteners in two-fastener row

The total tensile load on the fastener group from prying about the strongback edge is:

$$F_{\text{yg}} = F_x \frac{-L_1}{L_2 + y_{\text{bar}}}$$

The tensile load per fastener is:

$$F_{\text{xb}} = F_{\text{yg}}/3$$

The direct shear load per fastener in the y-direction is:

$$F_{\text{yb}} = F_y/3$$

The direct shear load per fastener in the z-direction is:

$$F_{\text{zb}} = F_z/3$$

The shear force per fastener from the torsional moment about the x-axis is:

$$F' = -F_z \frac{L_1 + L_2 + y_{\text{bar}}}{3 \times y_{\text{bar}}}$$

The total shear,  $f_v$ , is the square root sum of the squares for the worst fastener, which is the front single fastener:

$$f_v = \sqrt{(F_{yb} + F'_y)^2 + (F_{ab} + F'_z)^2}$$

where  $F'$  is orthogonal to the bolt moment arm and may be decomposed into the coordinate system for combination. The total tensile load per fastener is  $f_t = F_{xb}$ . The tensile stress is  $\sigma = f_t/A_t$  and the shear stress is  $\tau = f_v/A_s$ , where the tensile stress area,  $A_t = 0.078 \text{ in}^2$ , and the shear stress area,  $A_s = 0.068 \text{ in}^2$ , from Shigley<sup>10</sup>, Table 8.2. The margin of safety and interaction equations are calculated using the same allowable stresses and methods as in Section 2.12.5.12, *Fastener Analysis*. The results are given in Table 2.12.5-15. As shown, all of the lock plate fastener stresses are acceptable.

### Hinge Mounting Bracket Fasteners

The top and bottom hinge mounting brackets are each bolted to the strongback angle plate with four 3/8–16UNC countersunk socket screws in a square pattern. The bolt loads and stresses for each load case are calculated using an excel spreadsheet, summarized in Table 2.12.5-16. All of the hinge mounting block bolt stresses are acceptable. The method and design information for finding the loads and stresses are as follows.

The reaction loads for the hinge block from the FEA runs are used (as equal and opposite) for the loads applied to the hinge mounting brackets. However, the reaction loads are first rotated thirty degrees to be perpendicular and parallel with the surface of the hinge mounting brackets. In Figure 2.12.5-5, the hinge mounting bracket (pinned to the hinge block) is at angle with the coordinate system. The strongback triangular core is an equilateral triangle, which has internal angles of sixty degrees. The attached angle plate has a ninety degree bend, therefore the hinge mounting brackets are at an angle of thirty degrees with the x-axis in Figure 2.12.5-5. The rotated x and y loads are in Table 2.12.5-16 as  $F_{rx}$  and  $F_{ryt}$ . The hinge mounting brackets are supported by the strongback. The hinge mounting brackets are assumed to pivot about their back edge against the strongback angle plate creating tensile “prying” loads on the bolts. The bolts are also subjected to shear stresses in the two orthogonal directions perpendicular to the tensile load. The shear loads come directly from in-plane loads and a torsional moment created by the axial acceleration.

The parameters affecting the load calculations, as depicted on Figure 2.12.5-28 and Figure 2.12.5-29, are (inches):

w = 2.44	width
l = 3.16	length
b <sub>e</sub> = 0.70	bolt hole edge distance
b <sub>s</sub> = 1.20	bolt hole spread, square
p <sub>e</sub> = 0.44	pin edge distance
b <sub>p</sub> = 0.82	1st row bolt to pin spread
r = 0.85	bolt pattern radius

The total tensile load per bolt from out-of-plane force component and “prying” about the back hinge mounting bracket edge is:

<sup>10</sup> Shigley, J. E., Mischke, C. R., *Mechanical Engineering Design*, Fifth Edition, McGraw-Hill, 1989, New York, NY.

$$f_t = \frac{F_{\text{ryt}} \times (b_p + b_e + b_s)}{4 \times \left( b_e + \frac{b_s}{2} \right)}$$

The total shear,  $f_v$ , is  $F_{\text{ryt}}$  plus torsion about the y-axis from  $F_z$ , combined (SRSS) with for the worst bolt, which is one of the front bolts.

$$f_v = \sqrt{\left( \frac{F_{\text{ryt}}}{4} + \sin(45) \times F_z \times \frac{\left( b_p + \frac{b_s}{2} \right)}{(4 \times r)} \right)^2 + \left( \frac{F_z}{4} + \cos(45) \times F_z \times \frac{\left( b_p + \frac{b_s}{2} \right)}{(4 \times r)} \right)^2}$$

The results are presented in Table 2.12.5-16. In the referenced table, the tensile stress, sigma ( $\sigma$ ), is simply  $f_t/A_t$ . The shear stress, tau ( $\tau$ ), is similarly  $f_v/A_s$ .

**Minimum Edge Distance**

The minimum edge distance calculated is for the single front bolt of the lock plate, which is the bolt nearest to the edge of the strongback angle plate. The load is conservatively assumed to be ‘fv’ from LC 1, Table 2.12.5-15. The load  $f_v$  includes the shear force in the direction of the plate edge combined with the shear force (that is not directed towards the plate edge) from the moment generated by the axial acceleration. See also, Figure 2.12.5-30.

Projected bolt area on angle:  $A_p = (\text{bolt head mean diameter}^{11})(\text{angle plate thickness})$   
 $= 1/2(0.720 + 0.375)(0.25) = 0.55(0.25) = 0.14 \text{ in}^2$   
 $P = 3,343 \text{ lb}_f$  (from Table 2.12.5-15, LC1)

Projected Area Stress:  $f_p = P/A_p = 3,343/0.14 = 23,879 \text{ psi}$

Check Angle Minimum Bolt Edge Distance:

$$L/d \geq [0.5 + 1.2(f_p/S_u)] \Rightarrow 0.73/0.55 \geq [0.5 + 1.2(23,879/71,000)] \Rightarrow 1.33 \geq 0.90$$

$$f_p/S_u \leq 2.1 \Rightarrow 23,879/71,000 \leq 2.1 \Rightarrow 0.34 \leq 2.1$$

**Bolt Pull-Out:**

The strongback angle plate is evaluated for pull-out of the countersunk socket heads. The shear area of the angle plate is assumed to be the cylindrical area under the countersunk head diameter. The maximum tensile bolt load is ‘ft’ from the top bracket, LC1 in Table 2.12.5-16.

Net shear area:  $A_s = \pi(t)(\text{head diameter}) = \pi(0.25)(0.720) = 0.57 \text{ in}^2$

Bounding reaction load:  $P = 3,269 \text{ lb}_f$  (from Table 2.12.5-16, LC1)

Shear Stress:  $\tau = P/A_s = 3,269/0.57 = 5,735 \text{ psi}$

Allowable:  $\tau_{\text{allow}} = 0.42S_u = 0.42(71,000) = 29,820 \text{ psi}$

Margin of Safety:  $MS = (\tau_{\text{allow}} / \tau) - 1.0 = (29,820/5,735) - 1.0 = +4.20$

<sup>11</sup> Industrial Fasteners Institute, *Manufacturers' Capability Guide*, 1986, Cleveland, Ohio

**2.12.5.13.3 Net Section Bending Stress**

The lock plate and hinge mounting brackets are subjected to bending stresses from the “prying” loads discussed in the fastener evaluation, Section 2.12.5.13.2, *Fastener Analysis*. The lock plate moment arm is assumed to be from the pin centerline to the edge of the strongback angle plate. The hinge mounting bracket moment arm is assumed to be from the pin centerline to the first row of bolts. The pin and hinge blocks are fabricated from Type XM-19 stainless steel. The allowable primary-plus-membrane stress ( $S_{m+b}$ ) is  $S_u = 99,400$  psi, based on the elastic analyses stress criteria in Table 2.12.5-3 and the material properties of Type XM-19 stainless steel at 200 °F. The analysis results and the resultant margin of safety (MS) are summarized below.

<b>Lock Plate</b>	
Net section, $I_{net}$ (in <sup>4</sup> )	$I_{net} = ((2 \times \text{lug width})(\text{lug height})^3)/12$ $= ((2 \times 0.59)(0.67)^3)/12 = 0.030$
Maximum load, P (lb <sub>f</sub> )	$P = 8,893$ (LC2, Table 2.12.5-15)
Moment, M (in-lbs)	$M = P \times L = 8,893 \times 0.46 = 4,091$
Bending Stress, $\sigma_b$ (psi)	$\sigma_b = \frac{Mc}{I_{net}} = \frac{4,091 \left( \frac{0.67}{2} \right)}{0.030} = 45,683$
Margin of Safety (MS)	$MS = \frac{S_{m+b}}{\sigma_b} - 1.0 = \frac{99,400}{45,683} - 1.0 = +1.18$
<b>Hinge Mounting Bracket</b>	
Net section, $I_{net}$ (in <sup>4</sup> )	$I_{net} = (\text{width} - 2(\text{hole OD}))[(\text{Height})^3/12]$ $= (2.44 - 2(0.41))[(0.69)^3/12] = 0.044$
Net Area, $A_{net}$ (in <sup>2</sup> )	$A_{net} = (\text{width} - 2(\text{Hole OD}))(\text{Height})$ $= (2.44 - 2(0.41))(0.69) = 1.12$
Maximum load (lb <sub>f</sub> )	$P_y = 6,250$ (LC1, Table 2.12.5-16)
	$P_x = 3,816$ (LC1, Table 2.12.5-16)
Moment, M (in-lbs)	$M = P_y(L) = 6,250(0.82) = 5,125$
Bending Stress, $\sigma_b$ (psi)	$\sigma_b = \frac{Mc}{I_{net}} = \frac{5,125(1/2(0.69))}{0.044} = 40,185$
Membrane Stress, $\sigma_m$ (psi)	$\sigma_m = \frac{P_x}{A_{net}} = \frac{3,816}{1.12} = 3,407$
Membrane + Bending Stress, $\sigma_{b+m}$ (psi)	$\sigma_{b+m} = \sigma_b + \sigma_m = 43,592$
Margin of Safety (MS)	$MS = \frac{S_{m+b}}{\sigma_{b+m}} - 1 = \frac{99,400}{43,592} - 1 = +1.28$

**2.12.5.14 Strongback Global Stability**

The strongback is constrained by the body such that, under axial loads, only very small lateral displacements are possible. Thus, it is not possible for the strongback to undergo a typical "lower order" elastic buckling mode failure. Stability is controlled by plastic stability of the structure. However, the following calculation is included to demonstrate the large margin against global elastic collapse.

The strongback longitudinal weldment ("core") is evaluated for axial stability under loads resulting from a postulated 120g end drop. The core is modeled as a bar with a uniformly distributed axial load with the base fixed and top end free, using closed form solutions from Article 2.12 of Timoshenko<sup>12</sup> (See Equation 'n' on p. 103):

$$(qL)_{CR} = \frac{7.837EI}{L^2}$$

L	Axial length of the core, use 160 inches																		
E	27.6 × 10 <sup>6</sup> psi, Table TM-1 at 200 °F (Table 2.2-2).																		
A	Cross sectional area of the three (3) plate angles which form the primary axial member in the Core.  Calculated as 12.72 in <sup>2</sup> when neglecting the tube stiffeners on the free edges of the plate angles. See Figure 2.12.5-56.  Considering the tube stiffeners, the area is:  A <sub>CORE</sub> = 12.72 in <sup>2</sup> + (3 stiffeners)[(2.0 in) <sup>2</sup> - (1.5 in) <sup>2</sup> ] = 12.72 in <sup>2</sup> + 5.25 in <sup>2</sup> = 17.97 in <sup>2</sup>																		
I	274 in <sup>4</sup> , determined using ANSYS <sup>®</sup> for the three (3) plate angles that form the primary axial member in the core (see Figure 2.12.5-56)																		
q	Unit weight/load of the strongback assembly and payload. From Table 2.1-3, Section 2.1.3, <i>Weights and Centers of Gravity</i> , the weights are ( <b>bold numbers</b> ):  <table style="margin-left: auto; margin-right: auto;"> <thead> <tr> <th></th> <th style="text-align: center;"><u>Weight (pounds)</u></th> </tr> </thead> <tbody> <tr> <td>Top Endplate Assembly</td> <td style="text-align: right;">190</td> </tr> <tr> <td>Bottom Endplate Assembly</td> <td style="text-align: right;">168</td> </tr> <tr> <td>Fuel Control Structures</td> <td style="text-align: right;">855</td> </tr> <tr> <td> Total Strongback (w/o FCS, w/ endplates)</td> <td style="text-align: right;"> 2,175</td> </tr> <tr> <td>Total Strongback (w/ FCS, w/ endplates)</td> <td style="text-align: right;"><b>3,030</b></td> </tr> <tr> <td><u>Payload</u></td> <td style="text-align: right;"><b>4,740</b></td> </tr> <tr> <td>Strongback w/ FCS + Payload</td> <td style="text-align: right;"><b>7,770</b></td> </tr> <tr> <td>Strongback w/o FCS + Payload:</td> <td style="text-align: right;">6,915</td> </tr> </tbody> </table>		<u>Weight (pounds)</u>	Top Endplate Assembly	190	Bottom Endplate Assembly	168	Fuel Control Structures	855	 Total Strongback (w/o FCS, w/ endplates)	 2,175	Total Strongback (w/ FCS, w/ endplates)	<b>3,030</b>	<u>Payload</u>	<b>4,740</b>	Strongback w/ FCS + Payload	<b>7,770</b>	Strongback w/o FCS + Payload:	6,915
	<u>Weight (pounds)</u>																		
Top Endplate Assembly	190																		
Bottom Endplate Assembly	168																		
Fuel Control Structures	855																		
 Total Strongback (w/o FCS, w/ endplates)	 2,175																		
Total Strongback (w/ FCS, w/ endplates)	<b>3,030</b>																		
<u>Payload</u>	<b>4,740</b>																		
Strongback w/ FCS + Payload	<b>7,770</b>																		
Strongback w/o FCS + Payload:	6,915																		

<sup>12</sup> Timoshenko & Gere, *Theory of Elastic Stability*, Second Edition, McGraw-Hill Book Company, New York, 1961.

From the values above, addition of the FCSs increases the total load by  $\approx 12\%$  or the structure load (less payload) by  $\approx 40\%$ . Using the length listed above, and conservatively including the fuel/payload weight, the (maximum) unit load is:

$$\begin{aligned} \frac{q}{L} &= \frac{7,770}{160} = 48.6 \text{ lb}_f @ (1 \text{ g}) \\ &= 5,828 \text{ lb}_f/\text{in} @ (120 \text{ g}) \end{aligned}$$

Substituting into the stability equation:

$$(qL)_{CR} = \frac{7.837EI}{L^2} = \frac{7.837(27.6 \times 10^6)(274 \text{ in}^4)}{(160 \text{ in})^2} = 2.32 \times 10^6 \text{ lb}_f$$

And the critical distributed load is:

$$q_{CR} = \frac{2.32 \times 10^6}{L} = \frac{2.32 \times 10^6 \text{ lb}_f}{160 \text{ in}} = 14,470 \text{ lb}_f/\text{in}$$

Based on ASME B&PV Code, Appendix F, Subsection F-1331.5(a), the allowable load for free drop conditions is assumed to be 2/3 of the calculated critical value:

$$q'_{CR} = 2/3(14,470) = 9.65 \times 10^3 \text{ lb}_f/\text{in}$$

The margin of safety for the "applied load" to the postulated 120g axial free drop is:

$$MS = \frac{9.65 \times 10^3}{5.83 \times 10^3} - 1.0 = +0.66$$

Therefore, elastic stability criteria for the global structure are satisfied for the 120g end drop.

### 2.12.5.15 Strongback Local Stability

This section evaluates local stability of the "plate" section(s) extending from the central core using formulas for stability of plates from *Stress Analysis Manual*<sup>13</sup>:

$$\sigma_{CR} = \eta \bar{\eta} \frac{k\pi^2 E}{12(1-\nu^2)} \left(\frac{t}{b}\right)^2$$

where:

- Panel width is approximately 9 inches, use  $b = 9$ .
- Maximum panel height is the free span between clamp arm assemblies, considering the distance between the bolted connections and the "height" of the clamp arms, the free span is less than 18 inches for all locations except the bottom span which is less than 22 inches.
- $\eta$  is a plasticity reduction factor. Because the applied stress is much less than the yield stress,  $\eta$  is assumed to be 1.0.

<sup>13</sup> Air Force Flight Dynamics Laboratory, *Stress Analysis Manual*, Chapter 6 - Analysis of Plates, Wright Patterson AFB, Ohio, October 1986 (NTIS AD759199).

- $\bar{\eta}$  is a cladding reduction factor. The strongback is solid plate (no cladding), therefore  $\bar{\eta}$  is 1.0.
- $k$  is a function of aspect ratio ( $a/b$ ), where  $a$  = length and  $b$  = width (see Figure 6-1 of Stress Analysis Manual provided as Figure 2.12.5-57 of this calculation).

Plates are stiffened by the clamp arms (and FCSs) which provide connections between the adjacent plates. In addition, the fuel is pressed against the plates by the clamp arms, which will restrict "out-of-plane" motion of the plates.

**Span Length Reduced By FCS Stiffener**

As described above, the bottom nominal span length between clamp arms is 22 inches. Since the FCS channel stiffener on the FCS provides significant restraint of the plate and thus the span length is reduced by a factor of 2. Therefore  $a = 22/2 = 11$  and the constant,  $k = 3.6$  (i.e., from curve D (dashed) at  $a/b=1.2$ ,  $k=3.6$  for 3 edges clamped and 1 edge free):

$$F_{CR} = \frac{3.6 \pi^2 (27,600 \text{ ksi})}{12(1-.3^2)} \left( \frac{0.25 \text{ in}}{9.0 \text{ in}} \right)^2 = 69.3 \text{ ksi}$$

This value is significantly above the minimum yield stress of the material.

**"Free" Edge Pinned**

The addition of the tube stiffener on the free edge of the strongback angles stiffens the plate angles. This added stiffness is evaluated by considering the "free" edge to be simply supported and ignoring the effect of the FCS channel stiffener. Therefore  $a = 22$ ,  $a/b = 2.4$ , and the constant,  $k = 5.6$  (i.e., from curve B at  $a/b=2.2$ ,  $k=5.6$ , conservatively for simply supported on all edges):

$$F_{CR} = \frac{5.6 \pi^2 (27,600 \text{ ksi})}{12(1-.3^2)} \left( \frac{0.25 \text{ in}}{9.0 \text{ in}} \right)^2 \geq 100 \text{ ksi}$$

This value is significantly above the material yield stress.

**Summary of Local Stability**

Critical stresses are significantly greater than the yield stress. Therefore, elastic instability is not considered a viable failure mode.

<b>Case</b>	<b>Critical Stress</b>	<b>Notes</b>
$a = b = 9$ : Considers restraint provided by the FCS stiffener assembly	69.3 ksi	Critical stress $\gg S_y$
$a = 22, b = 9$ : Neglects restraint provided by the FCS stiffener/hinge assembly but considers free edge "simply supported" based on tube stiffener	$> 100$ ksi	Critical stress $\gg S_y$

**2.12.5.16 Strongback Width-Thickness Ratio - Triangular Core**

The sections comprising the triangular core are evaluated using the rules for flanges of box sections from ASME B&PV Code, Subsection NF-3322.2(d)(2)(b)(1):

$$\frac{238}{\sqrt{S_y}} = \frac{238}{\sqrt{25.0 \text{ ksi}}} = 47.6$$

Calculating the actual width/thickness ratio and comparing it to the allowable value:

$$\frac{b}{t} \approx \frac{8.3 \text{ in}}{0.25 \text{ in}} = 33.2 < 47.6$$

Therefore, the triangular core section is fully effective.

### 2.12.5.17 Strongback Width-Thickness Ratio - Plate Extensions

The plate sections extending from the triangular core are considered stiffened elements under compression (NF-3322.2(d)(2), where the sections are stiffened on one side by the continuous connection to the triangular core and on the "free" edge by the 2 inches square tubes. The effective width is evaluated using NF-3322.2(d)(2)(b)(3):

$$\frac{253}{\sqrt{S_y}} = \frac{253}{\sqrt{25.0 \text{ ksi}}} = 50.6$$

The actual width/thickness ratio is:

$$\frac{b}{t} \approx \frac{9 \text{ in}}{0.25 \text{ in}} = 36 < 50.6$$

Therefore, when stiffened by the tube sections, the plate extensions of the strongback are fully effective in carrying compressive loads.

Although neglected here, the FCS stiffener assembly (stiffener, hinge, and latch) provide additional connections between the plates, reducing the unbraced span by a factor of  $\approx 2$ . This conservatism further ensures that the extensions are fully effective in transmitting axial (compressive) loads.

### 2.12.5.18 Strongback Axial Stress

Assuming that the FAs are supported by the endplate assembly and the end of the package, the strongback assembly supports only its own weight. The nominal axial stress,  $f_a$ , results from the weight of strongback assembly less the weight of the (impact end) endplate assembly, which will rest on the end of the package. Stresses are calculated with and without the FCS assemblies:

Excluding FCS assemblies:
$f_a = \frac{2175 - 168}{12.7} = 158 \text{ psi @ (1.0g)}$ $= 19.0 \text{ ksi @ (120g)}$

Including FCS and Tube Stiffeners
$f_a = \frac{3,030 - 168}{17.9} = 160 \text{ psi @ (1.0g)}$ $= 19.2 \text{ ksi @ (120g)}$

Comparing these impact stresses with the minimum yield stress of Type 304 stainless steel results in the following margins of safety:

Configuration	Calculated Stress (ksi)	Yield Stress (ksi)	M.S.
w/o FCSs	19.0	25.0	+0.32
w/ FCSs & tube stiffeners	19.2		+0.30

**2.12.5.19 Evaluation of Strongback Response to FCS Loads**

Under axial drop conditions, out-of-plane loads are imposed on the strongback core by the FCS. These loads are shown in Table 2.12.5-8 through Table 2.12.5-11, and are transmitted from the FCS by the hinges and the lock bar/pin block to their connecting points on the strongback longitudinal weldment.

A simple ANSYS® model using Shell43 elastic-plastic elements is used to estimate the impact of the pin block loads on the strongback longitudinal weldment.

**FEA Model Geometry**

The model includes the 1/4-inch thick plate angle and the 2-inch square × 1/4-inch thick tube stiffener at the "free" edge. The plate was modeled as 9 inches wide × 17 inches and 20.6 inches long (high). The tube area where the lock bar is attached is modeled as being identical (material and thickness) with the tube. This area is shown in Figure 2.12.5-32. The plate and stiffener tubes are modeled as Type 304 stainless steel.

**Connections (contact element & couples)**

Connections between the plate angle and stiffener tube are made as follows:

- The threaded fasteners used to connect the parts are modeled using a node coupled in the three translational directions. These are shown with green triangles in the geometry plots.
- Compressive connections between the parts are modeled by including Contac52 (point-to-point) contact elements between the plate and the tube (meshes are aligned such that the contact elements are oriented completely in the global 'X' direction). The contact elements are shown in Figure 2.12.5-33.

**Boundary Conditions**

As shown in Figure 2.12.5-31, the plate is assumed restrained (fixed in translation and rotation) at the upper and lower clamp arms and at the strongback "core". No boundary conditions are applied to the stiffener tube.

**Applied Loads**

As noted above, the area where the lock bar is attached is modeled with an increased thickness. The loads from Table 2.12.5-17 are distributed equally to all nodes within the lock bar (thicker) area (i.e., Force per node = Total Load/Number of Nodes). This simplification eliminates moments which might result from loads with opposite sign at the two ends of the pin (e.g., for case 1, the Fz load changes sign). However, the resulting stresses are expected to be small.

**Stress Results**

Stress results are summarized in Table 2.12.5-18. The table contains maximum stress intensities at the mid-thickness and top surface of the shell elements for the 1/4-inch thick plate angle and the 1/4-inch thick stiffener tube. Stresses are listed for the complete part and for the part with elements connected to the coupled nodes removed. Stress results are also shown in the following figures:

<b>Load Case</b>	<b>Mid-thickness Stress Intensities</b>	<b>Top Surface Stress Intensities</b>	<b>Bottom Surface Stress Intensities</b>
1	Figure 2.12.5-36	Figure 2.12.5-37	Figure 2.12.5-38
2	Figure 2.12.5-39	Figure 2.12.5-40	Figure 2.12.5-41
3	Figure 2.12.5-42	Figure 2.12.5-43	Figure 2.12.5-44
4	Figure 2.12.5-45	Figure 2.12.5-46	Figure 2.12.5-47

**Strain Results**

Stress results are described above. The tangent modulus used in the stress analyses is relatively small. Therefore, stresses will increase slowly after reaching the yield point, but strains may become large prior to stresses reaching their allowable values.

To ensure that results are reasonable, plastic strains are reviewed for the three axial drop load cases. The maximum strains occur as a result of the Load Step 3, and are 1.7% and 1.8% at the middle and outer fiber, respectively. Considering the magnitude and type of loading, these values are reasonable and will not result in loss of function. Therefore, the strongback and stiffener tube are acceptable. Note also that increases in yield under dynamic loading will decrease the plastic strains.

**Fastener Loads**

Load on the coupled nodes used to represent the fasteners are extracted from the ANSYS® analysis and are listed in Table 2.12.5-17. All fasteners are assumed to have a nominal size of 3/8 inch and the shear plane(s) are assumed to pass through the threaded part of the fasteners such that root areas are used for calculating shear stress.

**Bearing**

For each load condition, the bearing stress imposed by the fasteners on the connected members is calculated using the maximum shear load.

Load Condition 20.6-inch span	Max Shear (lb <sub>f</sub> )	Bearing			Bearing Stress (ksi)
		Diameter (in)	Thickness (in)	Area (in <sup>2</sup> )	
Condition 1 (Table 2.12.5-8)	2,267	0.375	0.25	0.0938	24.2
Condition 2 (Table 2.12.5-9)	3,513	0.375	0.25	0.0938	37.5
Condition 3 (Table 2.12.5-10)	2,760	0.375	0.25	0.0938	29.4
Condition 4 (Table 2.12.5-11)	3,634	0.375	0.25	0.0938	38.8
<b>17.0-inch Span</b>					
Condition 4 (Table 2.12.5-11)	4,095	0.375	0.25	0.0938	43.7

The ASME B&PV Code Level A allowable stress for bearing per NF-3322.1(f)(3), Equation (24b) or NF-3324.6(a)(5) is:

$$F_p = 1.5S_u = 1.5(71.0 \text{ ksi}) = 106.5 \text{ ksi}$$

Since all of the HAC bearing stresses are less than the NCT allowable stress, bearing is acceptable.

**Edge Distance Check**

Spacing along the row of fasteners is 1.5 inches. Minimum edge distance is approximately 1 inch (at the end of the tube stiffener). This distance exceeds the required edge distance per Table NF-3324.6(b)(1)-1 for 1/2-inch bolts (3/4-inch for cut edges). Therefore, edge distance is acceptable.

**2.12.5.20 Strongback Stress Calculations – Horizontal Loads**

Under horizontal (side) drop conditions, loads imposed on the strongback angle by the lock plate are provided by Table 2.12.5-11. The lock plate loads are summarized in Table 2.12.5-17 of this calculation.

Stress plots for the long FCS are included as Figure 2.12.5-45 through Figure 2.12.5-47 and for the standard FCS as Figure 2.12.5-48 and Figure 2.12.5-50 (for mid-thickness and surface stresses, respectively).

**Component Stresses & Strains - Side Drop Loading**

Side drop evaluations are provided for both long FCS and standard FCS spans. Stress results are summarized in Table 2.12.5-22 (long FCS) and Table 2.12.5-23 (standard FCS). The table contains maximum stress intensities at the mid-thickness and surface of the shell elements for the 1/4-inch thick plate angle and the 1/4-inch thick stiffener tube. Stresses are listed for the complete part, and for the part with elements connected to the coupled nodes removed. As shown by Table 2.12.5-23, all stresses in the 17.0-inch section are within the allowable values.

As shown by Table 2.12.5-22, all stresses in the long FCS are within the allowable values.

As noted previously, the tangent modulus used in this analysis is relatively small so strains may increase rapidly while stresses remain below the allowable values. Therefore, plastic strains are reviewed as listed in Table 2.12.5-26. The maximum calculated plastic strain intensity is approximately 14%. This value is much less than the ductility of Type 304 stainless steel. For example, the minimum specified elongation of annealed ASTM A-479/SA-479 Type 304 is 30%,

cold working which could decrease the available elongation will also provide significant increases in yield strength.

Based on the magnitude of the strains, additional side drop stress analyses are performed using a tangent modulus of .05E. This value is considered an upper bound for strains of the magnitude of those listed in Table 2.12.5-26. Using a large  $E_{tan}$  will result in larger calculated stresses. Stresses for these analyses are listed in Table 2.12.5-27 and Table 2.12.5-28.

As shown by Table 2.12.5-28, all stresses in the 17.0-inch span are within the allowable values.

As shown by Table 2.12.5-27, with the exception of 2 nodes in the stiffener tube, all stresses in the 20.6-span are within the allowable stress limits. Excluding the stresses at these nodes is acceptable as described below:

- The tubes perform their function (stiffening the free edge of the plate angle) by acting as beams. As such, the critical loading is beam bending. As shown by Figure 2.12.5-54 and Table 2.12.5-27, when the two nodes are removed, stresses in the beam are within the allowable stress limits.
- The large stresses at the single nodes are a result of concentrated loads being transmitted through the contact elements. Redistribution of these loads resulting from local yielding will not result in loss of support to the strongback plate.
- Since the tubes perform their stiffening function and will not fail from the isolated high stresses, the tubes are acceptable.

Therefore, the strongback is acceptable for side drop loads imposed by the Lock Plate.

#### Fastener Loads - Side Drop Loading

Fasteners are evaluated using the same methods as described in Section 2.12.5.13.2, *Fastener Analysis* (see Table 2.12.5-24 (long FCS) and Table 2.12.5-25 (standard FCS)). As shown, all stress ratios are less than 1. Therefore, the 3/8-inch fasteners (threads excluded from the shear plane) are acceptable.

Bearing and edge distance is included in the evaluation in Section 2.12.5.13.2, *Fastener Analysis*.

**Table 2.12.5-1 – Fuel Assembly Physical Characteristics**

Parameter	Mark-BW
Rod Array	17 × 17
Rods per Assembly	264
Guide Thimbles per Assembly	24
Instrument Sheaths per Assembly	1
Rod Pitch, inches	0.496
Rod Length, inches	152.4
Rod OD, inches	0.374
Fuel Rod Weight, pounds (each)	5.33
Cladding thickness, inches	0.0225
Cladding Yield Strength at 200 °F, psi	31,222
Cladding Modulus of Elasticity at 200 °F, psi	12.8(10 <sup>6</sup> )

**Table 2.12.5-2 – FCS Evaluation Material Properties Summary**

Material Specification	Temperature, °F	Yield Strength (S <sub>y</sub> ), psi	Ultimate Strength (S <sub>u</sub> ), psi	Design Stress Intensity (S <sub>m</sub> ), psi	Elastic Modulus, ×10 <sup>6</sup> psi
XM-19 Stainless Steel	200	47,100	99,400	33,100	27.6
Type 304 Stainless Steel	200	25,000	71,000	20,000	27.6
A574 Grade 4037 or 4042	200	131,600	180,000	35,000	28.5
A564 Grade 630, H1100	200	106,300	140,000	28,000	28.5

**Table 2.12.5-3 – Criticality Control Structure Allowable Stress Limits**

Stress Category	HAC	
	Elastic Analyses	Plastic Analyses <sup>①</sup>
General Primary Membrane Stress Intensity	Lesser of: $2.4S_m$ $0.7S_u$	Greater of: $0.7S_u$ $S_y + 1/3(S_u - S_y)$
Local Primary Membrane Stress Intensity	Lesser of: $3.6S_m$ $S_u$	$0.9S_u$
Primary Membrane + Bending Stress Intensity	Lesser of: $3.6S_m$ $S_u$	$0.9S_u$
Range of Primary + Secondary Stress Intensity	Not Applicable	Not Applicable
Pure Shear Stress	$0.42S_u$	$0.42S_u$
Bearing Stress	$2.1S_u$	
Fatigue	Not Applicable	Not Applicable
<b>Fastener HAC Allowable Stress Limits<sup>②③</sup></b>		
Stress Category	Elastic Analyses <sup>④</sup>	Plastic Analyses <sup>①</sup>
Bolt Average Tensile Stress	Lesser of: $0.9S_y$ $2/3S_u$	Lesser of: $S_y$ $0.7S_u$
Bolt Average Shear Stress	$0.6S_y$	Lesser of: $0.6S_y$ $0.42S_u$
Bolt Tension + Shear	$f_t^2/F_{tb}^2 + f_v^2/F_{vb}^2 \leq 1$	$f_t^2/F_{tb}^2 + f_v^2/F_{vb}^2 \leq 1$
Minimum Edge Distance	n/a	$L/d \geq [0.5 + 1.2(f_p/S_u)]$ $f_p/S_u \leq 2.1$

**Notes:**

- ① Plastic Analysis: ASME B&PV Code, Section III, Appendix F, F-1341.2.
- ② Bolt Joints: ASME B&PV Code, Section III, Appendix F, F-1335.
- ③ Bearing for Pinned Joints: ASME B&PV Code, Section III, Appendix F, F-1336.
- ④ Elastic Analysis for Pinned Joints: ASME B&PV Code, Section III, Appendix F, F-1331

**Table 2.12.5-4 – FCS Force Calculations**

Row No. (i) <sup>①</sup>	Rod Quan. (n) <sup>②</sup>	x <sub>i</sub> (inches) <sup>③</sup>	M <sub>i</sub> (in-lb <sub>f</sub> ) <sup>④</sup>	F <sub>i</sub> per rod (lb <sub>f</sub> ) <sup>⑤</sup>	F, Row (lb <sub>f</sub> ) <sup>⑥</sup>	Cumulative Rows (lb <sub>f</sub> )
1	17	0.250	23.2	45	773	773
2	17	0.372	37.3	68	1,151	1,924
3	14	0.494	51.4	90	1,258	3,182
4	15	0.616	65.5	112	1,681	4,863
5	17	0.738	79.7	134	2,283	7,146
6	12	0.860	86.9	161	1,937	9,083
7	17	0.982	86.9	189	3,215	12,298
8	17	1.104	86.9	217	3,686	15,985
9	12	1.226	86.9	122	1,467	<b>17,452</b>

**Notes:**

- ① Row 1 is on the outside of the assembly adjacent to the FCS; row 9 is the center row.
- ② See Figure 2.12.5-1.
- ③ Rod lateral deflection,  $x_i = C + (i - 1)G_r$ , where  $C = 0.25$  inches and  $G_r = 0.122$  inches.
- ④ Rod bending moment,  $M_i = 115.8x_i$ , up to a maximum of 86.9 in-lb<sub>f</sub>.
- ⑤ Lateral force of a single rod,  $F_i = 8(Px_i - M_i)/L$ . In row 9, the force is half this value.
- ⑥ Equal to F<sub>i</sub> times rod quantity n.

**Table 2.12.5-5 – Low and High Tangent Modulus Results Comparison**

Run	Component	Low Tangent Modulus <sup>①</sup>		High Tangent Modulus <sup>②</sup>	
		Max Stress, psi	Max Disp, in	Max Stress, psi	Max Disp, in
Load Case 1	Pin Block	54,162	0.0219	58,071	0.0211
	Hinge Block	54,590	0.0075	52,564	0.0072
	Stiffener	56,152	0.0264	54,404	0.0257
	Angle	36,598	0.0258	42,366	0.0251
Load Case 2	Pin Block	53,451	0.0098	52,970	0.0095
	Hinge Block	57,634	0.0187	66,770	0.0179
	Stiffener	55,168	0.0233	60,547	0.0225
	Angle	34,618	0.0246	37,847	0.0238
Load Case 3	Pin Block	47,153	0.0060	46,589	0.0060
	Hinge Block	52,521	0.0055	53,630	0.0054
	Stiffener	48,220	0.0077	48,480	0.0076
	Angle	29,814	0.0084	29,820	0.0084

**Notes:**

- ① Tangent modulus is calculated in Section 2.12.5.4 (291,933 psi for XM-19 and 219,970 psi for Type 304).
- ② Tangent modulus is assumed to be 5% of the Modulus of Elasticity at 200 °F (1,380,000 psi for both materials).

**Table 2.12.5-6 – FCS General Primary Membrane Stress Intensity ( $P_m$ )**

Run	Component	Material	Allowable Stress (psi)	Path	$P_m$ (psi)	Margin of Safety
Load Case 1 (LC1)	Pin Block	XM-19	69,580	2	30,160	+1.31
	Hinge Block	XM-19	69,580	3B	26,340	+1.64
	Stiffener	XM-19	69,580	C2	39,350	+0.77
	Angle	304	49,700	14	9,847	+4.05
Load Case 2 (LC2)	Pin Block	XM-19	69,580	1	20,390	+2.41
	Hinge Block	XM-19	69,580	5	25,610	+1.72
	Stiffener	XM-19	69,580	13	27,390	+1.54
	Angle	304	49,700	15	9,274	+4.36
Load Case 3 (LC3)	Pin Block	XM-19	69,580	1	13,400	+4.19
	Hinge Block	XM-19	69,580	3B	18,030	+2.86
	Stiffener	XM-19	69,580	C1	15,570	+3.47
	Angle	304	49,700	14	8,053	+5.17

**Table 2.12.5-7 – FCS Local Primary Membrane Stress Intensity**

Run	Component	Material	Allowable Stress (psi)	Figure	P <sub>max</sub> (psi)	Margin of Safety
Load Case 1 (LC1)	Pin Block	XM-19	89,460	2.12.5-11	54,162	+0.66
	Hinge Block	XM-19	89,460	2.12.5-12	54,590	+0.64
	Stiffener	XM-19	89,460	2.12.5-13	56,152	+0.59
	Angle	304	63,900	2.12.5-14	36,598	+0.75
Load Case 2 (LC2)	Pin Block	XM-19	89,460	2.12.5-16	53,451	+0.67
	Hinge Block	XM-19	89,460	2.12.5-17	57,634	+0.55
	Stiffener	XM-19	89,460	2.12.5-18	55,168	+0.62
	Angle	304	63,900	2.12.5-19	34,616	+0.85
Load Case 3 (LC3)	Pin Block	XM-19	89,460	2.12.5-21	47,153	+0.90
	Hinge Block	XM-19	89,460	2.12.5-22	52,521	+0.70
	Stiffener	XM-19	89,460	2.12.5-23	48,220	+0.86
	Angle	304	63,900	2.12.5-24	29,814	+1.14

**Table 2.12.5-8 – Reactions for Load Condition 1 (lb<sub>f</sub>)**

Load Condition 1, Pressure Applied to Pin Block Side					
Component	NODE	F <sub>x</sub>	F <sub>y</sub>	SRSS (F <sub>x</sub> &F <sub>y</sub> )	F <sub>z</sub> (Axial)
Pin Block	50000	1,522	4,367	4,625	0
	50006	-1,028	4,026	4,155	1,126
<b>Pin Block Total</b>				<b>8,780</b>	<b>1,126</b>
Hinge Block Top	50003	-201	4,372	<b>4,377</b>	741
Hinge Block Center	50004	-22	2,948	2,948	0
	50008	-261	1,868	1,886	1,974
<b>Hinge Block Center Total</b>				<b>4,834</b>	<b>1,974</b>
Hinge Block Bottom	50007	-54	155	164	0
Top Hinge Mounting Bracket	50003	-201	4,372	4,377	741
	50004	-22	2,948	2,948	0
<b>Top Hinge Mounting Bracket Total</b>				<b>7,325</b>	<b>741</b>
Bottom Hinge Mounting Bracket	50008	-261	1,868	1,886	1,974
	50007	-54	155	164	0
<b>Bottom Hinge Mounting Bracket Total</b>				<b>2,050</b>	<b>1,974</b>
Lock Plate (reciprocal to Pin Block Total)				<b>8,780</b>	<b>1,126</b>
<b>Total Reactions (Sum of Nodes 50000 thru 50008)</b>		<b>0</b>	<b>17,736</b>	<b>17,736</b>	<b>3,840</b>

**Table 2.12.5-9 – Reactions for Load Condition 2 (lb<sub>f</sub>)**

<b>Load Condition 1, Pressure Applied to Pin Block Side</b>					
<b>Component</b>	<b>NODE</b>	<b>F<sub>x</sub></b>	<b>F<sub>y</sub></b>	<b>SRSS (F<sub>x</sub>&amp;F<sub>y</sub>)</b>	<b>F<sub>z</sub> (Axial)</b>
Pin Block	50000	5,076	165	<b>5,078</b>	
	50006	3,818	-138	3,820	1,022
<b>Pin Block Total</b>				<b>8,898</b>	1,022
Hinge Block Top	50003	733	1,308	1,500	1,616
Hinge Block Center	50004	3,615	1,250	3,825	
	50008	3,685	769	3,765	1,203
<b>Hinge Block Center Total</b>				<b>7,590</b>	1,203
Hinge Block Bottom	50007	809	-3,355	3,451	
Top Hinge Mounting Bracket	50003	733	1,308	1,500	1,616
	50004	3,615	1,250	3,825	
<b>Top Hinge Mounting Bracket Total</b>				<b>5,325</b>	1,616
Bottom Hinge Mounting Bracket	50008	3,685	769	3,765	1,203
	50007	809	-3,355	3,451	
<b>Bottom Hinge Mounting Bracket Total</b>				<b>7,216</b>	1,203
Lock Plate (Same as Pin Block Total)				<b>8,898</b>	1,022
<b>Total Reactions</b> (Sum of Nodes 50000 thru 50008)		<b>17,736</b>	<b>0</b>	<b>17,736</b>	<b>3,840</b>

**Table 2.12.5-10 – Reactions for Load Condition 3 (lb<sub>f</sub>)**

<b>Load Condition 1, Pressure Applied to Pin Block Side</b>					
<b>Component</b>	<b>NODE</b>	<b>F<sub>x</sub></b>	<b>F<sub>y</sub></b>	<b>SRSS (F<sub>x</sub>&amp;F<sub>y</sub>)</b>	<b>F<sub>z</sub> (Axial)</b>
Pin Block	50000	3,554	2,272	4,219	
	50006	1,143	1,935	2,247	1,113
<b>Pin Block Total</b>				<b>6,466</b>	1,113
Hinge Block Top	50003	210	2,566	2,575	1,099
Hinge Block Center	50004	1,865	2,328	2,983	
	50008	1,780	1,516	2,338	1,629
<b>Hinge Block Center Total</b>				<b>5,321</b>	1,629
Hinge Block Bottom	50007	317	-1,750	1,779	
Top Hinge Mounting Bracket	50003	210	2,566	2,575	1,099
	50004	1,865	2,328	2,983	
<b>Top Hinge Mounting Bracket Total</b>				<b>5,558</b>	1,099
Bottom Hinge Mounting Bracket	50008	1,780	1,516	2,338	1,629
	50007	317	-1,750	1,779	
<b>Bottom Hinge Mounting Bracket Total</b>				<b>4,117</b>	1,629
Lock Plate (Same as Pin Block Total)				<b>6,466</b>	1,113
<b>Total Reactions</b> (Sum of Nodes 50000 thru 50008)		<b>8,868</b>	<b>8,868</b>	<b>12,541</b>	<b>3,840</b>

**Table 2.12.5-11 – Reactions for Load Condition 4 (lb<sub>f</sub>)**

<b>Load Condition 1, Pressure Applied to Pin Block Side</b>					
<b>Component</b>	<b>NODE</b>	<b>F<sub>x</sub></b>	<b>F<sub>y</sub></b>	<b>SRSS (F<sub>x</sub>&amp;F<sub>y</sub>)</b>	<b>F<sub>z</sub> (Axial)</b>
Pin Block	50000	6,729	16	6,729	441
	50006	6,728	15	6,728	-441
<b>Pin Block Total</b>				13,457	0
Hinge Block Top	50003	1,488	-921	1,750	912
Hinge Block Center	50004	4,025	905	4,126	-262
	50008	4,024	907	4,125	262
<b>Hinge Block Center Total</b>				8,251	0
Hinge Block Bottom	50007	1,488	-922	1,751	-912
Top Hinge Mounting Bracket	50003	1,488	-921	1,750	912
	50004	4,025	905	4,126	-262
<b>Top Hinge Mounting Bracket Total</b>				5,876	650
Bottom Hinge Mounting Bracket	50008	4,024	907	4,125	262
	50007	1,488	-922	1,751	-912
<b>Bottom Hinge Mounting Bracket Total</b>				5,876	-650
Lock Plate (Same as Pin Block Total)				13,457	0
<b>Total Reactions (Sum of Nodes 50000 thru 50008)</b>		<b>24,482</b>	<b>0</b>	<b>24,482</b>	<b>0</b>

**Table 2.12.5-12 – Bolt Loads for Load Condition 1 (lb<sub>f</sub>)**

<b>Bolt Loads Pressure Applied to Pin Block Side</b>							
<b>Hinge Block</b>	<b>(x-axis is tensile load for bolt)</b>						<b>SRSS (Y &amp; Z)</b>
<b>NODE</b>	<b>F<sub>X</sub></b>	<b>F<sub>Y</sub></b>	<b>F<sub>Z</sub></b>	<b>M<sub>X</sub> (in-lb<sub>f</sub>)</b>	<b>M<sub>Y</sub> (in-lb<sub>f</sub>)</b>	<b>M<sub>Z</sub> (in-lb<sub>f</sub>)</b>	
744**	-217	1,161	122	0	0	0	1,167
6280‡	-152	794	278	0	0	0	841
8234‡	-203	1,080	68	0	0	0	1,182
8713	-55	913	549	0	0	0	1,065
8855	-76	1,054	412	0	0	0	1,132
17523‡	-85	391	49	0	0	0	394
19477‡	-13	25	-18	0	0	0	31
19956	-62	492	244	0	0	0	549
20098	-7	24	166	0	0	0	167
max	-217						1,167
<b>Pin Block</b>	<b>(y-axis is tensile load for bolt)</b>						<b>SRSS (Y &amp; Z)</b>
<b>NODE</b>	<b>F<sub>X</sub></b>	<b>F<sub>Y</sub></b>	<b>F<sub>Z</sub></b>	<b>M<sub>X</sub> (in-lb<sub>f</sub>)</b>	<b>M<sub>Y</sub> (in-lb<sub>f</sub>)</b>	<b>M<sub>Z</sub> (in-lb<sub>f</sub>)</b>	
2605*	-1,653	77	43	0	0	0	1,654
5625‡	-1,306	-48	290	0	0	0	1,338
5698	-1,244	-226	199	0	0	0	1,260
16868‡	-1,379	-92	60	0	0	0	<b>1,380</b>
16941	-1,245	-240	95	0	0	0	1,249
max		<b>-240</b>					1,654
<b>Stiffeners</b>	<b>(y-axis is tensile load for bolt)</b>						<b>SRSS (Y &amp; Z)</b>
<b>pin block side</b>	<b>F<sub>X</sub></b>	<b>F<sub>Y</sub></b>	<b>F<sub>Z</sub></b>	<b>M<sub>X</sub> (in-lb<sub>f</sub>)</b>	<b>M<sub>Y</sub> (in-lb<sub>f</sub>)</b>	<b>M<sub>Z</sub> (in-lb<sub>f</sub>)</b>	
3495*	1,653	-75	-43	0	0	0	1,654
3498	978	49	84	0	0	0	981
3870	2,202	236	-103	0	0	0	<b>2,204</b>
5303	1,940	96	-23	0	0	0	1,940
max		236					2,204
<b>hinge block side</b>	<b>(x-axis is tensile load for bolt)</b>						<b>SRSS (Y &amp; Z)</b>
<b>NODE</b>	<b>F<sub>X</sub></b>	<b>F<sub>Y</sub></b>	<b>F<sub>Z</sub></b>	<b>M<sub>X</sub> (in-lb<sub>f</sub>)</b>	<b>M<sub>Y</sub> (in-lb<sub>f</sub>)</b>	<b>M<sub>Z</sub> (in-lb<sub>f</sub>)</b>	
2509	-130	-1,801	-134	0	0	0	1,809
5883	-118	-580	211	0	0	0	617
5927**	217	-1,161	-122	0	0	0	1,167
6121	-213	-1,293	36	0	0	0	1,293
max	-213						1,809

**Notes:**

Starred nodes belong to same couple set between stiffener and hinge or pin block.

‡ nodes closest to angle sheet edge

**Table 2.12.5-13 – Bolt Loads for Load Condition 2 (lb<sub>f</sub>)**

<b>Bolt Loads Pressure Applied to Pin Block Side</b>							
<b>Hinge Block</b>	<b>(x-axis is tensile load for bolt)</b>						<b>SRSS (Y &amp; Z)</b>
<b>NODE</b>	<b>F<sub>X</sub></b>	<b>F<sub>Y</sub></b>	<b>F<sub>Z</sub></b>	<b>M<sub>X</sub> (in-lb<sub>f</sub>)</b>	<b>M<sub>Y</sub> (in-lb<sub>f</sub>)</b>	<b>M<sub>Z</sub> (in-lb<sub>f</sub>)</b>	
744**	56	-1,486	112	0	0	0	1,490
6280‡	-5	-715	-316	0	0	0	782
8234‡	-23	-56	-190	0	0	0	198
8713	-188	-674	241	0	0	0	716
8855	-106	87	101	0	0	0	133
17523‡	-7	-1,149	587	0	0	0	1,290
19477‡	-100	-1,187	318	0	0	0	1,229
19956	-228	-1,164	555	0	0	0	1,290
20098	-184	-991	498	0	0	0	1,108
max	-228						1,490
<b>Pin Block</b>	<b>(y-axis is tensile load for bolt)</b>						<b>SRSS (X &amp; Z)</b>
<b>NODE</b>	<b>F<sub>X</sub></b>	<b>F<sub>Y</sub></b>	<b>F<sub>Z</sub></b>	<b>M<sub>X</sub> (in-lb<sub>f</sub>)</b>	<b>M<sub>Y</sub> (in-lb<sub>f</sub>)</b>	<b>M<sub>Z</sub> (in-lb<sub>f</sub>)</b>	
2605*	1,321	-205	72	0	0	0	1,323
5625‡	961	-197	58	0	0	0	962
5698	1,014	-101	4	0	0	0	1,014
16868‡	1,089	-206	326	0	0	0	1,137
16941	1,167	-128	191	0	0	0	1,183
max		-206					1,323
<b>Stiffeners</b>							
<b>pin block side</b>	<b>(y-axis is tensile load for bolt)</b>						<b>SRSS (X &amp; Z)</b>
<b>NODE</b>	<b>F<sub>X</sub></b>	<b>F<sub>Y</sub></b>	<b>F<sub>Z</sub></b>	<b>M<sub>X</sub> (in-lb<sub>f</sub>)</b>	<b>M<sub>Y</sub> (in-lb<sub>f</sub>)</b>	<b>M<sub>Z</sub> (in-lb<sub>f</sub>)</b>	
3495*	-1,321	205	-72	0	0	0	1,323
3498	-531	-86	91	0	0	0	538
3870	-1,762	-147	-25	0	0	0	1,762
5303	-1,285	-181	-67	0	0	0	1,287
max		-181					1,762
<b>hinge block side</b>	<b>(x-axis is tensile load for bolt)</b>						<b>SRSS (Y &amp; Z)</b>
<b>NODE</b>	<b>F<sub>X</sub></b>	<b>F<sub>Y</sub></b>	<b>F<sub>Z</sub></b>	<b>M<sub>X</sub> (in-lb<sub>f</sub>)</b>	<b>M<sub>Y</sub> (in-lb<sub>f</sub>)</b>	<b>M<sub>Z</sub> (in-lb<sub>f</sub>)</b>	
2509	238	2,059	-96	0	0	0	2,061
5883	84	842	207	0	0	0	867
5927**	-54	1,486	-112	0	0	0	1,490
6121	6	1,809	-22	0	0	0	1,809
max	238						2,061

**Notes:**

Starred nodes belong to same couple set between stiffener and hinge or pin block.

‡ nodes closest to angle sheet edge

**Table 2.12.5-14 – Bolt Loads for Load Condition 3 (lb<sub>f</sub>)**

<b>Bolt Loads Pressure Applied to Pin Block Side</b>							
<b>Hinge Block</b>	<b>(x-axis is tensile load for bolt)</b>						<b>SRSS (Y &amp; Z)</b>
<b>NODE</b>	<b>F<sub>X</sub></b>	<b>F<sub>Y</sub></b>	<b>F<sub>Z</sub></b>	<b>M<sub>X</sub> (in-lb<sub>f</sub>)</b>	<b>M<sub>Y</sub> (in-lb<sub>f</sub>)</b>	<b>M<sub>Z</sub> (in-lb<sub>f</sub>)</b>	
744**	40	-280	155	0	0	0	320
6280‡	-5	-13	-2	0	0	0	13
8234‡	-82	487	-34	0	0	0	489
8713	-43	58	366	0	0	0	371
8855	-30	503	257	0	0	0	565
17523‡	-1	-405	305	0	0	0	507
19477‡	-59	-619	121	0	0	0	630
19956	-91	-393	393	0	0	0	555
20098	-93	-498	326	0	0	0	595
Max	-93						630
<b>Pin Block</b>	<b>(y-axis is tensile load for bolt)</b>						<b>SRSS (Y &amp; Z)</b>
<b>NODE</b>	<b>F<sub>X</sub></b>	<b>F<sub>Y</sub></b>	<b>F<sub>Z</sub></b>	<b>M<sub>X</sub> (in-lb<sub>f</sub>)</b>	<b>M<sub>Y</sub> (in-lb<sub>f</sub>)</b>	<b>M<sub>Z</sub> (in-lb<sub>f</sub>)</b>	
2605*	-291	67	84	0	0	0	303
5625‡	-235	-8	166	0	0	0	288
5698	-237	-46	97	0	0	0	256
16868‡	-289	-18	177	0	0	0	339
16941	-236	-54	167	0	0	0	289
max		67					339
<b>Stiffeners</b>							
<b>pin block side</b>	<b>(y-axis is tensile load for bolt)</b>						<b>SRSS (X &amp; Z)</b>
<b>NODE</b>	<b>F<sub>X</sub></b>	<b>F<sub>Y</sub></b>	<b>F<sub>Z</sub></b>	<b>M<sub>X</sub> (in-lb<sub>f</sub>)</b>	<b>M<sub>Y</sub> (in-lb<sub>f</sub>)</b>	<b>M<sub>Z</sub> (in-lb<sub>f</sub>)</b>	
3495*	291	-67	-84	0	0	0	303
3498	-39	106	115	0	0	0	121
3870	1,157	65	-126	0	0	0	1,164
5303	500	44	-16	0	0	0	500
max		106					1,164
<b>hinge block side</b>	<b>(x-axis is tensile load for bolt)</b>						<b>SRSS (Y &amp; Z)</b>
<b>NODE</b>	<b>F<sub>X</sub></b>	<b>F<sub>Y</sub></b>	<b>F<sub>Z</sub></b>	<b>M<sub>X</sub> (in-lb<sub>f</sub>)</b>	<b>M<sub>Y</sub> (in-lb<sub>f</sub>)</b>	<b>M<sub>Z</sub> (in-lb<sub>f</sub>)</b>	
2509	60	960	-129	0	0	0	968
5883	37	-1	229	0	0	0	229
5927**	-40	280	-155	0	0	0	320
6121	61	550	47	0	0	0	552
max	61						968

**Notes:**

Starred nodes belong to same couple set between stiffener and hinge or pin block.

‡ nodes closest to angle sheet edge

**Table 2.12.5-15 – Lock Plate Bolt Force Summary (lb<sub>f</sub>)**

Item	LC1	LC2	LC3	LC4
F <sub>x</sub>	-494	-8,893	-4,697	-13,457
F <sub>y</sub>	-8,393	-35	-4,207	-30
F <sub>z</sub>	-1,126	-1,022	-1,113	0
F <sub>xg</sub>	199	3,578	1,890	5,414
F <sub>xb</sub>	66	1,193	630	1,805
F <sub>yb</sub>	2,798	9	1,402	10
F <sub>zb</sub>	375	341	371	0
F'	1,455	1,321	1,439	0
f <sub>t</sub>	66	1,193	630	1,805
f <sub>v</sub>	3,343	1,661	2,290	10
σ (psi)	850	15,291	8,076	23,138
τ (psi)	49,167	24,431	33,676	149
MS, σ	+147.29	+7.24	+14.60	+4.45
MS, τ	+0.54	+2.09	+1.24	+505
Interaction Check	0.42 < 1.0	0.12 < 1.0	0.20 < 1.0	0.03 < 1.0

**Table 2.12.5-16 – Hinge Mounting Bracket Bolt Summary**

Top Bracket									
Item	F <sub>rx</sub> (lb <sub>f</sub> )	F <sub>ry</sub> (lb <sub>f</sub> )	f <sub>t</sub> (lb <sub>f</sub> )	f <sub>v</sub> (lb <sub>f</sub> )	Σ (psi)	MS (on σ)	τ (psi)	MS (on τ)	Interac. Ratio
LC1	3,816	-6,250	-3,269	1,241	41,914	+2.01	18,247	+3.14	0.17
LC2	-2,487	-4,389	-2,296	-1,410	29,436	+3.28	20,732	+2.65	0.13
LC3	650	-5,276	-2,760	773	35,383	+2.56	11,365	+5.65	0.10
LC4	-4,783	-2,743	-1,435	1,433	18,392	+5.85	21,069	+2.59	0.10
Bottom Bracket									
Item	F <sub>rx</sub> (lb <sub>f</sub> )	F <sub>ry</sub> (lb <sub>f</sub> )	f <sub>t</sub> (lb <sub>f</sub> )	f <sub>v</sub> (lb <sub>f</sub> )	σ (psi)	MS (on σ)	τ (psi)	MS (on τ)	Interac. Ratio
LC1	1,284	-1,594	-834	1,407	10,690	+10.79	20,690	+2.65	0.08
LC2	-5,185	-8	-4	1,778	55	+2,292	26,141	+1.89	0.12
LC3	-1,932	-846	-442	1,312	5,671	+21.22	19,291	+2.92	0.07
LC4	-4,781	-2,744	-1,435	1,432	18,399	+5.85	21,062	+2.59	0.10

**Table 2.12.5-17 – Loads on the Strongback from the Fuel Control Structures (lb<sub>f</sub>)**

<b>Node</b>	<b>Out-Of-Plane F<sub>x</sub></b>	<b>In-Plane F<sub>y</sub></b>	<b>In-Plane/Axial F<sub>z</sub></b>
<b>Load Condition 1 From Table 2.12.5-8</b>			
50000	1,522	4,367	--
50006	-1,028	4,026	1,126
Total	494	8,393	1,126
<b>Applied</b>	-500	-8,400	-1,150
<b>Load Condition 2 From Table 2.12.5-9</b>			
50000	5,076	165	--
50006	3,818	-138	1,022
Total	8,893	27	1,022
<b>Applied</b>	-8,900	-50	-1,050
<b>Load Condition 3 From Table 2.12.5-10</b>			
50000	3,554	2,272	--
50006	1,143	1,935	1,113
Total	4,697	4,207	1,113
<b>Applied</b>	-4,700	-4,250	-1,150
<b>Load Condition 4 - Horizontal From Table 2.12.5-11</b>			
50000	6,729	16	441
50006	6,728	15	-441
Total	13,457	31	0
<b>Applied</b>	-13,500	-50	50

**Table 2.12.5-18 – Summary of Strongback Stress Results LC1-LC3**

Load Case 1	Calculated Stress (ksi)		Margin of Safety <sup>①</sup>	
	P <sub>m</sub>	P <sub>m</sub> +P <sub>b</sub>	P <sub>m</sub>	P <sub>m</sub> +P <sub>b</sub>
Strongback Angle	19.0	19.1	+1.62	+2.35
Strongback Angle w/o <sup>②</sup> Bolt Nodes	13.4	13.5	+2.71	+3.73
Stiffener Tube	18.0	18.0	+1.76	+2.55
Stiffener Tube w/o Bolt Nodes	10.6	10.7	+3.69	+4.97
<b>Load Case 2</b>				
Strongback Angle	20.2	29.1	+1.46	+1.20
Strongback Angle w/o Bolt Nodes	20.6	29.1	+1.41	+1.20
Stiffener Tube	27.9	30.6	+0.78	+1.09
Stiffener Tube w/o Bolt Nodes	28.2	30.3	+0.76	+1.11
<b>Load Case 3</b>				
Strongback Angle	19.3	25.0	+1.58	+1.56
Strongback Angle w/o Bolt Nodes	17.4	25.0	+1.86	+1.56
Stiffener Tube	21.3	23.7	+1.33	+1.70
Stiffener Tube w/o Bolt Nodes	21.3	23.7	+1.33	+1.70

**Notes:**

- ① Allowable stresses are 49.7 ksi and 63.9 ksi for P<sub>m</sub> and P<sub>m</sub> + P<sub>b</sub>, respectively
- ② "w/o" indicates that the coupled nodes (used at fastener locations) and connected elements are excluded from the listed results.

**Table 2.12.5-19 – Fastener Evaluation for Lock Bar/Pin Block Loads**

Load Case 1										
NODE	F <sub>X</sub>	F <sub>Y</sub>	F <sub>Z</sub>	Axial, lb <sub>f</sub> (F <sub>V</sub> )	Shear, lb <sub>f</sub>	f <sub>t</sub> (ksi)	f <sub>v</sub> (ksi)	f <sub>t</sub> / F <sub>tb</sub>	f <sub>v</sub> / F <sub>vb</sub>	Interaction
4573	10	136	250	10	284	0.13	2.58	0.00	0.03	0.00
4580	9	-32	132	9	136	0.11	1.23	0.00	0.02	0.00
4586	12	-87	66	12	109	0.16	0.99	0.00	0.01	0.00
4593	19	-222	2	19	222	0.24	2.02	0.00	0.03	0.00
4600	27	-756	-90	27	762	0.34	6.92	0.00	0.09	0.01
4798	23	-2,256	-140	23	2,260	0.29	20.55	0.00	0.27	0.07
4429	42	-1,723	-155	42	1,730	0.54	15.73	0.00	0.21	0.04
4804	23	-2,260	-179	23	2,267	0.30	20.61	0.00	0.27	0.07
4630	26	-749	-58	26	751	0.34	6.82	0.00	0.09	0.01
4637	19	-220	-102	19	243	0.24	2.21	0.00	0.03	0.00
4644	12	-86	-156	12	178	0.15	1.62	0.00	0.02	0.00
4650	8	-30	-242	8	244	0.11	2.22	0.00	0.03	0.00
4657	10	139	-443	10	464	0.13	4.22	0.00	0.06	0.00
<b>Max:</b>				<b>42</b>	<b>2,267</b>	<b>Max:</b>				<b>0.07</b>

**Notes:**

- ① Stresses based on fastener areas of 0.078 in<sup>2</sup> and 0.110 in<sup>2</sup> for tension and shear, respectively.
- ② Allowable stresses are 126.0 ksi and 75.6 ksi for tension and shear, respectively.
- ③ Shear load is:  $(F_x^2 + F_z^2)^{1/2}$

**Table 2.12.5-20 – Fastener Evaluation for Lock Bar/Pin Block Loads (lb<sub>f</sub>)**

Load Case 2										
NODE	F <sub>X</sub>	F <sub>Y</sub>	F <sub>Z</sub>	Axial, lb <sub>f</sub> (F <sub>V</sub> )	Shear, lb <sub>f</sub>	f <sub>t</sub> (ksi)	f <sub>v</sub> (ksi)	f <sub>t</sub> / F <sub>tb</sub>	f <sub>v</sub> / F <sub>vb</sub>	Interaction
4573	206	68	3,444	206	3,445	2.64	31.32	0.02	0.41	0.17
4580	194	-100	3,371	194	3,372	2.48	30.66	0.02	0.41	0.16
4586	151	-71	3,305	151	3,306	1.94	30.05	0.02	0.40	0.16
4593	274	49	3,259	274	3,259	3.51	29.63	0.03	0.39	0.15
4600	699	169	3,114	699	3,119	8.96	28.35	0.07	0.38	0.15
4798	94	-133	900	94	909	1.21	8.27	0.01	0.11	0.01
4429	692	-58	-112	692	126	8.87	1.15	0.07	0.02	0.01
4804	57	-116	-1,351	57	1,356	0.73	12.33	0.01	0.16	0.03
4630	686	177	-3,214	686	3,219	8.79	29.26	0.07	0.39	0.15
4637	280	57	-3,356	280	3,356	3.59	30.51	0.03	0.40	0.16
4644	155	-63	-3,404	155	3,405	1.98	30.95	0.02	0.41	0.17
4650	193	-91	-3,461	193	3,462	2.47	31.47	0.02	0.42	0.17
4657	202	64	-3,512	202	3,513	2.59	31.93	0.02	0.42	0.18
<b>Max:</b>				<b>699</b>	<b>3,513</b>	<b>Max:</b>				<b>0.18</b>

**Notes:**

- ① Stresses based on fastener areas of 0.078 in<sup>2</sup> and 0.110 in<sup>2</sup> for tension and shear, respectively.
- ② Allowable stresses are 126.0 ksi and 75.6 ksi for tension and shear, respectively.
- ③ Shear load is:  $(F_x^2 + F_z^2)^{1/2}$

**Table 2.12.5-21 – Fastener Evaluation for Lock Bar/Pin Block Loads**

Load Case 3										
NODE	F <sub>X</sub>	F <sub>Y</sub>	F <sub>Z</sub>	Axial, lb <sub>f</sub> (F <sub>v</sub> )	Shear, lb <sub>f</sub>	f <sub>t</sub> (ksi)	f <sub>v</sub> (ksi)	f <sub>t</sub> / F <sub>tb</sub>	f <sub>v</sub> / F <sub>vb</sub>	Interaction
4573	110	117	2,621	110	2,624	1.42	23.85	0.01	0.32	0.10
4580	61	-64	1,843	61	1,844	0.78	16.76	0.01	0.22	0.05
4586	38	-75	1,487	38	1,489	0.48	13.54	0.00	0.18	0.03
4593	58	-112	1,277	58	1,282	0.75	11.65	0.01	0.15	0.02
4600	142	-357	1,047	142	1,106	1.82	10.05	0.01	0.13	0.02
4798	105	-1,143	228	105	1,165	1.35	10.60	0.01	0.14	0.02
4429	441	-870	-156	441	884	5.65	8.03	0.04	0.11	0.01
4804	107	-1,141	-552	107	1,267	1.37	11.52	0.01	0.15	0.02
4630	141	-349	-1,199	141	1,249	1.81	11.35	0.01	0.15	0.02
4637	57	-109	-1,384	57	1,388	0.73	12.62	0.01	0.17	0.03
4644	37	-74	-1,589	37	1,591	0.47	14.46	0.00	0.19	0.04
4650	62	-63	-1,976	62	1,977	0.79	17.97	0.01	0.24	0.06
4657	109	118	-2,757	109	2,760	1.40	25.09	0.01	0.33	0.11
<b>Max:</b>				<b>441</b>	<b>2,760</b>	<b>Max:</b>				<b>0.11</b>

**Notes:**

- ① Stresses based on fastener areas of 0.078 in<sup>2</sup> and 0.110 in<sup>2</sup> for tension and shear, respectively.
- ② Allowable stresses are 126.0 ksi and 75.6 ksi for tension and shear, respectively.
- ③ Shear load is:  $(F_x^2 + F_z^2)^{1/2}$

**Table 2.12.5-22 – Summary of Strongback Stress Results (20.6-inch model) LC4**

Load Case 4	Allowable Stresses (ksi)		Margin of Safety <sup>①</sup>	
	P <sub>m</sub>	P <sub>m</sub> +P <sub>b</sub>	P <sub>m</sub>	P <sub>m</sub> +P <sub>b</sub>
Strongback Angle	30.2	42.3	+0.65	+0.51
Strongback Angle w/o <sup>②</sup> Bolt Nodes	28.3	42.3	+0.76	+0.51
Stiffener Tube	44.6	45.7	+0.11	+0.40
Stiffener Tube w/o Bolt Nodes	44.6	45.7	+0.11	+0.40

**Notes:**

- ① Allowable stresses are 49.7 ksi and 63.9 ksi for P<sub>m</sub> and P<sub>m</sub> + P<sub>b</sub>, respectively
- ② "w/o" indicates that the coupled nodes (used at fastener locations) and connected elements are excluded from the listed results.

**Table 2.12.5-23 – Summary of Strongback Stress Results (17.0-inch model) LC4**

Load Case 4	Allowable Stresses (ksi)		Stress Ratio <sup>①</sup>	
	P <sub>m</sub>	P <sub>m</sub> +P <sub>b</sub>	P <sub>m</sub>	P <sub>m</sub> +P <sub>b</sub>
Strongback Angle	25.8	35.1	+0.93	+0.82
Strongback Angle w/o <sup>②</sup> Bolt Nodes	25.3	35.1	+0.96	+0.82
Stiffener Tube	38.0	39.1	+0.31	+0.63
Stiffener Tube w/o Bolt Nodes	38.0	39.1	+0.31	+0.63

**Notes:**

- ① Allowable stresses are 49.7 ksi and 63.9 ksi for P<sub>m</sub> and P<sub>m</sub> + P<sub>b</sub>, respectively
- ② "w/o" indicates that the coupled nodes (used at fastener locations) and connected elements are excluded from the listed results.

**Table 2.12.5-24 – Fastener Evaluation for Lock Bar/Pin Block Loads – Side Free Drop on 20.6-inch Section**

Load Case 4										
NODE	F <sub>x</sub>	F <sub>y</sub>	F <sub>z</sub>	Axial, lb <sub>r</sub> (F <sub>y</sub> )	Shear, lb <sub>r</sub>	f <sub>t</sub> (ksi)	f <sub>v</sub> (ksi)	f <sub>t</sub> / F <sub>tb</sub>	f <sub>v</sub> / F <sub>vb</sub>	Interaction
4573	230	-1,155	2,086	230	2,384	2.95	21.68	0.02	0.29	0.08
4580	398	608	3,539	398	3,591	5.10	32.64	0.04	0.43	0.19
4586	463	923	3,414	463	3,536	5.93	32.15	0.05	0.43	0.18
4593	795	536	3,594	795	3,634	10.19	33.03	0.08	0.44	0.20
4600	1,042	68	3,421	1,042	3,422	13.36	31.11	0.11	0.41	0.18
4798	248	-890	919	248	1,280	3.18	11.63	0.03	0.15	0.02
4429	1,000	-227	6	1,000	227	12.82	2.07	0.10	0.03	0.01
4804	247	-891	-904	247	1,269	3.17	11.54	0.03	0.15	0.02
4630	1,041	67	-3,416	1,041	3,417	13.35	31.06	0.11	0.41	0.18
4637	795	535	-3,591	795	3,631	10.19	33.01	0.08	0.44	0.20
4644	462	922	-3,409	462	3,532	5.93	32.10	0.05	0.42	0.18
4650	397	609	-3,535	397	3,587	5.09	32.61	0.04	0.43	0.19
4657	230	-1,154	-2,076	230	2,375	2.95	21.59	0.02	0.29	0.08
<b>Max:</b>				<b>1,042</b>	<b>3,634</b>				<b>Max:</b>	<b>0.20</b>

**Notes:**

- ① Stresses based on fastener areas of 0.078 in<sup>2</sup> and 0.110 in<sup>2</sup> for tension and shear, respectively.
- ② Allowable stresses are 126.0 ksi and 75.6 ksi for tension and shear, respectively.
- ③ Shear load is:  $(F_x^2 + F_z^2)^{1/2}$

**Table 2.12.5-25 – Fastener Evaluation for Lock Bar/Pin Block Loads – Side Free Drop on 17.0-inch Section**

Load Case 4										
NODE	F <sub>x</sub>	F <sub>y</sub>	F <sub>z</sub>	Axial, lb <sub>f</sub> (F <sub>v</sub> )	Shear, lb <sub>f</sub>	f <sub>t</sub> (ksi)	f <sub>v</sub> (ksi)	f <sub>t</sub> / F <sub>tb</sub>	f <sub>v</sub> / F <sub>v<b>b</b></sub>	Interaction
3805	169	-222	3,971	169	3,977	2.17	36.16	0.02	0.48	0.23
3811	424	72	4,094	424	4,095	5.44	37.22	0.04	0.49	0.24
3818	563	362	4,074	563	4,090	7.22	37.18	0.06	0.49	0.25
3825	980	363	3,788	980	3,805	12.57	34.59	0.10	0.46	0.22
3990	165	-624	1,006	165	1,184	2.12	10.76	0.02	0.14	0.02
3685	1,025	51	7	1,025	51	13.14	0.46	0.10	0.01	0.01
3996	164	-624	-985	164	1,166	2.11	10.60	0.02	0.14	0.02
3853	980	363	-3,782	980	3,799	12.57	34.54	0.10	0.46	0.22
3860	563	362	-4,069	563	4,085	7.22	37.14	0.06	0.49	0.24
3867	424	72	-4,090	424	4,091	5.44	37.19	0.04	0.49	0.24
3873	169	-223	-3,966	169	3,972	2.17	36.11	0.02	0.48	0.23
<b>Max:</b>				<b>1,025</b>	<b>4,095</b>	<b>Max:</b>				<b>0.25</b>

**Notes:**

- ① Stresses based on fastener areas of 0.078 in<sup>2</sup> and 0.110 in<sup>2</sup> for tension and shear, respectively.
- ② Allowable stresses are 126.0 ksi and 75.6 ksi for tension and shear, respectively.
- ③ Shear load is:  $(F_x^2 + F_z^2)^{1/2}$

**Table 2.12.5-26 – Side Drop Plastic Strain Intensity**

Plastic Strain Intensity	E <sub>tan</sub> ≅ .008E		E <sub>tan</sub> = .05E	
	Middle Fiber	Extreme Fiber	Middle Fiber	Extreme Fiber
<b>20.6-inch Span - Load Step 4 (Side Drop)</b>				
Plate	5.5	9.8	1.04	1.48
Stiffener Tube	13.4	13.9	3.07	3.15
<b>17.0-inch Span - Load Step 4 (Side Drop)</b>				
	Middle Fiber	Extreme Fiber	Middle Fiber	Extreme Fiber
Plate	3.0	4.9	0.73	0.98
Stiffener Tube	8.8	9.2	2.05	2.23

**Table 2.12.5-27 – Summary of Strongback Stress Results (20.6-inch model) LC4**

Load Case 4 (High Tangent Modulus)	Allowable Stresses (ksi)		Margin of Safety <sup>①</sup>	
	$P_m$	$P_m+P_b$	$P_m$	$P_m+P_b$
Strongback Angle	30.3	42.0	+0.64	+0.52
Strongback Angle w/o <sup>②</sup> Bolt Nodes	30.3	42.0	+0.64	+0.52
Stiffener Tube	54.5	55.4	③	+0.15
Stiffener Tube w/o Bolt Nodes	54.5	55.4		+0.15
Stiffener Tube w/o 2 Nodes (Note 3)	46.4	N/A	+0.07	N/A

**Notes:**

- ① Allowable stresses are 49.7 ksi and 63.9 ksi for  $P_m$  and  $P_m + P_b$ , respectively
- ② "w/o" indicates that the coupled nodes (used at fastener locations) and connected elements are excluded from the listed results.
- ③ Nodes 5802 & 5803 at stiffener tube ends are peak stresses and excluded from comparison to allowable stresses. Conservatively, the outer surface stresses are compared to the membrane-plus-bending allowable stress. See Section 2.12.5.20, *Strongback Stress Calculations - Horizontal Loads*, for further discussion.

**Table 2.12.5-28 – Summary of Strongback Stress Results (17.0-inch model) LC4**

Load Case 4 (High Tangent Modulus)	Allowable Stresses (ksi)		Stress Ratio <sup>①</sup>	
	$P_m$	$P_m+P_b$	$P_m$	$P_m+P_b$
Strongback Angle	27.7	37.4	+0.79	+0.71
Strongback Angle w/o <sup>②</sup> Bolt Nodes	26.0	37.4	+0.91	+0.71
Stiffener Tube	44.8	46.7	+0.11	+0.37
Stiffener Tube w/o Bolt Nodes	44.8	46.7	+0.11	+0.37

**Notes:**

- ① Allowable stresses are 49.7 ksi and 63.9 ksi for  $P_m$  and  $P_m + P_b$ , respectively
- ② "w/o" indicates that the coupled nodes (used at fastener locations) and connected elements are excluded from the listed results.

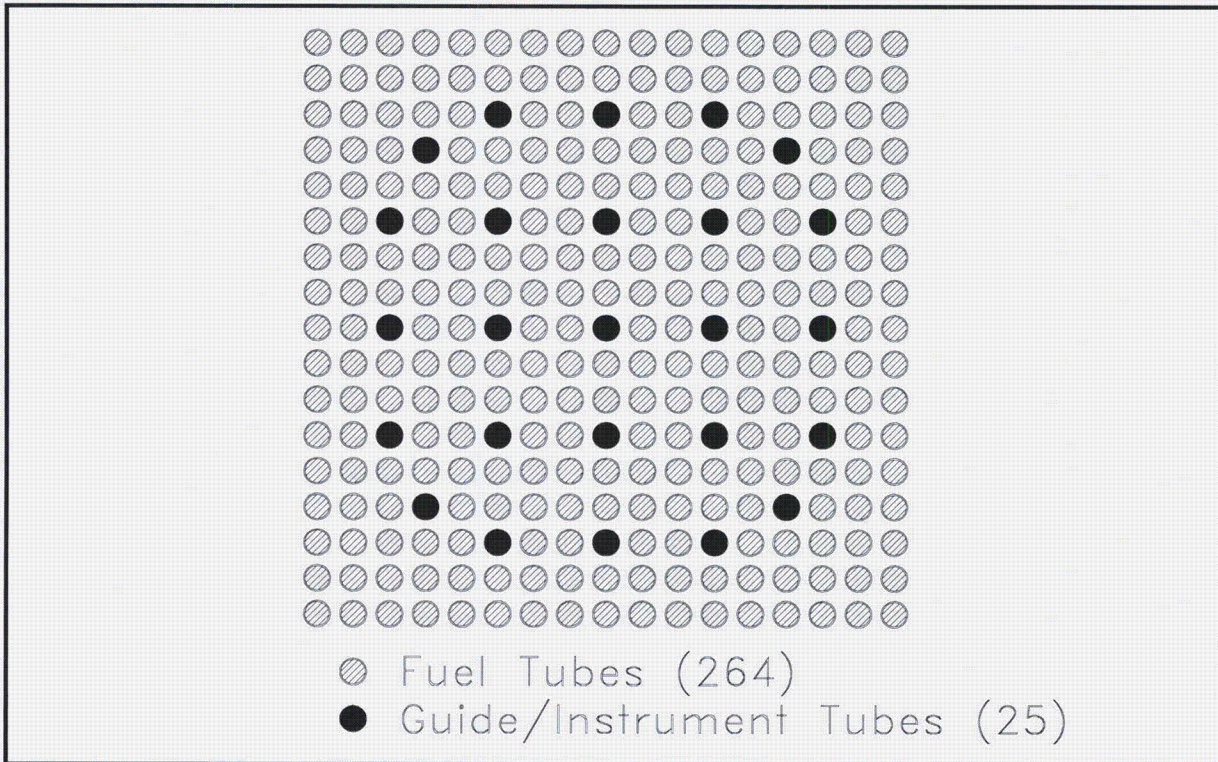


Figure 2.12.5-1 – MOX Fuel Assembly Rod Locations



Figure 2.12.5-2 – Buckled Shape of Fuel Rod from Certification Test

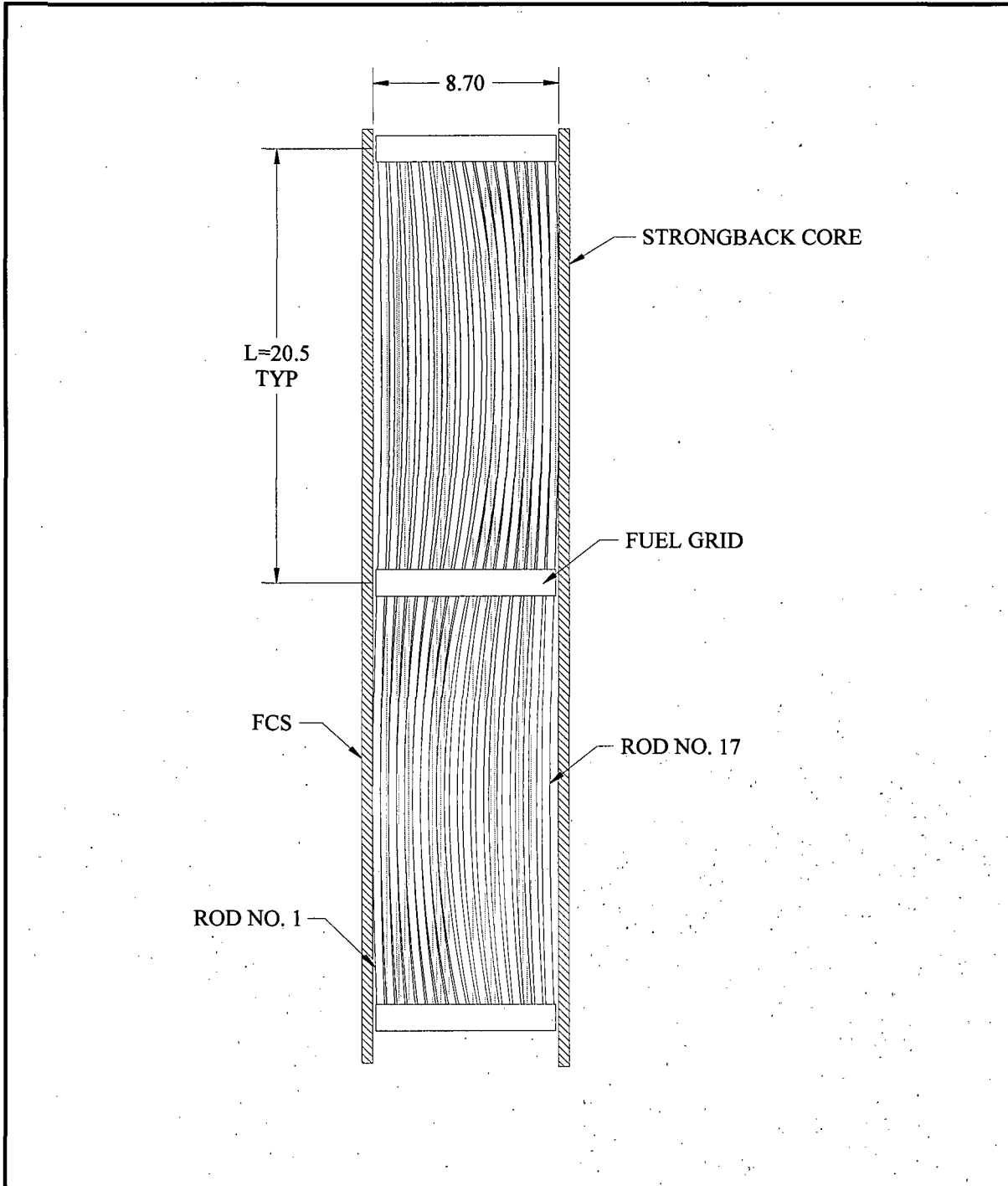


Figure 2.12.5-3 – Buckled Configuration of Fuel Rods

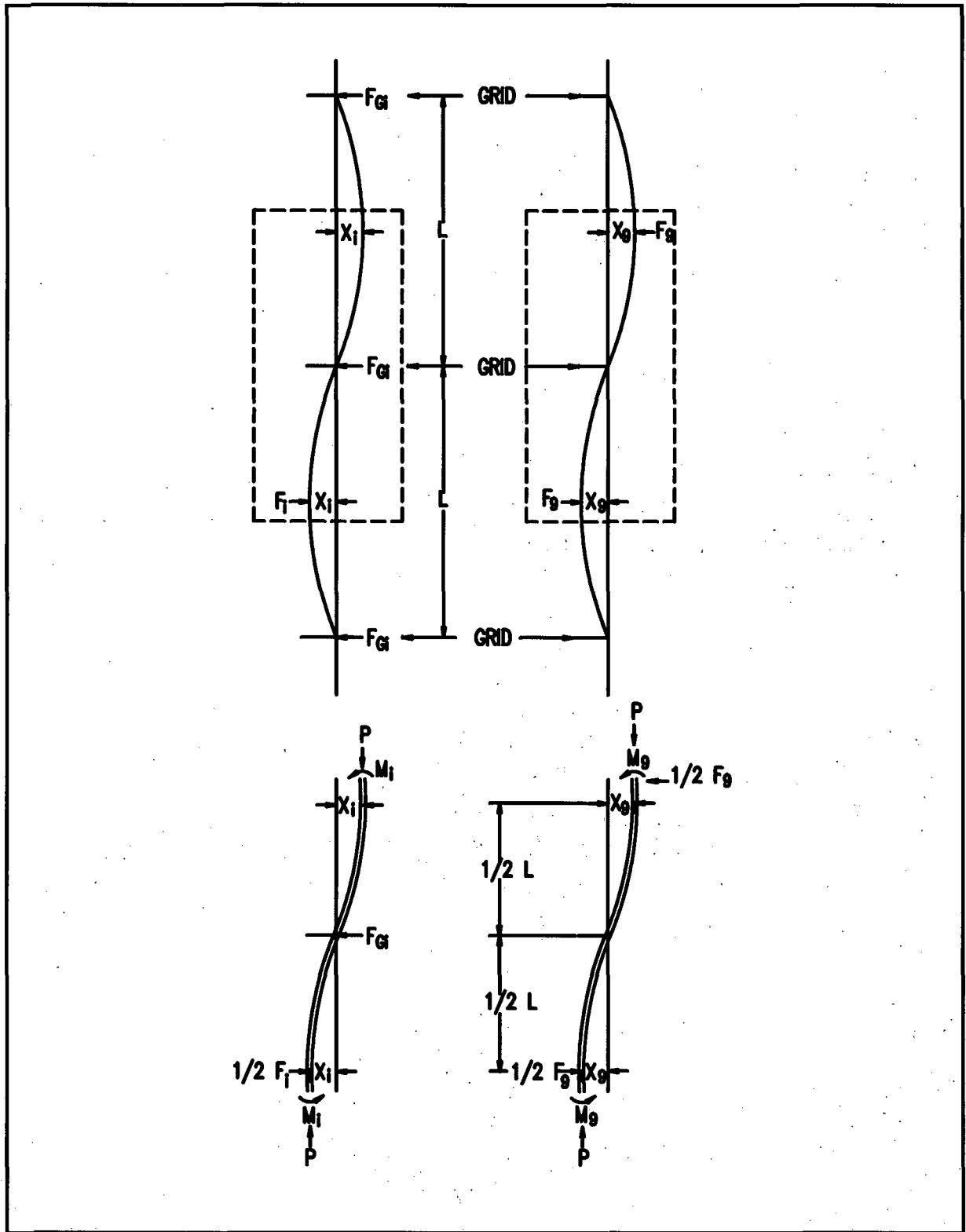
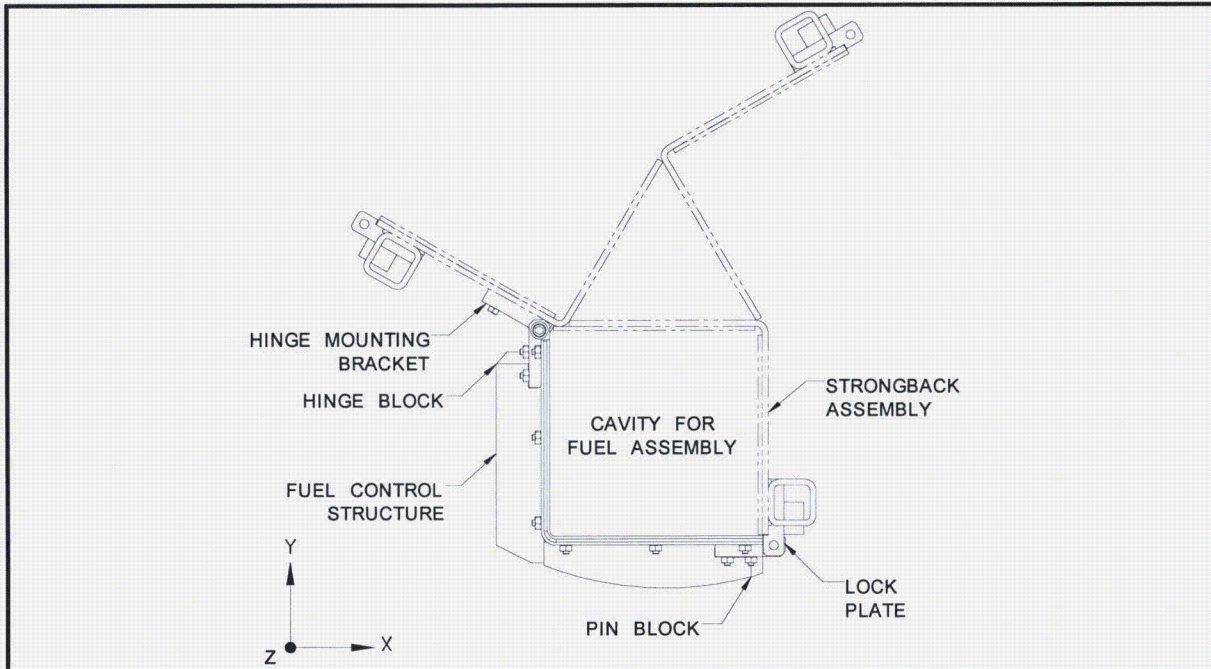
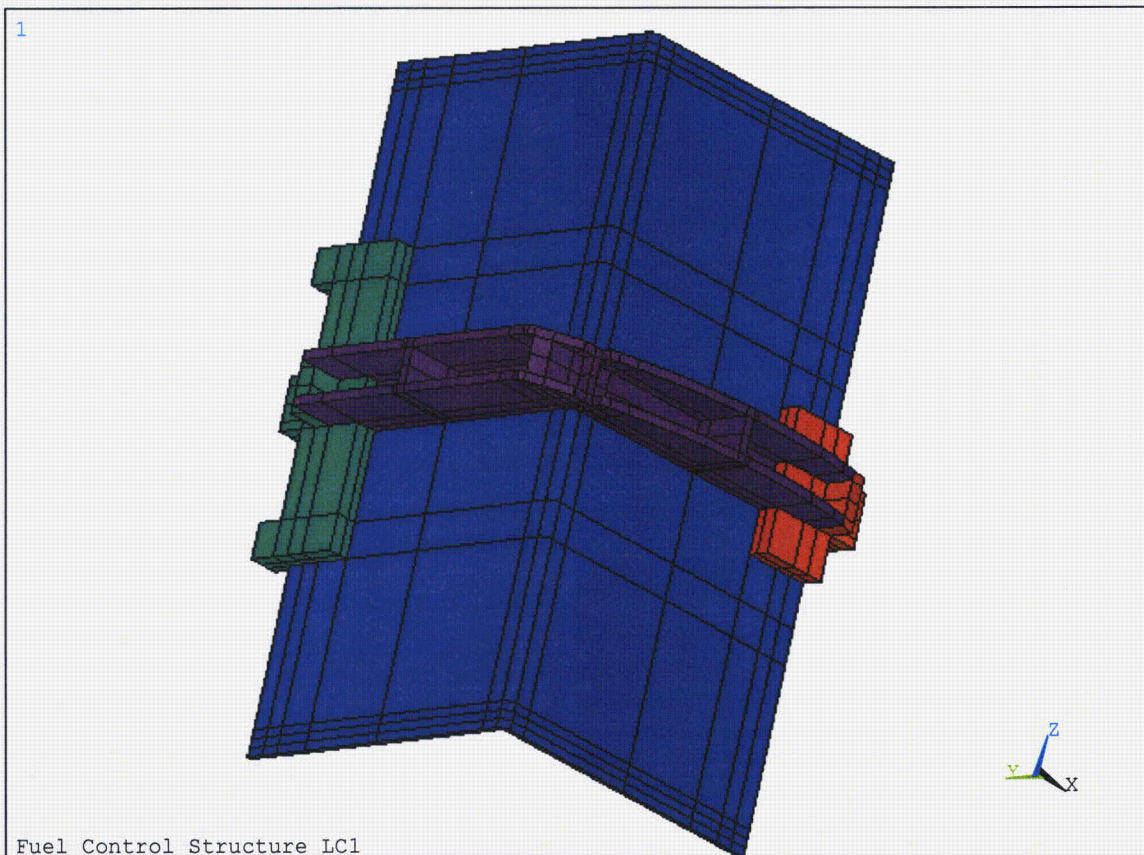


Figure 2.12.5-4 – Free Body Diagrams of Fuel Rods



**Figure 2.12.5-5 – FCS and Strongback Cross-Section**



**Figure 2.12.5-6 – FEA Volumes**

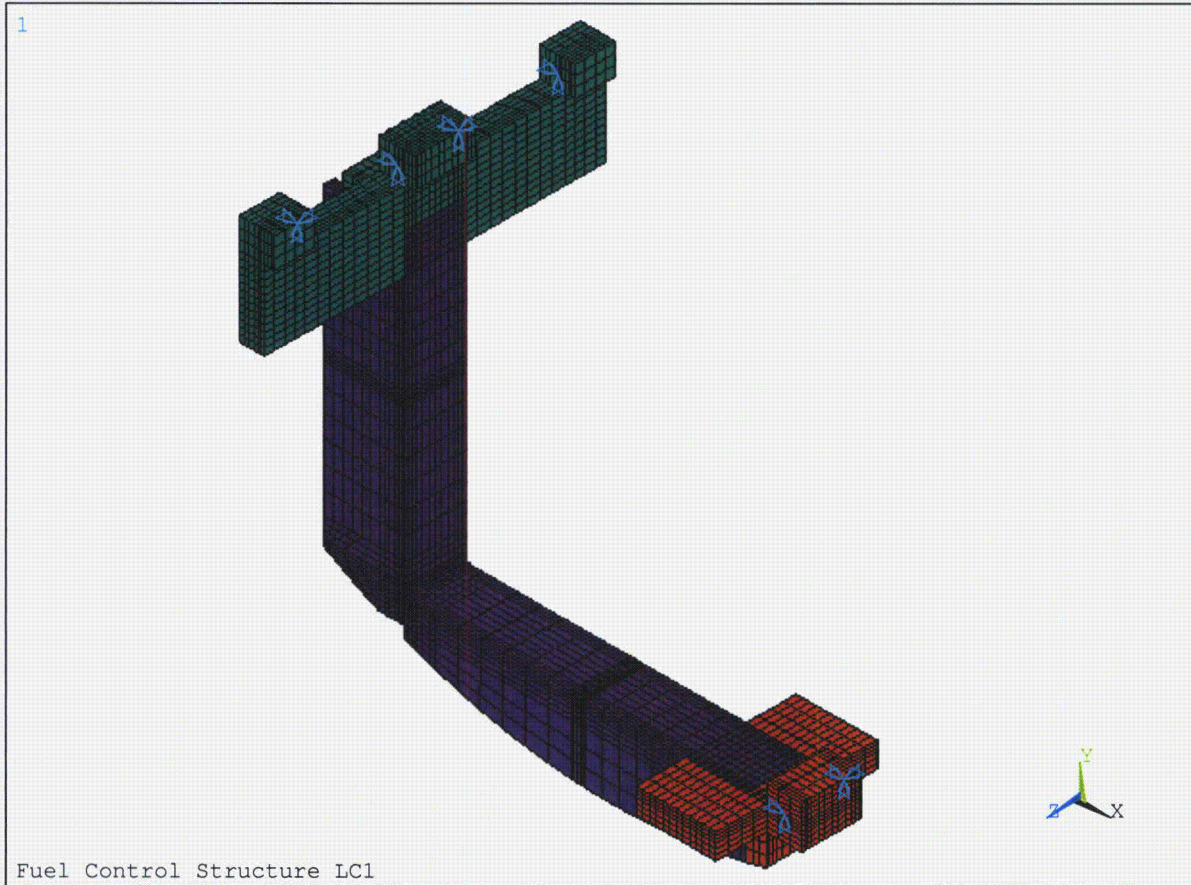


**Figure 2.12.5-7** – Elements and Boundary Constraints (Shown without Angle)

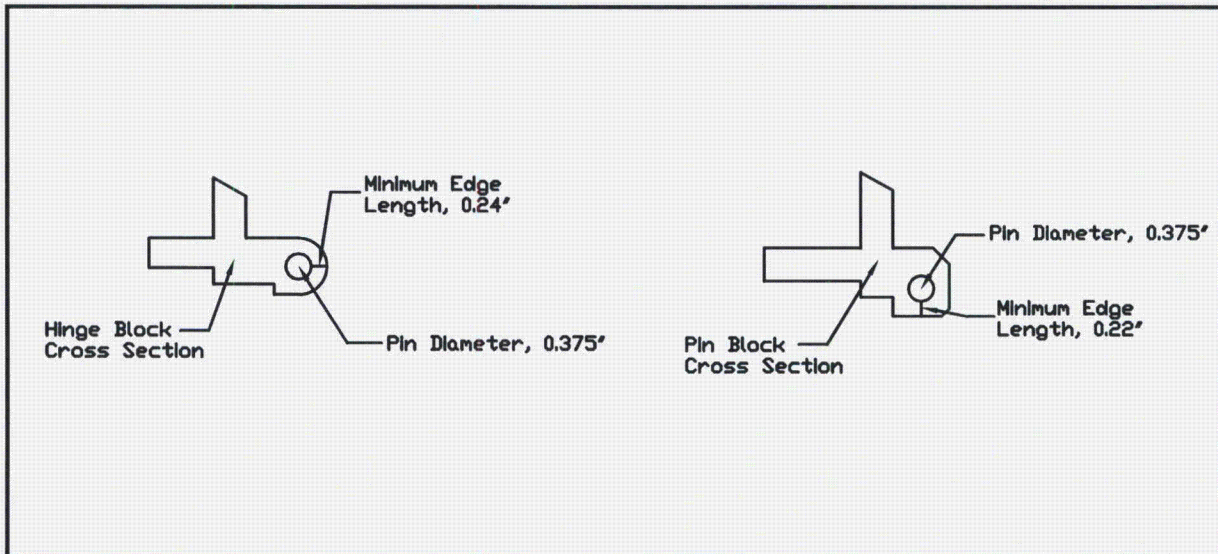


**Figure 2.12.5-8** – Pin Diameters and Minimum Edge Lengths

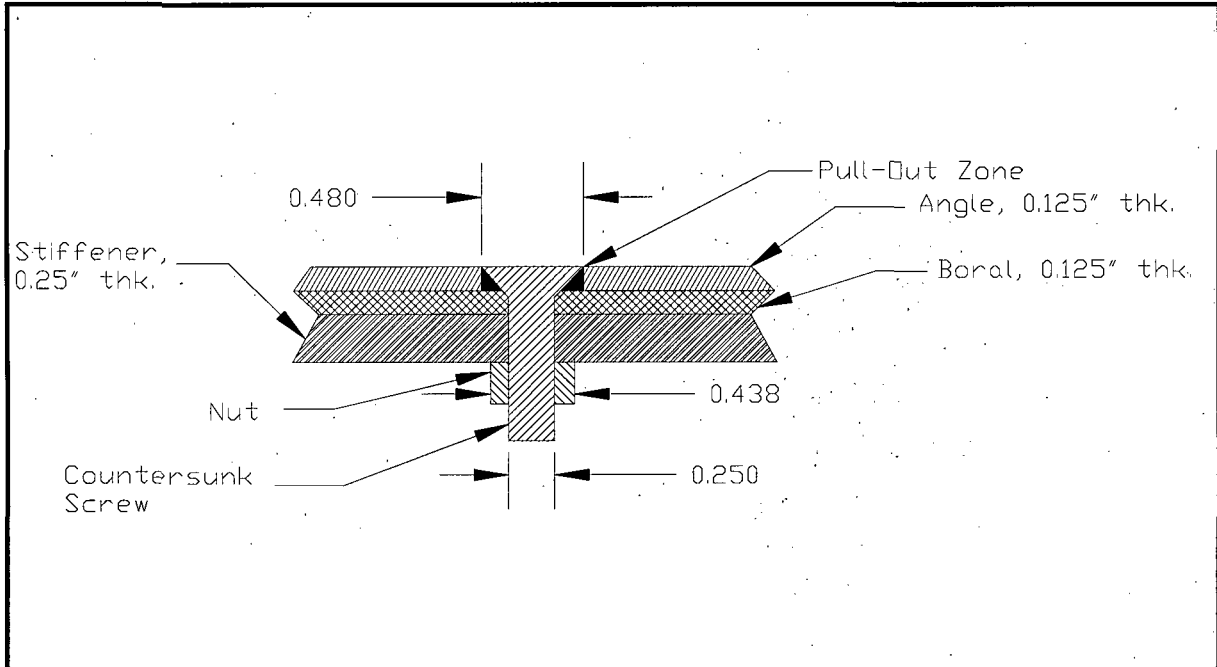


Figure 2.12.5-9 – Typical FCS Fastener Connection

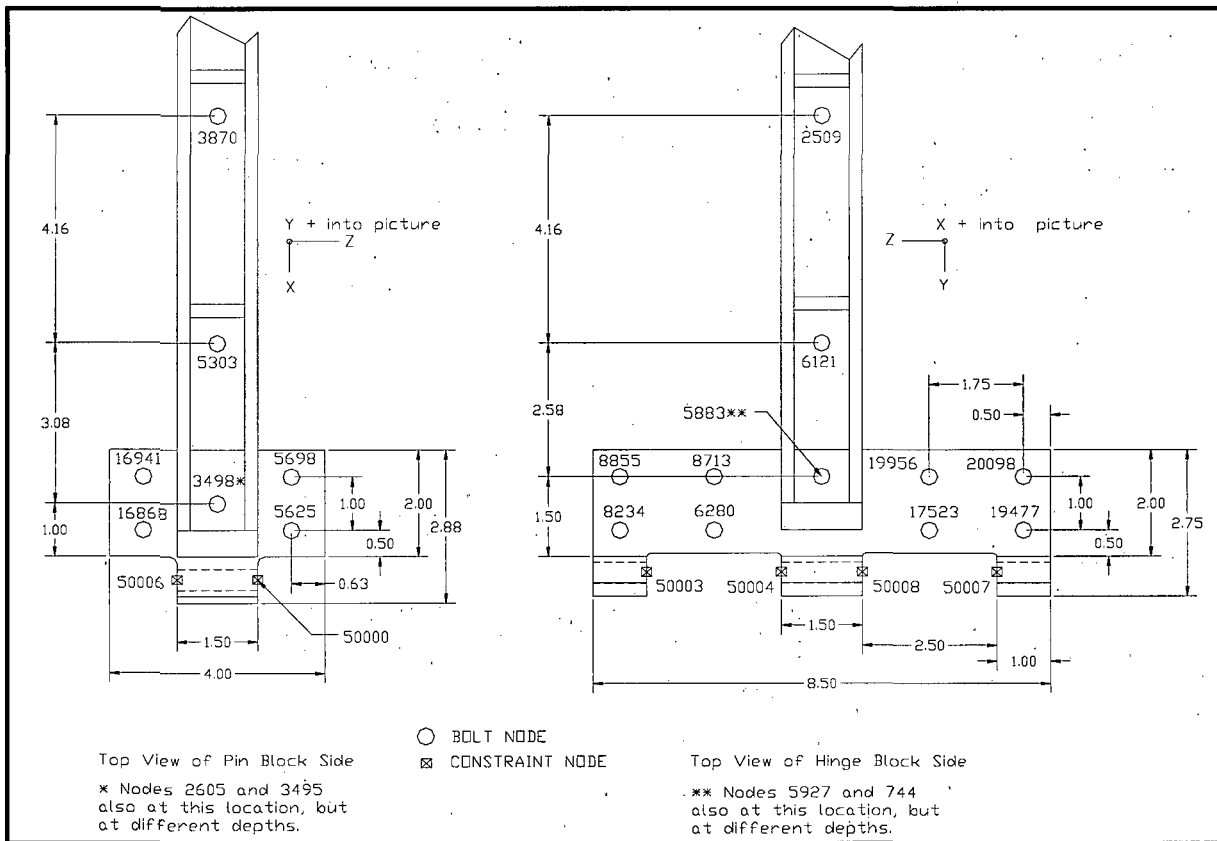


Figure 2.12.5-10 – Hinge and Pin Block Constraint and Bolt Locations

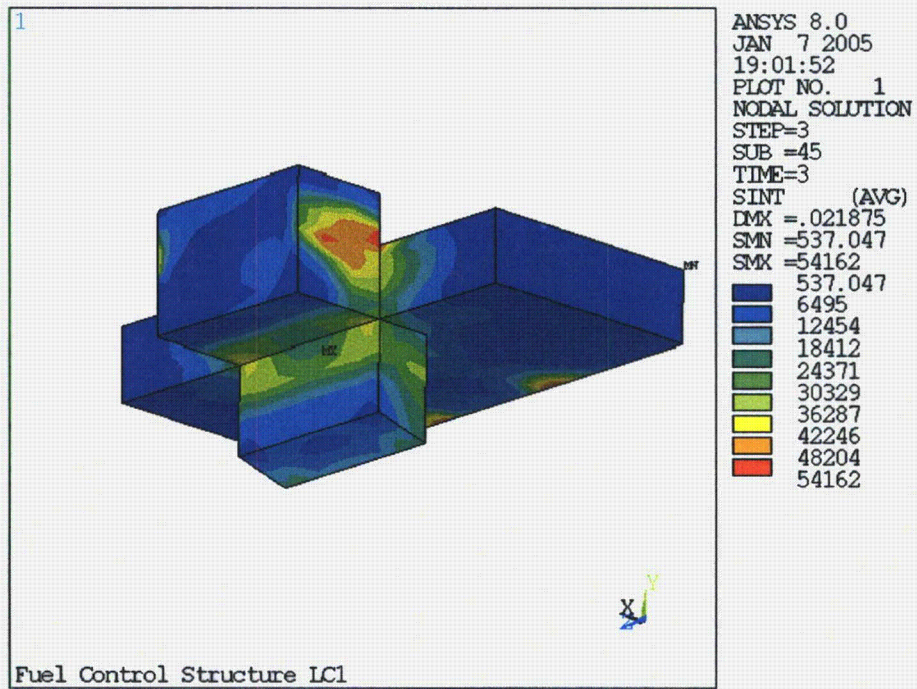


Figure 2.12.5-11 – LC1 Pin Block Stress Intensity

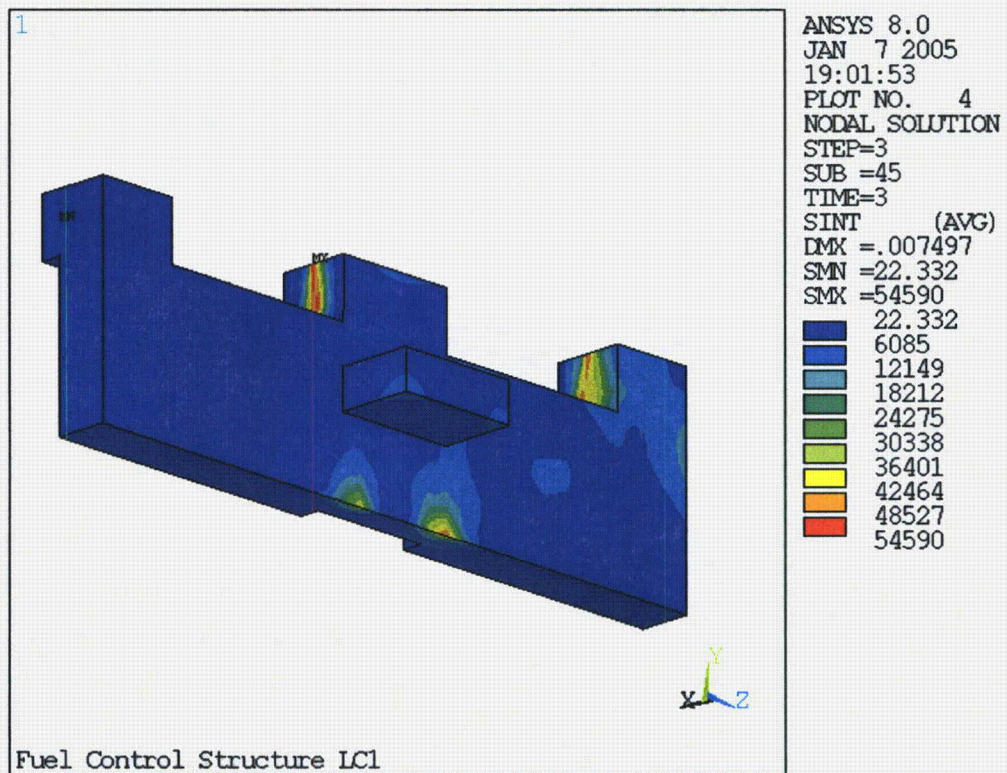


Figure 2.12.5-12 – LC1 Hinge Block Stress Intensity

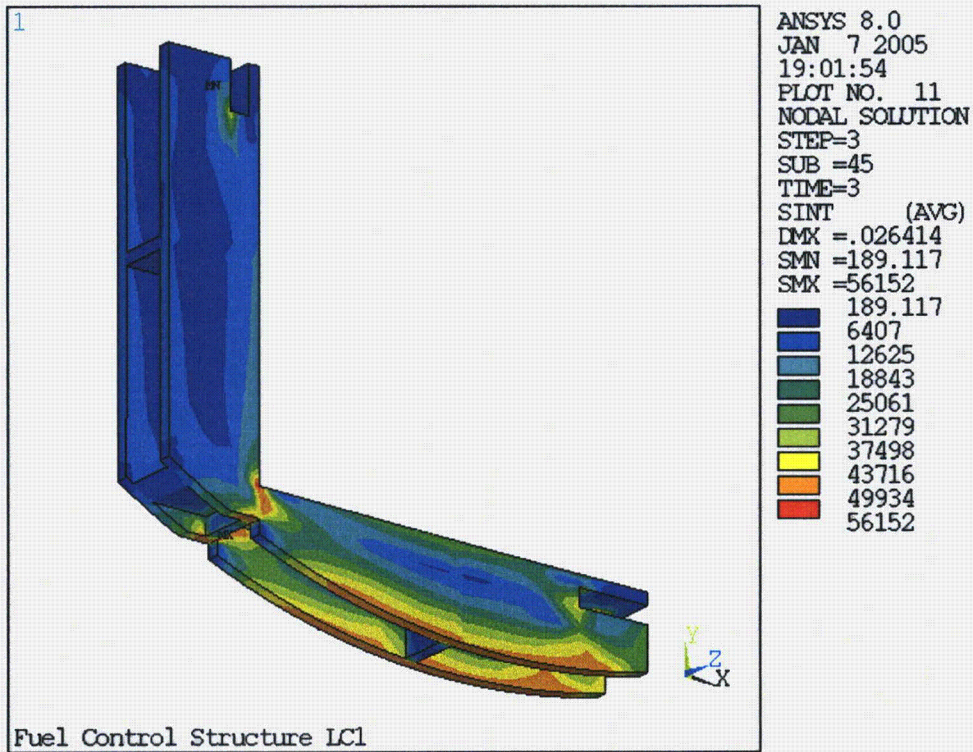


Figure 2.12.5-13 – LC1 Stiffener Stress Intensity

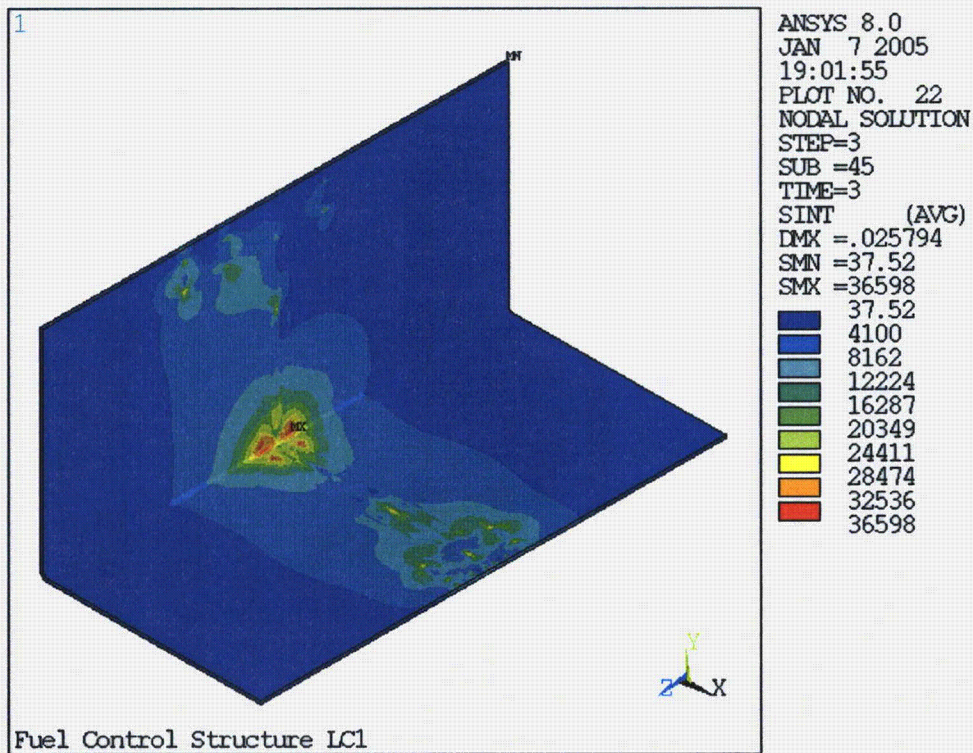


Figure 2.12.5-14 – LC1 Angle Stress Intensity

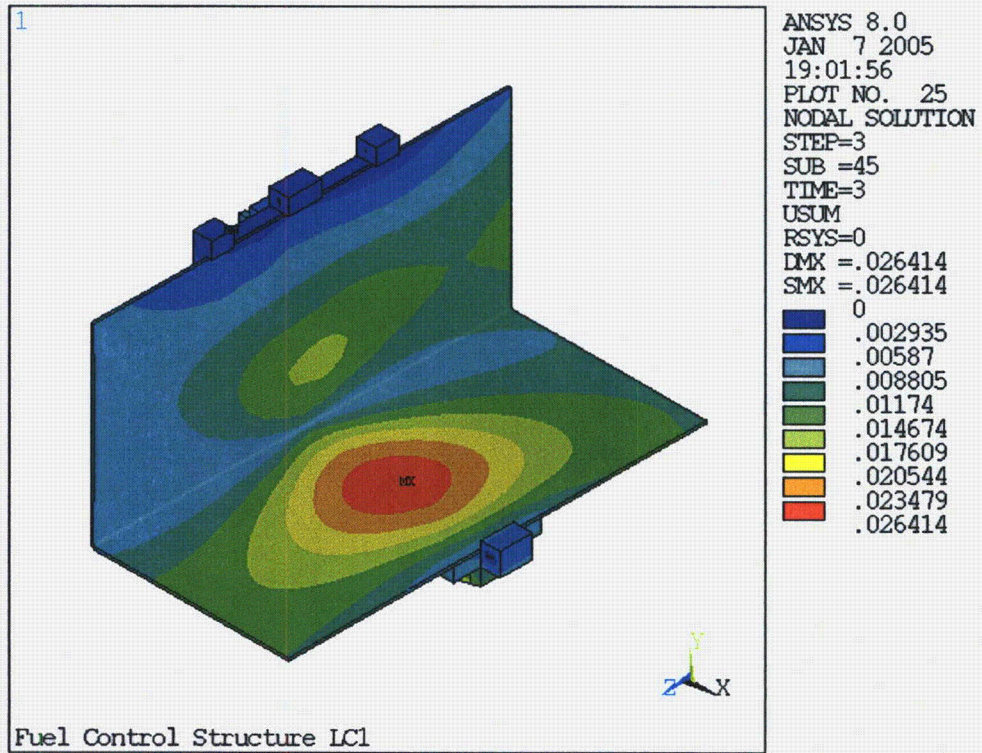


Figure 2.12.5-15 – LC1 Total Displacement

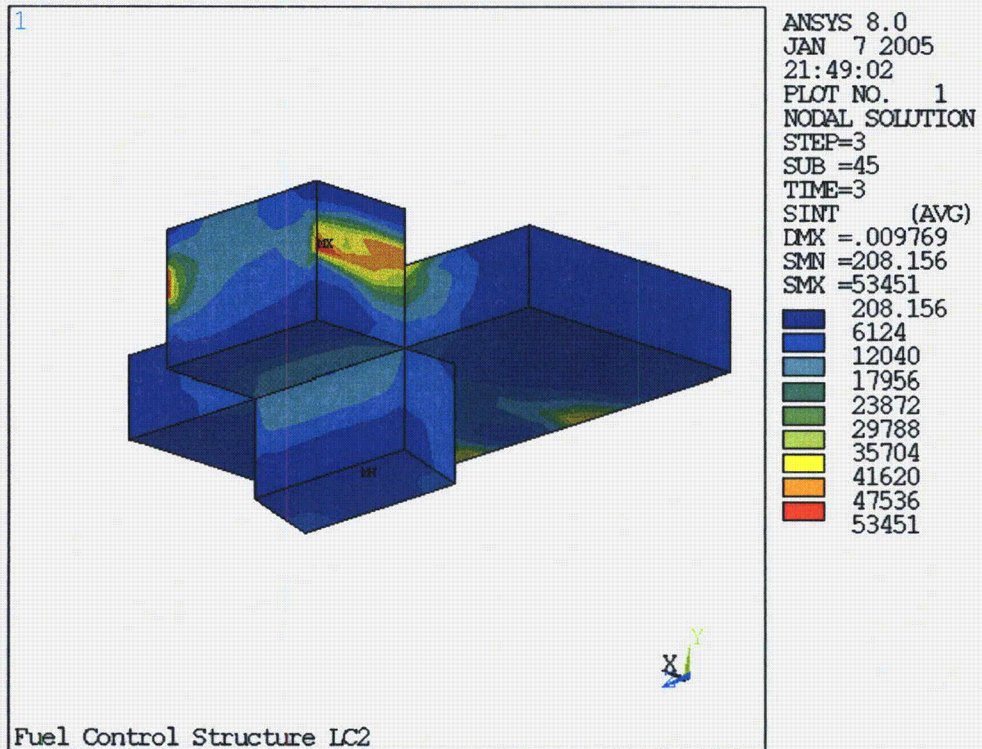


Figure 2.12.5-16 – LC2 Pin Block Stress Intensity

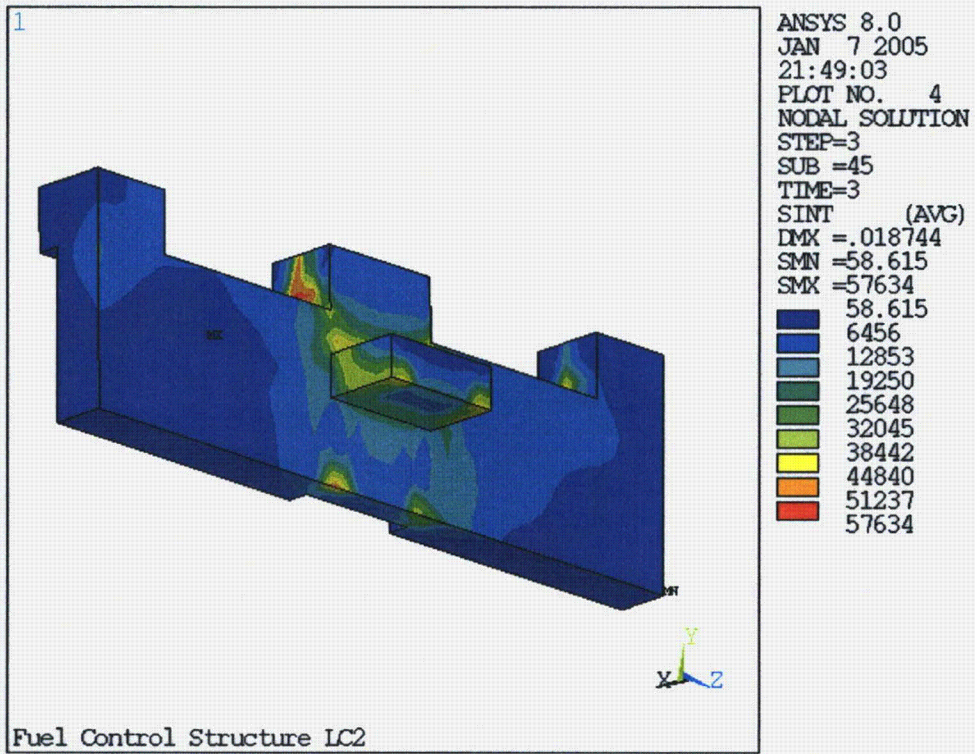


Figure 2.12.5-17 – LC2 Hinge Block Stress Intensity

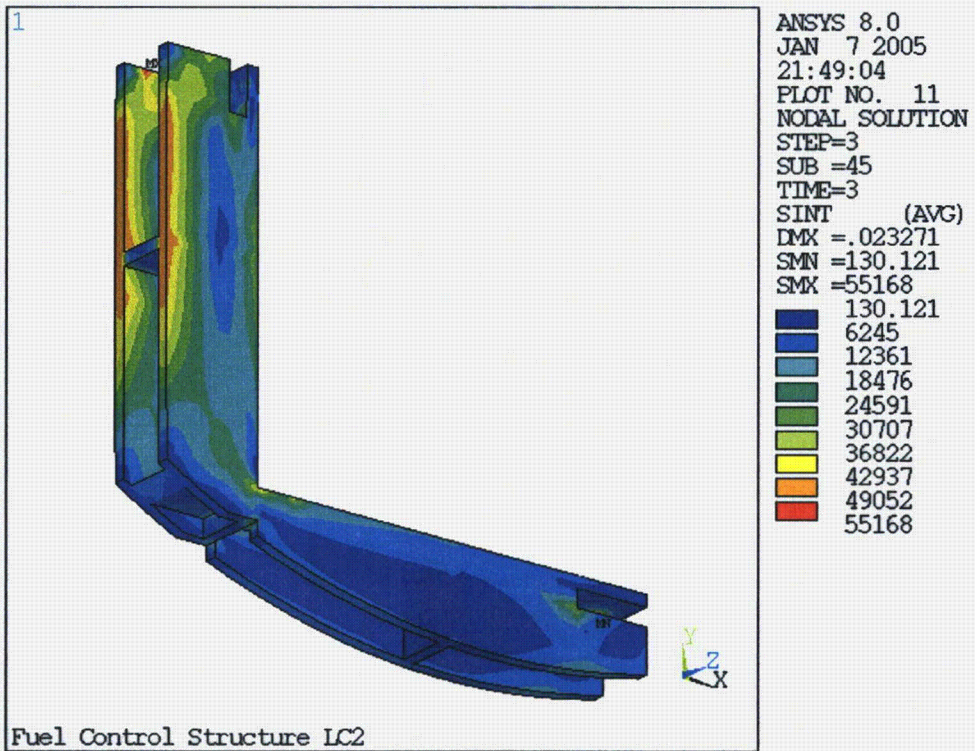


Figure 2.12.5-18 – LC2 Stiffener Stress Intensity

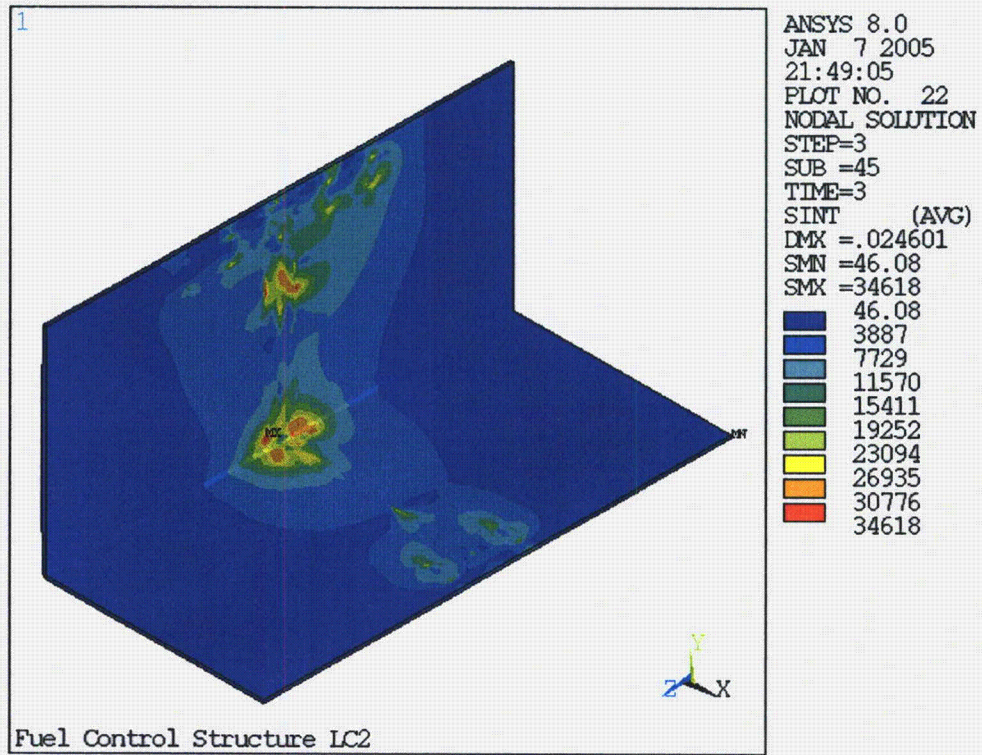


Figure 2.12.5-19 – LC2 Angle Stress Intensity

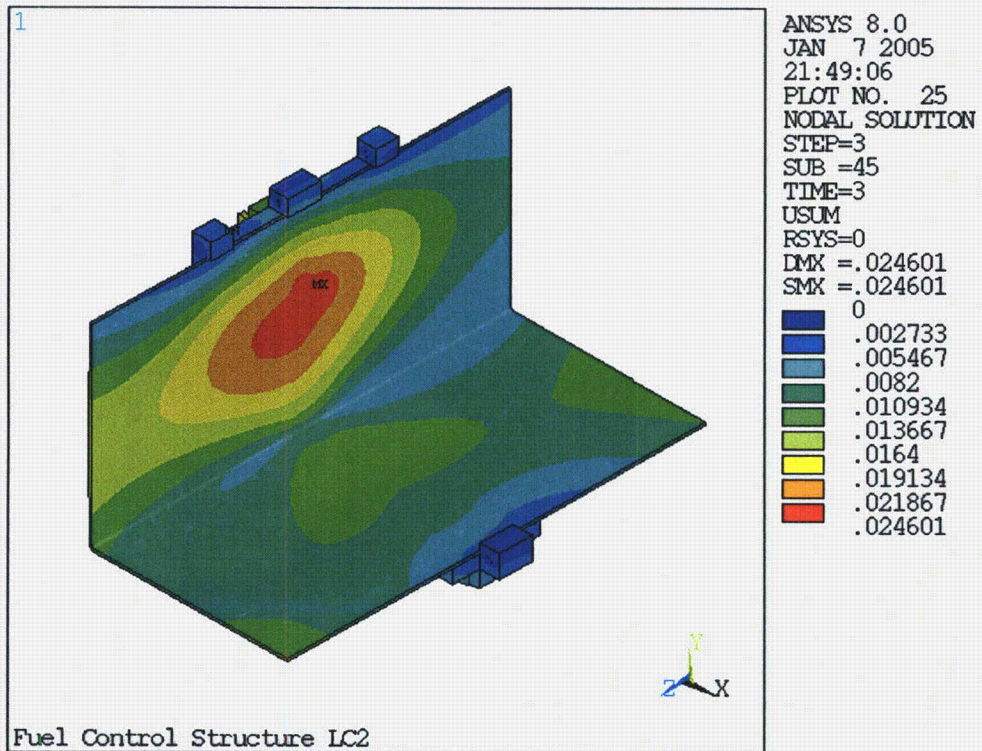


Figure 2.12.5-20 – LC2 Total Displacement

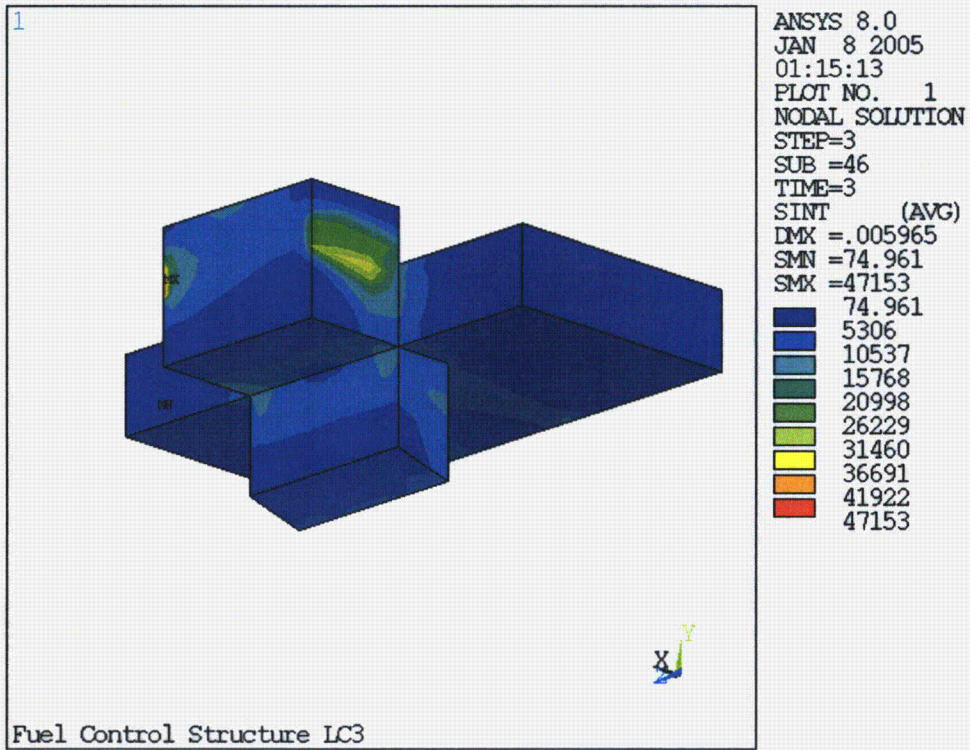


Figure 2.12.5-21 – LC3 Pin Block Stress Intensity

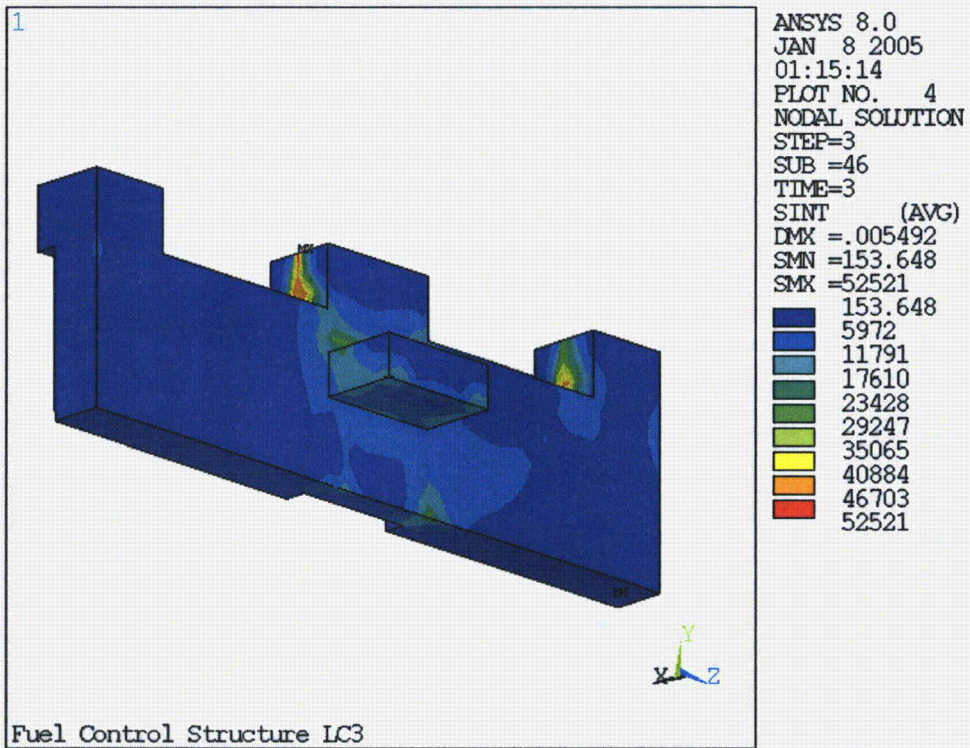


Figure 2.12.5-22 – LC3 Hinge Block Stress Intensity

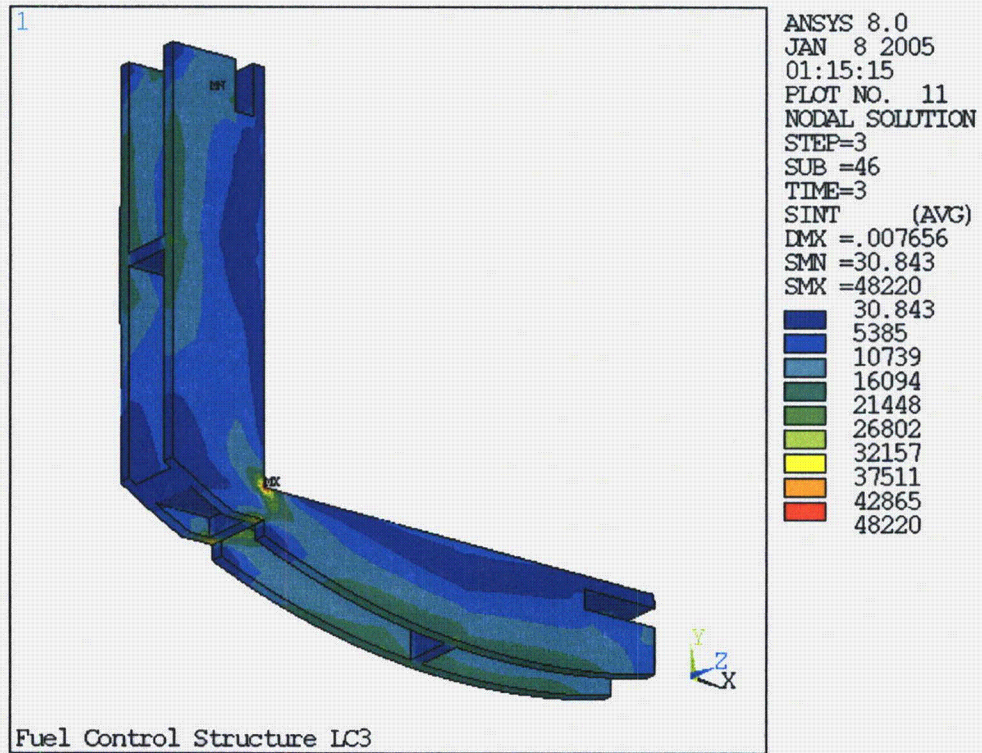


Figure 2.12.5-23 – LC3 Stiffener Stress Intensity

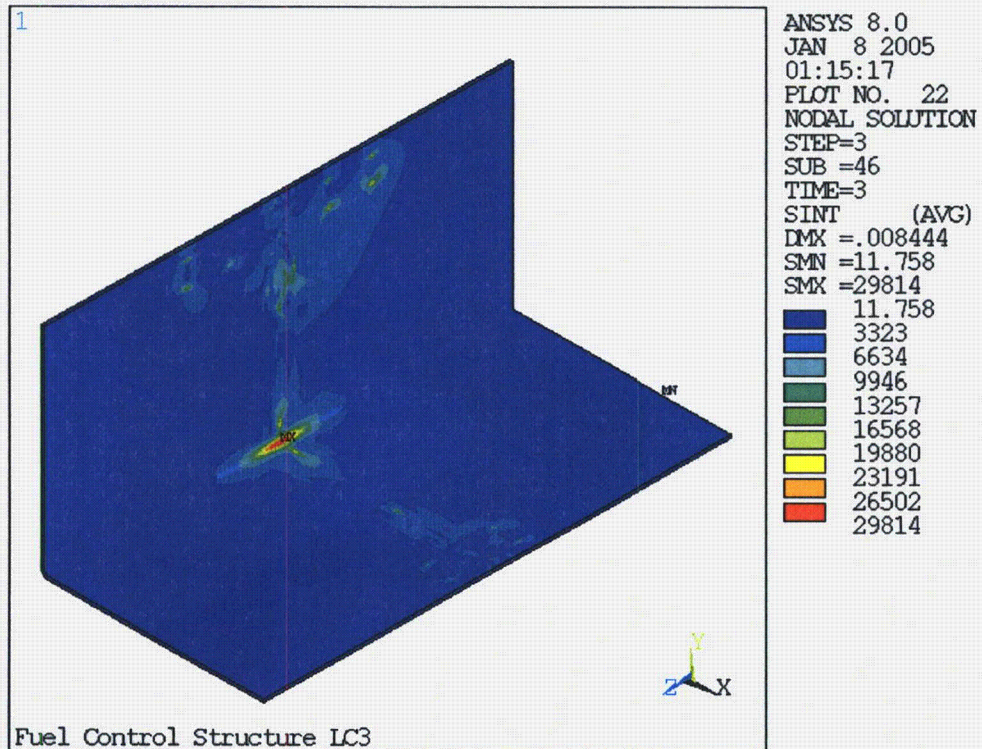


Figure 2.12.5-24 – LC3 Angle Stress Intensity

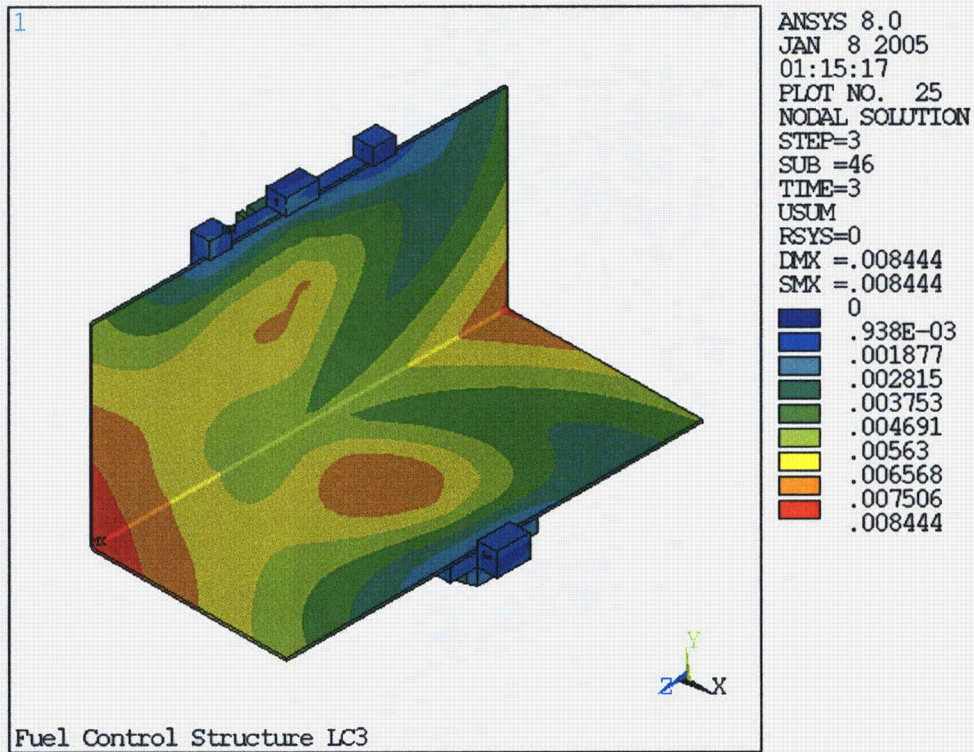


Figure 2.12.5-25 – LC3 Total Displacement

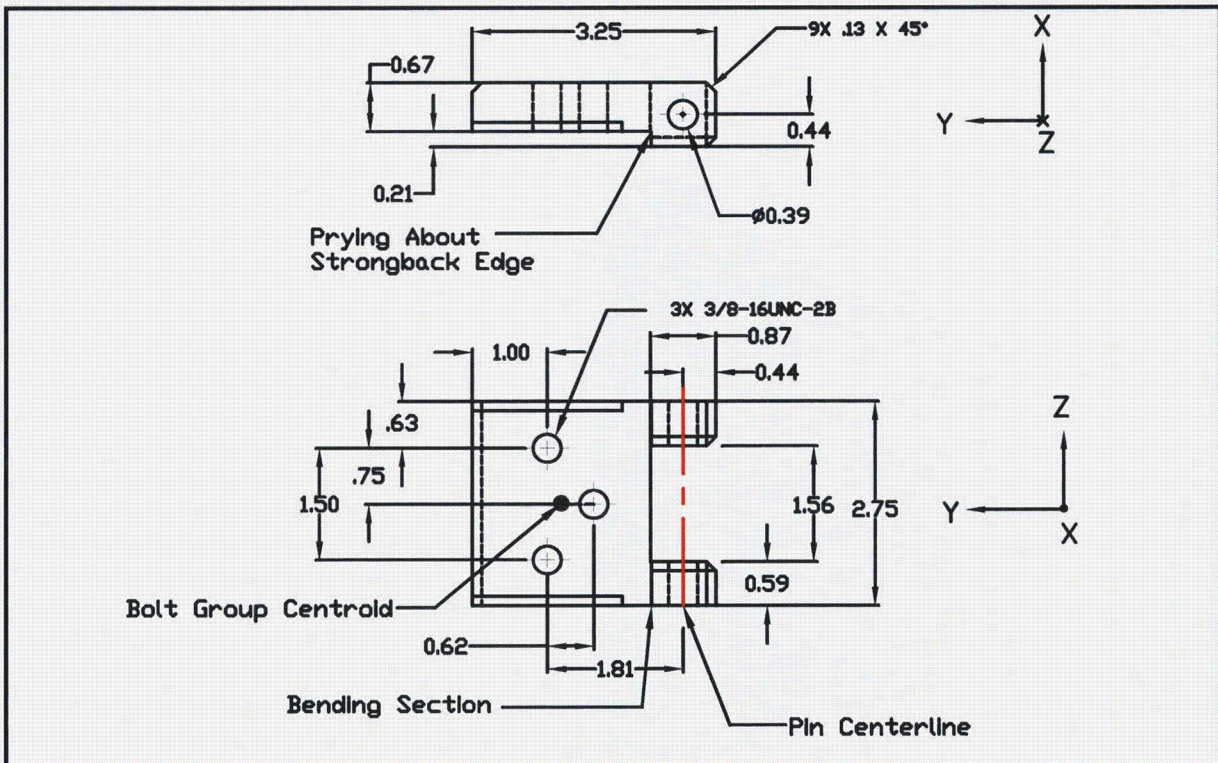


Figure 2.12.5-26 – Lock Plate Details

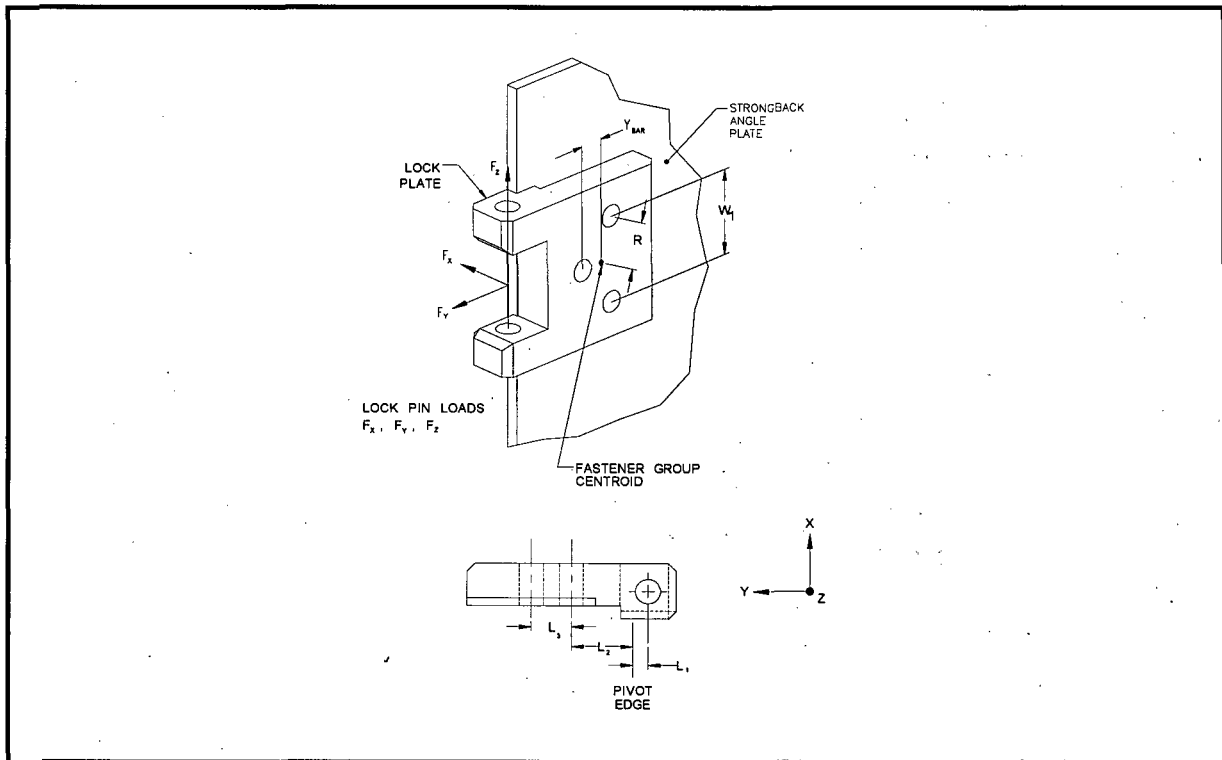


Figure 2.12.5-27 – Lock Plate (Refer to Figure 2.12.5-26 for Dimensions)

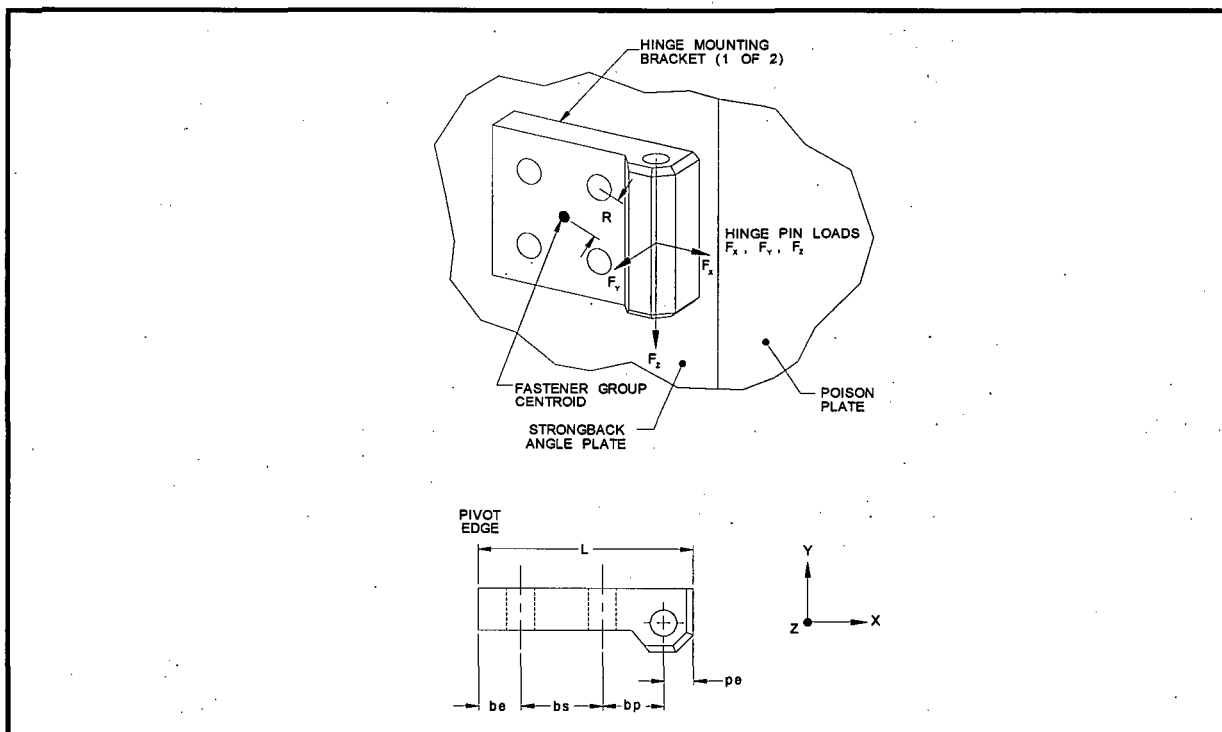


Figure 2.12.5-28 – Hinge Mounting Bracket (Refer to Figure 2.12.5-29 for Dimensions)

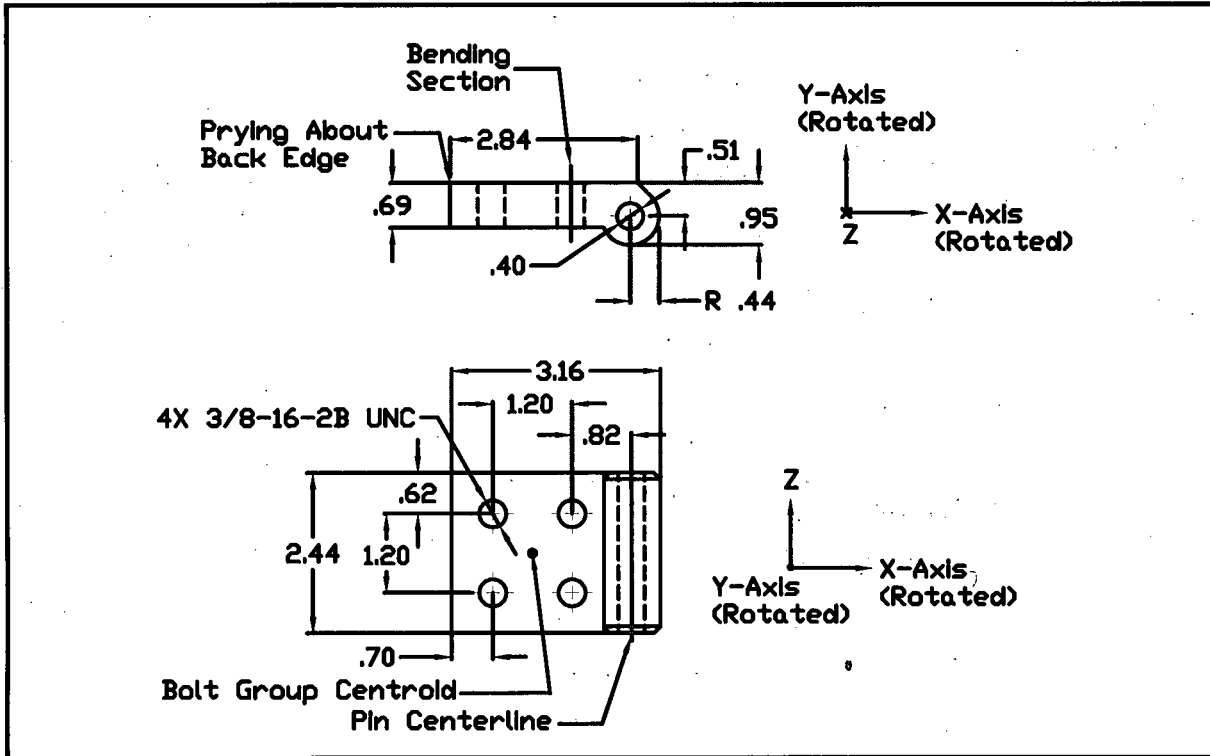


Figure 2.12.5-29 – Hinge Mounting Bracket

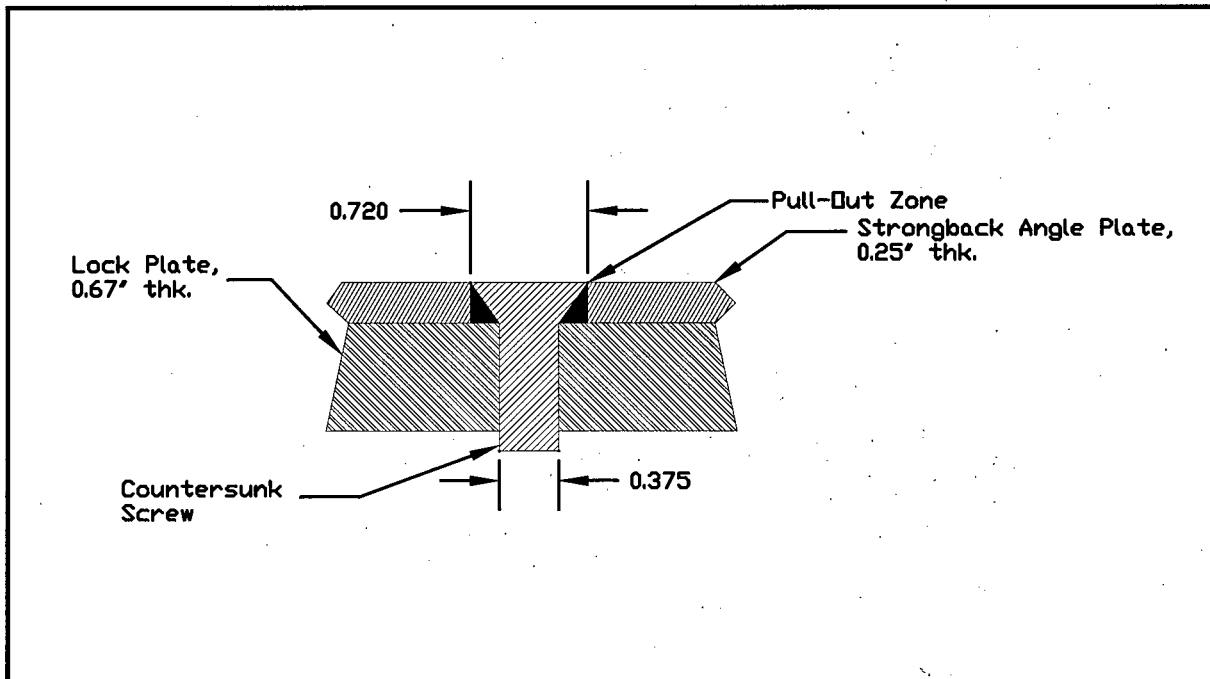


Figure 2.12.5-30 – Typical FCS Fastener Connection to Strongback

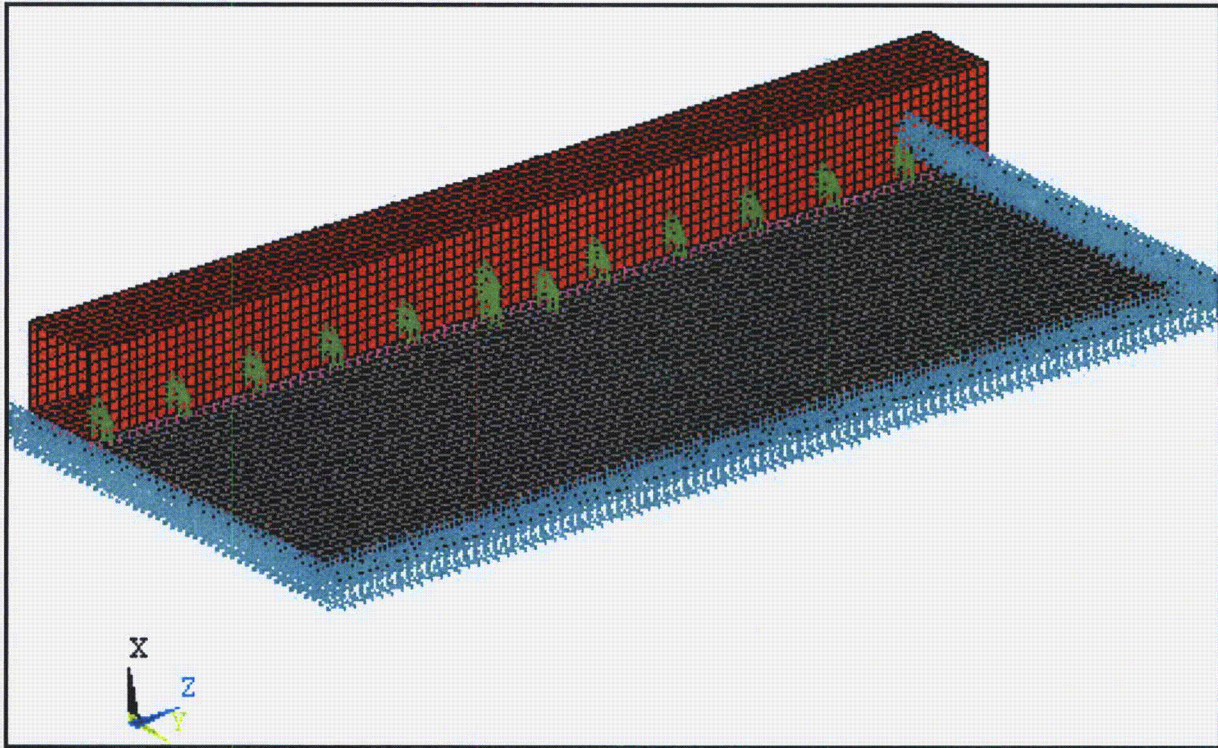


Figure 2.12.5-31 – Plate Angle Model for FCS Loads (w/ Boundary Conditions)

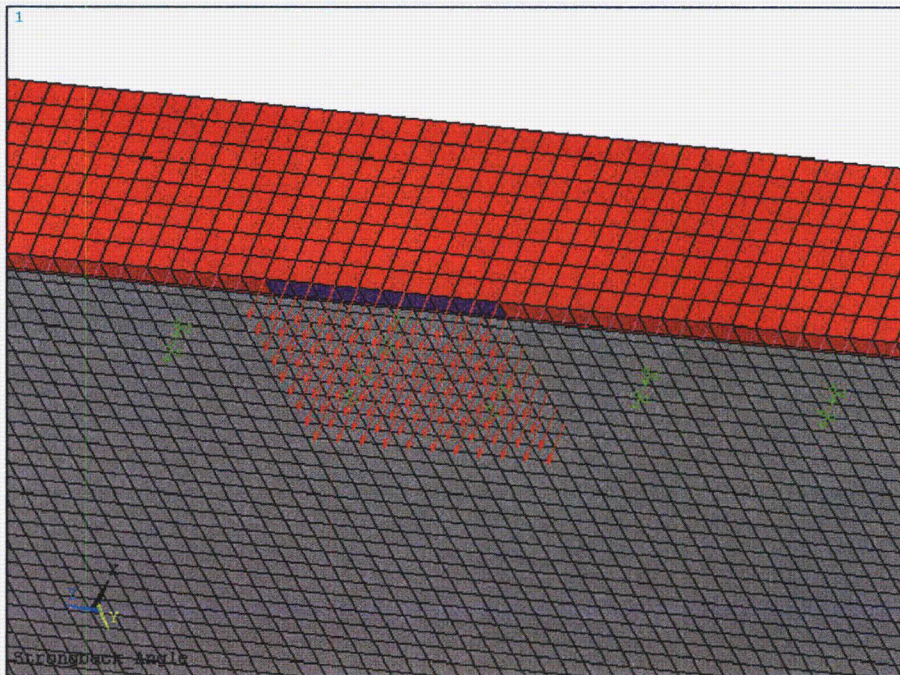
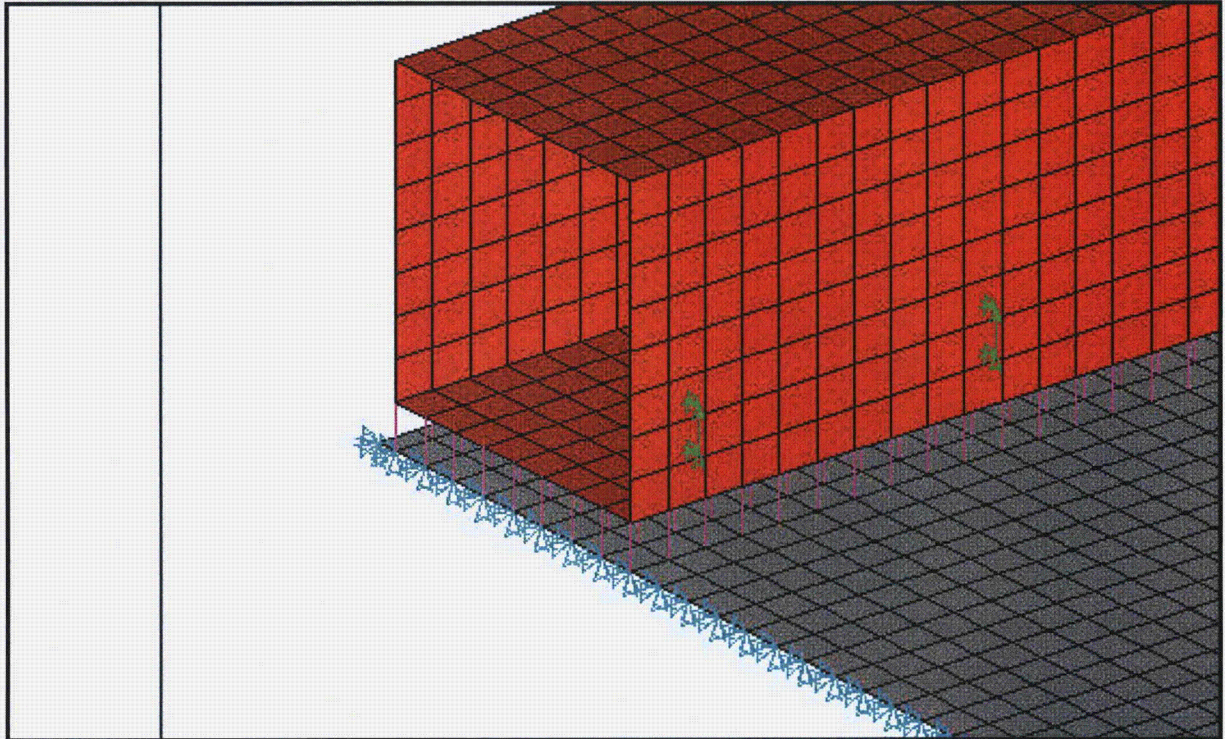
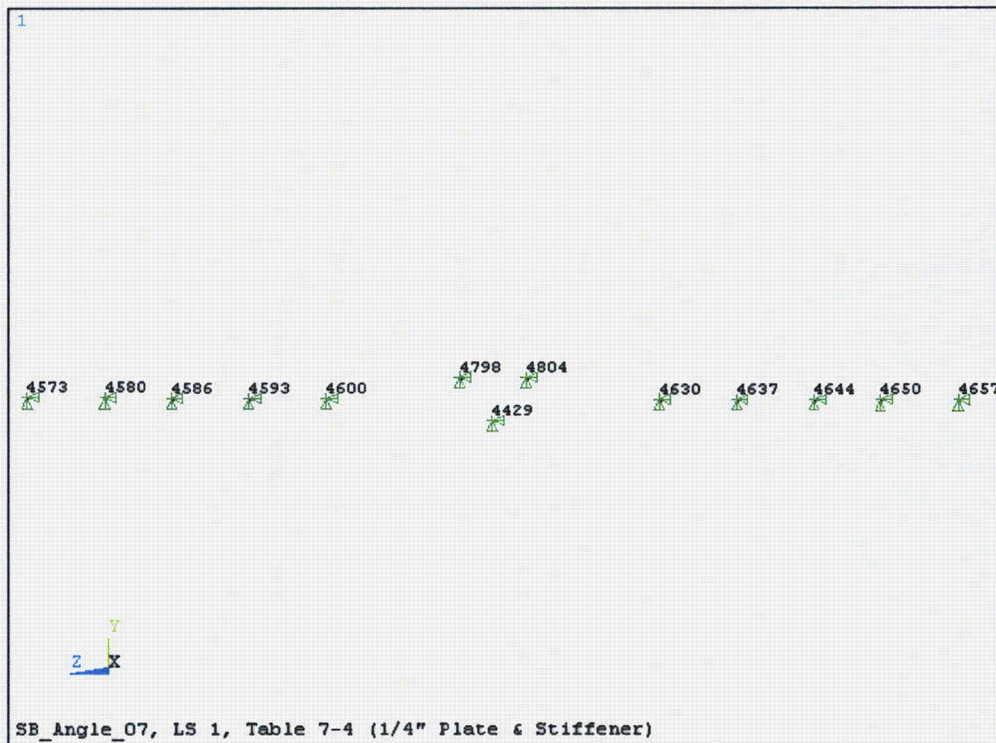


Figure 2.12.5-32 – Plate Angle Model for FCS Loads (Bottom View Showing “Thick” Section Where Loads Are Applied)



**Figure 2.12.5-33** – Plate Angle Model for FCS Loads (Close-Up Showing Contact52 Elements Between Tube And Plate)



**Figure 2.12.5-34** – Fastener Locations and Node Point IDs (Long FCS)

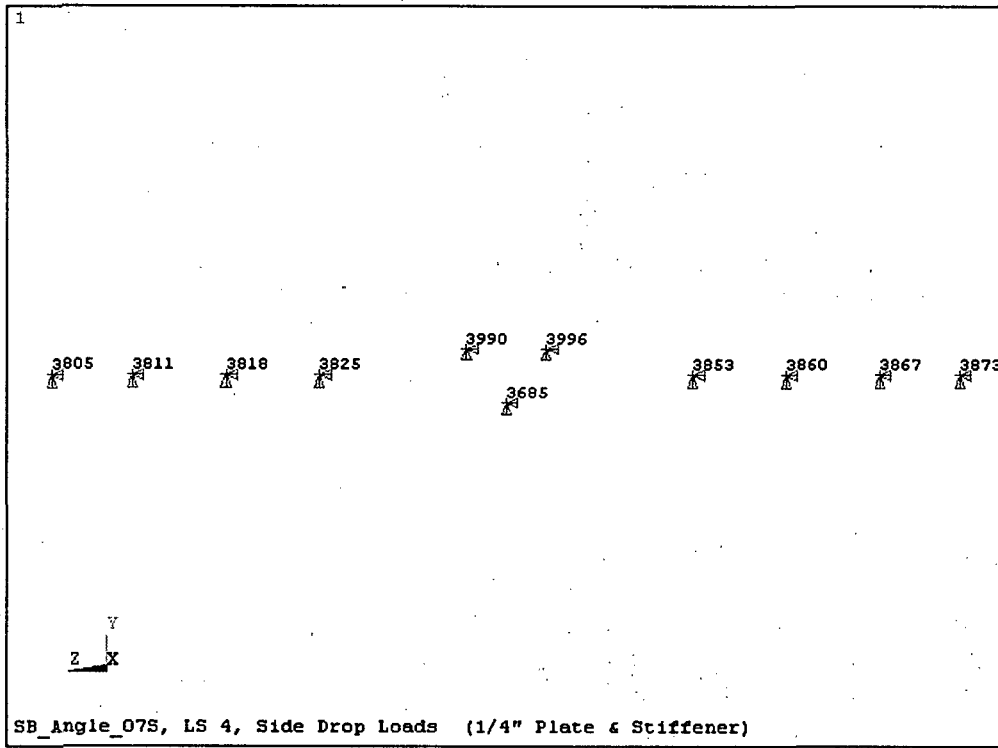


**Figure 2.12.5-35 – Fastener Locations and Node Point IDs (Standard FCS)**

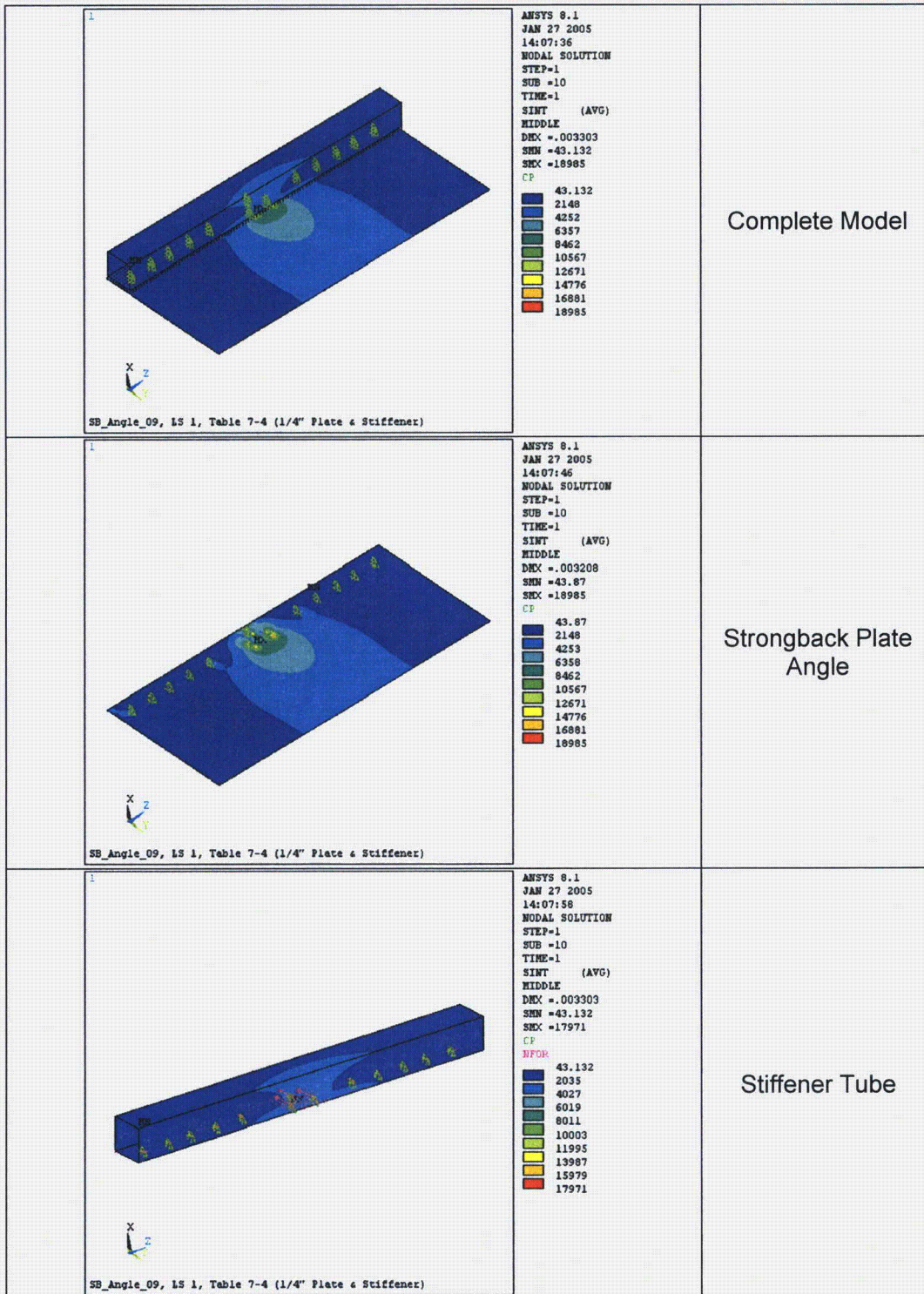


Figure 2.12.5-36 – Mid-thickness Stresses in Plate Angle Under Pin Block Load Case 1

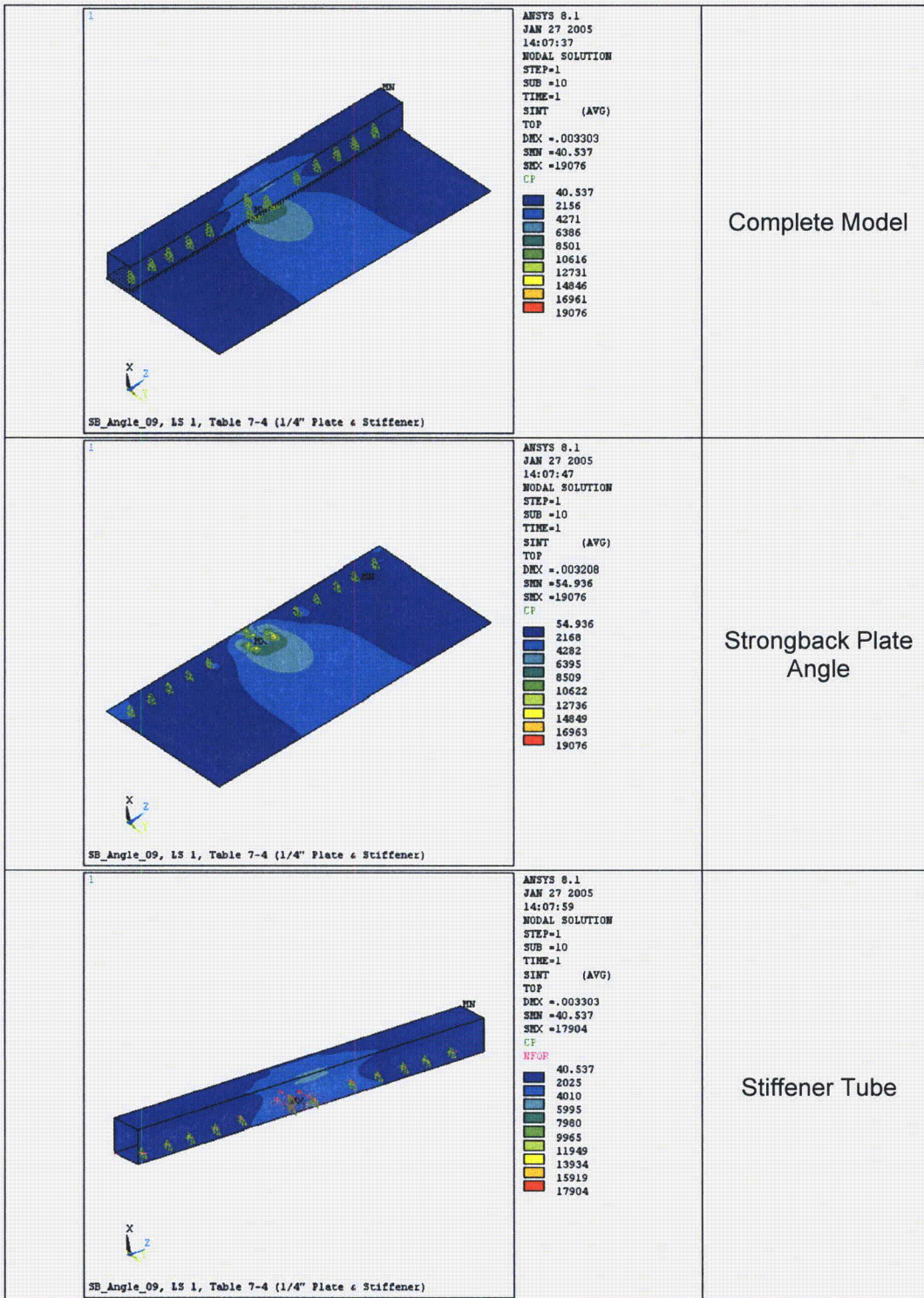


Figure 2.12.5-37 –Top Surface Stresses in Plate Angle Under Pin Block Load Case 1

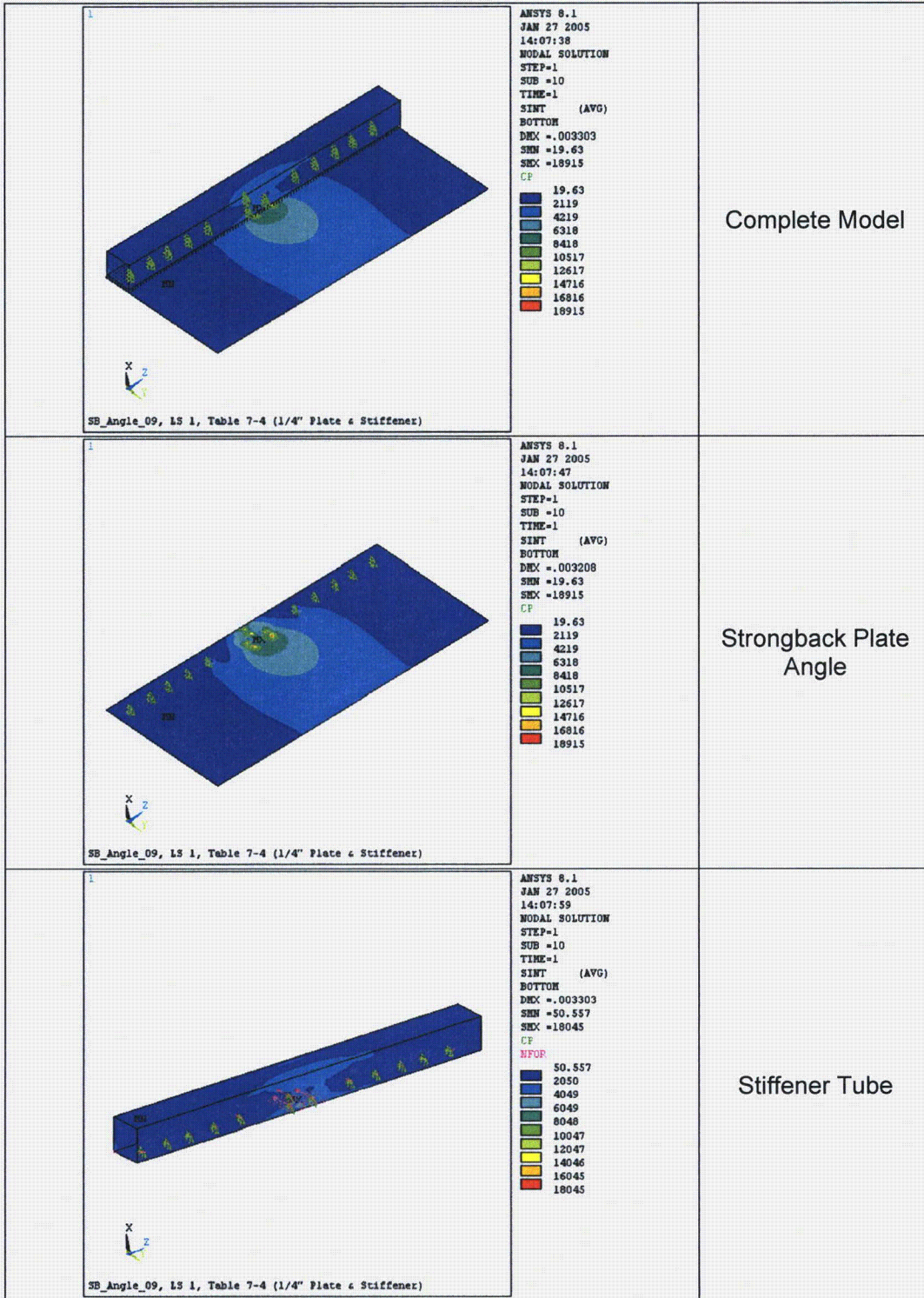


Figure 2.12.5-38 –Bottom Surface Stresses in Plate Angle Under Pin Block Load Case 1

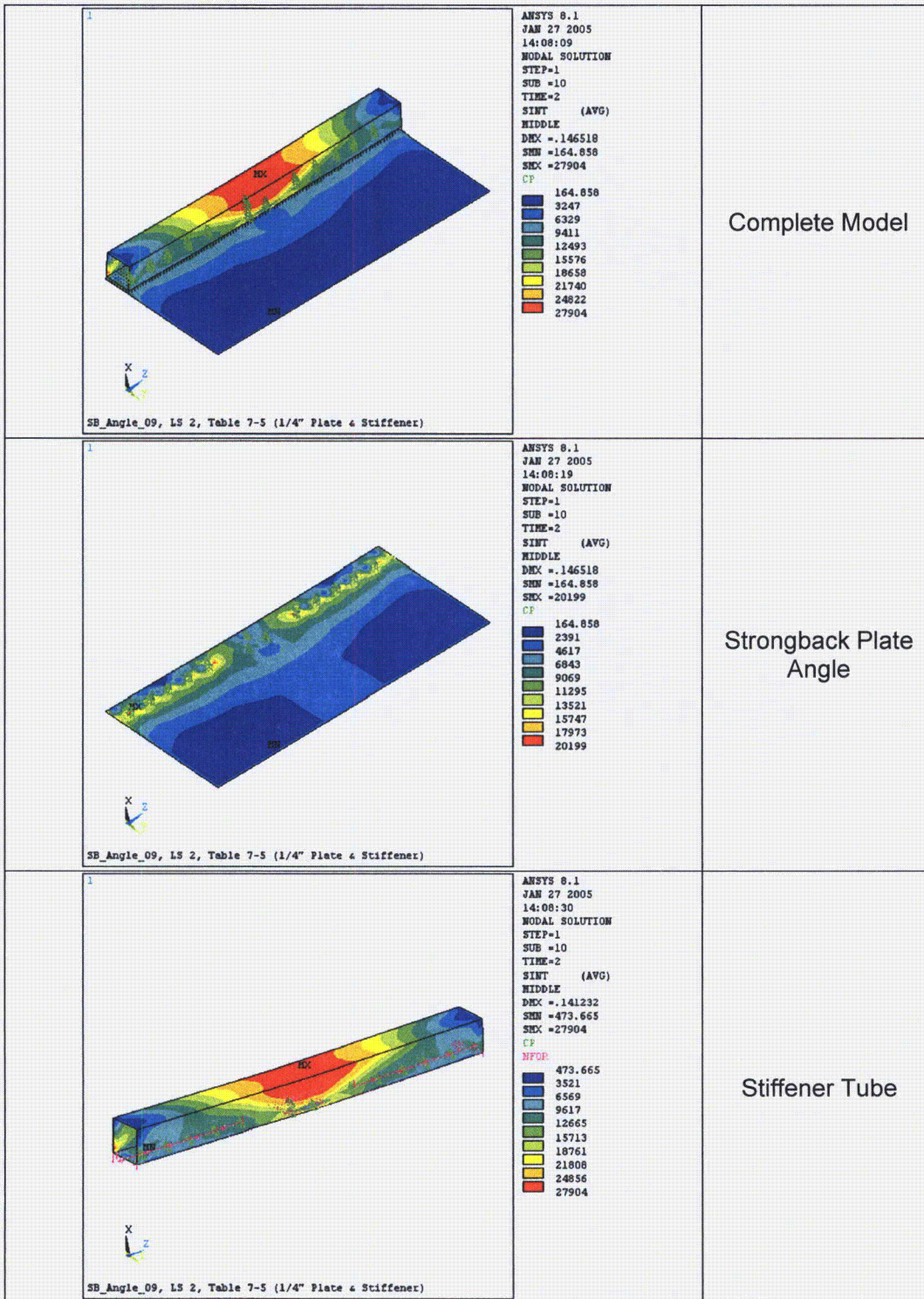


Figure 2.12.5-39 – Mid-thickness Stresses in Plate Angle Under Pin Block Load Case 2

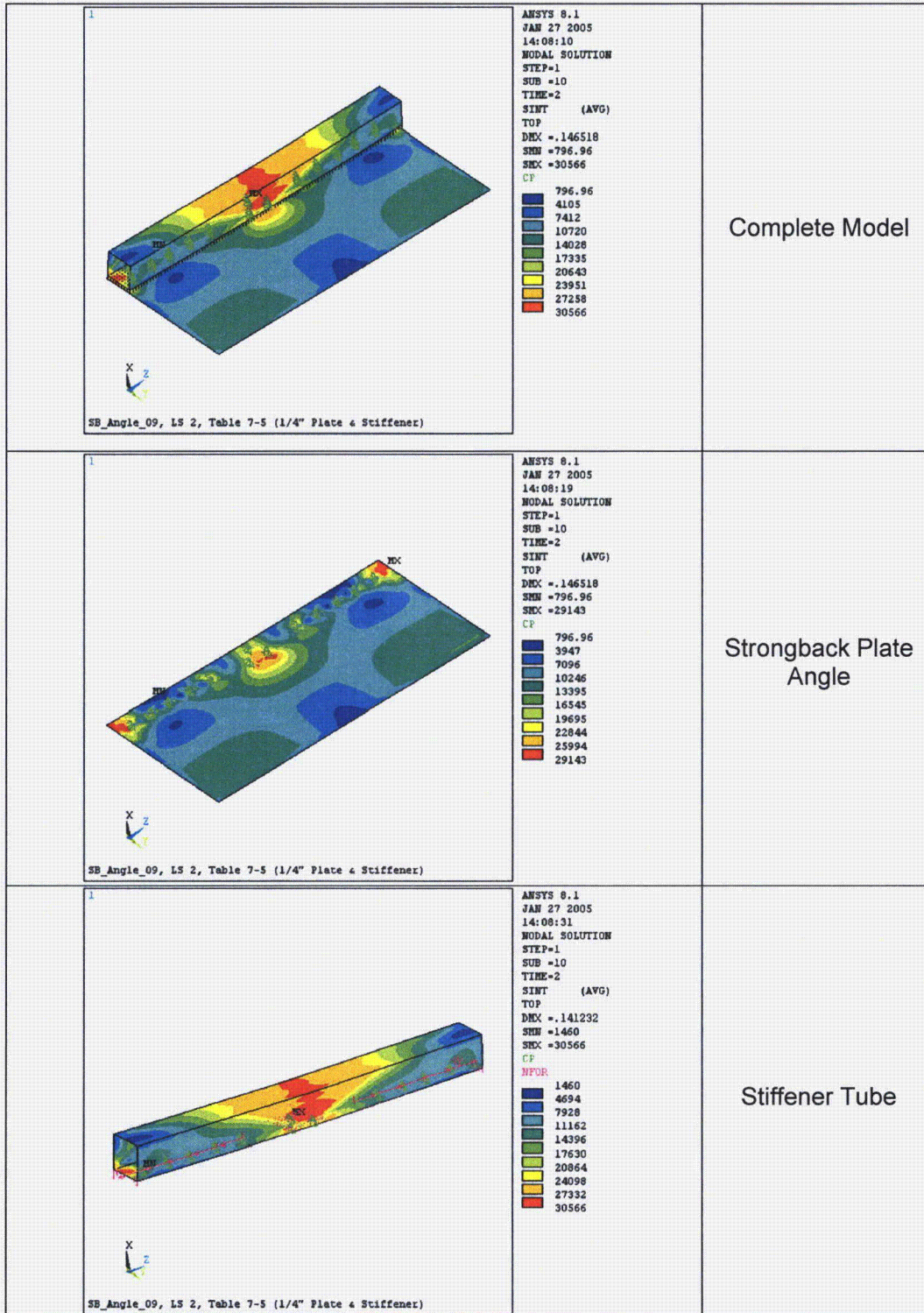


Figure 2.12.5-40 – Top Surface Stresses in Plate Angle Under Pin Block Load Case 2

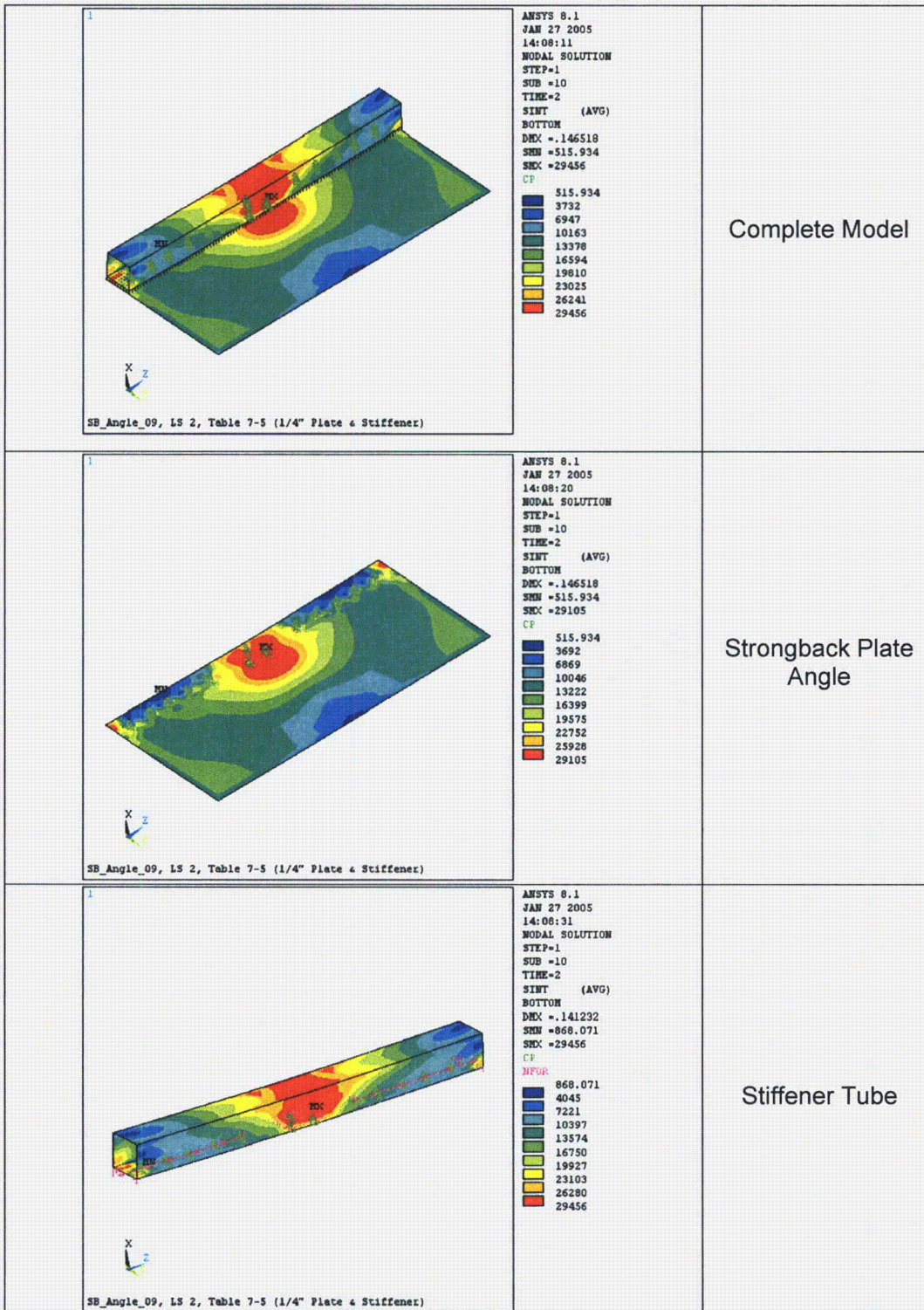


Figure 2.12.5-41 – Bottom Surface Stresses in Plate Angle Under Pin Block Load Case 2

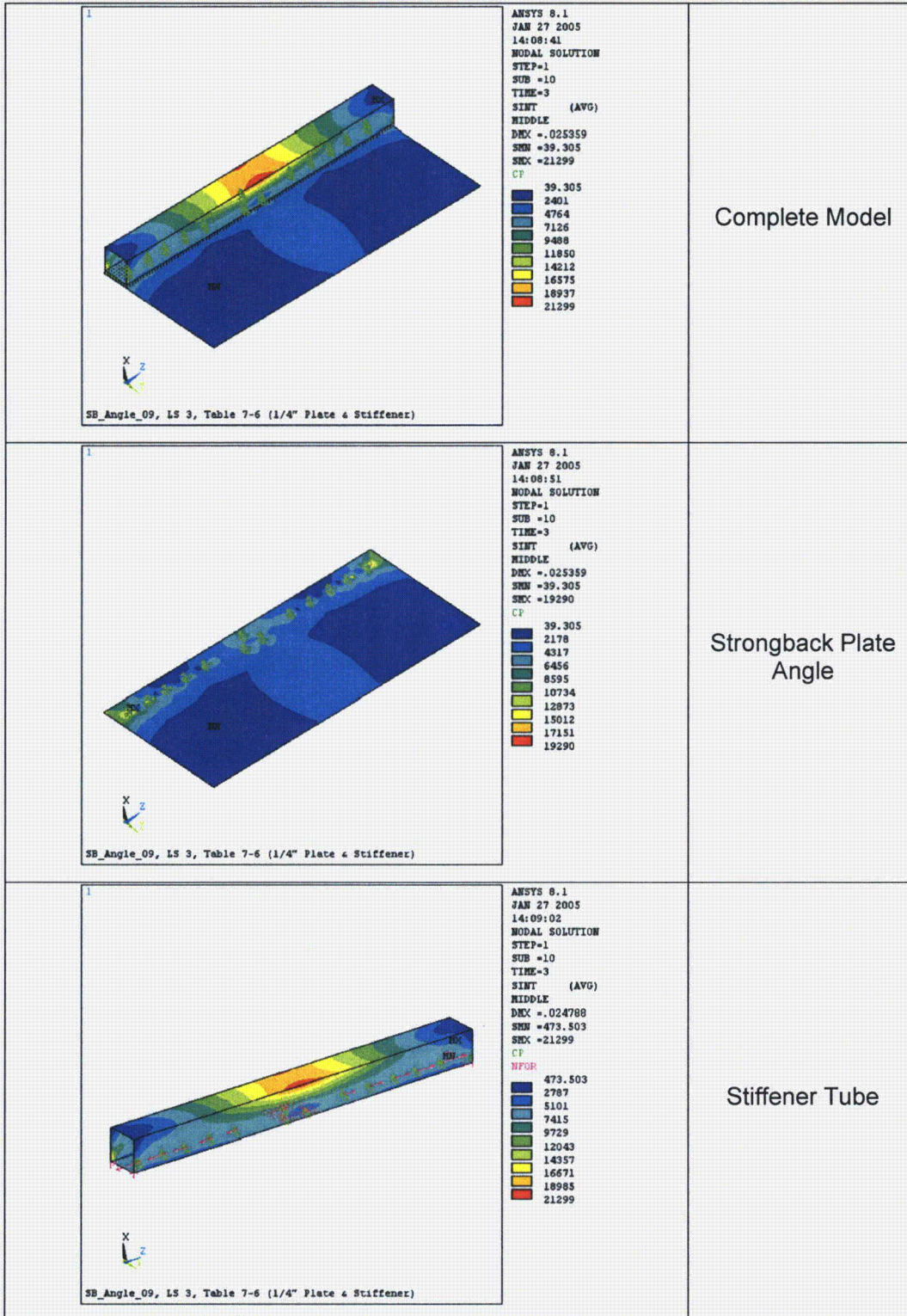


Figure 2.12.5-42 – Mid-thickness Stresses in Plate Angle Under Pin Block Load Case 3

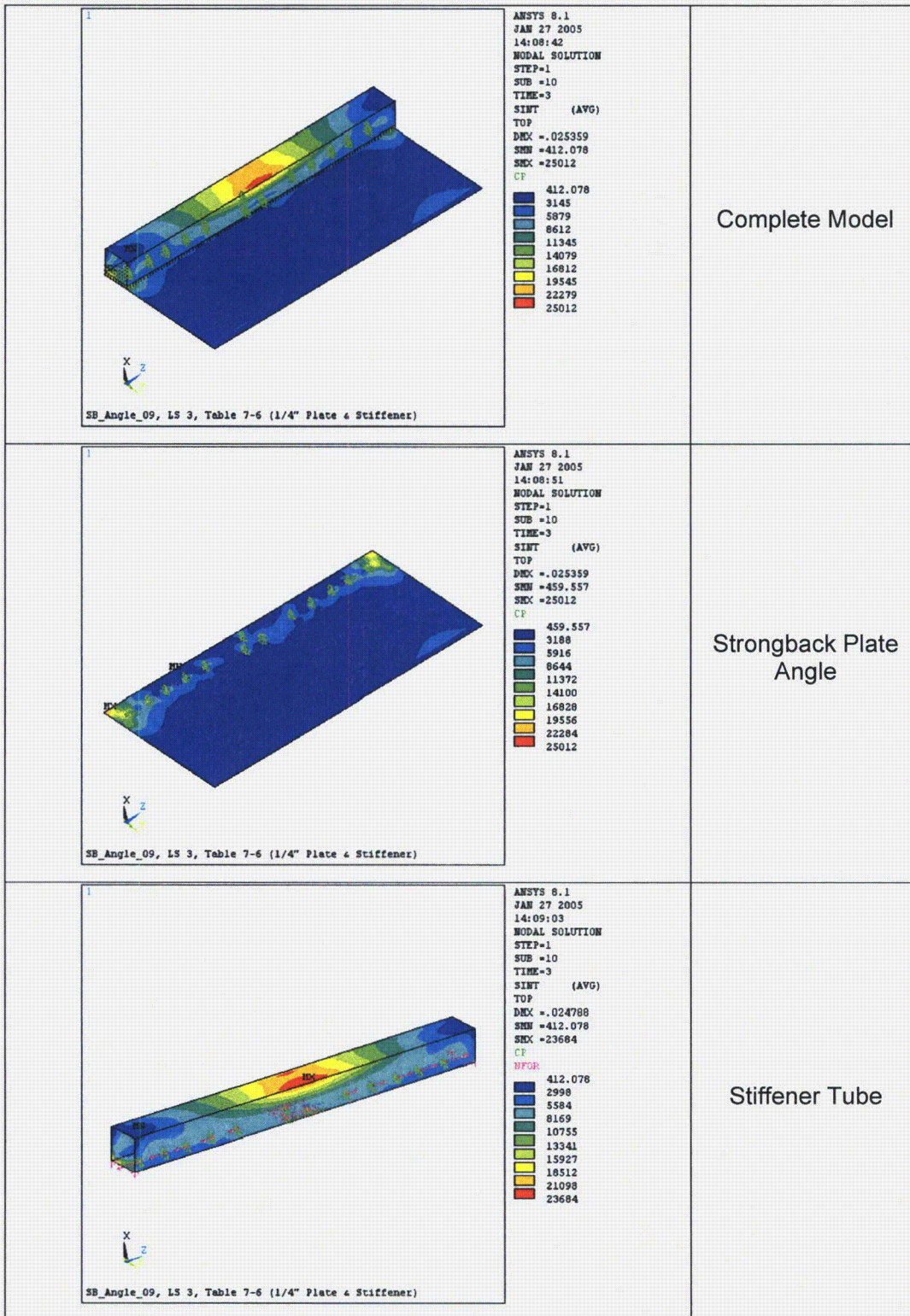


Figure 2.12.5-43 – Top Surface Stresses in Plate Angle Under Pin Block Load Case 3

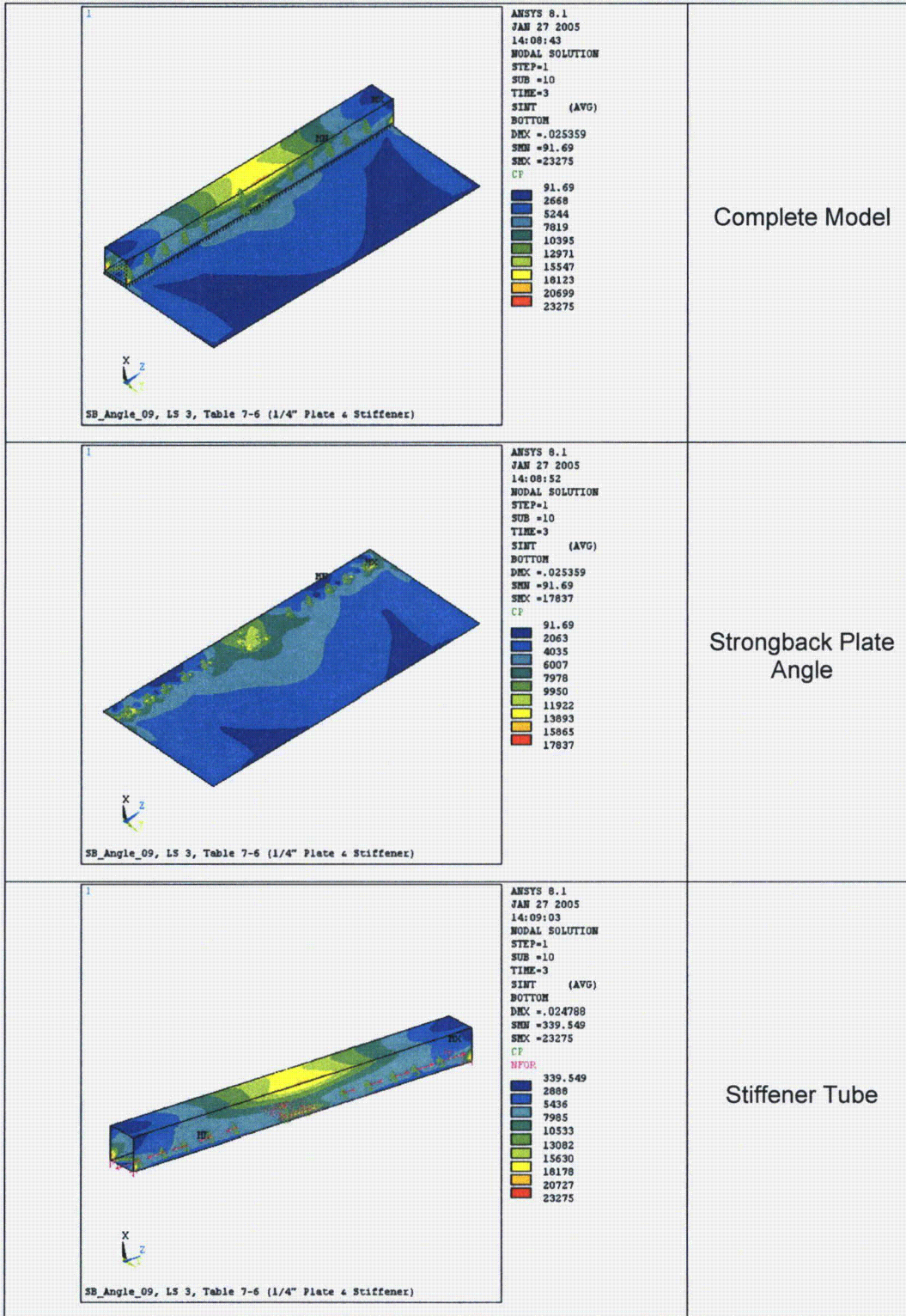


Figure 2.12.5-44 – Bottom Surface Stresses in Plate Angle Under Pin Block Load Case 3

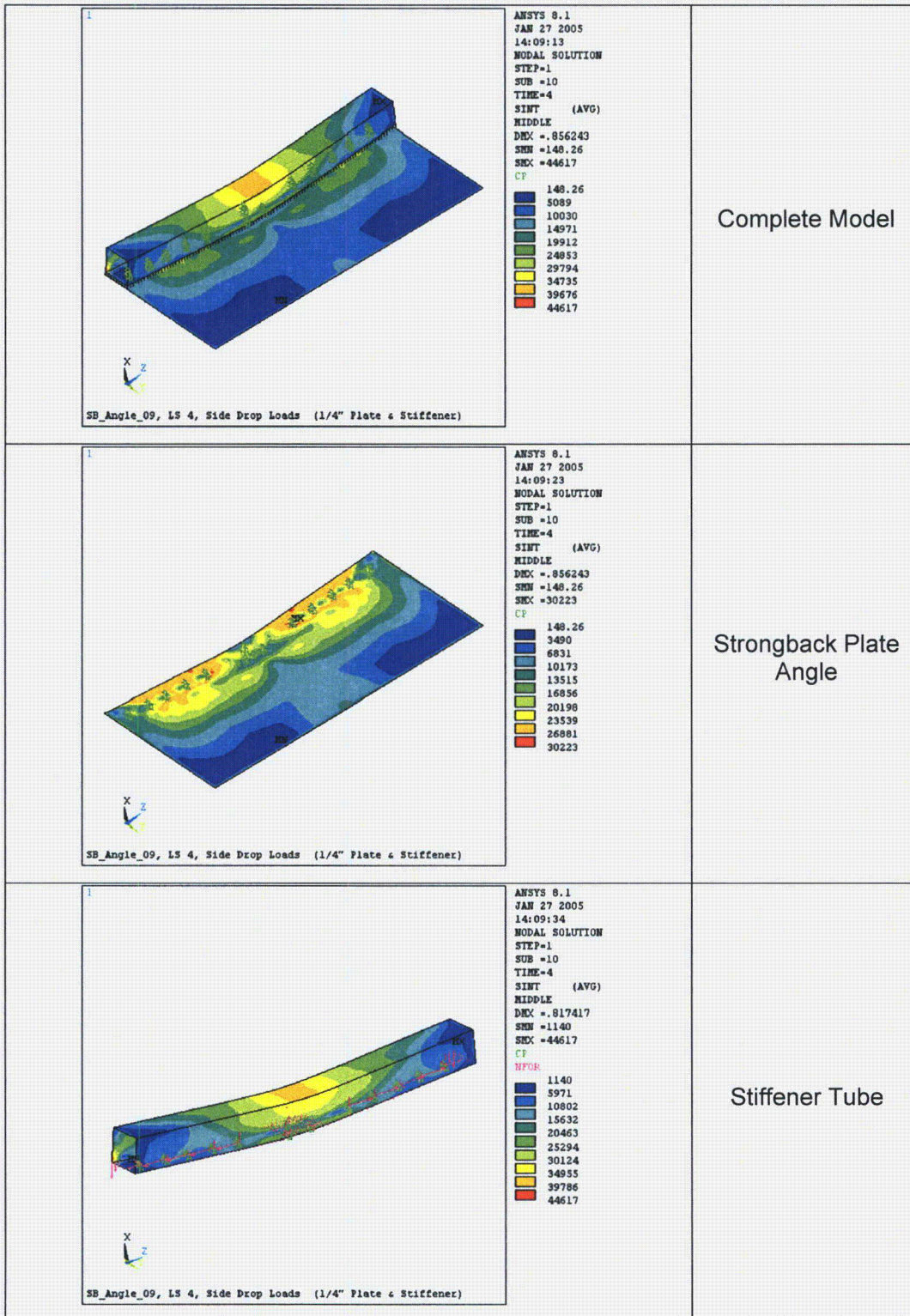


Figure 2.12.5-45 – Mid-thickness Stresses in Plate 20.6-inch Angle Under Pin Block Load Case 4

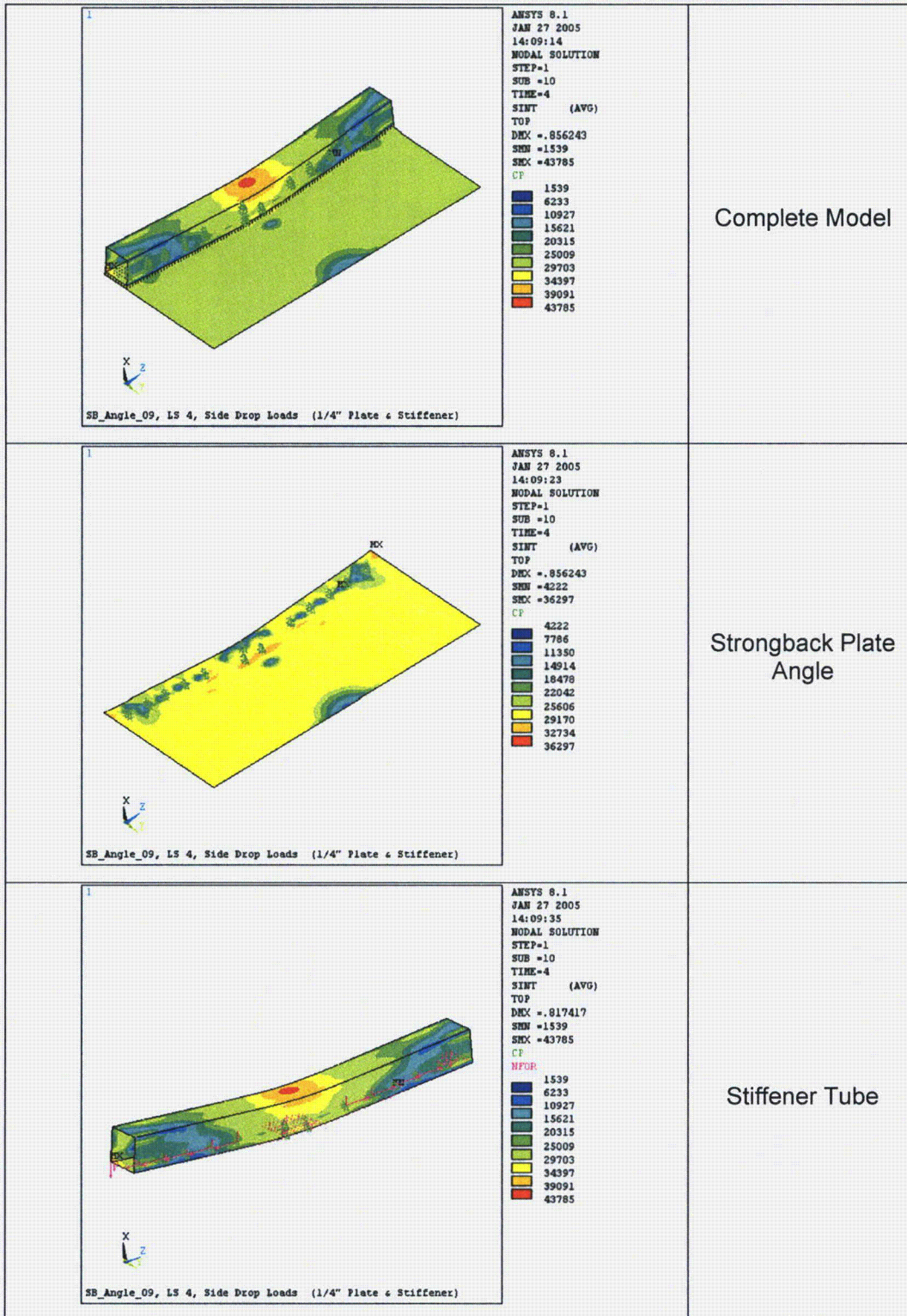


Figure 2.12.5-46 – Top Surface Stresses in 20.6-inch Plate Angle Under Pin Block Load Case 4

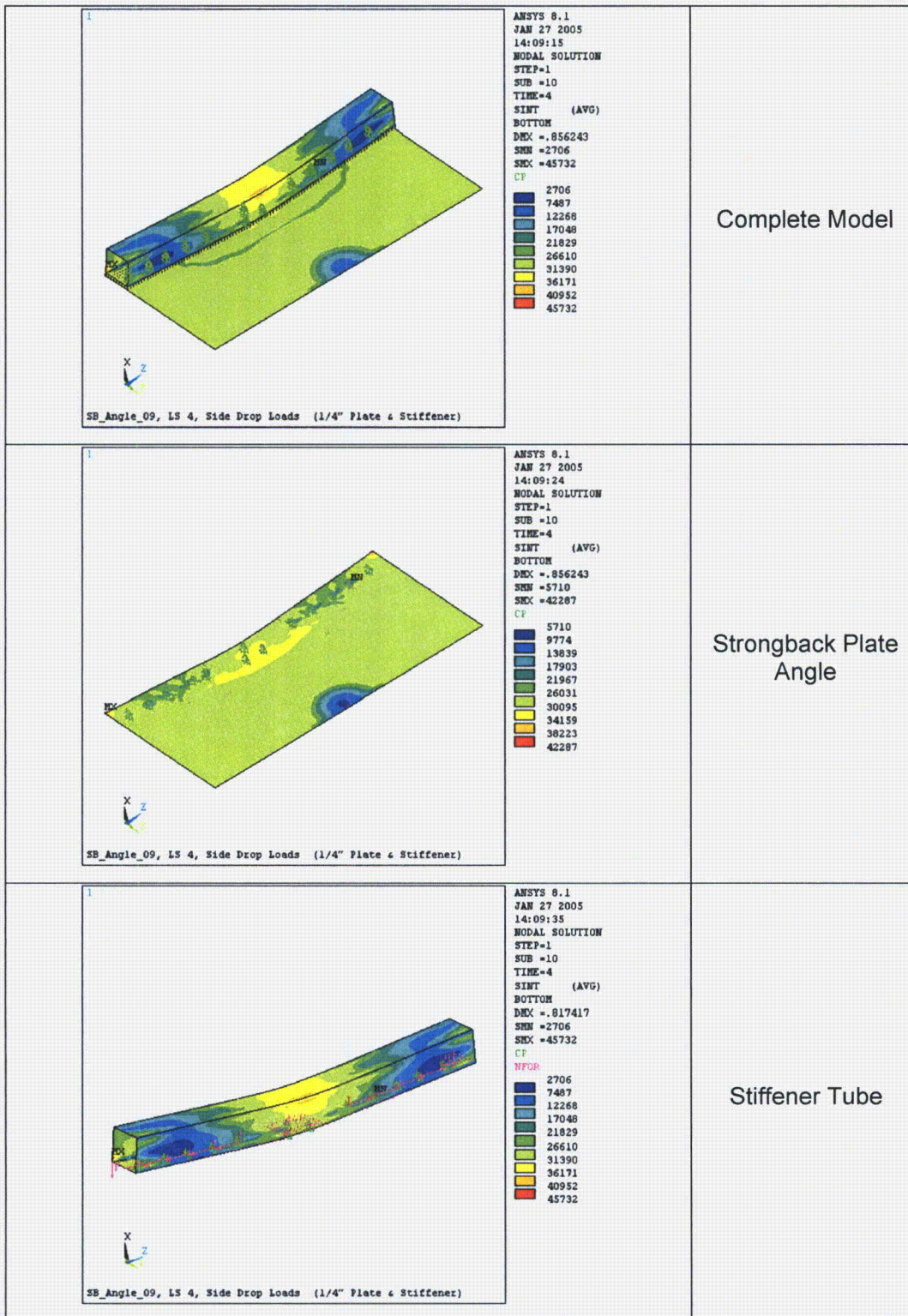


Figure 2.12.5-47 – Bottom Surface Stresses in 20.6-inch Plate Angle Under Pin Block Load Case 4

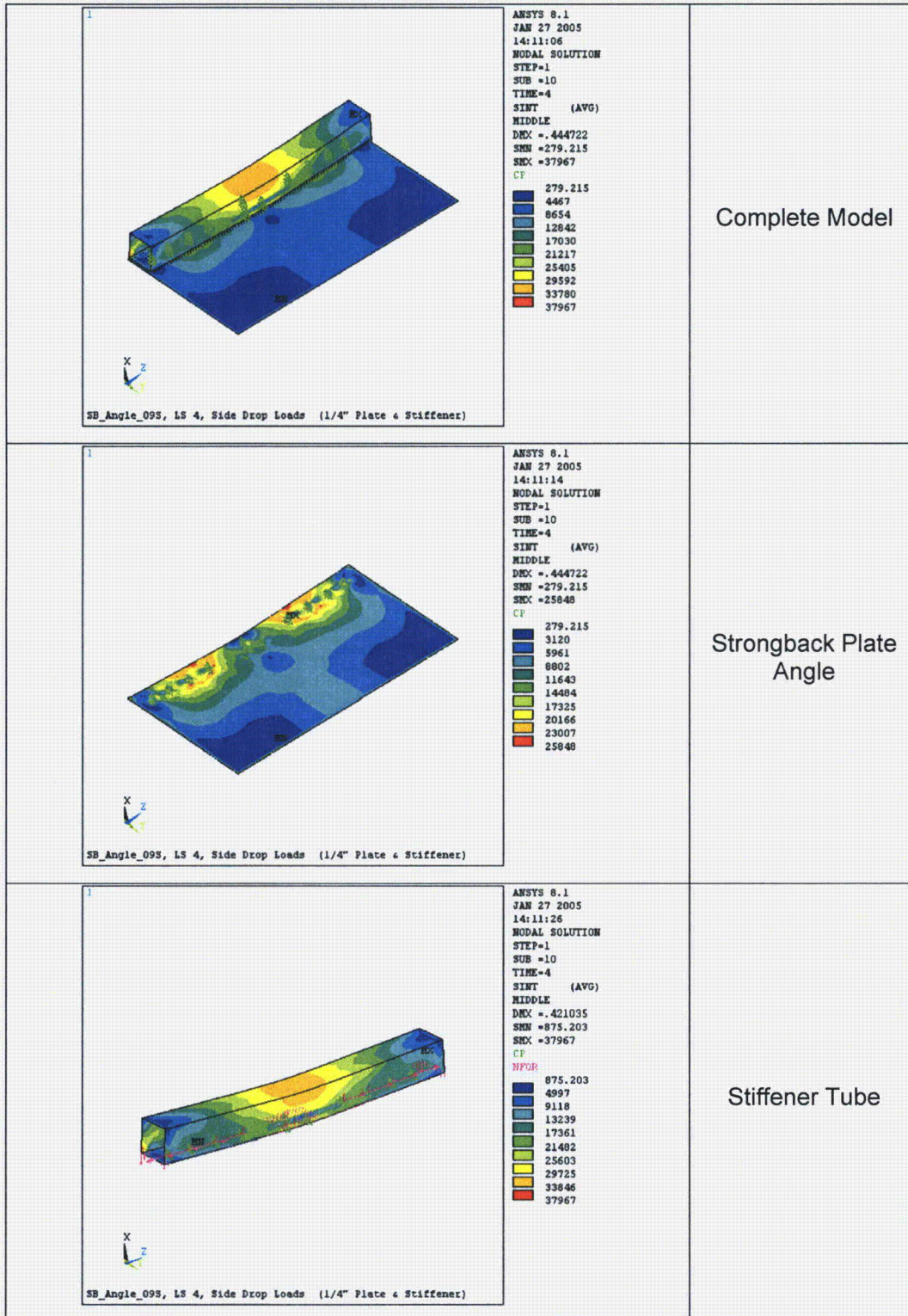


Figure 2.12.5-48 – Mid-thickness Stresses in Plate 17.0-inch Angle Under Pin Block Load Case 4

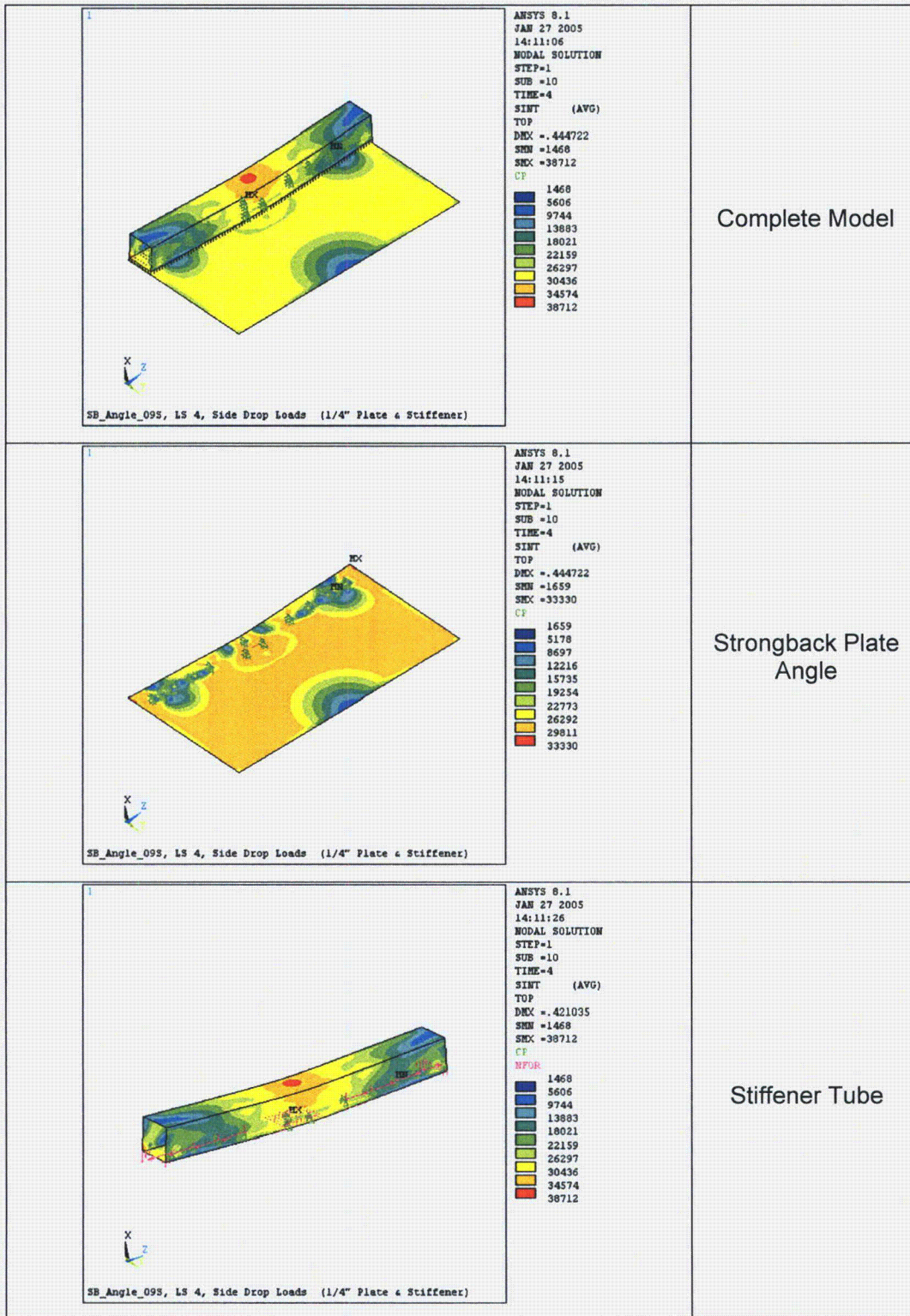


Figure 2.12.5-49 – Top Stresses in Plate 17.0-inch Angle Under Pin Block Load Case 4

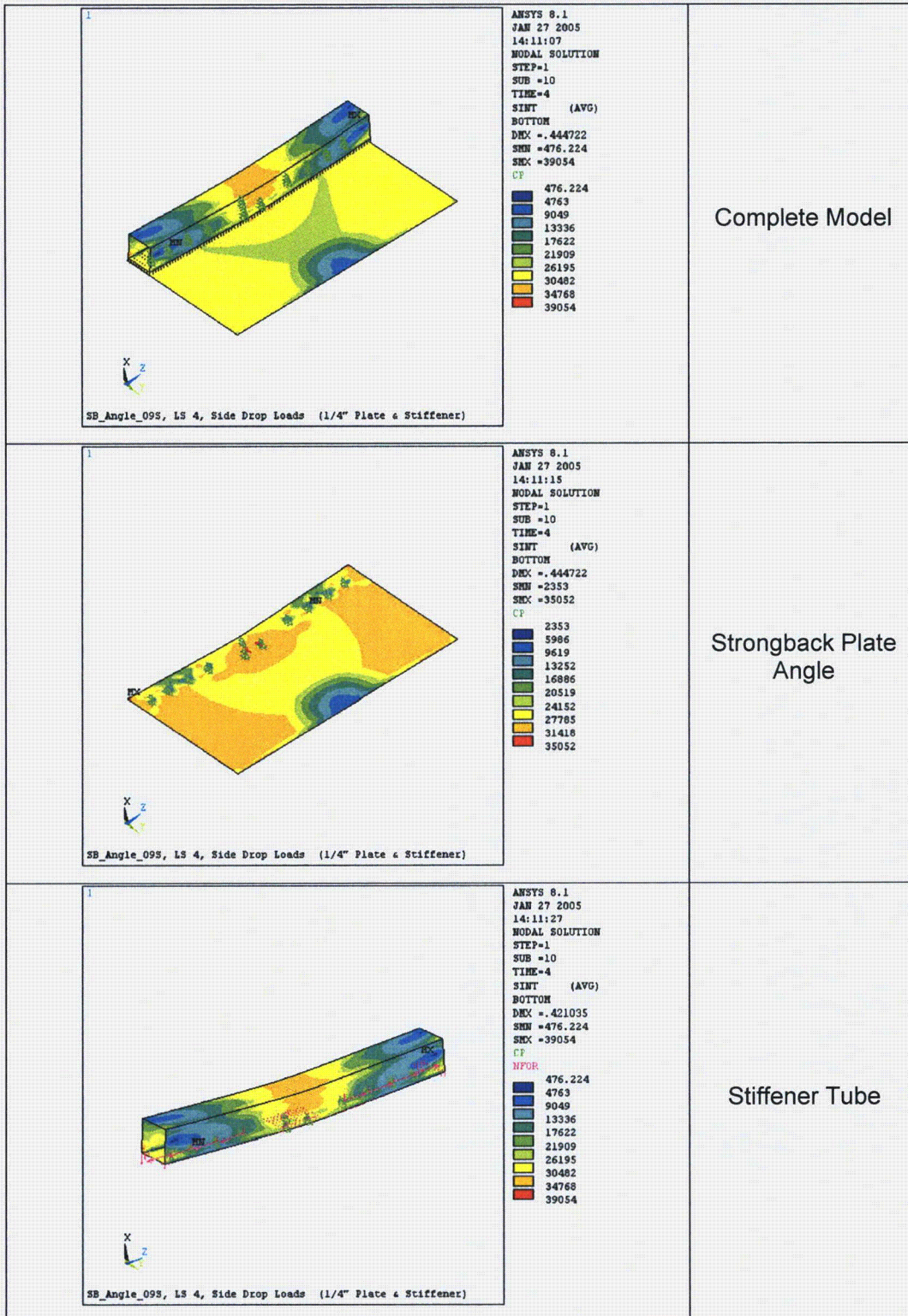
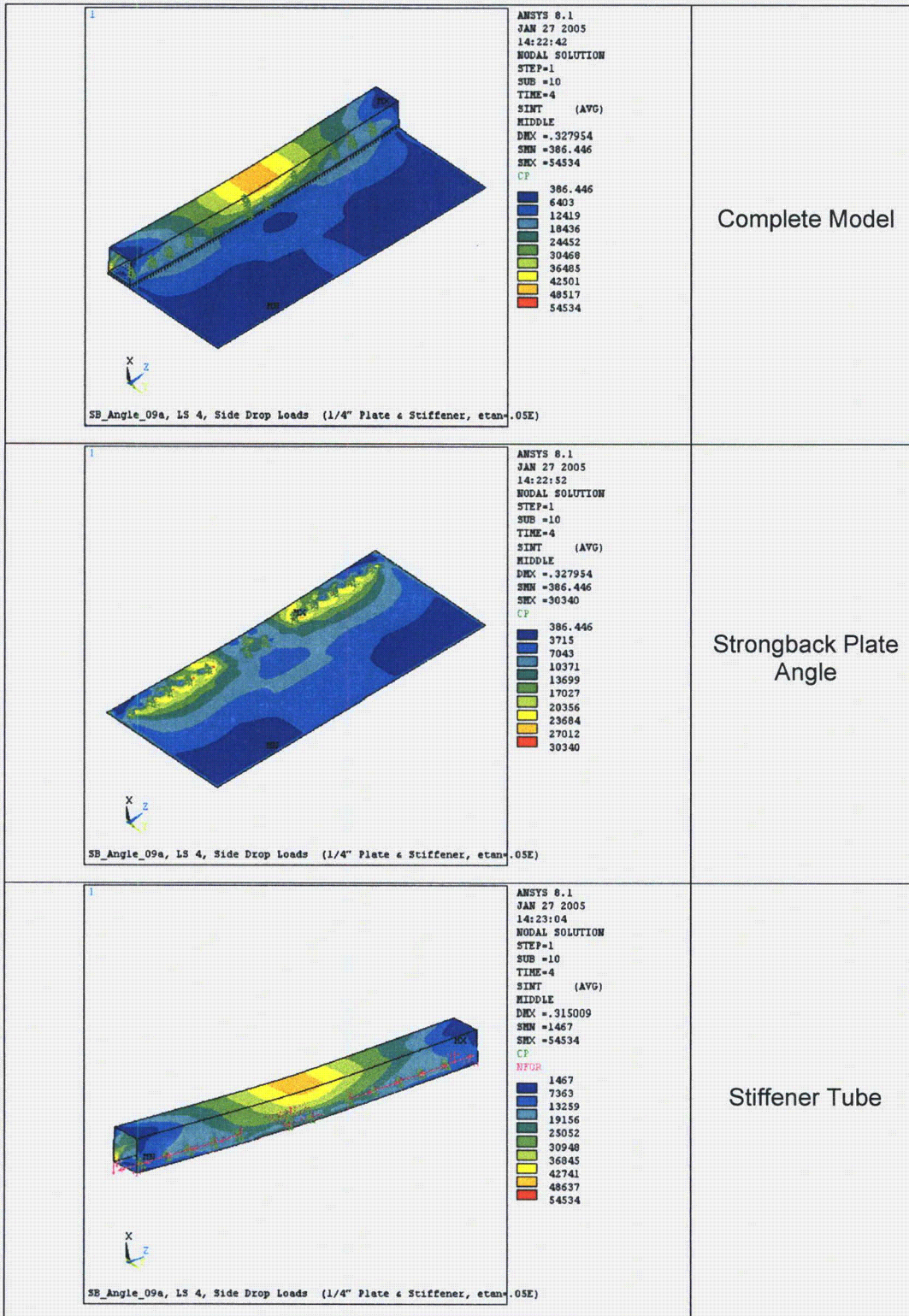


Figure 2.12.5-50 – Bottom Stresses in Plate 17.0-inch Angle Under Pin Block Load Case 4



**Figure 2.12.5-51** – Midthickness Stresses in 20.6-inch Angle w/  $E_{TAN}=.05E$  Under Pin Block Load Condition 4 (Side Drop)

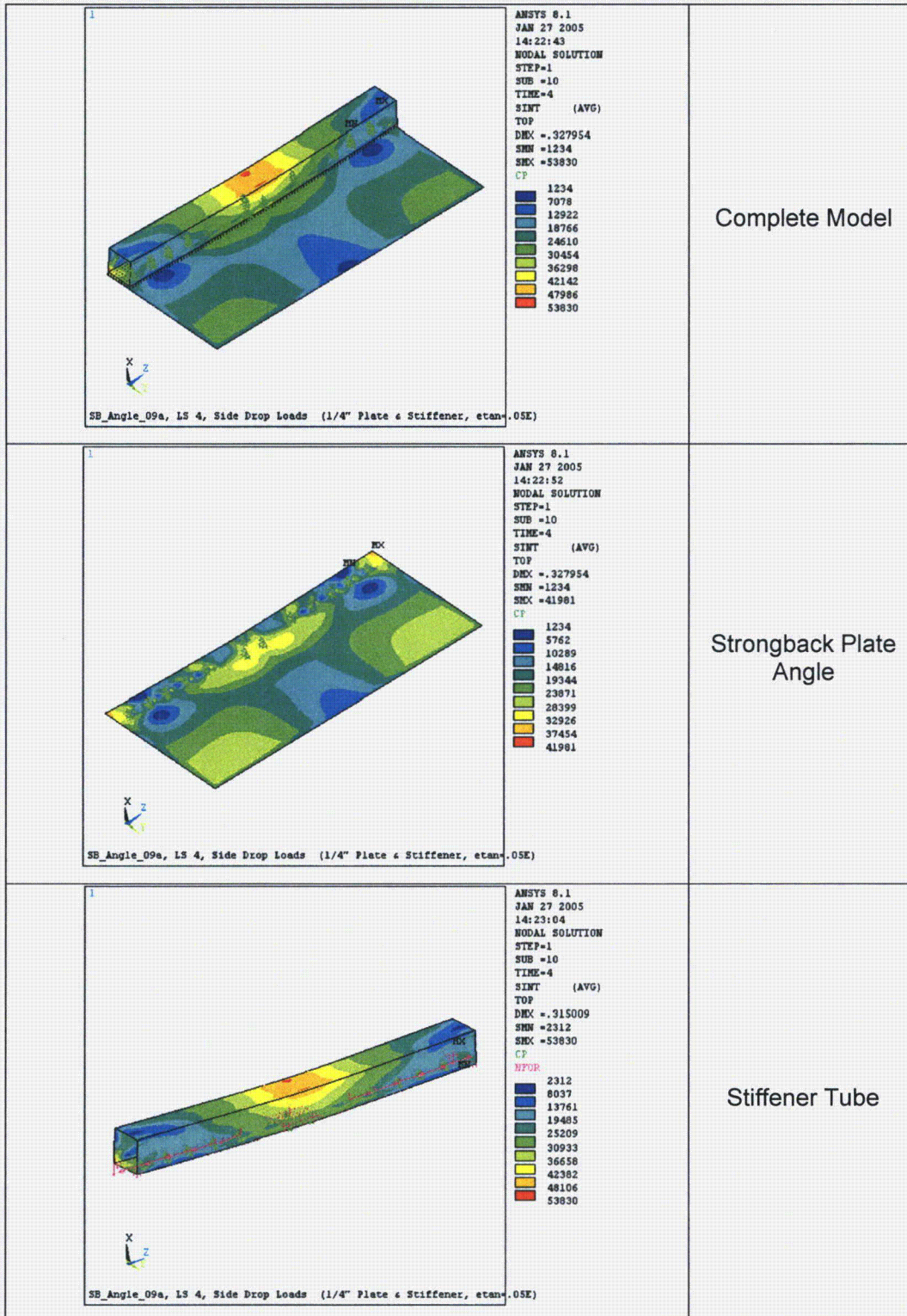


Figure 2.12.5-52 – Top Stresses in 20.6-inch Plate w/  $E_{Tan} = .05E$  Under Pin Block Load Condition 4 (Side Drop)

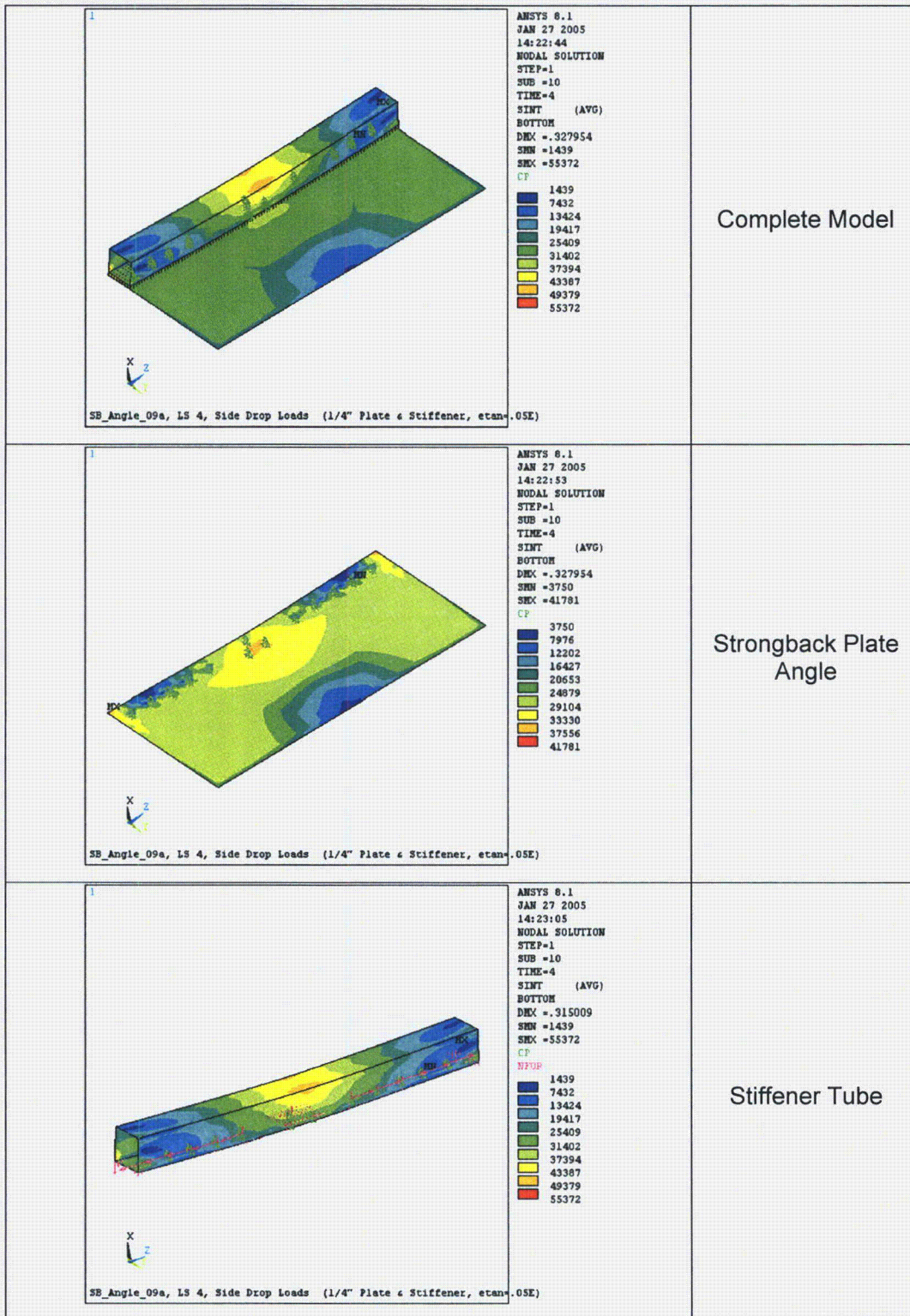
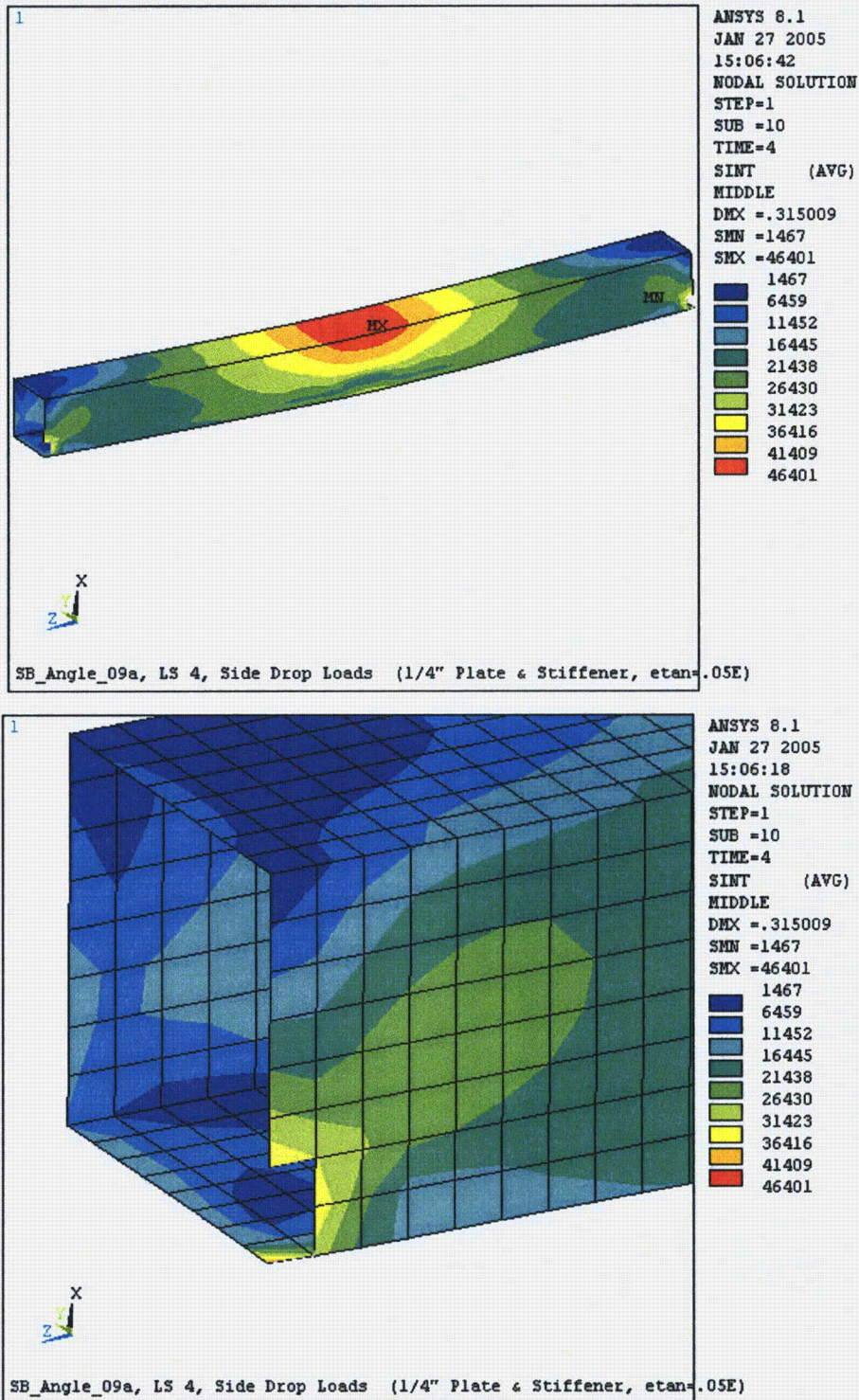


Figure 2.12.5-53 – Bottom Stresses in 20.6-inch Angle w/  $E_{Tan} = .05E$  Under Pin Block Load Condition 4 (Side Drop)



**Figure 2.12.5-54** – Stiffener Tube Side Drop Midthickness Stress, 2 nodes Removed (Top) and Detail (Bottom),  $E_{Tan} = .05E$

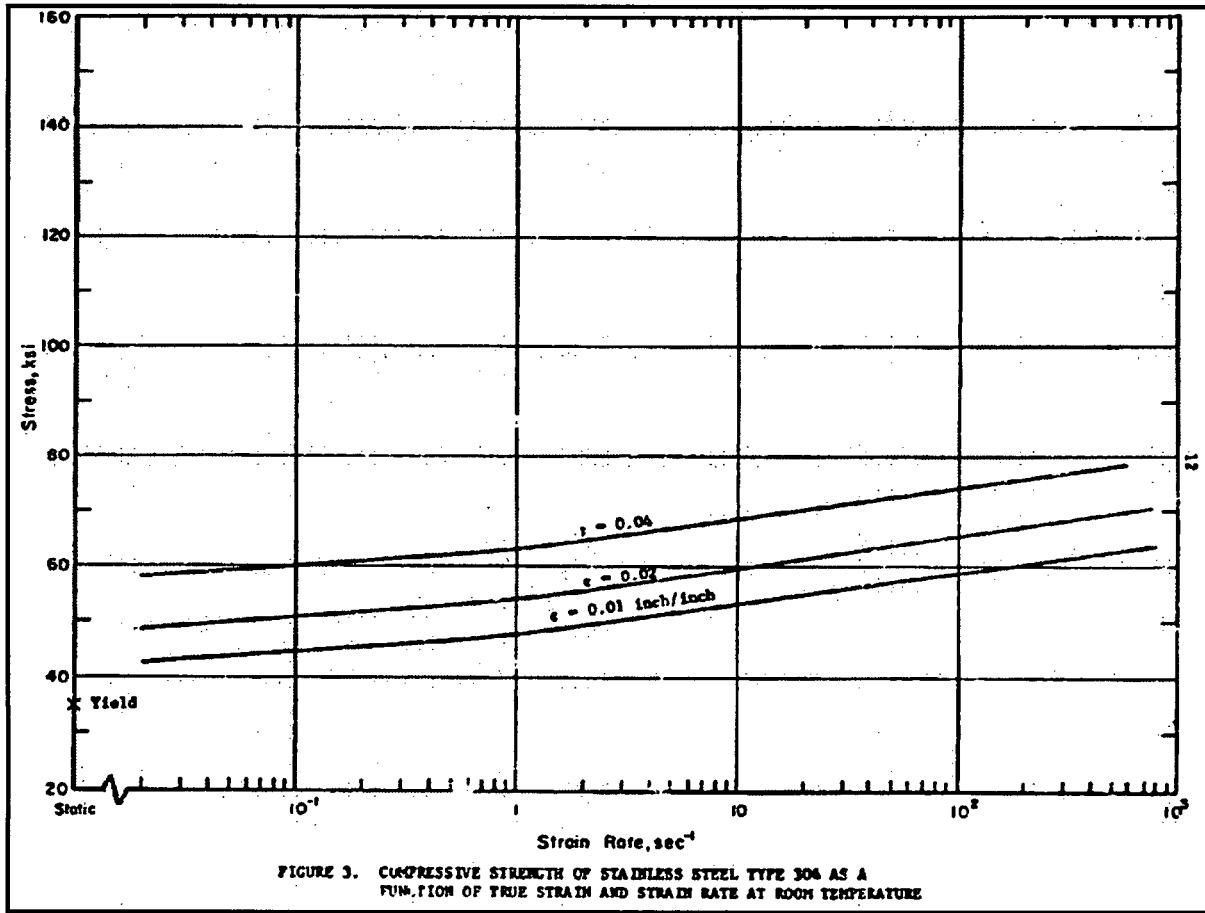
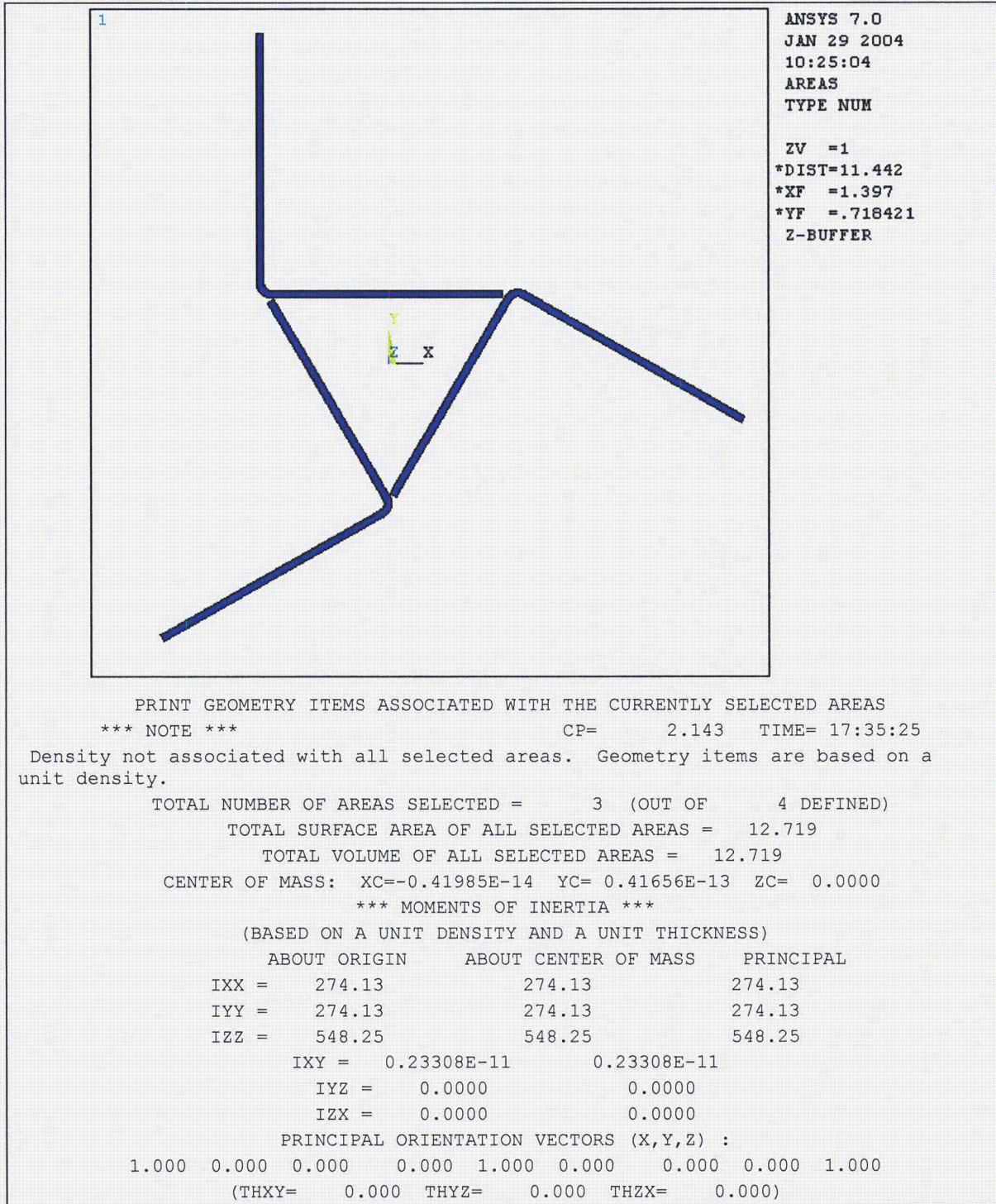


Figure 2.12.5-55 – Strain Rate Data for Type 304 Stainless Steel



**Figure 2.12.5-56 – Geometry Used to Determine Section Properties**

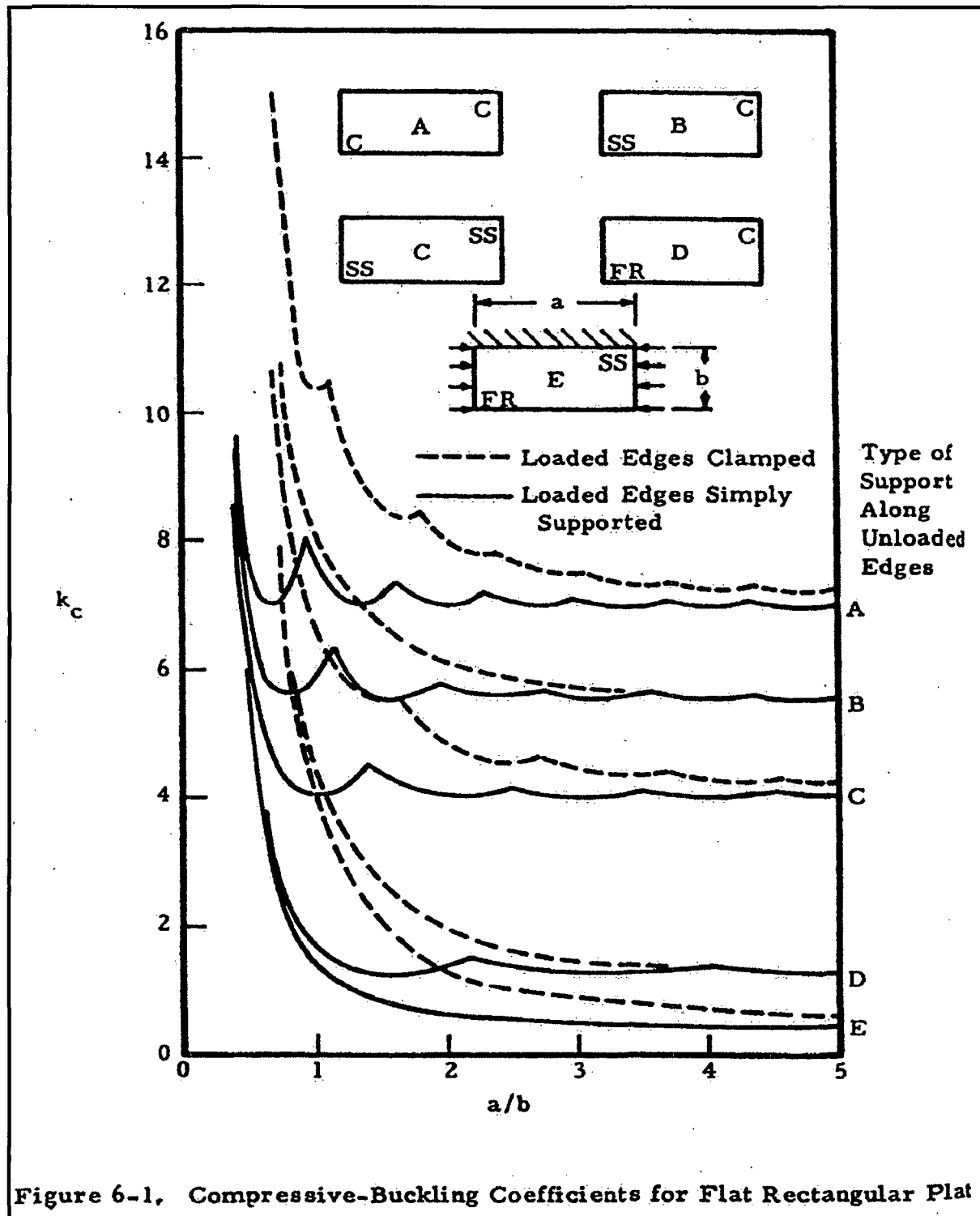


Figure 2.12.5-57 - Plate Stability Constants from Stress Analysis Manual

## 2.12.5.21 Representative ANSYS® Input Files

### 2.12.5.21.1 FCS Finite Element Model

This input file is representative of the FCS finite element analysis described in Section 2.12.5.10.

```

/prep7
!"Box"
ET,1,SOLID45
nuxy,1,.29
ex,1,27.6e6
TB,bkin,1,1,2,
TBTEMP,0
TBDATA,,25000,219970
!"Stiffener"
ET,2,SOLID45
nuxy,2,.29
dens,2,493/1728 ! weight density
ex,2,27.6e6
TB,bkin,2,1,2,
TBTEMP,0
TBDATA,,47100, 291933
!Gap Stiffness Value
gstiff=4e6
!Contact for the stiffener
et,5,contac49
!mp,mu,5,0.25
r,5,gstiff
keyopt,5,3,0
keyopt,5,7,1
!Contact for the Pin Block
et,7,contac49
!mp,mu,7,0.25
r,7,gstiff
keyopt,7,3,0
keyopt,7,7,1
!Contact for the Hinge Block
et,9,contac49
!mp,mu,9,0.25
r,9,gstiff
keyopt,9,3,0
keyopt,9,7,1
!"Pin Block"
ET,10,SOLID45
nuxy,10,.29
dens,10,493/1728 ! weight density
ex,10,27.6e6
TB,bkin,10,1,2,
TBTEMP,0
TBDATA,,47100, 291933
!"Hinge Block"
ET,11,SOLID45
nuxy,11,.29
dens,11,493/1728 ! weight density
ex,11,27.6e6
TB,bkin,11,1,2,
TBTEMP,0
TBDATA,,47100, 291933
ET,12,beam4
R,12,10*0.05,10*0.000192,10*0.000192
10*0.25,10*0.25
nuxy,12,.29
dens,12,0 ! weight density
ex,12,27.6e6
pi=3.1415926
!Global Box
b_len=17.5 !box length
b_wid=9.0 !box side length
b_thk=0.13 !box thickness
!stiffener
s_wid=1.5 !stiffener width
s_hgt=2.0 !stiffener height
s_thk=0.25 !stiffener
thickness
!End Piece
e_wid=0.5 !width
e_hgt=1.0 !height
e_thk=0.13 !thickness
!Pin Block Piece
p_wid=s_wid-s_thk*2 !width
p_len=2.0 !height
p_thk=0.375 !thickness
!Hinge Block Piece
h_wid=8.50/2 !width (z)
h_len=2.0 !height (y)
h_thk=0.375 !thickness (x)
!Stiffener Locations
z1=b_len/2-0.5 !center of 1st
stiffener
z2=b_len/2 !center of 2nd stiffener
z3=b_len-5 !center of 3rd stiffener

!Generate Box
k,1,0,0,0
k,2,b_wid,0,0
k,3,b_wid,b_thk,0
k,4,b_thk,b_thk,0
k,5,b_thk,b_wid,0
k,6,0,b_wid,0
1,1,2
1,2,3
1,3,4
1,4,5
1,5,6
1,6,1
LFILLT,4,3,b_thk,
LFILLT,1,6,b_thk*2,
a,9,2,3,8
a,9,8,7,10
a,7,5,6,10
vext,all,,,0,0,s_wid/2-s_thk
asel,s,area,,4
asel,a,area,,9
asel,a,area,,13
vext,all,,,0,0,s_thk
asel,s,area,,17
asel,a,area,,22
asel,a,area,,26
vext,all,,,0,0,z1-e_wid/2
asel,s,area,,30
asel,a,area,,35
asel,a,area,,39
vext,all,,,0,0,e_wid/2
asel,s,area,,43
asel,a,area,,48
asel,a,area,,52
vext,all,,,0,0,e_wid/2
asel,s,area,,56
asel,a,area,,61
asel,a,area,,65
vext,all,,,0,0,b_len/2-z1-e_wid/2
alls
!Generate Stiffener
real,2
type,2
mat,2
k,100,2*b_thk,0,0
k,101,2*b_thk,-s_thk,0
k,103,b_wid,0,0
k,102,b_wid,-s_thk,0
a,100,101,102,103
vext,82,,,0,0,s_wid/2-s_thk
vext,83,,,0,0,s_thk
vext,90,,,0,0,-s_hgt+s_thk
asel,s,area,,84
asel,a,area,,89
asel,a,area,,97
vext,all,,,2*b_thk-s_hgt
local,11,0,0,0,1,45,0,
vsymm,y,19,24,1,500
FLST,2,6,6,ORDE,4
FITEM,2,22
FITEM,2,-24
FITEM,2,28
FITEM,2,-30
VOVLAP,P51X
FLST,5,15,6,ORDE,4
FITEM,5,2
FITEM,5,5
FITEM,5,31
FITEM,5,-43
!Pin Block
csys,0
k,1000,b_wid,-s_thk,0
k,1001,b_wid-p_len,-s_thk,0
k,1002,b_wid-p_len,-s_thk-p_thk,0
k,1003,b_wid,-s_thk-p_thk,0
a,1000,1001,1002,1003
vext,99,,,,,p_wid/2
!Hinge Block
k,2000,-s_thk,b_wid,0
k,2001,-s_thk,b_wid-h_len,0
k,2002,-s_thk-h_thk,b_wid-h_len,0
k,2003,-s_thk-h_thk,b_wid,0
a,2000,2001,2002,2003
vext,106,,,,s_wid/2-s_thk
vext,108,,,,s_thk

vext,130,,,,h_wid-s_wid/2
vext,137,,,,s_thk
alls
!Devide things up by temporary Areas
!block,x1,x2,y1,y2,z1,z2
block,b_wid-0.5,-5,b_wid-0.5,-5,-5,b_len
vsel,u,volu,,30
VSBA,all, 197
VSBA,all, 199
alls
vdele,30,,,1
block,b_wid-1.0,-5,b_wid-1.0,-5,-5,b_len
vsel,u,volu,,1
VSBA,all, 7
VSBA,all, 18
alls
vdele,1,,,1
block,b_wid/2,-5,b_wid/2,-5,-5,b_len
vsel,u,volu,,1
VSBA,all, 7
VSBA,all, 18
alls
vdele,1,,,1
block,b_thk*2+0.5,-5,b_thk*2+0.5,-5,-5,b_len
vsel,u,volu,,1
VSBA,all, 7
VSBA,all, 18
alls
vdele,1,,,1
!Devide the where the pin block is
block,b_wid,b_wid-p_len,0.5,-s_hgt,-5,b_len
vsel,u,volu,,1
VSBA,all, 17
alls
vdele,1,,,1
block,b_wid,-s_hgt*2,0.5,-s_thk-p_thk,-5,b_len
vsel,u,volu,,1
VSBA,all, 5
alls
vdele,1,,,1
!Devide the where the hinge block is
block,1,-s_hgt*2,b_wid+1,b_wid-h_len,-5,b_len
vsel,u,volu,,1
VSBA,all, 5
alls
vdele,1,,,1
block,b_wid+1,-s_thk-h_thk,b_wid+1,-s_hgt*2,-5,h_wid
vsel,u,volu,,1
VSBA,all, 4
VSBA,all, 17
alls
vdele,1,,,1
block,b_wid+1,-s_thk-h_thk,b_wid+1,-s_hgt*2,-5,3.25
hinge block key !2.5
vsel,u,volu,,1
VSBA,all, 4
alls
vdele,1,,,1
VSEL,S,loc,x,0,b_wid
VSEL,r,loc,y,0,b_wid
!Add mass of borol and end angles to main angle
vsum
*get,vangle,volu,all,volu
dplus=8/(2*vangle)
dtotal=dplus+(493/1728)
dens,1,dtotal
vatt,1,1,1
vsel,inve
vatt,2,2,2
vsel,s,volu,,66
vsel,a,volu,,76
vsel,a,volu,,99
vatt,10,10,10
vsel,s,volu,,20
vsel,a,volu,,77
vsel,a,volu,,86

```



```

vsel,a,volu,,90
vsel,a,volu,,63
vsel,a,volu,,65
vsel,a,volu,,125
vsel,a,volu,,158
vsel,a,volu,,162
vsel,a,volu,,189
vsel,a,volu,,191,199
vsel,u,volu,,195
vatt,11,11,11
vsel,s,volu,,49
vsel,a,volu,,68
vsel,a,volu,,185
vdele,all,,1
alls
!Add Pin Hole
vext,105,,875,,
vsel,s,volu,,1
vatt,10,10,10
alls
!Add Hinge Hole
vext,129,,75,
vsel,s,volu,,24
vatt,11,11,11
alls
vext,805,,75,
vsel,s,volu,,49
vatt,11,11,11
alls
!pin block mods
vext,5,,0,s_thk
vsel,s,volu,,67
vatt,10,10,10
alls
vsel,s,volu,,116
vsel,a,volu,,145
vsel,a,volu,,151
vatt,10,10,10
alls
asel,s,area,,619
asel,a,area,,627
asel,a,area,,647
vext,all,,0,0,2
alls
asel,s,area,,316
asel,a,area,,348
asel,a,area,,391
vext,all,,0,s_thk,0
alls
vsel,s,volu,,68,69,1
vsel,a,volu,,71,75,4
vsel,a,volu,,78,79,1
vatt,10,10,10
alls
vext,622,,0,0,-p_wid/2
vsel,s,volu,,91
vsel,a,volu,,144
vatt,10,10,10
alls
!hinge block stiffener
vext,362,,0,0,-p_wid/2
vsel,s,volu,,50
vsel,a,volu,,92
vatt,11,11,11
alls
!stiffener reinforcement mods
!hinge block side
vsel,s,volu,,8,10,2
vsel,a,volu,,15,18,3
vsel,a,volu,,42,43,1
vgen,2,all,,0,4.375,0
alls
vsbv,123,167,,dele,keep
vsbv,124,169,,dele,keep
vsbv,183,164,,dele,keep
vsbv,184,107,,dele,keep
vsel,s,volu,,123,124,1
vsel,a,volu,,172,173,1
vsel,a,volu,,175,178,3
vsel,a,volu,,183,185,2
vatt,2,2,2
alls
!pin block side
vsel,s,volu,,42,43,1
vsel,a,volu,,108,109,1
vsel,a,volu,,114,115,1
vgen,2,all,,4.375,0,0
alls
vsbv,132,184,,dele,keep
vsbv,133,216,,dele,keep
vsbv,149,220,,dele,keep
vsbv,150,218,,dele,keep
vsel,s,volu,,132,133,1
vsel,a,volu,,149
vsel,a,volu,,221,225,1

```

```

vatt,2,2,2
alls
!fix touching connected components
hinge
vdele,92,,1
vdele,50,,1
asel,s,area,,275
asel,a,area,,282
vext,all,,-s_hgt+h_thk+s_thk,0,0
vsel,s,volu,,50
vsel,a,volu,,92
vatt,11,11,11
alls
!fix touching connected components
pin
vdele,91,,1
vdele,144,,1
vdele,68,69,,1
vdele,78,79,,1
vdele,71,75,4,1
vdele,116,,1
vdele,145,,1
vdele,151,,1
asel,s,area,,7
asel,a,area,,293
asel,a,area,,328
asel,a,area,,399
asel,a,area,,426
vext,all,,0,0,s_thk
alls
asel,s,area,,392
asel,a,area,,330
vext,all,,0,-s_hgt+h_thk+s_thk,0
alls
asel,s,area,,431
asel,a,area,,438
asel,a,area,,352
vext,all,,0,0,1.25
alls
asel,s,area,,701
asel,a,area,,621
asel,a,area,,627
vext,all,,0,s_thk,0
alls
vsel,s,volu,,68,69,1
vsel,a,volu,,71,75,4
vsel,a,volu,,78,79,1
vsel,a,volu,,91,116,25
vsel,a,volu,,144,145,1
vsel,a,volu,,150,151,1
vsel,a,volu,,226
vatt,10,10,10
alls
!move hinge block web stiffener back
for clearance
vdele,82,,1
vdele,92,,1
vdele,50,,1
asel,s,area,,388
asel,a,area,,375
vext,all,,-
s_hgt+s_thk-h_thk+0.4583,0,0
vsel,s,volu,,50,82,32
vatt,11,11,11
alls
asel,s,area,,134
asel,a,area,,191
vext,all,,0.25,0,0
vsel,s,volu,,92
vsel,a,volu,,227
vatt,11,11,11
alls
!bring pin block down
asel,s,area,,288
asel,a,area,,348
vext,all,,0,0.435,0
vsel,s,volu,,228,229,1
vatt,10,10,10
alls
!bring hinge block down and over
asel,s,area,,578
asel,a,area,,974
vext,all,,0.25,0,0
vsel,s,volu,,230,231,1
vatt,11,11,11
alls
asel,s,area,,136
asel,a,area,,644
asel,a,area,,990
vext,all,,0,0,0.25
vsel,s,volu,,232,234,1
vatt,11,11,11
alls
asel,s,area,,274
asel,a,area,,281

```

```

asel,a,area,,374
asel,a,area,,387
vext,all,,0.25,0,0
vsel,s,volu,,235,238,1
vatt,11,11,11
alls
vsel,s,type,,11
alls,below,volume
nummrg,kp
alls
vdele,58,,1
vdele,60,,1
vdele,87,,1
vdele,88,,1
alls
!pin block/web mod
vdele,70,,1
vdele,72,,1
asel,s,area,,329
asel,a,area,,390
vext,all,,0,0.25,0
vsel,s,volu,,58,60,2
vatt,10,10,10
alls
vsel,s,type,,10
alls,below,volume
nummrg,kp
alls
!Cut Stiffener for interface with
cask
cyl4,5.175,11.819,0,,13.75,,2
vsba,all,264
vdele,70,,1
local,11,1,5.175,11.819,0
csys,11
vsel,s,loc,x,13.75,20
vdele,all,,1
csys,0
alls
vsel,s,,245,246
vatt,10,10,10
alls
vsel,u,type,,10
vsel,u,type,,11
vsel,u,type,,1
vatt,2,2,2
alls
vsel,s,,272
alls,below,volume
adrag,530,,618
vsba,272,32
vsel,s,,8,10,2
vatt,2,2,2
alls
accat,34,41
vdele,72,,1
!accat,306,1071
vdele,249,,1
vdele,250,,1
vdele,264,,1
!Set Up Mesh
LESIZE,121,,3,,1
LESIZE,125,,3,,1
LESIZE,137,,3,,1
LESIZE,140,,3,,1
LESIZE,167,,3,,1
LESIZE,183,,3,,1
LESIZE,186,,3,,1
LESIZE,740,,1,,0
LESIZE,1096,,8,,0
LESIZE,1183,,4,,0
LESIZE,992,,10,,0
LESIZE,82,,1,,0
LESIZE,100,,1,,0
LESIZE,118,,1,,0
LESIZE,28,,3,,0
LESIZE,1198,,4,,0
LESIZE,469,,6,,0
LESIZE,567,,6,,0
LESIZE,818,,6,,0
LESIZE,922,,6,,0
LESIZE,934,,6,,0
LESIZE,1039,,6,,0
LESIZE,1031,,3,,0
LESIZE,1364,,4,,0
LESIZE,1027,,4,,0
LESIZE,1375,,4,,0
LESIZE,434,,3,,0
LESIZE,686,,3,,0
LESIZE,426,,3,,0
LESIZE,1458,,3,,0
LESIZE,682,,3,,0
lsel,s,loc,x,b_wid-p_len+0.2,b_wid-
p_len+0.5
LESIZE,all,,6,,0

```

```

alls
lset,s,loc,y,b_wid-h_len+0.2,b_wid-
h_len+0.5
LESIZE,all,,,6,,,,,0
alls
lset,s,loc,x,b_wid-p_len-0.2,b_wid-
p_len-1.5
LESIZE,all,,,6,,,,,0
alls
lset,s,loc,y,b_wid-h_len-0.2,b_wid-
h_len-1.5
LESIZE,all,,,6,,,,,0
alls
lset,s,loc,x,1.0,3.0
LESIZE,all,,,6,,,,,0
alls
lset,s,loc,y,1.0,3.0
LESIZE,all,,,6,,,,,0
alls
lset,s,loc,x,b_thk/2
LESIZE,all,,,1,,,,,0
alls
lset,s,loc,y,b_thk/2
LESIZE,all,,,1,,,,,0
alls
vsel,s,type,,11
alls,below,volume
lset,r,loc,x,-0.01,-0.24
LESIZE,all,,,3,,,,,0
alls
MSHAPE,0,3D
MSHKEY,1
VMESH,all
alls
!generate other symmetry half
vsymm,z,all,,,0,0
esel,s,type,,1
nsle,s
nummrg,node,0.001
alls
esel,s,type,,2
nsle,s
nummrg,node,0.001
alls
esel,s,type,,10
nsle,s
nummrg,node,0.001
alls
esel,s,type,,11
nsle,s
nummrg,node,0.001
alls
!Add Bolt couples
!pin block
nset,s,loc,x,b_wid-0.5
nset,r,loc,z,1.375
cpintf,ux,0.01
cpintf,uy,0.01
cpintf,uz,0.01
alls
nset,s,loc,x,b_wid-0.5
nset,r,loc,z,-1.375
cpintf,ux,0.01
cpintf,uy,0.01
cpintf,uz,0.01
alls
nset,s,loc,x,b_wid-1.5
nset,r,loc,z,1.375
cpintf,ux,0.01
cpintf,uy,0.01
cpintf,uz,0.01
alls
nset,s,loc,x,b_wid-1.5
nset,r,loc,z,-1.375
cpintf,ux,0.01
cpintf,uy,0.01
cpintf,uz,0.01
alls
!Pin
n,50000,b_wid+0.875-0.437,-0.002,.75
e,50000,node(9.292,-0.083,0.75)
e,50000,node(9.583,-0.083,0.75)
e,50000,node(9.292,0,0.75)
e,50000,node(9.583,0,0.75)
e,50000,node(9.292,0.109,0.75)
e,50000,node(9.583,0.109,0.75)
n,50006,b_wid+0.875-0.437,-0.002,-
.75
e,50006,node(9.292,-0.083,-0.75)
e,50006,node(9.583,-0.083,-0.75)
e,50006,node(9.292,0,-0.75)
e,50006,node(9.583,0,-0.75)
e,50006,node(9.292,0.109,-0.75)
e,50006,node(9.583,0.109,-0.75)
!Hinge
n,50003,-.187,b_wid+0.75-0.437,3.25
e,50003,node(-0.167,9.25,3.25)
e,50003,node(-0.167,9.50,3.25)
e,50003,node(-.25,9.25,3.25)
e,50003,node(-.25,9.50,3.25)
n,50004,-.187,b_wid+0.75-0.437,0.75
e,50004,node(-0.167,9.25,0.750)
e,50004,node(-0.167,9.50,0.750)
e,50004,node(-.25,9.25,0.750)
e,50004,node(-.25,9.50,0.750)
!n,50005,-.187,b_wid+0.75-0.437,5
!e,50005,node(-0.167,9.25,5)
!e,50005,node(-0.167,9.50,5)
!e,50005,node(-.25,9.25,5)
!e,50005,node(-.25,9.50,5)
n,50007,-.187,b_wid+0.75-0.437,-3.25
e,50007,node(-0.167,9.25,-3.25)
e,50007,node(-0.167,9.50,-3.25)
e,50007,node(-.25,9.25,-3.25)
e,50007,node(-.25,9.50,-3.25)
n,50008,-.187,b_wid+0.75-0.437,-0.75
e,50008,node(-0.167,9.25,-0.750)
e,50008,node(-0.167,9.50,-0.750)
e,50008,node(-.25,9.25,-0.750)
e,50008,node(-.25,9.50,-0.750)
!n,50009,-.187,b_wid+0.75-0.437,-5
!e,50009,node(-0.167,9.25,-5)
!e,50009,node(-0.167,9.50,-5)
!e,50009,node(-.25,9.25,-5)
!e,50009,node(-.25,9.50,-5)
alls
!generate gaps
!box walls to stiffeners
!stiffeners are the 'target'
vsel,s,type,,2
vsel,a,type,,10
vsel,a,type,,11
alls,below,volu
nset,r,loc,x,0
nset,r,loc,y,0,b_wid
nset,r,loc,z,-s_wid/2,s_wid/2
cm,stiff,node
alls,below,volu
nset,r,loc,y,0
nset,r,loc,x,0,b_wid
nset,r,loc,z,-s_wid/2,s_wid/2
cmset,a,stiff,node
cm,stiff,node
alls
!box walls are the 'Contact'
vsel,s,type,,1
alls,below,volu
nset,r,loc,x,0
nset,r,loc,y,0,b_wid
nset,r,loc,z,-s_wid/2,s_wid/2
cm,box,node
alls,below,volu
nset,r,loc,y,0
nset,r,loc,x,0,b_wid
nset,r,loc,z,-s_wid/2,s_wid/2
cmset,a,box,node
cm,box,node
alls
type,5
mat,5
real,5
gngen,box,stiff,2
alls
!pin block to stiffener and box
!pin block is 'target'
vsel,s,type,,10
alls,below,volu
nset,r,loc,y,-s_thk
nset,r,loc,z,-s_wid/2,s_wid/2
cm,p_block,node
alls,below,volu
nset,r,loc,y,0
nset,r,loc,x,b_wid,b_wid-p_len
nset,r,loc,z,1.25+s_wid/2,s_wid/2
cmset,a,p_block,node
cm,p_block,node
alls,below,volu
nset,r,loc,y,0
nset,r,loc,x,b_wid,b_wid-p_len
nset,r,loc,z,-1.25-s_wid/2,-s_wid/2
cmset,a,p_block,node
cm,p_block,node
alls
!stiffener and box are 'contact'
vsel,s,type,,2
alls,below,volu
nset,r,loc,y,-s_thk
nset,r,loc,x,b_wid-0.5,b_wid-p_len
nset,r,loc,z,-s_wid/2,s_wid/2
cm,parea,node
vsel,a,type,,1
alls,below,volu
nset,r,loc,y,
nset,r,loc,x,b_wid,b_wid-p_len
nset,r,loc,z,1.25+s_wid/2,s_wid/2
cmset,a,parea,node

```

```

cm,parea,node
alls,below,volu
nset,r,loc,y,
nset,r,loc,x,b_wid,b_wid-p_len
nset,r,loc,z,-1.25-s_wid/2,-s_wid/2
cmset,a,parea,node
cm,parea,node
alls
type,7
mat,7
real,7
gcgen,parea,p_block,2
alls
!Hinge Block to stiffener and box
wall
!hinge block is 'target'
vsel,s,type,,11
alls,below,volu
nset,r,loc,x,-s_thk
nset,r,loc,y,b_wid-1,b_wid-h_len
nset,r,loc,z,s_wid/2,-s_wid/2
cm,h_block,node
alls,below,volu
nset,r,loc,x,0
nset,r,loc,z,h_wid,s_wid/2
cmset,a,h_block,node
cm,h_block,node
alls,below,volu
nset,r,loc,x,0
nset,r,loc,z,-h_wid,-s_wid/2
cmset,a,h_block,node
cm,h_block,node
alls
!stiffener and box are 'contact'
vsel,s,type,,2
alls,below,volu
nset,r,loc,x,-s_thk
nset,r,loc,y,b_wid-1,b_wid-h_len
cm,harea,node
vsel,a,type,,1
alls,below,volu
nset,r,loc,x,
nset,r,loc,y,b_wid,b_wid-h_len
nset,r,loc,z,h_wid,s_wid/2
cmset,a,harea,node
cm,harea,node
alls,below,volu
nset,r,loc,x,
nset,r,loc,y,b_wid,b_wid-h_len
nset,r,loc,z,-h_wid,-s_wid/2
cmset,a,harea,node
cm,harea,node
alls
type,9
mat,9
real,9
gcgen,harea,h_block,2
alls
!Weld Pin Block to Stiffener
vsel,s,type,,2
vsel,a,type,,10
alls,below,volu
nset,r,loc,y,-s_thk-h_thk,-s_hgt
CPINTF,ALL,0.001,
alls
!Weld Hinge Block to Stiffener
vsel,s,type,,2
vsel,a,type,,11
alls,below,volu
nset,r,loc,x,-s_thk-h_thk,-s_hgt
CPINTF,ALL,0.001,
alls
!Pin Side
d,50000,Ux,
d,50000,Uy,
!d,50000,Uz,
d,50006,Ux,
d,50006,Uy,
d,50006,Uz,
!Hinge Side
d,50003,Ux,
d,50003,Uy,
d,50003,Uz,
d,50004,Ux,
d,50004,Uy,
!d,50004,Uz,
!d,50005,Ux,
!d,50005,Uy,
!d,50005,Uz,
d,50007,Ux,
d,50007,Uy,
!d,50007,Uz,
d,50008,Ux,
d,50008,Uy,
d,50008,Uz,
!d,50009,Ux,
!d,50009,Uy,
!d,50009,Uz,
alls
/solu
antype,static
solcontrol,on,on
autots,on
nropt,auto
!Load Step 1
!Apply g-Load
g=120
acel,0,0,g
NSUBST,10,25,1
lswrite,1
!Load Step 2
!Apply Initial Pressure
fp=18000/100/(b_wid-b_thk)/s_wid
esel,s,type,,1
nsle,s
nset,r,loc,y,b_thk
nset,r,loc,x,b_thk,b_wid
nset,r,loc,z,-s_wid/2,s_wid/2
sf,all,pres,fp
alls
NSUBST,10,25,1
lswrite,2
!Load Step 3
!Apply Full Pressure
fp=18000/(b_wid-b_thk)/s_wid
esel,s,type,,1
nsle,s
nset,r,loc,y,b_thk
nset,r,loc,x,b_thk,b_wid
nset,r,loc,z,-s_wid/2,s_wid/2
sf,all,pres,fp
alls
NSUBST,10,50,1
lswrite,3
lssolve,1,3,1
save
finish

```

**2.12.5.21.2 Strongback Evaluation Finite Element Model**

This input file is representative of the FCS finite element analysis described in Section 2.12.5.19.

```

/PREP7
/com Plate Dimensions
A_Plate=17.0
B=9
A2_Plate=A_Plate/2
tol=.001
T_Plate=0.25
/com Stiffener Dimensions
H_Stiff=2.0
T_Stiff=0.25
/com Loads
Fx_1=-500 $
Fy_1=-8400 $
Fz_1=-1150
Fx_2=-8900 $
Fy_2=-50 $
Fz_2=-1050
Fx_3=-4700 $
Fy_3=-4250 $
Fz_3=-1150
Fx_4=-13500 $
Fy_4=-50 $
Fz_4=50
et,1,shell43 $ r,1,T_Plate
et,2,shell43 $ r,2,T_Stiff
et,3,shell43 $ r,3,T_Stiff
et,52,contac52,,1,0
keyopt,52,7,1
r,52,1.0e+06,,2.0
! initially closed & sliding
mu,52,0
/com Material 1 - Type 304
nuxy,1,0.3
mptemp,1,0,300
dens,1,493/1728
! weight density
mpdata,ex,1,1,27.6e+06,27.6e+06
pmod=0.05
tb,bkin,1,2
tbtemp,0
tbdata,,25000,219970
! c1=sy, c2=tangent modulus
tbtemp,300
tbdata,,25000,219970
! c1=sy, c2=tangent modulus
/com Dimensions for Geometry
tempA=T_Stiff/2
tempB=H_Stiff-T_Stiff/2
temp1=(T_Plate+T_Stiff)/2
temp2=temp1+H_Stiff-T_Stiff
/com Define Plate
wprotae,0,0,90 ! match 99008-20
coordinates
mat,1
real,1
type,1
rect,-A2_Plate,A2_Plate,0,B
rect,-A2_Plate,A2_Plate,0,B
rect,-A2_Plate,A2_Plate,TempA,TempB
aovlap,all
wpstyle
esize,0.22
amesh,all
cm,PlateA,area
cm,PlateL,line
cm,PlateK,kp
cm,PlateE,elem
cm,PlateN,node
cmgrp,Plate,PlateA,PlateL,PlateK,PlateE,PlateN
/com Define Stiffener.....
mat,1
real,3
type,3
block,-
A2_Plate,A2_Plate,tempA,tempB,temp1,temp2
vdele,all
! delete vol, keep areas
ksel,s,loc,z,-A2_Plate-tol,-
A2_Plate+tol ! ends only
lslk,s,1
! line w/all kp
asll,s,1
! area w/all line
adele,all
! delete block ends
wpstyle
alls
cmsetl,u,Plate
real,3
amesh,all
cm,StiffA,area
cm,StiffL,line
cm,StiffK,kp
cm,StiffE,elem
cm,StiffN,node
cmgrp,Stiff,StiffA,StiffL,StiffK,StiffE,StiffN
/com Pin Block Location (Welded Into Tube Stiffener)
cmsetl,s,Stiff
nset,r,loc,z,-1.25,1.25
nset,r,loc,x,Temp1-tol,Temp1+tol
esln,s,1
cm,Pin_n,node
cm,Pin_e,elem
cmgrp,Pin,Pin_n,Pin_e
emodif,all,type,2 ! at Pin Block
emodif,all,real,2 ! at Pin Block
*get,iPin_n,node,0,count
alls
/com Connect Plate and Stiffener
nset,s,loc,Y,H_Stiff/2-tol,H_Stiff/2+tol
nset,r,loc,X,0,H_Stiff/2
cm,TempN,node
cmsetl,r,PlateN $ cm,TempP,node
cmsetl,s,TempN
cmsetl,r,StiffN $ cm,TempS,node
nset,none
cm,BoltN,node ! initialize group
for connected nodes
*do,i,-7.5,-3.0,1.5
cmsetl,s,TempP
nodeP=node(0,T_Stiff/2,i)
cmsetl,s,TempS
nodeS=node(0,T_Stiff/2,i)
nall
cp,next,ux,Nodes,NodeP
cp,next,uy,Nodes,NodeP
cp,next,uz,Nodes,NodeP
cmsetl,s,BoltN ! add nodes
to group
nset,a,node,,NodeP
nset,a,node,,NodeS
cm,BoltN,node
*enddo
*do,i,3.0,7.5,1.5
cmsetl,s,TempP
nodeP=node(0,T_Stiff/2,i)
cmsetl,s,TempS
nodeS=node(0,T_Stiff/2,i)
nall
cp,next,ux,Nodes,NodeP
cp,next,uy,Nodes,NodeP
cp,next,uz,Nodes,NodeP
cmsetl,s,BoltN ! add nodes
to group
nset,a,node,,NodeP
nset,a,node,,NodeS
cm,BoltN,node
*enddo
/com 3 Fasteners at Pin Block
cmsetl,s,PlateN $ nodeP1=node(0,1.37,-.75)
cmsetl,s,StiffN $
nodeS1=node(T_Stiff,1.37,-.75)
nall
cp,next,ux,Nodes1,NodeP1
cp,next,uy,Nodes1,NodeP1
cp,next,uz,Nodes1,NodeP1
cmsetl,s,PlateN $ nodeP2=node(0,0.62,.00)
cmsetl,s,StiffN $
nodeS2=node(T_Stiff,0.62,.00)
nall
cp,next,ux,Nodes2,NodeP2
cp,next,uy,Nodes2,NodeP2
cp,next,uz,Nodes2,NodeP2
cmsetl,s,PlateN $ nodeP3=node(0,1.37,.75)
cmsetl,s,StiffN $
nodeS3=node(T_Stiff,1.37,.75)
nall
cp,next,ux,Nodes3,NodeP3
cp,next,uy,Nodes3,NodeP3
cp,next,uz,Nodes3,NodeP3
cmsetl,s,BoltN ! add nodes
to group
nset,a,node,,NodeP1 $
nset,a,node,,NodeP2 $
nset,a,node,,NodeP3
nset,a,node,,NodeS1 $
nset,a,node,,NodeS2 $
nset,a,node,,NodeS3
cm,BoltN,node
/com Contact Elements
asel,s,area,,3
alls,below,area
cmsetl,u,BoltN ! unselect
Bolted nodes
cm,TempP,node ! plate
nodes
cm,Temp,node
cmsetl,s,Stiff
*get,Xmin,Node,0,MNLOC,X
nset,r,loc,X,Xmin-tol,Xmin+tol
cmsetl,u,BoltN ! unselect
Bolted nodes
cm,TempS,node !
stiffener nodes
*get,HowMany,node,,count
esel,none
type,52
real,52
mat,52
node1=0
*do,i,1,HowMany
cmsetl,s,Temp
node1=ndnext(node1)
yloc=ny(node1)
zloc=nz(node1)
cmsetl,s,TempS
node2=node(Xmin,yloc,zloc)
cmsetl,a,TempP
e,node1,node2
*enddo
eplot
*get,N_Elem,elem,,count
*if,N_Elem,GT,HowMany,then
*msg,warn,N_Elem,HowMany
CONTACT GENERATION MAY BE
MESSUED UP, %I Elements from %I Nodes
*endif
alls
/com Groups for Boundary Conditions
cmsetl,s,PlateN
nset,r,loc,y,0
nset,r,loc,z,-A2_Plate+tol,A2_Plate-tol
cm,free_edge,node
cmsetl,s,PlateN
nset,r,loc,y,B-tol,B+tol
cm,fix_edge,node
cmsetl,s,PlateN
nset,r,loc,z,-A2_Plate-tol,-
A2_Plate+tol
cm,top_edge,node
cmsetl,s,PlateN
nset,r,loc,z,+A2_Plate-tol,+A2_Plate+tol
cm,bot_edge,node
alls
/com Apply Boundary Conditions
(Plate (not stiffener) Edges Only)
cmsetl,s,top_edge
cmsetl,a,bot_edge
cmsetl,a,fix_edge
d,all,ux,0,,,uy,uz
alls
/com Load Step 1
/title,SB_Angle_075,LS 1, Table 7-4
(1/4" Plate & Stiffener)
time,1

```

```

nlgeom,on
autots,on
nsubst,10,20,10,off
cnvtol,f,,.01,,10      !
modified convergence tolerance
neqit,100
nropt,auto
pred,on,,on
cmsel,s,Pin_n
f,all,fx, Fx_1/iPin_n
! out-of-plane
f,all,fz, Fz_1/iPin_n
! in-plane (axial)
f,all,fy, Fy_1/iPin_n
! in-plane
alls
lswrite
/com Load Step 2
fdele,all,all
/title,SB_Angle_07S, LS 2, Table 7-5
(1/4" Plate & Stiffener)
time,2
nlgeom,on
autots,on
nsubst,10,20,10,off
cnvtol,f,,.01,,10      !
modified convergence tolerance
neqit,100
nropt,auto
pred,on,,on
cmsel,s,Pin_n
f,all,fx, Fx_2/iPin_n
! out-of-plane
f,all,fz, Fz_2/iPin_n
! in-plane (axial)
f,all,fy, Fy_2/iPin_n
! in-plane
alls
lswrite
/com Load Step 3
fdele,all,all
(1/4" Plate & Stiffener)
time,3
nlgeom,on
autots,on
nsubst,10,20,10,off
cnvtol,f,,.01,,1      !
modified convergence tolerance
neqit,100
nropt,auto
pred,on,,on
cmsel,s,Pin_n
f,all,fx, Fx_3/iPin_n
! out-of-plane
f,all,fz, Fz_3/iPin_n
! in-plane (axial)
f,all,fy, Fy_3/iPin_n
! in-plane
alls
lswrite
! save,SB_Angle_07S-3,db      ! /com
Load Step 4
fdele,all,all
/title,SB_Angle_07S, LS 4, Side Drop
Loads (1/4" Plate & Stiffener)
time,4
nlgeom,on
autots,on
nsubst,10,20,10,off
cnvtol,f,,.01,,1      !
modified convergence tolerance
neqit,100
nropt,auto
pred,on,,on
cmsel,s,Pin_n
! no axial force
f,all,fx, Fx_4/iPin_n
! out-of-plane
f,all,fz, Fz_4/iPin_n
! in-plane (axial)
f,all,fy, Fy_4/iPin_n
! in-plane
alls
lswrit

```

This page left intentionally blank.

## **2.12.6 CASKDROP Computer Program**

This appendix briefly documents the methodology employed by the PacTec proprietary computer program CASKDROP. Used in conjunction with an appropriate packaging dynamic analysis computer code, such as SCANS<sup>1</sup> or SLAPDOWN<sup>2</sup>, the computer program CASKDROP is used to demonstrate compliance of the package with 10 CFR §71.71(c)(7)<sup>3</sup> and 10 CFR §71.73(c)(1) for normal conditions of transport (NCT) and hypothetical accident conditions (HAC) of transport free drop analyses, respectively.

A summary of the appendix subsections is as follows:

- describes the CASKDROP analysis methodology.
- provides an example problem with input and output.

### **2.12.6.1 Using CASKDROP to Determine Impact Limiter Deformation Behavior**

The package is protected by polyurethane foam-filled, energy absorbing end buffers, called impact limiters. For purposes of the regulatory free drop analyses using the CASKDROP computer program, the impact limiters are assumed to absorb, in plastic deformation of the polyurethane foam, all of the potential energy of the drop event. In other words, the drop analyses assume that none of the potential energy of the free drop event is transferred to kinetic or strain energy of the target (i.e., the “unyielding” surface assumption of 10 CFR 71), nor strain energy in the package body itself.

CASKDROP evaluates all angles of drop from 0° (horizontal) to 90° (vertical) by performing a quasi-static analysis that ignores rotational effects. At orientations where rotational effects are important, use of a dynamic analysis computer program such as SCANS or SLAPDOWN is required utilizing the force-deflection data developed by CASKDROP. Three orientations where rotational motions (or pitch) play no role in the evaluation of the free drop analyses are:

- *END DROP* on the circular end surface of the impact limiter,
- *SIDE DROP* on the cylindrical side surfaces of the impact limiters, and
- *CORNER DROP* with the package center of gravity directly over the impact limiter corner.

For all orientations of impact, the prediction of impact limiter deformation behavior can be approached from straightforward energy balance principles:

$$E = W(h + \delta) = \int_0^{\delta} F_x dx$$

<sup>1</sup> SCANS (*Shipping Cask ANalysis System*), A Microcomputer Based Analysis System for Shipping Cask Design Review, NUREG/CR-4554 (UCID-20674), Lawrence Livermore National Laboratory.

<sup>2</sup> G. D. Sjaardema, G. W. Wellman, *Numerical and Analytical Methods for Approximating the Eccentric Impact Response (Slapdown) of Deformable Bodies*, SAND88-0616 (UC-71), Sandia National Laboratories.

<sup>3</sup> Title 10, Code of Federal Regulations, Part 71 (10 CFR 71), *Packaging and Transportation of Radioactive Materials*, Final Rule, 01-26-04.

where  $W$  is the package gross weight,  $h$  is the drop height,  $\delta$  is the maximum impact limiter deformation, and  $F_x$  is the force imposed on target at an impact limiter deformation of  $x$ . The left-hand term represents the potential energy of the free drop. The right-hand term represents the strain energy of the deformed impact limiter(s).

Given a specific drop angle,  $\theta$ , and impact limiter deformation,  $\delta$ , as illustrated in Figure 2.12.6-1, the result is an impact limiter crush plane "footprint." Integration of the impact limiter crush plane yields a total crush force and centroidal distance of:

$$F = \iint \sigma\{\varepsilon\} dA \quad \text{and} \quad \bar{X} = \left(\frac{1}{F}\right) \iint \bar{x}\sigma\{\varepsilon\} dA$$

respectively, where  $F$  is the total integrated force,  $\sigma\{\varepsilon\}$  is the differential stress as a function of strain,  $dA$  is the differential area (i.e.,  $dA$  is a function of the "x" and "y" directions, or  $dx$  and  $dy$ ),  $\bar{X}$  is the total integrated centroidal distance from the package center of gravity, and  $\bar{x}$  is the differential centroidal distance from the package center of gravity.

With reference to Figure 2.12.6-1, the geometric calculations for the impact surface (crush plane) and the associated strains are carried out using a translating X'-Y'-Z' coordinate system, with the X'-Y' plane corresponding to the crush plane. Due to the cylindrical nature of the problem, the overall crush plane is comprised of a segment of an ellipse corresponding to the outside surface of the impact limiter. The optional end hole requires removal of its associated elliptical segment. Similarly, the optional conical surface is an elliptical, parabolic, or hyperbolic segment depending on both the drop angle,  $\theta$ , and angle of the cone.

Calculation of the differential strain is somewhat more complex. As illustrated in Figure 2.12.6-2, the differential strain,  $\varepsilon\{x,y\}$ , is calculated at the center of the differential area,  $dA$ . The differential strain is determined by calculating the amount of vertical deformation at the (x, y) location on the crush plane. The vertical distance from point (x, y) on the impact surface to the package or upper impact limiter surface is found and denoted  $z_{TOP}$ . Similarly, the vertical distance from point (x, y) on the impact surface to the undeformed lower impact limiter surface is found and denoted  $z_{BOT}$ . In equation format the differential strain at location (x, y) is simply:

$$\varepsilon = \frac{z_{BOT}}{z_{BOT} + z_{TOP}}$$

This strain is used to determine the corresponding crush stress from an implicit tabular definition of the crushable media stress-strain characteristics. For each differential area,  $dA$ , the differential force,  $dF$ , is found. The total force,  $F$ , is therefore the summation of the differential forces. Similarly, the centroidal distance,  $\bar{X}$ , is the summation of the moments,  $\bar{x} \times dF$ , divided by the total force.

Unbacked regions are defined as having an (x, y) location where  $z_{TOP}$  is calculated to occur outside the package's "shadow" (i.e., or backing, occurring on the impact limiter surface). Unbacked regions usually utilize the nominal crush strength of the crushable media (typically 10% for polyurethane foam material) for integrated force purposes. The crush strength for unbacked regions is user-definable in the program CASKDROP.

For most drop angles,  $\theta$ , and impact limiter deformations,  $\delta$ , the impact limiter crush force,  $F$ , is transmitted to the package body in direct compression. Hence, the forces transmitted to the circumferential impact limiter attachments are essentially zero. However, for nearly vertical or

horizontal orientations at small deformations where the crush force occurs beyond the edge of the package, the forces transmitted to the impact limiter attachments can be substantially large. It is important to note that only the nearly vertical or nearly horizontal orientations are required to produce the prying motion; all other orientations will always compress the impact limiter onto the package body. Figure 2.12.6-3 illustrates the near vertical and near horizontal orientations producing impact limiter separation forces.

For the near vertical orientation, the moment about point “a” determines whether a separation force exists at the impact limiter attachments. Assuming for this case that a counterclockwise moment is positive (i.e., will tend to “pry” the impact limiter off the package), the equation for the moment about point “a,”  $M_a$ , is:

$$M_a = Fx_F + F_{IL}x_{IL}$$

Similarly, for the near horizontal orientation, the moment about point “b” determines whether a separation force exists at the impact limiter attachments. Assuming for this case that a clockwise moment is positive (i.e., will tend to “pry” the impact limiter off the package), the equation for the moment about point “b,”  $M_b$ , is:

$$M_b = Fx_F - F_{IL}x_{IL}$$

If  $M_a$  or  $M_b$  are positive, a separation force will occur at the impact limiter attachments whereas if  $M_a$  or  $M_b$  are zero or negative, a separation force will not occur. Note that use of a conically shaped impact limiter typically eliminates the impact limiter separation force by causing the crush force,  $F$ , to almost always occur between points “a” and “b.”

### **2.12.6.2 An Example Problem for the CASKDROP Program**

An example problem is illustrated in Figure 2.12.6-4. The CASKDROP program utilizes a variety of physical input data to determine package and impact limiter geometry. In all cases, the package and impact limiter are assumed axisymmetric. The package is cylindrical, as is the impact limiter. Two fundamental variations in the basic cylindrical shape of the impact limiter are an optional end hole and optional conical end. The end hole may extend part or all of the way from the outside surface of the impact limiter to the package end. The conical end may be a truncated or fully developed cone, defined by a cone diameter and a cone length at the outside surface of the impact limiter. By varying the impact limiter dimensions the result is a wide variety of possible impact limiter shapes, from a totally enclosing “overpack” to pointed end-only buffers.

The CASKDROP program was primarily developed as an impact limiter design tool. Geometry and analysis control input to the CASKDROP program is fully interactive allowing changes “on the fly.” Figure 2.12.6-5 illustrates the CASKDROP screen for data entry into the *Input Window*.

The CASKDROP program allows for three types of crushable media definition:

1. **CONSTANT:** a constant crush stress independent of calculated strain.
2. **VARIABLE:** a variable, user-defined stress-strain definition.
3. **POLYFOAM:** a built-in polyurethane foam database providing accurate stress-strain definition for 5 to 25 pound per cubic foot (pcf) density and temperatures of -20 °F to +300 °F based on extensive sample testing.

The example problem assumes 20 pcf polyurethane foam at a temperature of -20 °F. A +60% bias is applied to the temperature-corrected stress-strain data to account for dynamic strain rate effects for the example problem. Figure 2.12.6-6 illustrates the CASKDROP input screen for the polyurethane foam crush media for the example problem.

For the example problem, the CASKDROP program utilizes polyurethane foam where “parallel to rise” foam curing occurs in the axial direction and “perpendicular to rise” foam curing occurs in the radial direction, although the difference between these two directions is small. The user may optionally select the “parallel-to-rise” or “perpendicular-to-rise” properties to be reversed or global for all drop orientations. For orientations other than axial (end drop) and radial (side drop), the CASKDROP program interpolates foam properties using an ellipse function. For the case where crush stress “parallel-to-rise” is in the axial direction,  $\sigma_{PAR}$ , and crush stress “perpendicular-to-rise” is in the radial direction,  $\sigma_{PER}$ , the interpolation equation at drop angle,  $\theta$ , is:

$$\sigma_{\theta} = \sqrt{\frac{1}{\left(\frac{\sin \theta}{\sigma_{PAR}}\right)^2 + \left(\frac{\cos \theta}{\sigma_{PER}}\right)^2}}$$

Similarly, for the case where crush stress “perpendicular-to-rise” is in the axial direction,  $\sigma_{PER}$ , and crush stress “parallel-to-rise” is in the radial direction,  $\sigma_{PAR}$ , the interpolation equation is:

$$\sigma_{\theta} = \sqrt{\frac{1}{\left(\frac{\sin \theta}{\sigma_{PER}}\right)^2 + \left(\frac{\cos \theta}{\sigma_{PAR}}\right)^2}}$$

The *Control Window* allows the user to specify various analysis and output controls. The *Control Window* is separated into *Analysis*, *Crush*, *Angle*, *Static*, *Dynamic*, *Print*, and *File*.

Three *Analysis* options are available: dXY defines the number of integration elements in the crush plane, 25 for the example problem; Sln defines the analysis methodology (Global versus Local Strain Theory), *Global* for the example problem;  $\epsilon/\sigma$  defines the strain (or crush stress) value to be utilized in unbacked regions (e.g., if a value is specified between 0 and 1, it is assumed a strain value and the corresponding crush stress at that strain is used; if a value is specified greater than 1, it is assumed to be a crush stress), 0.1 for the example problem corresponding to a crush stress at 10% strain from the polyurethane foam database.

The *Crush* options define the incremental deformations to be analyzed. The example problem specifies analyzing for crush deformations from 0.25 inch to 20 inch in 0.25 inch increments. Specifying a *Max* value greater than the actual maximum available crush depth (as determined geometrically) flags the CASKDROP program to not exceed the maximum available crush depth.

Similarly, the *Angle* options define the incremental angular orientations to be analyzed. The example problem specifies analyzing for drop angles from 0° to 90° in 15° increments.

The *Static* options allow the user to specify quasi-static analyses providing *Full* display output, *Smry* (summary) output, or *Both*. The example problem specifies *Full* output to the display only. Similarly, the *Dynamic* options allow the user to specify dynamic analyses providing *Full* display output, *Smry* (summary) output, or *Both*. The example problem does not specify a dynamic analysis as that module is not completed in the CASKDROP program.

The *Print* and *File* options allow the user to specify *Full* display output, *Smry* (summary) output, or *Both* to the printer or a file. The example problem specifies *Full* output to an output file only.

The *Output Window* provides the location for *Static* and *Dynamic* display output. A quasi-static solution is achieved when the strain energy of the crushable media (*SE*) is equal to the free-falling kinetic energy of the package (*KE*), or  $SE/KE = 1$ . The following tables provide a sample file output at 0° (side drop), at 45°, and at 90° (end drop).

This page left intentionally blank.



**MFFP Safety Analysis Report**

**Docket No. 71-9295  
Revision 8, June 2010**

Side Drop  
05-16-1995, 15:38:39

\*\*\* PACKAGING TECHNOLOGY \*\*\*

CASKDROP, v2.21  
Jul 01, 1994

SAMPLE PROBLEM FOR QUALITY ASSURANCE CHECK (AREAS AND VOLUMES)			
Impact Limiter Weight (each) -	1,000 lbs	Cask and Payload Weight -	10,000 lbs
Impact Limiter Outside Diameter -	60.0000 in	Cask Outside Diameter -	40.0000 in
Impact Limiter Overall Length -	24.0000 in	Cask Overall Length -	48.0000 in
Impact Limiter Conical Diameter -	48.0000 in	Dynamic Unloading Modulus -	1.000E+07 lbs/in
Impact Limiter Conical Length -	10.0000 in	Rad Mass Moment of Inertia -	12,235 lb-in-s <sup>2</sup>
Impact Limiter End Thickness -	12.0000 in	Frictional Coefficient -	0.0000
Impact Limiter Hole Diameter -	20.0000 in	Drop Height -	30.0000 ft
Impact Limiter Hole Length -	8.0000 in	Drop Angle from Horizontal -	0.0000°
Unbacked Area Threshold Strain -	0.1000 in/in	Crush Analysis Theory -	Global
Unbacked Area Crush Stress -	2,675 psi	Number of Integration Incs -	25

POLYFOAM CRUSH STRESS (Axial: "  " to rise)	
Density = 20.000 pcf Temp = -20.000 °F σ-yield = 2,552.3 psi Bias = 60.000%	
ε (in/in)	σ (psi)
0.000	0.0
0.100	2,552.3
0.200	2,687.0
0.300	2,868.8
0.400	3,302.9
0.500	4,115.1
0.600	6,074.3
0.650	7,942.0
0.700	10,925.0
0.750	15,001.8
0.800	26,829.5

POLYFOAM CRUSH STRESS (Radial: "⊥" to rise)	
Density = 20.000 pcf Temp = -20.000 °F σ-yield = 2,675.0 psi Bias = 60.000%	
ε (in/in)	σ (psi)
0.000	0.0
0.100	2,675.0
0.200	2,785.4
0.300	2,959.9
0.400	3,345.9
0.500	4,147.7
0.600	6,062.8
0.650	7,868.8
0.700	10,180.0
0.750	15,554.4
0.800	29,704.8

POLYFOAM CRUSH STRESS (Actual Data @ 0.0°)	
Density = 20.000 pcf Temp = -20.000 °F σ-yield = 2,675.0 psi Bias = 60.000%	
ε (in/in)	σ (psi)
0.000	0.0
0.100	2,675.0
0.200	2,785.4
0.300	2,959.9
0.400	3,345.9
0.500	4,147.7
0.600	6,062.8
0.650	7,868.8
0.700	10,180.0
0.750	15,554.4
0.800	29,704.8

DEFL (in)	MAX ε (%)	AREA (in <sup>2</sup> )	VOLUME (in <sup>3</sup> )	XBAR (in)	IMPACT FORCE (lbs)	ACCEL (g's)	I/L MOMENT (in-lbs)	STRAIN ENERGY (in-lbs)	KINETIC ENERGY (in-lbs)	SE/KE RATIO
0.250	2.50	221	37	0.00	106,881	8.9	0	13,360	4,323,000	0.00
0.500	5.00	318	105	0.00	289,508	24.1	0	62,909	4,326,000	0.01
0.750	7.50	396	194	0.00	518,875	43.2	0	163,957	4,329,000	0.04
1.000	10.00	465	302	0.00	733,200	61.1	0	320,466	4,332,000	0.07



MFFP Safety Analysis Report

Docket No. 71-9295
Revision 8, June 2010

Side Drop
05-16-1995, 15:38:39

\*\*\* PACKAGING TECHNOLOGY \*\*\*
(continued...)

CASKDROP, v2.21
Jul 01, 1994

Table with 11 columns: DEFL (in), MAX ε (%), AREA (in2), VOLUME (in3), XBAR (in), IMPACT FORCE (lbs), ACCEL (g's), I/L MOMENT (in-lbs), STRAIN ENERGY (in-lbs), KINETIC ENERGY (in-lbs), SE/KE RATIO. Rows show data for various drop heights from 1.250 to 10.000 inches.



**MFFP Safety Analysis Report**

**Docket No. 71-9295**  
**Revision 8, June 2010**

Corner Drop  
 05-16-1995, 15:38:39

\*\*\* PACKAGING TECHNOLOGY \*\*\*

CASKDROP, v2.21  
 Jul 01, 1994

SAMPLE PROBLEM FOR QUALITY ASSURANCE CHECK (AREAS AND VOLUMES)			
Impact Limiter Weight (each) -	1,000 lbs	Cask and Payload Weight -	10,000 lbs
Impact Limiter Outside Diameter -	60.0000 in	Cask Outside Diameter -	40.0000 in
Impact Limiter Overall Length -	24.0000 in	Cask Overall Length -	48.0000 in
Impact Limiter Conical Diameter -	48.0000 in	Dynamic Unloading Modulus -	1.000E+07 lbs/in
Impact Limiter Conical Length -	10.0000 in	Rad Mass Moment of Inertia -	12,235 lb-in-s <sup>2</sup>
Impact Limiter End Thickness -	12.0000 in	Frictional Coefficient -	0.0000
Impact Limiter Hole Diameter -	20.0000 in	Drop Height -	30.0000 ft
Impact Limiter Hole Length -	8.0000 in	Drop Angle from Horizontal -	45.0000°
Unbacked Area Threshold Strain -	0.1000 in/in	Crush Analysis Theory -	Global
Unbacked Area Crush Stress -	2,611 psi	Number of Integration Incs -	25

POLYFOAM CRUSH STRESS (Axial: "  " to rise)	
Density = 20.000 pcf	
Temp = -20.000 °F	
σ-yield = 2,552.3 psi	
Bias = 60.000%	
ε (in/in)	σ (psi)
0.000	0.0
0.100	2,552.3
0.200	2,687.0
0.300	2,868.8
0.400	3,302.9
0.500	4,115.1
0.600	6,074.3
0.650	7,942.0
0.700	10,925.0
0.750	15,001.8
0.800	26,829.5

POLYFOAM CRUSH STRESS (Radial: "⊥" to rise)	
Density = 20.000 pcf	
Temp = -20.000 °F	
σ-yield = 2,675.0 psi	
Bias = 60.000%	
ε (in/in)	σ (psi)
0.000	0.0
0.100	2,675.0
0.200	2,785.4
0.300	2,959.9
0.400	3,345.9
0.500	4,147.7
0.600	6,062.8
0.650	7,868.8
0.700	10,180.0
0.750	15,554.4
0.800	29,704.8

POLYFOAM CRUSH STRESS (Actual Data @ 45.0°)	
Density = 20.000 pcf	
Temp = -20.000 °F	
σ-yield = 2,611.5 psi	
Bias = 60.000%	
ε (in/in)	σ (psi)
0.000	0.0
0.100	2,611.5
0.200	2,734.9
0.300	2,913.3
0.400	3,324.2
0.500	4,131.3
0.600	6,068.5
0.650	7,905.2
0.700	10,532.8
0.750	15,270.6
0.800	28,157.6

DEFL (in)	MAX ε (%)	AREA (in <sup>2</sup> )	VOLUME (in <sup>3</sup> )	XBAR (in)	IMPACT FORCE (lbs)	ACCEL (g's)	I/L MOMENT (in-lbs)	STRAIN ENERGY (in-lbs)	KINETIC ENERGY (in-lbs)	SE/KE RATIO
0.250	1.44	7	1	-8.30	1,351	0.1	0	169	4,323,000	0.00
0.500	2.88	20	4	-8.11	7,756	0.6	0	1,307	4,326,000	0.00
0.750	4.33	36	11	-7.90	21,631	1.8	0	4,981	4,329,000	0.00
1.000	5.79	55	22	-7.68	44,807	3.7	0	13,286	4,332,000	0.00
1.250	7.25	78	39	-7.44	78,737	6.6	0	28,729	4,335,000	0.01
1.500	8.71	102	61	-7.19	124,483	10.4	0	54,131	4,338,000	0.01
1.750	10.18	129	90	-6.92	182,320	15.2	0	92,481	4,341,000	0.02



**MFFP Safety Analysis Report**

**Docket No. 71-9295  
Revision 8, June 2010**

Corner Drop  
05-16-1995, 15:38:39

\*\*\* PACKAGING TECHNOLOGY \*\*\*  
(continued...)

CASKDROP, v2.21  
Jul 01, 1994

DEFL (in)	MAX ε (%)	AREA (in <sup>2</sup> )	VOLUME (in <sup>3</sup> )	XBAR (in)	IMPACT FORCE (lbs)	ACCEL (g's)	I/L MOMENT (in-lbs)	STRAIN ENERGY (in-lbs)	KINETIC ENERGY (in-lbs)	SE/KE RATIO
2.000	11.66	158	126	-6.65	250,919	20.9	0	146,636	4,344,000	0.03
2.250	13.14	189	169	-6.39	327,791	27.3	0	218,975	4,347,000	0.05
2.500	14.63	222	221	-6.15	409,985	34.2	0	311,197	4,350,000	0.07
2.750	16.12	256	280	-5.92	495,229	41.3	0	424,349	4,353,000	0.10
3.000	17.64	290	349	-5.70	581,988	48.5	0	559,001	4,356,000	0.13
3.250	19.14	321	425	-5.53	666,955	55.6	0	715,119	4,359,000	0.16
3.500	21.04	350	509	-5.39	750,161	62.5	0	892,258	4,362,000	0.20
3.750	23.53	379	600	-5.30	832,241	69.4	0	1,090,058	4,365,000	0.25
4.000	26.04	407	698	-5.24	913,114	76.1	0	1,308,228	4,368,000	0.30
4.250	28.58	435	804	-5.21	993,967	82.8	0	1,546,613	4,371,000	0.35
4.500	31.14	462	916	-5.20	1,075,026	89.6	0	1,805,237	4,374,000	0.41
4.750	33.55	490	1,035	-5.22	1,157,389	96.4	0	2,084,289	4,377,000	0.48
5.000	35.86	517	1,161	-5.24	1,240,678	103.4	0	2,384,048	4,380,000	0.54
5.250	38.16	545	1,293	-5.27	1,325,202	110.4	0	2,704,783	4,383,000	0.62
5.500	40.44	573	1,433	-5.30	1,413,119	117.8	0	3,047,073	4,386,000	0.69
5.750	42.71	600	1,579	-5.33	1,503,231	125.3	0	3,411,616	4,389,000	0.78
6.000	44.96	628	1,733	-5.37	1,596,230	133.0	0	3,799,049	4,392,000	0.86
6.250	47.21	656	1,894	-5.40	1,692,397	141.0	0	4,210,127	4,395,000	0.96
6.359	48.17	668	1,966	-5.41	1,735,814	144.7	0	4,396,303	4,396,303	1.00
6.500	49.43	684	2,061	-5.42	1,792,981	149.4	0	4,837,403	4,398,000	1.10
6.750	51.75	711	2,236	-5.44	1,897,584	158.1	0	5,298,723	4,401,000	1.20
7.000	54.19	739	2,417	-5.46	2,009,560	167.5	0	5,787,116	4,404,000	1.31
7.250	56.65	767	2,605	-5.47	2,128,316	177.4	0	6,304,351	4,407,000	1.43
7.500	59.12	795	2,800	-5.48	2,255,709	188.0	0	6,852,354	4,410,000	1.55
7.750	61.60	824	3,002	-5.48	2,392,365	199.4	0	7,433,363	4,413,000	1.68
8.000	64.10	852	3,212	-5.47	2,538,941	211.6	0	8,049,776	4,416,000	1.82
8.250	66.60	881	3,429	-5.47	2,701,943	225.2	0	8,704,887	4,419,000	1.97
8.500	69.12	909	3,652	-5.45	2,882,629	240.2	0	9,402,959	4,422,000	2.13
8.750	71.65	938	3,883	-5.43	3,079,002	256.6	0	10,148,162	4,425,000	2.29
9.000	74.19	967	4,121	-5.38	3,300,885	275.1	0	10,945,648	4,428,000	2.47
9.250	76.75	995	4,367	-5.32	3,573,055	297.8	0	11,804,891	4,431,000	2.66
9.500	79.31	1,024	4,619	-5.26	3,901,592	325.1	0	12,739,222	4,434,000	2.87
9.750	81.89	1,053	4,879	-5.17	4,292,510	357.7	0	13,763,484	4,437,000	3.10
10.000	84.49	1,082	5,146	-5.06	4,763,070	396.9	0	14,895,432	4,440,000	3.35
10.250	87.09	1,109	5,419	-4.95	5,316,128	443.0	0	16,155,332	4,443,000	3.64
10.500	89.71	1,134	5,698	-4.83	5,947,562	495.6	0	17,563,293	4,446,000	3.95
10.750	92.34	1,161	5,985	-4.74	6,665,548	555.5	0	19,139,932	4,449,000	4.30
11.000	94.98	1,184	6,270	-4.63	7,465,195	622.1	0	20,906,275	4,452,000	4.70
11.250	97.64	1,206	6,563	-4.54	8,360,345	696.7	0	22,884,467	4,455,000	5.14

End Drop  
05-16-1995, 15:38:39

\*\*\* PACKAGING TECHNOLOGY \*\*\*

CASKDROP, v2.21  
Jul 01, 1994

SAMPLE PROBLEM FOR QUALITY ASSURANCE CHECK (AREAS AND VOLUMES)			
Impact Limiter Weight (each) -	1,000 lbs	Cask and Payload Weight -	10,000 lbs
Impact Limiter Outside Diameter -	60.0000 in	Cask Outside Diameter -	40.0000 in
Impact Limiter Overall Length -	24.0000 in	Cask Overall Length -	48.0000 in
Impact Limiter Conical Diameter -	48.0000 in	Dynamic Unloading Modulus -	1.000E+07 lbs/in
Impact Limiter Conical Length -	10.0000 in	Rad Mass Moment of Inertia -	12,235 lb-in-s <sup>2</sup>
Impact Limiter End Thickness -	12.0000 in	Frictional Coefficient -	0.0000
Impact Limiter Hole Diameter -	20.0000 in	Drop Height -	30.0000 ft
Impact Limiter Hole Length -	8.0000 in	Drop Angle from Horizontal -	90.0000°
Unbacked Area Threshold Strain -	0.1000 in/in	Crush Analysis Theory -	Global
Unbacked Area Crush Stress -	2,552 psi	Number of Integration Incs -	25

POLYFOAM CRUSH STRESS (Axial: "  " to rise)	
Density = 20.000 pcf	
Temp = -20.000 F	
σ-yield = 2,552.3 psi	
Bias = 60.000%	
ε (in/in)	σ (psi)
0.000	0.0
0.100	2,552.3
0.200	2,687.0
0.300	2,868.8
0.400	3,302.9
0.500	4,115.1
0.600	6,074.3
0.650	7,942.0
0.700	10,925.0
0.750	15,001.8
0.800	26,829.5

POLYFOAM CRUSH STRESS (Radial: "⊥" to rise)	
Density = 20.000 pcf	
Temp = -20.000 F	
σ-yield = 2,675.0 psi	
Bias = 60.000%	
ε (in/in)	σ (psi)
0.000	0.0
0.100	2,675.0
0.200	2,785.4
0.300	2,959.9
0.400	3,345.9
0.500	4,147.7
0.600	6,062.8
0.650	7,868.8
0.700	10,180.0
0.750	15,554.4
0.800	29,704.8

POLYFOAM CRUSH STRESS (Actual Data @ 90.0°)	
Density = 20.000 pcf	
Temp = -20.000 F	
σ-yield = 2,552.3 psi	
Bias = 60.000%	
ε (in/in)	σ (psi)
0.000	0.0
0.100	2,552.3
0.200	2,687.0
0.300	2,868.8
0.400	3,302.9
0.500	4,115.1
0.600	6,074.3
0.650	7,942.0
0.700	10,925.0
0.750	15,001.8
0.800	26,829.5

DEFL (in)	MAX ε (%)	AREA (in <sup>2</sup> )	VOLUME (in <sup>3</sup> )	XBAR (in)	IMPACT FORCE (lbs)	ACCEL (g's)	I/L MOMENT (in-lbs)	STRAIN ENERGY (in-lbs)	KINETIC ENERGY (in-lbs)	SE/KE RATIO
0.250	2.08	1,518	377	0.00	810,360	67.5	0	101,295	4,323,000	0.02
0.500	4.17	1,541	759	0.00	1,592,808	132.7	0	401,691	4,326,000	0.09
0.750	6.25	1,564	1,147	0.00	2,311,804	192.7	0	889,768	4,329,000	0.21
1.000	8.33	1,587	1,541	0.00	2,931,701	244.3	0	1,545,206	4,332,000	0.36
1.250	10.42	1,610	1,941	0.00	3,416,844	284.7	0	2,338,774	4,335,000	0.54
1.500	12.50	1,634	2,346	0.00	3,752,646	312.7	0	3,234,960	4,338,000	0.75
1.750	14.58	1,657	2,758	0.00	3,971,661	331.0	0	4,200,498	4,341,000	0.97



**MFFP Safety Analysis Report**

**Docket No. 71-9295  
Revision 8, June 2010**

End Drop  
05-16-1995, 15:38:39

\*\*\* PACKAGING TECHNOLOGY \*\*\*  
(continued...)

CASKDROP, v2.21  
Jul 01, 1994

DEFL (in)	MAX ε (%)	AREA (in <sup>2</sup> )	VOLUME (in <sup>3</sup> )	XBAR (in)	IMPACT FORCE (lbs)	ACCEL (g's)	I/L MOMENT (in-lbs)	STRAIN ENERGY (in-lbs)	KINETIC ENERGY (in-lbs)	SE/KE RATIO
1.785	14.88	1,661	2,816	0.00	3,995,461	333.0	0	4,341,425	4,341,425	1.00
2.000	16.67	1,681	3,175	0.00	4,112,712	342.7	0	5,354,946	4,344,000	1.23
2.250	18.75	1,705	3,598	0.00	4,214,497	351.2	0	6,395,847	4,347,000	1.47
2.500	20.83	1,729	4,027	0.00	4,287,704	357.3	0	7,458,622	4,350,000	1.71
2.750	22.92	1,753	4,462	0.00	4,351,294	362.6	0	8,538,497	4,353,000	1.96
3.000	25.00	1,777	4,904	0.00	4,445,683	370.5	0	9,638,119	4,356,000	2.21
3.250	27.08	1,801	5,351	0.00	4,562,636	380.2	0	10,764,159	4,359,000	2.47
3.500	29.17	1,826	5,804	0.00	4,693,990	391.2	0	11,921,237	4,362,000	2.73
3.750	31.25	1,851	6,264	0.00	4,831,784	402.6	0	13,111,959	4,365,000	3.00
4.000	33.33	1,875	6,730	0.00	4,973,522	414.5	0	14,337,622	4,368,000	3.28
4.250	35.42	1,900	7,202	0.00	5,120,673	426.7	0	15,599,396	4,371,000	3.57
4.500	37.50	1,925	7,680	0.00	5,274,868	439.6	0	16,898,839	4,374,000	3.86
4.750	39.58	1,951	8,164	0.00	5,437,800	453.2	0	18,237,922	4,377,000	4.17
5.000	41.67	1,976	8,655	0.00	5,611,685	467.6	0	19,619,108	4,380,000	4.48
5.250	43.75	2,002	9,152	0.00	5,802,397	483.5	0	21,045,868	4,383,000	4.80
5.500	45.83	2,027	9,656	0.00	6,018,789	501.6	0	22,523,516	4,386,000	5.14
5.750	47.92	2,053	10,166	0.00	6,268,472	522.4	0	24,059,424	4,389,000	5.48
6.000	50.00	2,079	10,682	0.00	6,560,063	546.7	0	25,662,991	4,392,000	5.84
6.250	52.08	2,105	11,205	0.00	6,900,740	575.1	0	27,345,591	4,395,000	6.22
6.500	54.17	2,131	11,735	0.00	7,296,837	608.1	0	29,120,288	4,398,000	6.62
6.750	56.25	2,158	12,271	0.00	7,751,903	646.0	0	31,001,381	4,401,000	7.04
7.000	58.33	2,184	12,814	0.00	8,272,373	689.4	0	33,004,415	4,404,000	7.49
7.250	60.42	2,211	13,363	0.00	8,862,880	738.6	0	35,146,322	4,407,000	7.98
7.500	62.50	2,238	13,919	0.00	9,556,877	796.4	0	37,448,792	4,410,000	8.49
7.750	64.58	2,265	14,482	0.00	10,454,871	871.2	0	39,950,260	4,413,000	9.05
8.000	66.67	2,606	15,051	0.00	11,632,851	969.4	0	42,711,226	4,416,000	9.67
8.250	68.75	2,633	15,706	0.00	13,506,993	1,125.6	0	45,853,706	4,419,000	10.38
8.500	70.83	2,660	16,368	0.00	14,954,954	1,246.2	0	49,411,449	4,422,000	11.17
8.750	72.92	2,688	17,037	0.00	16,218,008	1,351.5	0	53,308,070	4,425,000	12.05
9.000	75.00	2,715	17,712	0.00	18,519,890	1,543.3	0	57,650,307	4,428,000	13.02
9.250	77.08	2,743	18,394	0.00	22,571,268	1,880.9	0	62,786,702	4,431,000	14.17
9.500	79.17	2,771	19,084	0.00	27,794,818	2,316.2	0	69,082,462	4,434,000	15.58
9.750	81.25	2,799	19,780	0.00	33,405,583	2,783.8	0	76,732,513	4,437,000	17.29
10.000	83.33	2,827	20,483	0.00	39,286,171	3,273.8	0	85,818,982	4,440,000	19.33
10.250	85.42	2,827	21,190	0.00	45,050,964	3,754.2	0	96,361,124	4,443,000	21.69
10.500	87.50	2,827	21,897	0.00	51,018,884	4,251.6	0	108,369,855	4,446,000	24.37
10.750	89.58	2,827	22,604	0.00	57,507,705	4,792.3	0	121,935,678	4,449,000	27.41
11.000	91.67	2,827	23,311	0.00	64,451,479	5,371.0	0	137,180,576	4,452,000	30.81
11.250	93.75	2,827	24,017	0.00	74,690,773	6,224.2	0	154,573,358	4,455,000	34.70
11.500	95.83	2,827	24,724	0.00	85,563,336	7,130.3	0	174,605,121	4,458,000	39.17
11.750	97.92	2,827	25,431	0.00	96,435,898	8,036.3	0	197,355,026	4,461,000	44.24
12.000	100.00	2,827	26,138	0.00	107,308,461	8,942.4	0	222,823,071	4,464,000	49.92

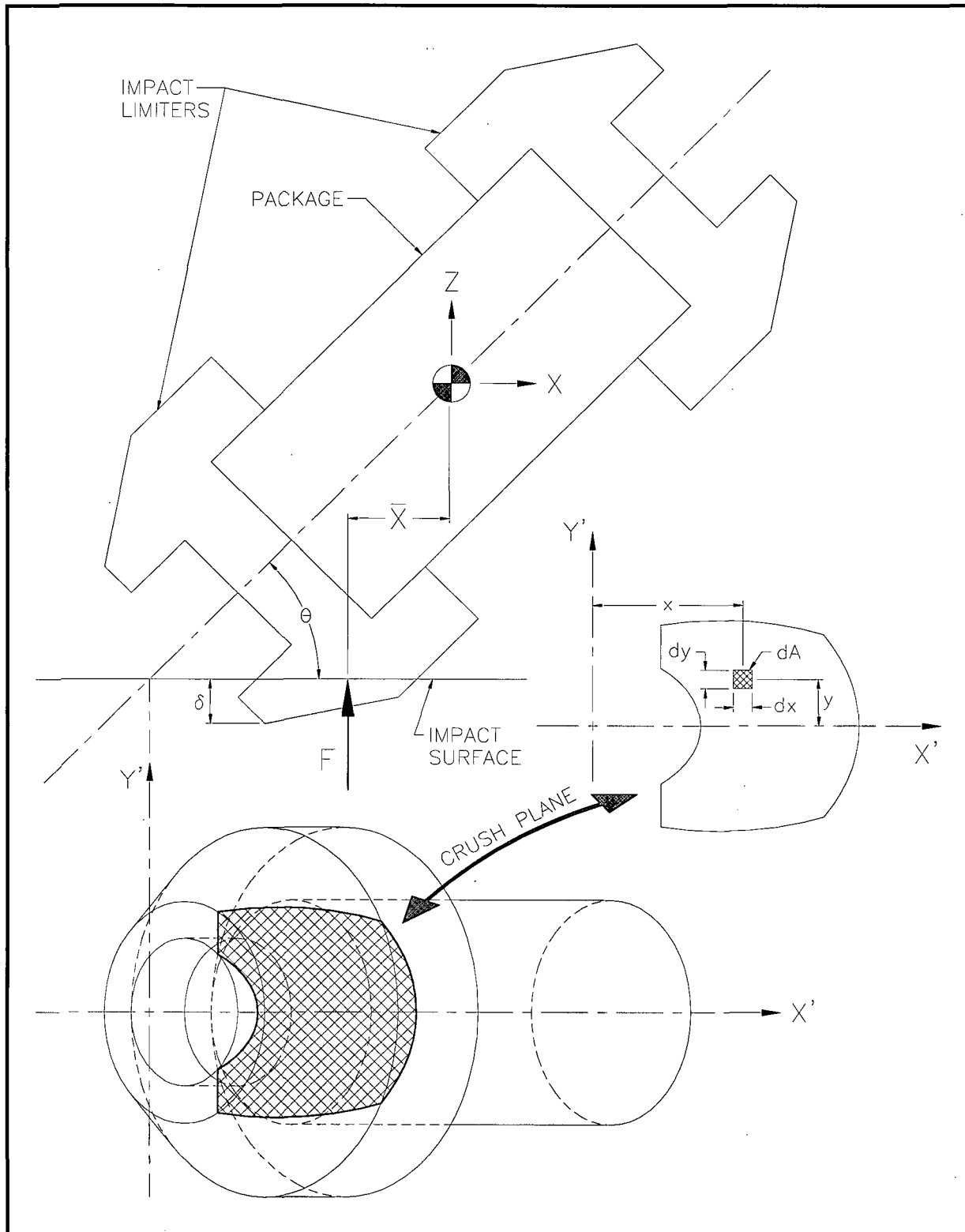


**FIGURE 2.12.6-1 – Impact Limiter Force and Centroid Development**

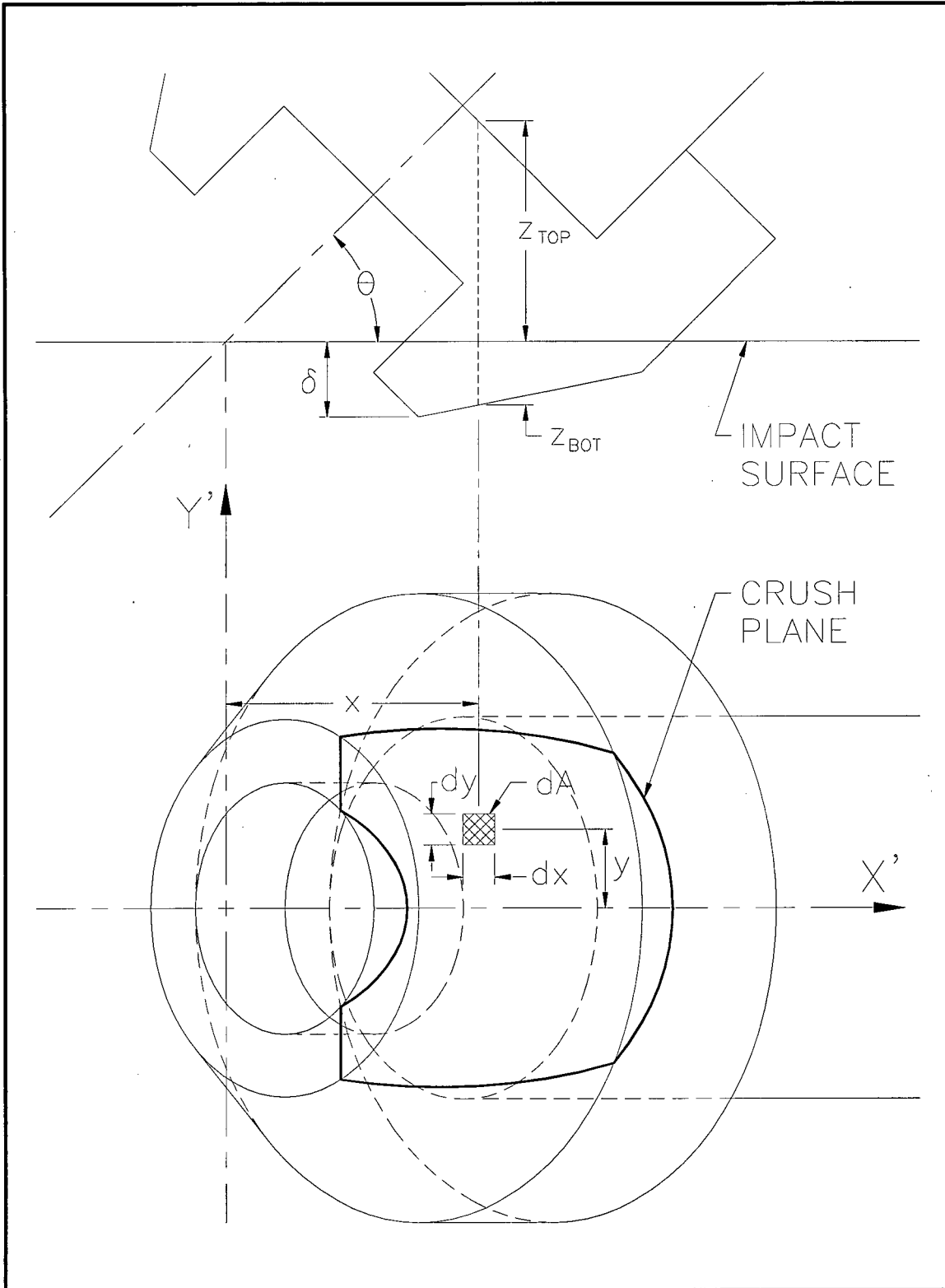


**FIGURE 2.12.6-2 – Strain Determination**

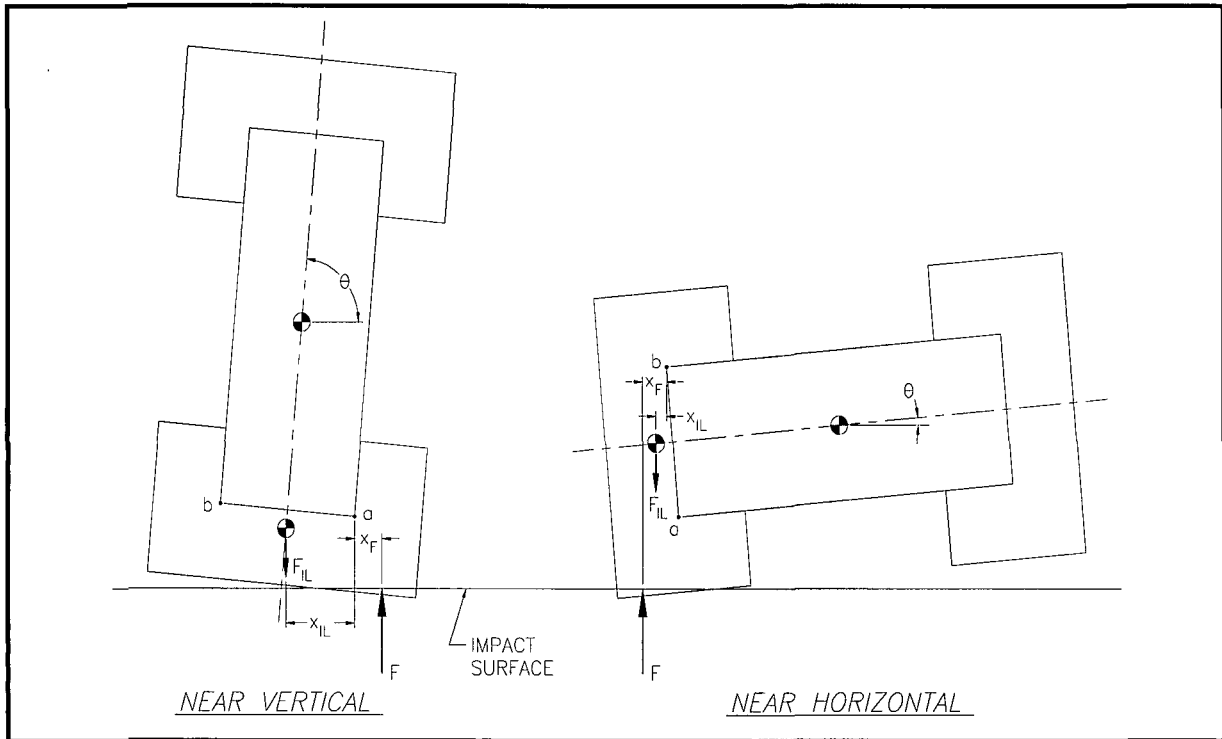


**FIGURE 2.12.6-3 – Determination of Impact Limiter Separation Moments**

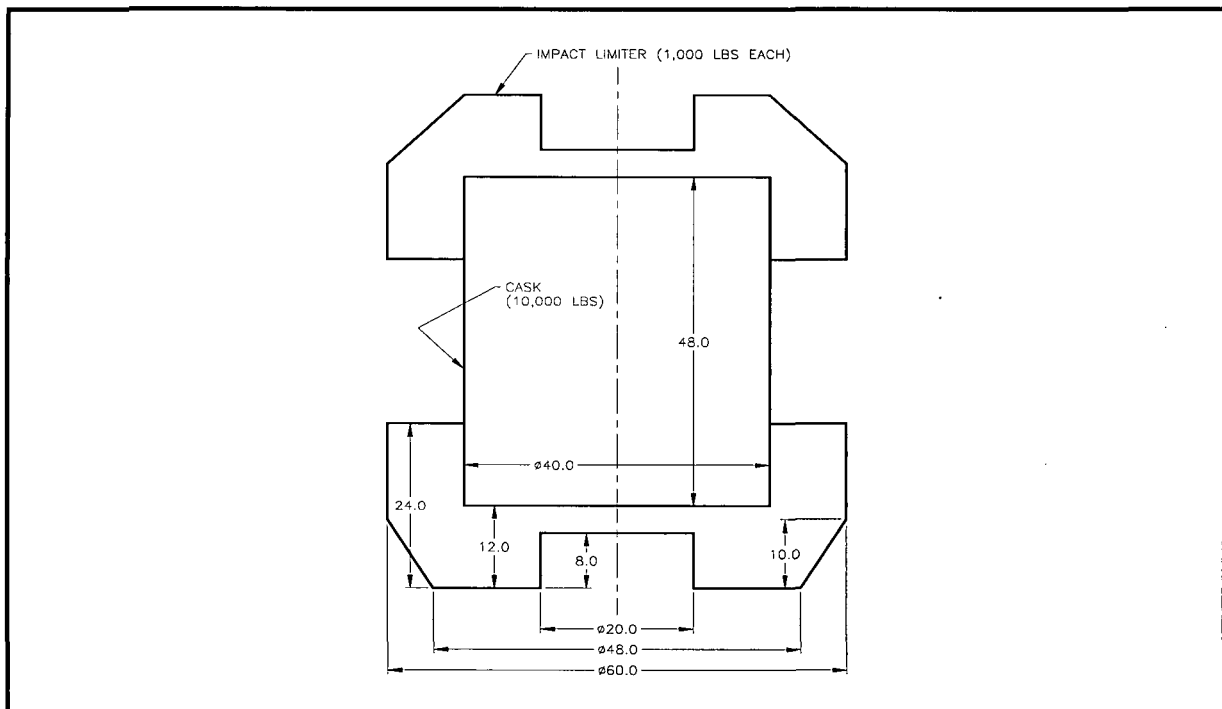


**FIGURE 2.12.6-4 – Example Problem for CASKDROP**

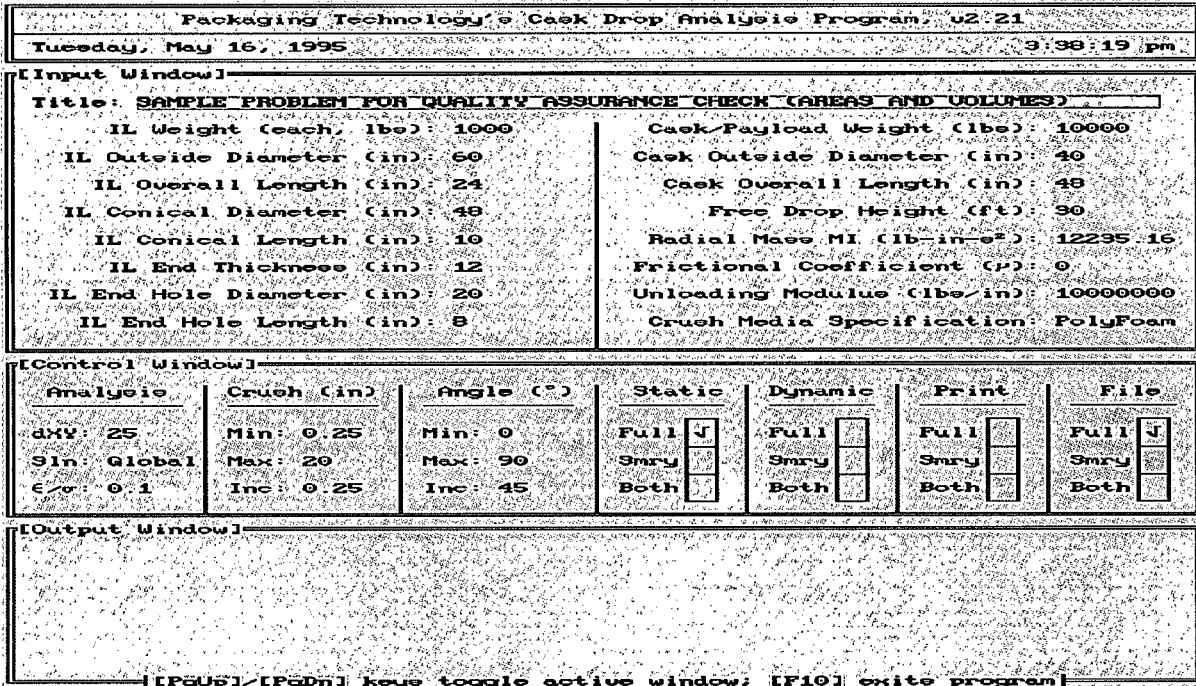


**FIGURE 2.12.6-5 – The CASKDROPP Program Input Window**

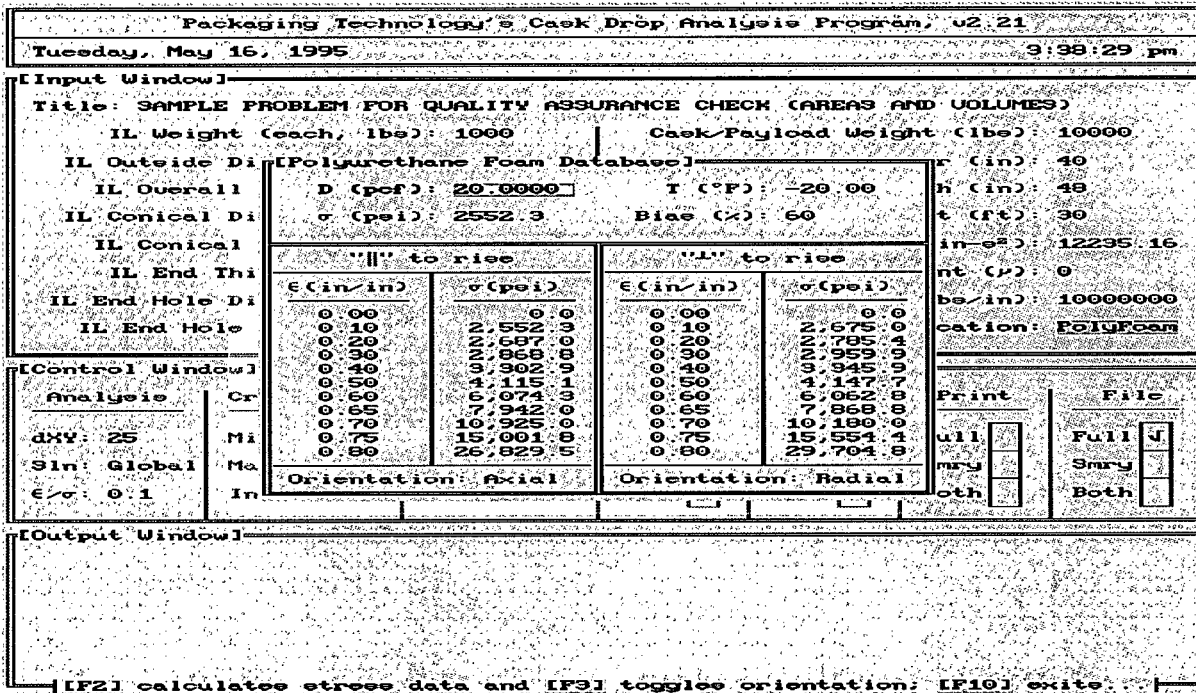


**FIGURE 2.12.6-6 – The CASKDROPP Program Polyurethane Foam Window**

## 2.12.7 Impact Limiter Weld Joint Test Results

This appendix documents the results of bench tests of MFFP impact limiter weld joint designs. As shown in Figure 2.12.3-7 of Appendix 2.12.3, *Certification Test Results*, the closure weld (top outer corner angle) of the certification test unit (CTU) lid end impact limiter failed due to the 30-foot side free drop. Although the damage was assessed in Chapter 3.0, *Thermal Evaluation*, and determined to preserve O-ring seal temperatures within acceptable limits, maintaining the structural integrity of the weld joint is desirable.

Two 12-inch × 12-inch × 18-inch long L-shaped test specimens were fabricated to demonstrate weld joint integrity. The first test specimen (TS-1) utilized the weld joint for the impact limiter closure weld, as shown in the packaging drawings in Appendix 1.4.2, *Packaging General Arrangement Drawings*. The second test specimen (TS-2) was prototypic of the weld joint utilized for the CTU impact limiter. Both specimens were fabricated using Type 304 stainless steel material, which was the same material used for the CTU impact limiters. The two weld joint designs are shown in Figure 2.12.7-1.

### 2.12.7.1 Packaging Weld Joint Design

The packaging closure weld joint design utilizes a V-groove butt weld between the steel top plate and the corner angle. Since both the plate and the angle are joined through their full thickness, full-strength of the material is developed as the joint is deformed. The polyurethane foam is then fully encased in the steel shell of the impact limiter. Without direct exposure, the polyurethane foam will not experience any significant damage for the subsequent puncture drop and thermal event of 10 CFR §71.73<sup>1</sup>.

### 2.12.7.2 Certification Test Unit Weld Joint Design

The closure weld of the CTU impact limiter consisted of a single-sided fillet weld between the corner angle and the 1/4-inch thick steel top plate, which included 1/2-inch deep slots at 5.2 inch spacing. Because the access to the inside of the plate and angle was not possible, the fillet weld was the only structural weld between the corner angle and the steel plate around the circumference of the impact limiter. During free drop impact, the plate/angle joint has to deform as a unit in order to maintain closure. However, the single-sided fillet weld is not adequate to cause the leg of the angle to deform with the plate. As the plate buckles and rotates due to compression of the impact, cracks develop in the fillet weld, which then leads to weld failure and separation between the angle and the 1/4-inch thick steel plate.

### 2.12.7.3 Bench Test Results

Each test specimen was placed in a hydraulic press so that the outside root of the angle was contacted by the hydraulic ram. The 1/4-inch plates were oriented at approximately 45 degrees with respect to the axis of the press. The test set-up is shown in Figure 2.12.7-2.

---

<sup>1</sup> Title 10, Code of Federal Regulations, Part 71 (10 CFR 71), *Packaging and Transportation of Radioactive Material*, Final Rule, 01-26-04.

Test Specimen 1 (TS-1) reflected the packaging weld joint design while Test Specimen 2 (TS-2) used the CTU weld joint design. Deforming TS-1 to nearly a flat condition resulted in no cracks developing in the welds. The fully deformed shape of TS-1 is shown in Figure 2.12.7-3. As shown in Figure 2.12.7-4, no cracks developed in the V-groove butt weld joint.

As TS-2 was deformed, cracks in the fillet welds initiated in the 1/2-inch slots. The cracks propagated beyond the slots into the straight section of the fillet weld as the specimen was further deformed. With continued deformation, the crack propagated until the fillet weld failed over its entire length. The plate was then separate from the angle leg, which did not bend. This behavior replicated the exact failure of the closure weld in the CTU impact limiters from the 30-foot side free drop. The TS-2 weld failure is shown in Figure 2.12.7-5 and Figure 2.12.7-6

#### 2.12.7.4 Conclusions

Based on the comparable testing of the two different weld joint designs, it has been demonstrated that the design shown in the packaging drawings in Appendix 1.4.2, *Packaging General Arrangement Drawings*, is capable of large deformation without failure of the weld joint, and hence, preventing exposure of the polyurethane foam.

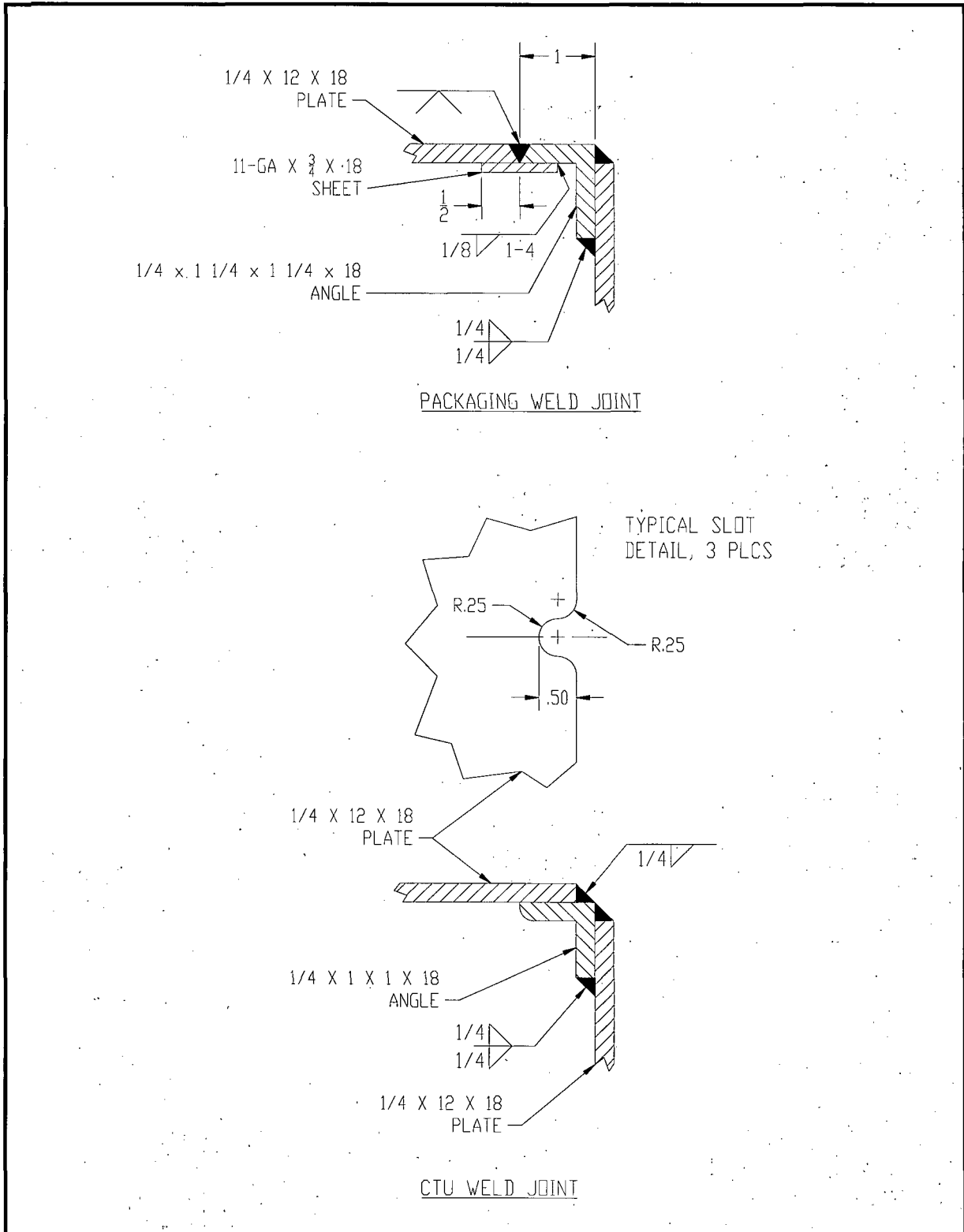
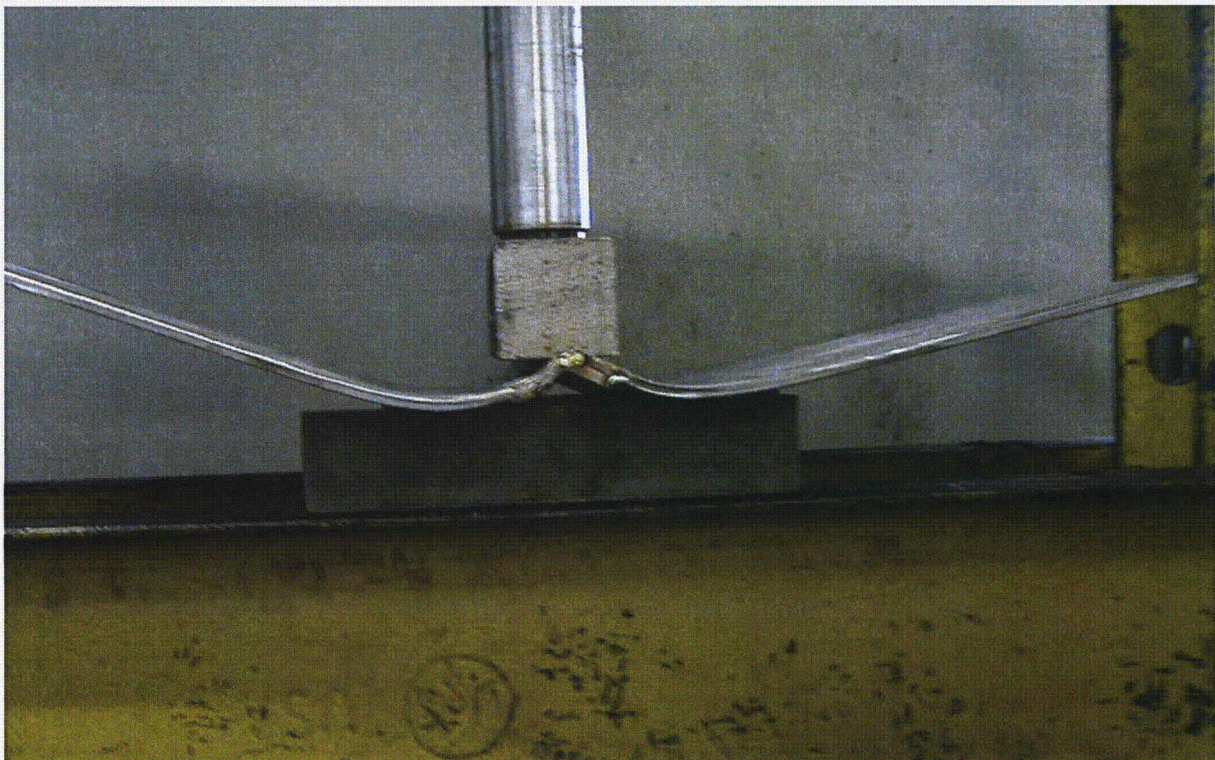


FIGURE 2.12.7-1 – Weld Joint Designs for Test Specimens



**FIGURE 2.12.7-2 – Bench Test Set-Up (TS-2 Shown)**



**FIGURE 2.12.7-3 – TS-1 Fully Deformed**

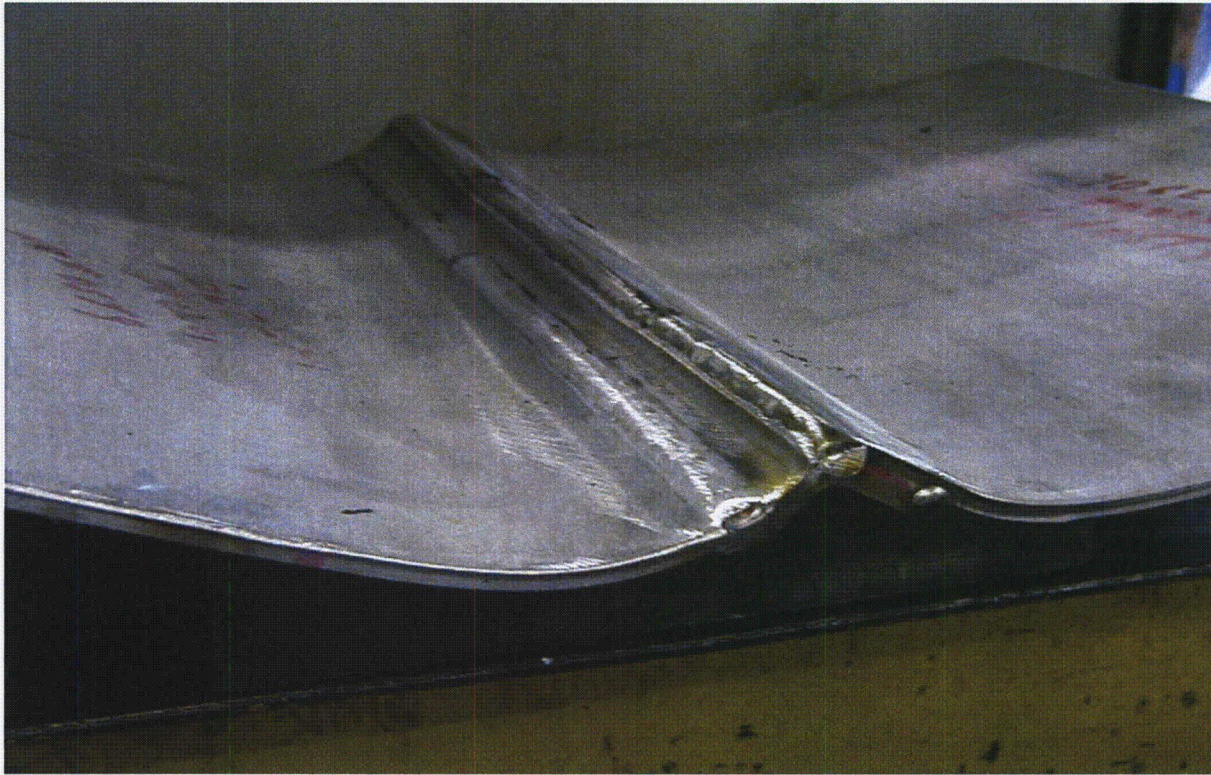


FIGURE 2.12.7-4 – View of V-Groove Weld of TS-1 (No weld cracks)

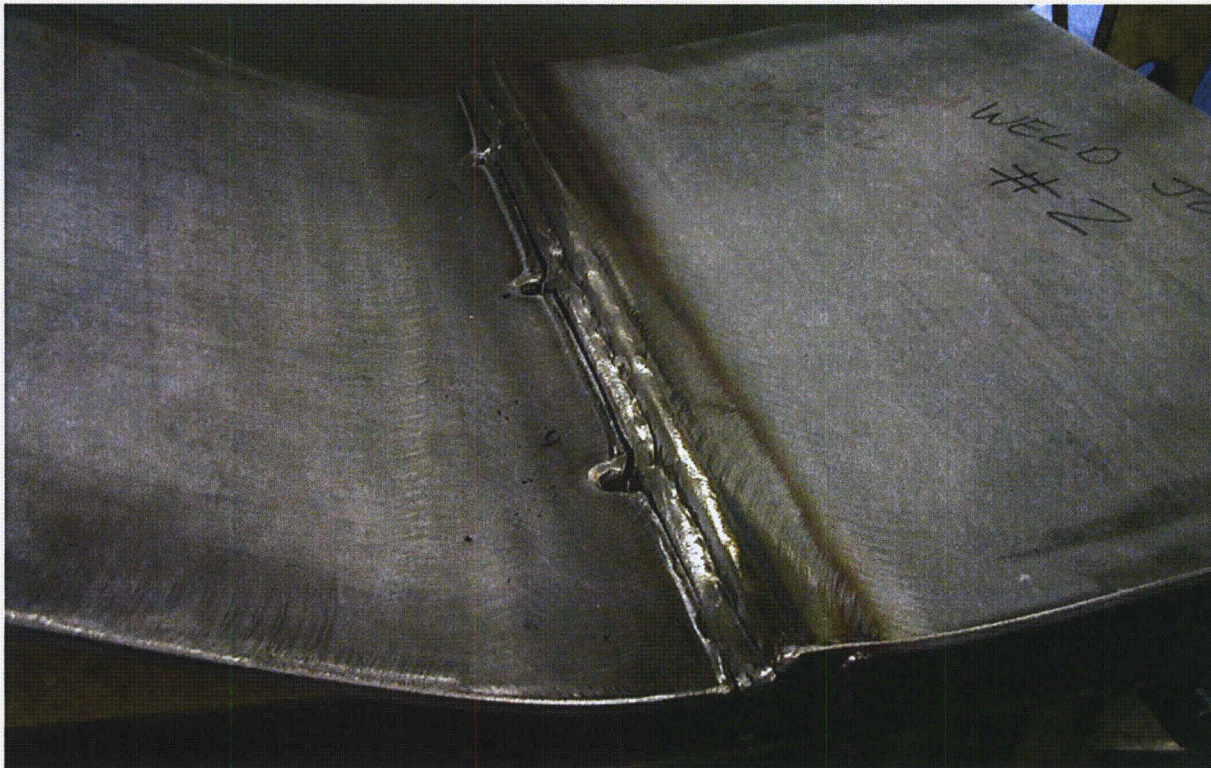


FIGURE 2.12.7-5 – View of Fillet Weld Failure of TS-2



**FIGURE 2.12.7-6 – Close-up View of TS-2 Failed Fillet Weld Joint**

## 2.12.8 Effect of Bounding Weight on Package Structural Responses

The free drop and puncture drop testing documented in Appendix 2.12.3, *Certification Test Results*, was performed without the presence of the fuel control structures (FCSs). Since the FCSs are integral with the strongback, they represent an additional contents weight that was not accounted for by the certification testing. Note that “contents” in this context refers to the fissile material contents (fuel assemblies) plus the strongback. This appendix documents the MFFP structural responses that would result from the increased weight of the contents consistent with the addition of the FCS.

### 2.12.8.1 Component Weights

As shown in Section 2.1.3, *Weights and Center of Gravity*, the maximum gross weight of the MFFP is 14,260 pounds, and the weight of the contents (including the FCS) is equal to the sum of the strongback (3,030 pounds) and three fuel assemblies (4,740 pounds), or 7,770 pounds. The certification test was performed in three series. The maximum gross weight and the weights of the certification test series are compared in Table 2.12.8-1 (Certification test weight data is extracted from Section 2.12.3.6, *Test Unit Description*).

### 2.12.8.2 Evaluations

The certification test series summary is given in Table 2.12.2-1. Each test is examined in the following paragraphs for the effect of the increased weight on the test results. Each evaluation focuses on the behavior of the package containment structure or impact limiters. The effect of the addition of the FCS on the strongback and fuel assembly behavior is evaluated separately in Appendix 2.12.5, *Fuel Control Structure Evaluation*. A buckling evaluation for the body shell is not needed since the increased weight, which is primarily associated with the contents, does not affect buckling response. The effect of maximum gross weight on the maximum impact limiter deformation in the warm condition is evaluated in Appendix 2.12.1, *Impact Limiter Evaluation*. The maximum deformations reported in Table 2.12.1-8 are evaluated using the maximum licensed package weight of 14,260 pounds (or 36.61 lb<sub>m</sub>-s<sup>2</sup>/in, as shown in Table 2.12.1-6). Impact limiter maximum crush responses are not further evaluated in this appendix.

#### 2.12.8.2.1 Test Series 1

The first test in Series 1 was a 30-ft horizontal free drop. The purpose of this test was to demonstrate that the containment shell would not experience excessive deformation or buckling from the lateral inertia forces. The payload of steel bars weighed 7,500 pounds, or 270 pounds less than the licensed contents weight. In reality, the weight of the containment shell itself contributes to the potential bending of the containment shell during the horizontal free drop. Therefore, taking into account the containment shell weight of 2,482 lbs, the additional weight of 270 lbs is only 2.6% of the licensed contents weight plus the shell weight. In the test, the containment shell did not experience any visible permanent deformation from the side drop impact. For this reason, the small increase of 270 pounds in contents weight will have no effect on the containment shell. Furthermore, as discussed in Section 2.12.2.2.1, *Mock Payload*, the steel bars together have a much smaller bending stiffness than the actual strongback used, and

consequently would exert somewhat less self-support than would the strongback, thus diminishing or even eliminating any possible effect due to the extra weight.

The next three tests in Series 1 were puncture bar attacks on various locations of the impact limiters. The weight of the certification test unit, 13,815 pounds, was 445 pounds (i.e., 3.1%) less than the maximum licensed weight of the MFFP of 14,260 lbs. Since the damage due to these impacts was minimal, as described in Section 2.12.3.8.1, *Certification Test Series No. 1*, it is reasonable to assume that an increase of only 3.1% in available puncture energy would have no effect. Thus, the extra contents weight would have little or no effect on the results from Test Series 1.

### **2.12.8.2.2 Test Series 2**

The first test in Series 2 was a 30-ft, C.G.-over-corner (near vertical) free drop. The purpose of this test was to demonstrate that the closure system could withstand the inertia loading of the contents, and to test fuel assembly integrity. The prototypic strongback, prototypic fuel assembly, and two dummy fuel assemblies together weighed 6,906 pounds, or 864 pounds (i.e., 11.1%) less than the licensed contents weight. Although small, this difference could cause an increase in the loading on the closure system, which is evaluated as follows.

The effect on the closure lid structure is evaluated in two ways:

- Gross bending of the closure lid
- Puncture shear of the closure lid

The effect on the closure bolts is also evaluated.

**Gross bending of the closure lid.** The MFFP closure lid is a weldment consisting of two plates (3/4-inch thick outer plate and a 5/8-inch thick inner plate), which are connected by an array of radial and ring-shaped stiffeners. The total thickness of the lid weldment is 4.38 inches. During an end impact, the inertia load of the contents is applied to the inner surface of the lid as a pressure. The applied pressure is:

$$q = \frac{(w_{\text{contents}} + w_{\text{lid}})g}{(\pi/4)D_i^2} + p = 1,575 \text{ psi}$$

where:  $w_{\text{contents}}$  = 7,770 pounds (licensed weight of contents)

$w_{\text{lid}}$  = 468 pounds (weight of closure lid)

$D_i$  = 28.5 inches (inner diameter of package/closure lid)

$g$  = 120g (end impact magnitude, from Section 2.12.5.2)

$p$  = 25 psi (design pressure from Section 2.6.1.3.1)

For a simply supported circular plate of radius  $a$ , the maximum moment per unit width is at the center of the plate. From Roark<sup>1</sup>, Table 24, Case 10a, the moment is:

<sup>1</sup> Young, W. C., *Roark's Formulas for Stress and Strain*, Sixth Edition, McGraw-Hill, 1989.

$$M_c = \frac{qa^2(3+\nu)}{16} = 76,541 \text{ lb} \cdot \text{in/in}$$

where  $\nu = 0.3$  and the radius  $a$  is conservatively based on the bolt circle diameter of the lid of 30.7 inches. In order to determine the bending stress in the closure lid, its moment of inertia per unit width ( $I_{\text{total}}$ ) is determined by ignoring the stiffeners and taking credit only for the inner and outer lid plates. The vertical centroid, measured from the inner face of the inner plate is:

$$\bar{y} = \frac{\sum Ay}{\sum A} = \frac{(0.75)(4.00) + (0.625)(0.312)}{0.75 + 0.625} = 2.32 \text{ in}$$

The moment of inertia per inch of circumference is:

$$I_{\text{total}} = \sum (I + Ad^2) = \frac{1}{12}(0.75^3 + 0.625^3) + 0.75(4.00 - 2.32)^2 + 0.625(0.312 - 2.32)^2 = 4.69 \text{ in}^4 / \text{in}$$

The bending stress at the center of the plate is then given by:

$$\sigma_c = \frac{M_c \bar{y}}{I_{\text{total}}} = 37,863 \text{ psi}$$

The yield strength of the lid material at a bounding temperature of 200 °F is 47,100 psi from Table 2.2-1. The margin of safety against yield stress is:

$$MS = \frac{47,100}{37,863} - 1.0 = +0.24$$

Therefore, the closure lid remains elastic with the full contents weight when conservatively combining the cold, -20 °F impact to the warm, 200 °F material allowable.

***Puncture shear of the closure lid.*** To evaluate puncture shear, a detailed evaluation of the load paths into and through the lid is made. During an end impact, the inertia load of the contents is sequentially supported as various parts of the strongback structure come into contact with the closure lid. Refer to Figure 2.12.8-1, which is a schematic representation of the structures which participate in the contact between the MFFP contents and the closure lid (the figure is to scale, but represents a composite cross section in order to show all of the elements in a single view). In the progress of the end impact, the first point of contact with the lid inner plate is at the outer rim of the top plate, as shown by the symbol ① in Figure 2.12.8-1. After undergoing approximately 0.3 inches of diaphragm deformation of the top plate, the BPRA Restraint Weldment comes in contact with the center portion of the lid, as shown by the symbol ②. All of the weight of the strongback and FCS is supported by either the top plate outer rim or the BPRA Restraint Weldment. A final contact can occur between the lid and the fuel assembly axial adjustment screws. As shown in Figure 2.12.8-1, these screws are located in the top plate and support the fuel assembly. Once the BPRA Restraint Weldment has come to rest against the closure lid, the fuel assemblies can cause further diaphragm deformation of the top plate by breaking the three, 1/2-13 UNC socket head cap screws which attach the top plate to the strongback (represented by a single bolt labeled 'B' in Figure 2.12.8-1). Note that the contact between the lid and the axial adjustment screws is driven solely by the weight of the fuel. The weight of the strongback and FCS continues to be carried into the closure lid by the top plate outer rim and the BPRA restraint weldment.

The structures of the closure lid which support the impact forces described above are also shown in Figure 2.12.8-1. The outer rim of the top plate is supported by the outer forging of the lid. The BPRA restraint weldment consists of three, 1-inch diameter hollow bars through which the bolts ('A' in the figure) pass. The three bars are placed on a 6.38-inch bolt circle, which are supported by the stiffening ring (7-inch diameter OD, 6-inch diameter ID) of the closure lid. The fuel assembly axial adjustment screws are supported by the inner plate of the closure lid.

The increase in contents weight from 6,906 pounds to 7,770 pounds arises from the following:

- Addition of 73 pounds to account for the maximum possible manufactured weight of the strongback.
- Addition of the FCS weight of 855 pounds.
- Reduction of 64 pounds since the simulated fuel weighed slightly more than the FA weight (including BPRA) of 4,740 pounds total.

As seen from this breakdown, all of the increase in weight is either part of the strongback structure, or, in the case of the FCS, is fully carried by the strongback. Consequently, in an end drop, the added weight will be carried into the closure lid by the same paths as was the weight of the strongback in the Series 2 free drop, namely, through the top plate outer rim and through the BPRA Restraint Weldment. Since these two pathways are well supported by internal closure lid structure, the added weight does not create a risk of puncture shear in the closure lid inner plate. The only source of load path into the closure lid that is not fully supported by internal structure is the fuel assembly axial adjustment screws. However, the licensed weight of the MOX FA is slightly less than the weight of the simulated fuel assembly actually tested. For this reason, no risk of puncture shear of the closure lid is presented by the increased contents weight.

**Closure bolts.** As for the normal conditions of transport bolt analysis given in Section 2.6.1.3.4, *Closure Bolt Evaluation*, NUREG/CR-6007<sup>2</sup> will be used to evaluate the closure bolts. The analysis makes the following assumptions:

- From Section 2.6.1.3.4, *Closure Bolt Evaluation*, the maximum force due to pre-load ( $F_{a_{max}}$ ) is equal to 22,420 pounds. Differential thermal expansion ( $F_{a_{therm}}$ ) is not applicable for HAC. Therefore,  $F_{a_{pt}}$  as discussed in Table 4.9 of NUREG/CR-6007 is equal to 22,420 pounds.
- The sum of the tensile forces for the remaining loads ( $F_{a_{al}}$ ) is equal to the sum of the forces resulting from the internal pressure load ( $F_{a_{pressure}} = 687$  pounds) as calculated in Section 2.6.1.3.4, *Closure Bolt Evaluation*, and the vertical component of the impact load ( $F_{a_{impact}}$ ) calculated below.
- In Appendix V of NUREG/CR-6007,  $F_{a_{impact}}$  is calculated based on the very conservative assumption that the package is supported only at the impact corner of the package, and ignores any support provided by the impact limiter. The following analysis assumes some support is provided by the impact limiter. A modified derivation of  $F_{a_{impact}}$  follows below.
- The closure lid has a step located at the bolt circle diameter that precludes prying forces.

---

<sup>2</sup> G.C. Mok, L.E. Fischer, S.T. Hsu, *Stress Analysis of Closure Bolts for Shipping Casks*, NUREG/CR-6007, UCRL-ED-110637, U.S. Nuclear Regulatory Commission, April 1992.

- There are no applied shear stresses from the horizontal component of the impact force since the shear load is carried by the closure lid.
- Per Table 6.3 of NUREG/CR-6007, the “tension plus shear plus bending plus residual torsion” stress limit is not evaluated for HAC. Therefore, the residual torsion stress is not considered in the calculation.

The maximum bolt impact force is now determined. Because of the cold conditions, the impact limiter crush zone has a minimum possible volume, resulting in the smallest possible crush foot print. Moreover, the regulatory test articles weighed slightly less than the maximum MFFP weight, which also results in a smaller crush volume. Consequently, the crush zone resulting from the regulatory drop predicts a conservative minimum backing of the closure bolts by the impact limiter.

The shape of the impact limiter crush zone is a wedge shape due to the impact angle as illustrated in Figure 2.12.8-2. The maximum depth of the deformation is measured as 6.1 inches as stated in Section 2.12.3.8.2.2, *Series 2, Test 1: HAC 80-Degree Oblique C.G.-Over-Corner 30-foot Drop*. Given this crush depth, the impact footprint extends nearly to the edge of the impact limiter’s 36 inch diameter face, as shown in Figure 2.12.8-2. The impact limiter has a 20-inch diameter hole on its end having a depth of 8 inches. Conservatively, no support is assumed for the area of the 20-inch diameter hole.

At a minimum, the impact limiter will provide support to the closure lid over the vertical projection of the footprint area onto the lid. Rather than assuming that the zone extends to the edge of the impact limiter’s 36 inch diameter face, it is conservatively assumed that the zone will extend only to the edge of the 20 inch hole. The force distribution will be a maximum at the impact corner of the closure lid, and will linearly decrease to zero at the opposite edge of the supported zone. Figure 2.12.8-2 illustrates the force distribution.

Using the nomenclature from NUREG/CR-6007 for the impact  $gs$  ( $a_i$ ) and the drop angle ( $\pi_i$ ), the total reaction force provided by the impact limiter equals the vertical component of the weight supported by the impact limiter multiplied by the impact  $gs$  and is given by:

$$R_{IL,y} = (W_{TOTAL-IL} \sin(\pi_i)) \times a_i$$

Because of the shape and distribution of the reaction force, the center of pressure of the distributed reaction force acts at location 8.28 inches from the impact corner of the closure lid as determined by 3D computer-aided design (CAD) software, and shown in Figure 2.12.8-2. This arm length is referred to as ( $y_f$ ).

As shown on the free body diagram V.1 in Appendix V of NUREG/CR-6007, the vertical component of the load applied by the lid ( $W_l$ ) and payload ( $W_c$ ) during impact is equal to  $L$ , or:

$$L = ((W_l + W_c) \sin(\pi_i)) \times a_i$$

Taking into consideration the support force  $R_{IL,y}$ , the summation of moments about the impact point (Appendix V, equation V.1) becomes:

$$\sum fb_yb = L(yL) - R_{IL,y}(y_f)$$

where ( $yL$ ) is the distance from the impact point to the center of the applied load ( $L$ ), which equals the outside radius of the lid ( $R_{lo}$ ). Following the derivation in Appendix V, the maximum bolt force,  $(fb)_{max}$ , for a bolt pattern having a total number of bolts ( $N_b$ ) becomes:

$$(fb)_{\max} = \frac{4 L(yL) - R_{IL,y}(yf)}{3 (Rlo)(Nb)}$$

In summary, the moment in the direction of opening the lid is  $L(yL)$ , the moment of the impact limiter in resisting that moment is  $R_{IL,y}(yf)$ , and the balance is resisted by the closure bolt forces.

Substituting the above equation into the equation for the axial force in Table 4.5 of NUREG/CR-6007 for an unprotected closure lid gives the following equation:

$$Fa_{\text{impact}} = \frac{1.34(ai) \sin(\pi i) [(Wl + Wc)Rlo - W_{\text{TOTAL-IL}}(yf)]}{Nb(Rlo)} = 11,157 \text{ lb}_m$$

where:  $Wl$  = 468 pounds (weight of closure lid)  
 $Wc$  = 7,770 pounds (licensed weight of contents)  
 $W_{\text{TOTAL-IL}}$  = 12,770 pounds (MFFP weight (14,260 lb<sub>m</sub>) - lower limiter weight (1,490 lb<sub>m</sub>)  
 $Rlo$  = 16.15 inches (outer radius of closure lid)  
 $yf$  = 8.28 inches (location of reaction force centroid from lid edge)  
 $\pi i$  = 80° (package orientation)  
 $ai$  = 120g (impact magnitude)  
 $Nb$  = 24 (number of bolts)

The combined maximum tensile bolt forces are equal to:

$$Fa_{\text{al}} = Fa_{\text{pressure}} + Fa_{\text{impact}} = 687 + 11,157 = 11,844 \text{ lb}$$

A comparison of  $Fa_{\text{pt}}$  with  $Fa_{\text{al}}$  per Table 4.9, Step 1.4 of NUREG/CR-6007, shows that  $Fa_{\text{pt}}$ , equal to 22,420 pounds, is greater than  $Fa_{\text{al}}$ . Therefore, calculation of the average bolt stress ( $Sba$ ) is based on the pre-load, not the impact loads:

$$Sba = (1.2732) \frac{Fa_{\text{pt}}}{Dba^2} = 66,943 \text{ psi}$$

where  $Dba = 0.653$  inches from Section 2.6.1.3.4. From Table 2.1-1, the HAC allowable average tensile stress is the lesser of  $S_y$  (equal to 106,300 psi) or  $0.7S_u$  (equal to  $0.7 \times 140,000 = 98,000$  psi), with material properties taken from Table 2.2-5 at 200 °F. The corresponding margin of safety on average tensile stress,  $Sba$ , is:

$$MS = \frac{98,000}{66,943} - 1.0 = +0.46$$

Since the calculated stress is less than the material yield strength of 106,300 psi, there is no plastic deformation in the closure lid or seal region. Because there is no resulting shear stress, the "Average Shear Stress" and the "Average Tensile + Average Shear" criteria are met.

The second test in Series 2 was a puncture drop test on the impact damage from the prior free drop. The weight of the certification test unit, 13,234 pounds, was 1026 pounds (i.e., 7.2%) less than the maximum licensed weight of the MFFP. However, based on the very minimal damage done to the impact limiter as a result of this test (see Figure 2.12.3-18), an increase in available

puncture energy of 7.2% will have a negligible effect. Thus, the extra contents weight would have little or no effect on the results from Test Series 2.

**2.12.8.2.3 Test Series 3**

The first two tests in Test Series 3 were 30-ft free drops in a slapdown orientation, one with the closure lid end striking first, and one with the closure lid end striking second. Each test also featured a different azimuth orientation of the strongback. As stated in Table 2.12.2-1, these two drops were planned to test the strongback and the closure system in the lateral direction. The effect of the added FCS weight on the strongback structure is evaluated in Appendix 2.12.5, *Fuel Control Structure Evaluation*. The added contents weight will have no effect on the behavior of the closure system in a slapdown orientation, since the secondary impact orientation was essentially horizontal.

The second two tests were puncture attacks on the containment boundary shell. The weight of the certification test unit, 13,217 pounds, was 1043 pounds (i.e., 7.3%) less than the maximum licensed weight of the MFFP. The governing case was Test 3, which was oriented perpendicular to the surface and directed through the package C.G. As stated in Section 2.12.3.8.3.4, *Series 3, Test 3: HAC Horizontal Puncture Drop*, the damage consisted of an indentation of approximately 2.13 inches deep. As shown in Figure 2.12.3-35, the deformation was not severe, and no cracking or loss of leaktight condition was noted from the test. An additional available puncture energy of 7.3% could produce an additional deformation of approximately  $0.073 \times 2.13 = 0.16$  inches. This modest increase in deformation would not cause containment boundary failure or loss of a leaktight condition. Thus, the extra contents weight would have little or no effect on the results from Test Series 3.

**2.12.8.3 Conclusions**

As shown in the foregoing calculations, the additional weight of the MFFP, up to the maximum licensed weight, will have little or no effect on the results obtained from full-scale certification testing.

**Table 2.12.8-1 – Summary of Certification Test Unit Weights (pounds)**

<b>Component</b>	<b>Licensed</b>	<b>Test Series 1</b>	<b>Test Series 2</b>	<b>Test Series 3</b>
Strongback	3,030	N/A	2,102	2,100
Fuel Assemblies	4,740	7,500*	4,804	4,788
<i>Contents Sum</i>	7,770	7,500	6,906	6,888
Empty Package**	6,490	6,315	6,328	6,329
<i>Gross Package</i>	14,260	13,815	13,234	13,217

\*Mock payload composed of small steel rods.

\*\*Empty package, without strongback.

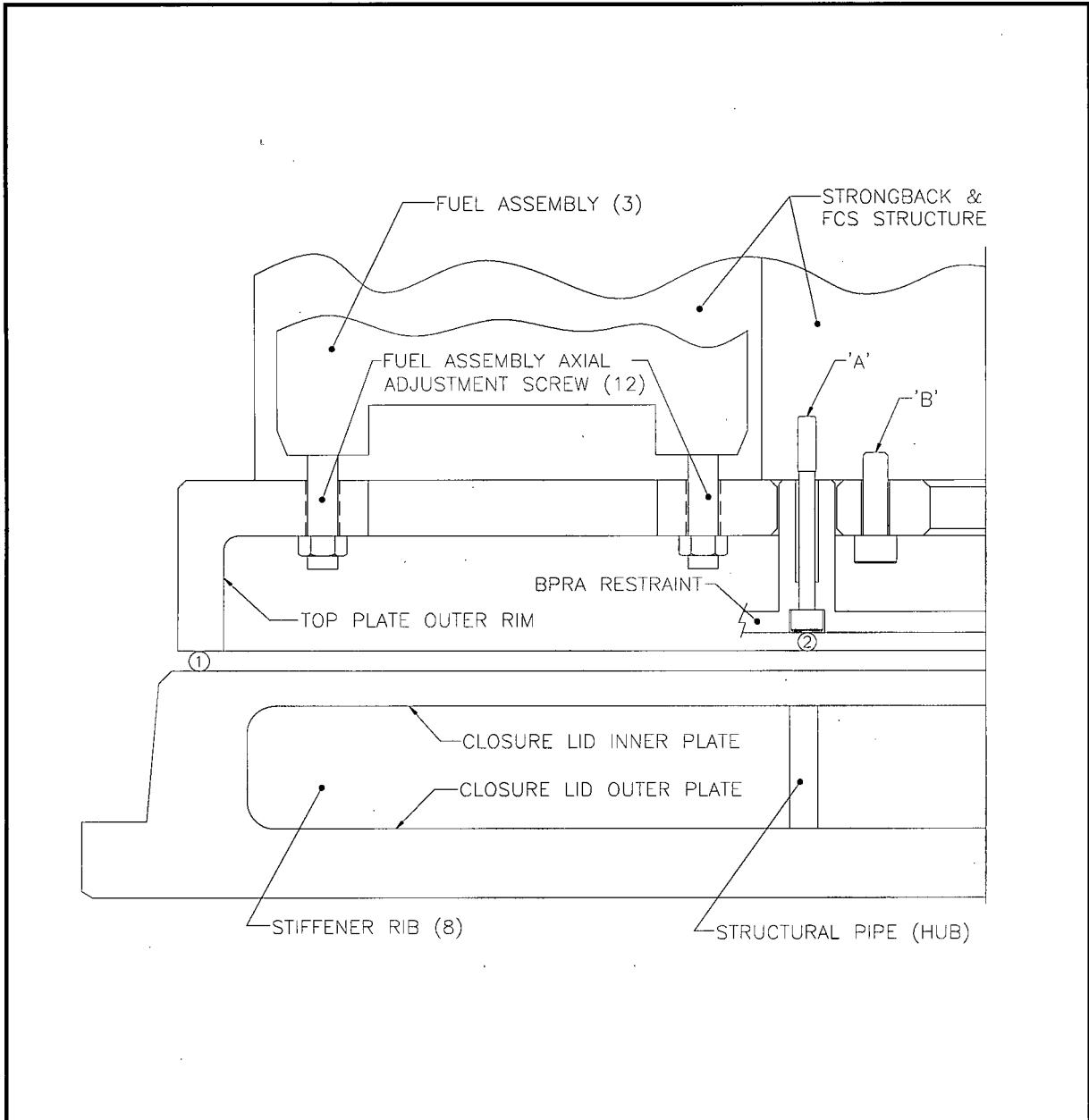


**FIGURE 2.12.8-1 – Impact Conditions at the Top Plate – Closure Lid Interface**

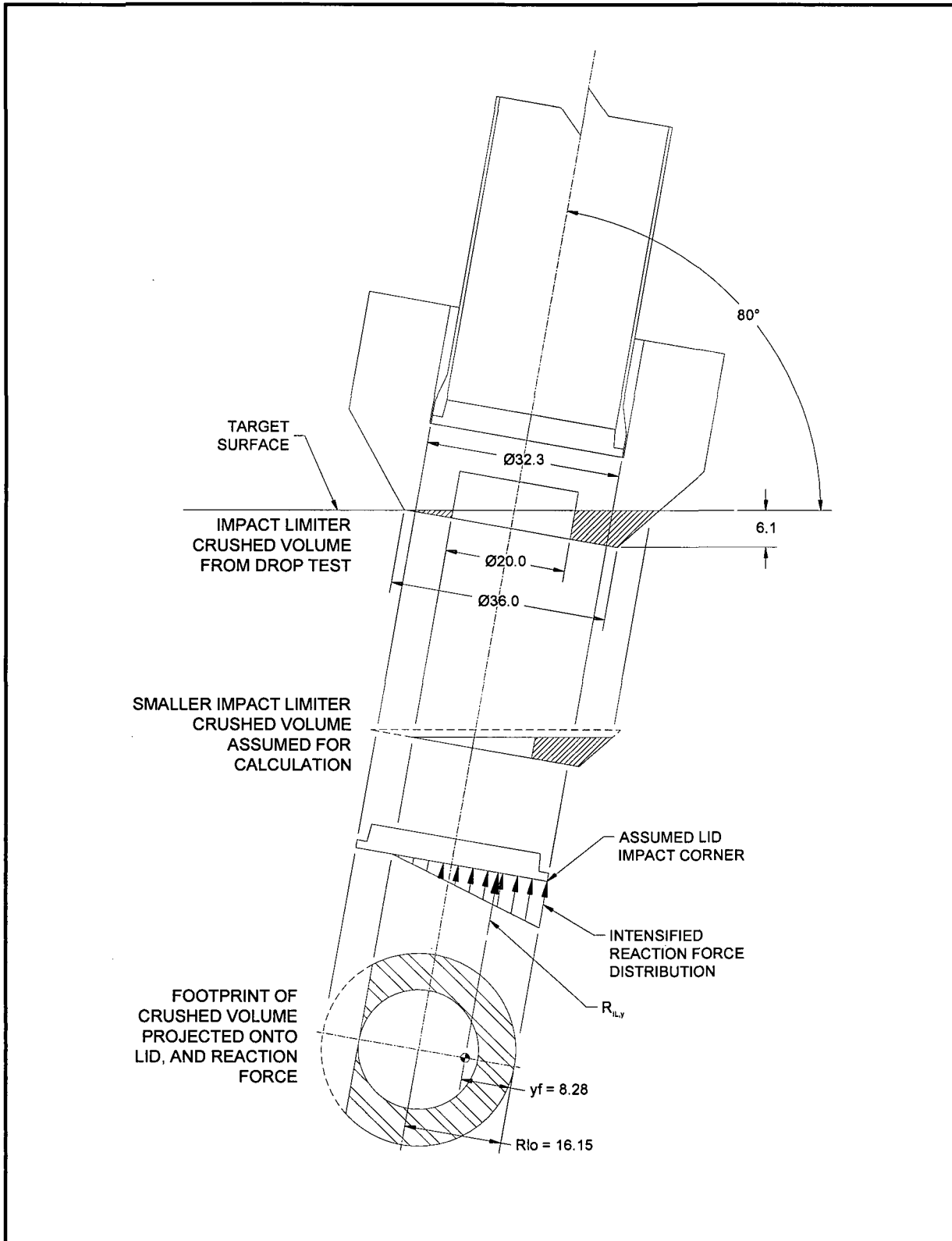


FIGURE 2.12.8-2 – Support Provided by the Impact Limiter

This page left intentionally blank.

## **3.0 THERMAL EVALUATION**

### **3.1 Description of Thermal Design**

This section identifies and describes the principal thermal design aspects of the MFFP. Further, this chapter demonstrates the thermal safety of the system and compliance with the thermal requirements of 10 CFR 71<sup>1</sup> when transporting a payload of up to three (3) mixed oxide fuel assemblies (MOX FAs) generating a maximum of 240 watts of decay heat. Specifically, all package components are shown to remain within their respective temperature limits under the normal conditions of transport (NCT). Further, per 10 CFR §71.43(g), the maximum accessible package surface temperature is demonstrated to be less than 122 °F for the maximum decay heat loading, an ambient temperature of 100 °F, and no insolation. The bulk temperature of the impact absorbing foam is shown to be less than 150 °F, based on NCT maximum temperature conditions. Therefore, the foam will retain sufficient structural integrity to protect the payload during the subsequent hypothetical accident condition (HAC) free drop scenarios described in Chapter 2.0, *Structural Evaluation*. Finally, the package is demonstrated to structurally withstand the damage arising from the HAC free drop scenarios and retain sufficient thermal protection to maintain all package component temperatures within their respective short term limits during the regulatory fire event and subsequent package cool-down.

#### **3.1.1 Design Features**

The MFFP packaging is designed to be a totally passive thermal system for transporting up to three (3) mixed oxide fuel assemblies (MOX FAs), with or without burnable poison assemblies installed. As described in Section 1.1, *Introduction*, the MFFP consists of a strongback assembly that provides support for three (3) fresh MOX PWR FAs, a stainless steel cylindrical vessel that provides leaktight containment, and energy absorbing impact limiters.

##### **3.1.1.1 Body**

The package body serves as a single containment boundary for the payload of MOX FAs. The components that form the containment boundary are the cylindrical shell, the bottom plate, the seal flange, the inner plate and seal ring of the closure lid, the vent port plug and elastomeric seal, the fill port plug and elastomeric seal, and the closure lid containment elastomeric O-ring. The cylindrical cavity formed by these components is 28½ inches in diameter and 165.45 inches in length.

The 9/16-inch thick body shell is fabricated from ASTM SA-240, XM-19 austenitic stainless steel. A circumferentially continuous doubler plate is used near each end of the shell to interface between the six impact limiter attachment lugs and the shell. The doubler plate also serves to provide an interface with the transportation skid for longitudinal restraint. The lid end of the body is locally thicker than the body shell to accommodate the closure lid sealing area and the closure bolt threaded holes. The wall thickness transition is a 3:1 minimum taper. The bottom end closure is fabricated from a 1½ inch thick forging. There are no containment penetrations located at the bottom end of the body.

---

<sup>1</sup> Title 10, Code of Federal Regulations, Part 71 (10 CFR 71), *Packaging and Transportation of Radioactive Material*, Final Rule, 01-26-04.

The closure lid is a weldment constructed of XM-19, and has a construction that provides significant strength and stiffness while also being weight efficient. The closure lid is constructed of a 3/4-inch thick outer plate and 5/8-inch thick inner plate, stiffened with eight, 1/2-inch thick radial ribs that are three inches deep. A 1/2-inch thick, 6-inch inner diameter cylinder forms a hub at the inner end of the radial ribs. The ribs are welded on all four edges to the adjacent structure. Each rib has a projection that passes through a slot in the outer plate, and the ribs and outer plate are securely welded together using 1/2-inch groove welds. The closure lid inner plate is welded to the outer ring using a full-penetration weld. The seal flange of the closure lid has a minimum thickness of one inch, and provides locations for three closure O-ring seals for leakage rate testing, as well as providing a location for the vent, fill, and test ports. The closure lid is attached to the body using twenty four (24) 3/4-10UNC ASTM A564, Grade 630 (H1100) socket head cap screws (SHCS).

Package closure is sealed using a single 3/8-inch cross-section diameter bore-type O-ring seal made from butyl rubber. O-rings of similar construction are located on either side of the containment O-ring to facilitate leakage rate testing. The inner O-ring creates a cavity, which is backfilled with helium during leakage rate tests. The outer O-ring is utilized to create a cavity for leakage rate testing. The body cavity is filled with atmospheric air during transport operations.

### 3.1.1.2 Impact Limiters

Impact limiters are installed at each end of the MFFP to provide thermal and impact protection under all regulatory conditions. The impact limiters are comprised of cylindrical and conical sections, with a maximum outer diameter of 60 inches. A recessed region at the bottom of the limiter is designed to reduce end drop impact forces. This recess has a diameter of 20 inches and a depth of eight inches. The impact limiter shells are constructed of ASTM A240, Type 304 stainless steel. The lid end impact limiter has 1/4-inch thick shells (5/16-inch thick for the recessed end plate) to resist perforation in the HAC puncture drop event, and to protect the closure lid and sealing area from damage due to the HAC puncture drop and thermal events. The bottom impact limiter has 11-gauge (0.12-inch thick) shells. Within the impact limiter shells is closed cell, rigid polyurethane foam. The polyurethane foam provides the majority of the energy absorption during the HAC free drop events, and thermal protection of the O-ring seals during the HAC fire event. Each impact limiter is secured to the body using six, relatively long, 1-8 UNC, ASTM A320, Grade L43 socket head cap screws (SHCS), with a majority of the shank length reduced to a diameter of 0.805 inches.

### 3.1.1.3 Strongback

The strongback assembly is fabricated primarily of ASTM A240, Type 304 stainless steel. The strongback longitudinal weldment is 1/4-inch thick plate, and provides support for the neutron poison plates and for the MOX FAs. Eight support disk assemblies, each of which are composed of three clamp arm assemblies, are attached to the strongback longitudinal weldment at each fuel assembly grid location. Between the clamp arm assemblies, the fuel control structures (FCSs) are attached to the strongback. The clamp arm assemblies are hinged to allow loading of the fuel assemblies. The clamp arms are designed with clamping mechanisms to securely clamp the fuel assemblies onto the strongback. Each clamp arm is constructed of two 3/8-inch thick plates, separated by the fuel clamping mechanism and stiffened to provide in-plane stability.

The FCS assemblies are constructed of a 1/8-inch thick angle plate constructed of Type 304 austenitic stainless steel. In the center of the longitudinal span of each FCS is a stiffener, constructed of 1/4-inch thick Type XM-19 austenitic stainless steel. Each FCS assembly is hinged to assist FA loading and unloading.

The top and bottom end plates clamp the top and bottom fuel assembly nozzles in the same way that the grids are clamped, and provide axial restraint to the fuel assembly. The loaded strongback is slid into and out of the body horizontally, aided by anti-friction plastic pads located in the top and bottom end disks. The top and bottom plate assemblies support the strongback such that the smaller support disks have no contact with the body shell.

When installed in the body, the inner end of the strongback is supported on a 2¼ inch diameter trunnion, which is bolted to the center of the inside of the bottom end closure. The upper end is supported by the contact between the top plate assembly and the body, and is secured to prevent axial motion of the strongback under normal over-the-road transportation forces using three removable SHCS that engage three lugs machined into the body weldment.

#### **3.1.1.4 Neutron Moderation and Absorption**

Criticality control is provided in the MFFP by the geometric spacing of the fuel assemblies and by borated neutron poison plates contained on the strongback assembly and the FCSs. The strongback weldment, clamp arm assemblies, and FCSs maintain the geometric spacing of the FAs within the packaging. The borated neutron poison plates are secured to the strongback weldment by cover pads at ten locations corresponding to the fuel assembly clamping locations. On the FCSs, the neutron poison plates are secured with flat head machine screws. The neutron poison plates do not support any structural loading except their own weight.

#### **3.1.1.5 Receptacles, Valves, Testing and Sample Ports**

The package design includes a seal test port, a fill port, and a vent port. The seal test port accesses the cavity between the middle (containment) and upper O-ring bore seals on the closure lid, thereby allowing leaktight verification prior to shipping the loaded package. The fill port allows helium to be placed on the inner side of the containment O-ring seal for leaktight verification. The vent port permits venting of the internal cavity during loading and unloading of the package. Each port is an integral, recessed part of the closure lid, which protects the ports. There are no receptacles or valves utilized on this package.

### **3.1.2 Content's Decay Heat**

The MFFP packaging is designed to transport up to three (3) MOX FAs, with or without burnable poison rod assemblies (BPRAs). As described in Section 1.2.3, *Contents of Packaging*, the MOX FAs are 17 × 17 un-irradiated, PWR commercial reactor fuel assemblies with 264 fuel rods, 24 guide tubes, and 1 instrument tube. A decay heat loading of 80 watts per assembly, evenly distributed over the 144 inch active fuel length, is utilized for the thermal evaluation.

### **3.1.3 Summary of Temperatures**

The maximum temperatures for the MFFP under NCT and HAC conditions are summarized in Table 3.4-1 and Table 3.5-1, respectively.



### 3.1.4 Summary of Maximum Pressures

The maximum normal operating pressure (MNOP) for the MFFP resulting from the NCT Hot condition and conservative assumptions is 10 psig. The NCT internal pressures are presented in Table 3.4-2. Further details of these analyses are presented in Section 3.4.2, *Maximum Normal Operating Pressure*.

The maximum peak pressure generated within the package cavity under HAC conditions is estimated to be 142.4 psia (127.7 psig) at the end of the fire when the peak cavity gas temperature is reached. The pressure will then decrease as the package cools, reaching 76.9 psia (62.2 psig) 9.5 hours after the end of the fire. The HAC internal pressures are presented in Table 3.5-2. Further details of the analyses are presented in Section 3.5.3, *Maximum Temperatures and Pressures*.

## 3.2 Material Properties and Component Specifications

### 3.2.1 Material Properties

The thermally significant materials used in the fabrication of the MFFP include the following:

- XM-19 stainless steel used for the body shell, bottom, and closure lid
- Type 304 stainless steel used for the strongback structure and the impact limiter shells
- ASTM A320 Type L43 alloy steel used for the impact limiter attachment bolts
- ASTM A564, Grade 630 used in the closure lid bolts
- Polyurethane foam (nominal density of 10 lb<sub>m</sub>/ft<sup>3</sup>) used in the lid end impact limiter
- Polyurethane foam (nominal density of 30 lb<sub>m</sub>/ft<sup>3</sup>) used to provide thermal protection around the collar of the body.

This section presents the thermal properties used in the heat transfer model and the references from which they are obtained.

Table 3.2-1 presents the thermal properties for the A240, Type 304 stainless steel and the XM-19 austenitic stainless steel. The density of Type 304 stainless steel is 495.9 lb<sub>m</sub>/ft<sup>3</sup>, while the density of XM-19 stainless steel is 492.5 lb<sub>m</sub>/ft<sup>3</sup>.

Table 3.2-2 presents the material properties for the neutron absorbing material (i.e., boral). The boral material is a composite of a core material (chemical composition 69% aluminum, 24% boron, 6% carbon, 0.5% iron, and 0.1% silicon, titanium, copper, and zinc) sandwiched in a protective aluminum clad layer. The thermal conductivity is listed as bi-directional since the composite material exhibits a different thermal conductivity across the layers than along the layers. The combined material properties for the composite panel are computed as a function of thicknesses of the clad and core matrix materials. These parameters, in turn, are a function of the desired boron loading (i.e., 0.035 g/cm<sup>2</sup>) and temperature. The manufacturer's procedure for calculating the thermal conductivity, specific heat, and density are used to arrive at the specific values presented in Table 3.2-2.

Table 3.2-3 presents thermal properties for the A320, Grade L43 material used for the impact limiter attachment bolts and the A564, Grade 630 material used for the closure lid bolts. The density of the ASTM A320, Grade L43 material is 489.0 lb<sub>m</sub>/ft<sup>3</sup>, while the density of the ASTM A564, Grade 630 material is 486.9 lb<sub>m</sub>/ft<sup>3</sup>.

The heat transfer within the MOX FA is a combination of conduction and radiation heat transfer within and between the individual rods of the fuel assembly. Rather than include the details of the fuel geometry in the thermal model, the fuel assemblies and the surrounding space between the edges of the FAs and the surrounding surfaces of the strongback structure are represented as homogenous solid region with anisotropic thermal properties. The thermal properties are based on a detailed model of the FA geometry (see Appendix 3.6.2.2, *Effective Thermal Conductivity of MOX Fuel Assemblies*). The model accounts for conduction and radiation heat transfer between the individual rods and across the space between the edges of the FA and the strongback surfaces. The results of this detailed modeling are used to compute an 'effective thermal conductivity' for the radial and the axial directions. The same thermal properties can be conservatively applied to both the vertical and horizontal orientations of the fuel assembly.

Table 3.2-4 presents the effective, anisotropic thermal properties for the homogenized fuel

region. Appendix 3.6.2, *Thermal Model Details*, presents the details of the methodology used to compute the various values.

Table 3.2-5 presents the thermal properties for the miscellaneous materials used in the thermal model. Material properties for the 11½ pcf polyurethane foam used in the lower impact limiter are not required since the 1/4-symmetry thermal model used for this safety calculation does not include the lower impact limiter. Specific thermal properties for the neoprene rubber and Delrin® plastic used for padding and bearing surfaces are not needed since the thermal model ignores the relatively small effect that these components have on the overall package conductivity. The impact of these materials on gas generation and maximum operating temperatures are considered. Table 3.2-6 presents the thermal conductivity of air. Because the thermal conductivity of air varies significantly with temperature, the computer model calculates the thermal conductivity as a function of the mean film temperature. The void spaces within the package are to be filled with air at one atmosphere.

Table 3.2-7 presents the important parameters in radiative heat transfer, emissivity ( $\epsilon$ ) for each radiating surface and solar absorptivity ( $\alpha$ ) value for the exterior surfaces. Under NCT conditions, the machined surfaces of the XM-19 stainless steel used for the body shell will have an emissivity of approximately 0.30 and a solar absorptivity of approximately 0.5. The surfaces of the XM-19 stainless steel used for the closure lid use a slightly lower emissivity of 0.25 to account for the high surface finish typically used for mating surfaces. In contrast, the 'as-rolled' and un-painted Type 304 stainless steel used for the shells of the impact limiter will yield a slightly higher emissivity of approximately 0.4. The solar absorptivity for the impact limiter surfaces will also be approximately 0.5.

The Type 304 stainless steel utilized for the strongback structure is assumed to have a conservatively low emissivity of 0.2, indicative of a bright finish. The surfaces of the boral neutron absorbing material use a nominal emissivity of 0.15.

### 3.2.2 Component Specifications

The materials that are considered temperature sensitive are the butyl rubber O-ring seals used for the closure lid and the vent/fill ports, the polyurethane foam used in the impact limiter, the neoprene rubber pads, and the Delrin® plastic.

The butyl rubber O-ring seals used for the containment seals are fabricated from Rainier Rubber compound RR0405-70 material meeting the requirements of ASTM D2000 M4AA710 A13 B13 F17 F48 Z Trace Element. The butyl rubber sealing material has a working temperature range of -65 °F to 225 °F<sup>2</sup>, and a short duration (8 hours) temperature range of 400 °F. Developmental O-ring seal testing, documented in the TRUPACT-II SAR<sup>3</sup>, investigated the butyl rubber O-ring seal's performance at reduced and elevated temperatures. Further developmental O-ring seal testing was conducted as part of the Radioisotope Thermoelectric Generator (RTG) Transportation System Packaging<sup>4</sup> design effort. This testing demonstrated that this specific butyl rubber compound has a

<sup>2</sup> Rainier Rubber Company, Company Standard Compounds, <http://www.rainierrubber.com>, Seattle, WA.

<sup>3</sup> U. S. Department of Energy (DOE), *Safety Analysis Report for the TRUPACT-II Shipping Package*, USNRC Certificate of Compliance 71-9218, U.S Department of Energy, Carlsbad Field Office, Carlsbad, New Mexico.

<sup>4</sup> DOE Docket No. 94-6-9904, *Radioisotope Thermoelectric Generator Transportation System Safety Analysis Report for Packaging*, WHC-SD-RTG-SARP-001, prepared for the U.S. Department of Energy Office of Nuclear Energy under Contract No. DE-AC06-87RL10930 by Westinghouse Hanford Company, Richland, WA. Per Appendix 2.10.6, elevated temperature tests were performed on Rainier Rubber Company butyl rubber compound No. RR-0405-70 O-ring seals with

peak temperature rating of 430 °F for durations of 1 hour or less, 400 °F for 8 hours or less, 375 °F for 24 hours or less, 350 °F for 168 hours or less, and 285 °F or less for the long-term (1 year) transportation duration. For conservatism, a long-term limit of 225 °F, a short-term limit of 400 °F for 8 hours or less, and a lower temperature limit of -40 °F are assumed for this analysis.

The NCT temperature range for the polyurethane foam material is -40 °F to 300 °F, per the foam manufacturer's recommendations<sup>5</sup>. Polyurethane foam is not subject to degradation with age when encased within the stainless steel shells.

The recommended maximum operating temperature for Delrin<sup>®</sup> plastic is 180 °F for continuous operation in air, with intermittent operation (based on the deflection temperature) up to 250 °F permitted<sup>6</sup>. Delrin<sup>®</sup> plastic has a minimum melting point of 347 °F. Except for material strength considerations, no limit exists for the minimum allowable operating temperature. The maximum operating temperature for the neoprene rubber is 180 °F for continuous operation in air, with intermittent use up to 250 °F<sup>6</sup>. A minimum allowable operating temperature -22 °F is recommended, primarily due to the potential loss of flexibility.

The other primary packaging materials are the Type 304 and XM-19 stainless steels and the aluminum material used in the boral. Stainless steel exhibits material property variations within the operating temperature range of the transportation package. In compliance with the ASME B&PV Code<sup>7</sup>, the maximum allowable temperature of stainless steel used for structural purposes is 800 °F for NCT conditions. The Type 304 and XM-19 stainless steels have a melting point above 2,500 °F, which is utilized as the upper bound temperature limit for HAC conditions. The minimum allowable temperature for stainless steel is below the -40 °F considered in this analysis.

The maximum operating temperature for boral<sup>8</sup> is 850 °F for continuous operation under dry conditions and 1,000 °F for non-continuous operation under dry conditions. No limit exists for the minimum allowable operating temperature.

From Section 1.2.3, *Contents of Packaging*, the MOX FAs have an allowable cladding temperature limit of 392 °F for NCT conditions<sup>9</sup> and 1,337 °F for HAC conditions<sup>10</sup>.

---

seal compressions as low as 10%. The specific time-temperature test parameters evaluated were 380 °F for 24 hours followed by 350 °F for 144 hours, for a total of 168 hours (1 week). At these temperatures, all elastomeric compounds are susceptible to relatively high helium permeability; thus, helium leakage rate testing was not performed. Instead, a hard vacuum of less than 0.15 torr was maintained on the test O-ring seals with no measurable pressure loss that would indicate leakage. At the end of the entire test sequence, the test O-ring seals were stabilized at -20 °F and shown, via helium leakage rate testing, to be leaktight (i.e., a leakage rate less than  $1 \times 10^{-7}$  standard -cubic centimeters per second (std-cc/s), air leakage).

<sup>5</sup> *LAST-A-FOAM FR-3700 for Crash and Fire Protection of Nuclear Material Shipping Containers*, General Plastics Manufacturing Company, Tacoma, WA.

<sup>6</sup> Mat Web On-Line Material Property Data (DuPont Delrin<sup>®</sup> Acetal, homopolymer, unfilled, extruded), [www.matls.com](http://www.matls.com).

<sup>7</sup> American Society of Mechanical Engineers (ASME) Boiler & Pressure Vessel Code, Section III, *Rules for Construction of Nuclear Facility Components*, Division 1, Subsection NB, *Class 1 Components*, & Subsection NG, *Core Support Structures*, 2001 Edition, 2002 and 2003 Addenda.

<sup>8</sup> AAR, *Standard Specification for Boral Composite Sheet*, AAR Advanced Structures.

<sup>9</sup> Temperature provided by fuel vendor.

<sup>10</sup> Sanders, et al, *A Method for Determining the Spent-Fuel Contribution to Transport Cask Containment Requirements*, Sandia National Laboratories, Albuquerque, NM, SAND90-2406, November 1992.

**Table 3.2-1 – Properties of Stainless Steels**

Material	Temperature (°F)	Density (lb <sub>m</sub> /ft <sup>3</sup> )	Thermal Conductivity (Btu/hr-ft-°F)	Specific Heat (Btu/lb <sub>m</sub> -°F)
Stainless Steel <sup>①</sup> Type 304	-40	495.9	8.23	0.1127
	70		8.6	0.1148
	100		8.7	0.1154
	200		9.3	0.1202
	300		9.8	0.1235
	400		10.4	0.1271
	500		10.9	0.1293
	600		11.3	0.1309
	700		11.8	0.1329
	800		12.2	0.1337
	1000		13.2	0.1372
	1200		14.0	0.1391
	1400		14.9	0.1417
	1500		15.3	0.1428
Stainless Steel <sup>②</sup> XM-19	-40	492.5	5.67	0.1037
	70		6.4	0.1130
	100		6.6	0.1155
	200		7.1	0.1191
	300		7.7	0.1241
	400		8.2	0.1261
	500		8.8	0.1295
	600		9.3	0.1321
	700		9.9	0.1349
	800		10.4	0.1362
	1000		11.4	0.1386
	1200		12.5	0.1426
	1400		13.5	0.1458
	1500		14	0.1488

**Notes:**

- ① American Society of Mechanical Engineers (ASME) Boiler and Pressure Vessel Code, Section II, *Materials, Part D – Properties*, Table TCD, Material Group J, 2001 Edition, 2002 Addenda, New York.
- ② American Society of Mechanical Engineers (ASME) Boiler and Pressure Vessel Code, Section II, *Materials, Part D – Properties*, Table TCD, Material Group E, 2001 Edition, 2002 and 2003 Addenda.

**Table 3.2-2 – Thermal Properties of Boral**

Material	Temperature (°F)	Thermal Conductivity (Btu/hr-in-°F)		Specific Heat (Btu/lb <sub>m</sub> -°F)	Density (lb <sub>m</sub> /in <sup>3</sup> )
		Through	Axial & 'Along'		
0.035 g/cc B10 loading, 0.118-inch total thickness <sup>①</sup>	-40	4.796	5.022	0.190	0.0917
	77	4.704	5.051	0.217	
	122	4.670	5.060	0.228	
	167	4.637	5.070	0.238	
	212	4.598	5.080	0.247	
	257	4.603	5.104	0.256	
	302	4.608	5.128	0.263	
	347	4.617	5.147	0.269	
	392	4.622	5.171	0.274	
	482	4.598	5.186	0.284	
	572	4.579	5.200	0.292	
	662	4.540	5.186	0.297	
	752	4.507	5.171	0.303	
	842	4.420	5.094	0.309	
	932	4.333	5.017	0.313	
1472	3.823	4.565	0.336		

**Notes:**

- ① Based on mean of manufacturer's suggested values, AAR, *Standard Specification for Boral Composite Sheet*, AAR Advanced Structures.

**Table 3.2-3 – Properties of Bolt Materials**

<b>Material</b>	<b>Temperature (°F)</b>	<b>Density (lb<sub>m</sub>/ft<sup>3</sup>)</b>	<b>Thermal Conductivity (Btu/hr-ft-°F)</b>	<b>Specific Heat (Btu/lb<sub>m</sub>-°F)</b>
Impact Limiter Bolt Material, A320, Gr L43 <sup>①</sup>	-40	489.0	17.8	0.0936
	70		19.3	0.1047
	100		19.7	0.1077
	200		20.6	0.1170
	300		21.2	0.1249
	400		21.4	0.1314
	500		21.4	0.1372
	600		21.2	0.1426
	700		20.9	0.1484
	800		20.5	0.1553
	1000		19.4	0.1710
	1200		18.0	0.2000
	1400		15.0	0.1723
	1500		15.0	0.1511
Closure Lid Bolt Material, A564, Gr 630 <sup>②</sup>	-40	486.9	9.2	0.1023
	70		9.9	0.1081
	100		10.1	0.1097
	200		10.6	0.1152
	300		11.2	0.1211
	400		11.7	0.1258
	500		12.2	0.1319
	600		12.7	0.1373
	700		13.2	0.1457
	800		13.5	0.1540
	1000		13.8	0.1771
	1200		14.2	0.2261
	1400		15.0	0.1665
	1500		15.4	0.1573

**Notes:**

- ① American Society of Mechanical Engineers (ASME) Boiler and Pressure Vessel Code, Section II, *Materials, Part D – Properties*, Table TCD, 2Ni-3/4Cr-1/3Mo, 1998 Edition.
- ② American Society of Mechanical Engineers (ASME) Boiler and Pressure Vessel Code, Section II, *Materials, Part D – Properties*, Table TCD, Material Group I, 2001 Edition, 2002 and 2003 Addenda.

**Table 3.2-4 – Effective Thermal Properties for Homogenized Fuel Region**

Material	Temperature (°F)	Thermal Conductivity (Btu/hr-in-°F) <sup>①</sup>		Specific Heat (Btu/lb <sub>m</sub> -°F)	Density (lb <sub>m</sub> /in <sup>3</sup> )
		Axial	Radial		
Homogenized MOX Fuel Region	46	0.02125	--	0.0638	0.1246
	80	0.02120	--		
	260	0.01873	--		
	440	0.01683	--		
	620	0.01533	--		
	800	0.01420	--		
	980	0.01352	--		
	1160	0.01326	--		
	-20	--	0.00232		
	50	--	0.00269		
	150	--	0.00321		
	275	--	0.00390		
	425	--	0.00479		
	575	--	0.00579		
	725	--	0.00694		
800	--	0.00754			

**Notes:**

- ① Homogenized fuel region is assumed to extend between the inner surfaces of the ‘fuel boxes’ on the strongback structure. See Appendix 3.6.2, *Thermal Model Details*, for development of the homogenized fuel region thermal properties.

**Table 3.2-5 – Properties of Miscellaneous Solids**

Material	Temperature (°F)	Density (lb <sub>m</sub> /ft <sup>3</sup> )	Thermal Conductivity (Btu/hr-ft-°F)	Specific Heat (Btu/lb <sub>m</sub> -°F)
Polyurethane Foam <sup>①</sup>	---	10	0.01975	0.353
Polyurethane Foam <sup>①</sup>	---	30	0.04	0.353
Neoprene Rubber <sup>②</sup>	---	89	--	--
Delrin <sup>®</sup> plastic <sup>②</sup>	---	88	0.208	--

**Notes:**

- ① Thermal conductivity and specific heat for 10 and 30 lb<sub>m</sub>/ft<sup>3</sup> (pcf) polyurethane foam taken from product data sheet for *LAST-A-FOAM FR-3700 for Crash and Fire Protection of Nuclear Material Shipping Containers*, General Plastics Manufacturing Company, Tacoma, WA.
- ② Impact of neoprene rubber and Delrin<sup>®</sup> plastic components not considered thermally significant. Data per Mat Web On-Line Material Property Data, [www.matls.com](http://www.matls.com).

**Table 3.2-6 – Properties of Air**

Temperature (°F)	Density (lb <sub>m</sub> /ft <sup>3</sup> )	Specific Heat (Btu/lb <sub>m</sub> -°F)	Dynamic Viscosity (lb <sub>m</sub> /ft-hr)	Thermal Conductivity (Btu/hr-ft-°F)	Prandtl No.	Coef. Of Thermal Exp. (°F <sup>-1</sup> )
-40	Use Ideal Gas Law w/ M = 28.966	0.240	0.0367	0.0121	Compute as Pr = c <sub>p</sub> μ / k	Compute as β = 1/(°F+459.67)
0		0.240	0.0395	0.0131		
50		0.240	0.0429	0.0143		
100		0.241	0.0461	0.0155		
200		0.242	0.0521	0.0178		
300		0.243	0.0576	0.0199		
400		0.245	0.0629	0.0220		
500		0.248	0.0678	0.0240		
600		0.251	0.0724	0.0259		
700		0.253	0.0768	0.0278		
800		0.256	0.0810	0.0297		
900		0.259	0.0850	0.0315		
1000		0.262	0.0889	0.0333		
1200		0.269	0.0962	0.0366		
1400		0.274	0.1031	0.0397		
1500	0.277	0.1063	0.0412			

**Note:** Properties based on curve fits in Rohsenow, Hartnett, and Choi, *Handbook of Heat Transfer*, 3rd edition, McGraw-Hill Publishers, 1998.

**Table 3.2-7 – Emissivities and Absorptivities for NCT**

Surface	Material And Assumed Condition	Emissivity ( $\epsilon$ )	Solar Absorptivity ( $\alpha$ )
Interior and exterior surfaces of body shell	Type XM-19 stainless steel <sup>①</sup> , slightly oxidized	0.30	0.50
Impact Limiter Shell	Type 304 Stainless Steel <sup>②</sup> , weathered	0.40	0.50
Strongback surfaces	Type 304 Stainless Steel <sup>③</sup> , unoxidized	0.20	N/A
Poison Surfaces	Aluminum <sup>④</sup> , bright	0.15	N/A
Closure lid/collar interface surfaces	Type XM-19 stainless steel <sup>⑤</sup> , clean	0.25	N/A
Ambient Environment	--	1.00	N/A

**Notes:**

- ① Optical properties assumed similar to those for Type 304 stainless steel. Listed properties based on the values for 'as-received' surface finish values in Frank, R. C., and W. L. Plagemann, *Emissivity Testing of Metal Specimens*, Boeing Analytical Engineering coordination sheet No. 2-3623-2-RF-C86-349, August 21, 1986.
- ② Assumes a weathered, 'as-received' surface finish, Gubareff, G. G., J. E. Janssen, and R. H. Torborg, *Thermal Radiation Properties Survey*, 2nd Edition, Honeywell Research Center, 1960.
- ③ Based on representative values for a unoxidized, 'bright' surface from Gubareff, G. G., J. E. Janssen, and R. H. Torborg, *Thermal Radiation Properties Survey*, 2nd Edition, Honeywell Research Center, 1960 and Wood, W. D., *Thermal Radiative Properties of Selective Materials - Volume I*, Battelle Memorial Institute, Report No. AD 294-345, 1962.
- ④ Based on mean of manufacturer's suggested values, AAR, *Standard Specification for Boral Composite Sheet*, AAR Advanced Structures.
- ⑤ Optical properties assumed similar to those for Type 304 stainless steel. Listed properties based on the lower values for 'as-received' surface finish values in Frank, R. C., and W. L. Plagemann, *Emissivity Testing of Metal Specimens*, Boeing Analytical Engineering coordination sheet No. 2-3623-2-RF-C86-349, August 21, 1986 and clean, un-oxidized surfaces from Gubareff, G. G., J. E. Janssen, and R. H. Torborg, *Thermal Radiation Properties Survey*, 2nd Edition, Honeywell Research Center, 1960 and Wood, W. D., *Thermal Radiative Properties Of Selective Materials - Volume I*, Battelle Memorial Institute, Report No. AD 294-345, 1962.

This page left intentionally blank.